Journal of Oncology

Cancer Metastasis: A Therapeutic Target

Lead Guest Editor: Peramaiyan Rajendran
Guest Editors: Wei-Ting Chao, Esaki Shankar, Ganapathy Ekambaram, and Kalayarasan Srinivasan

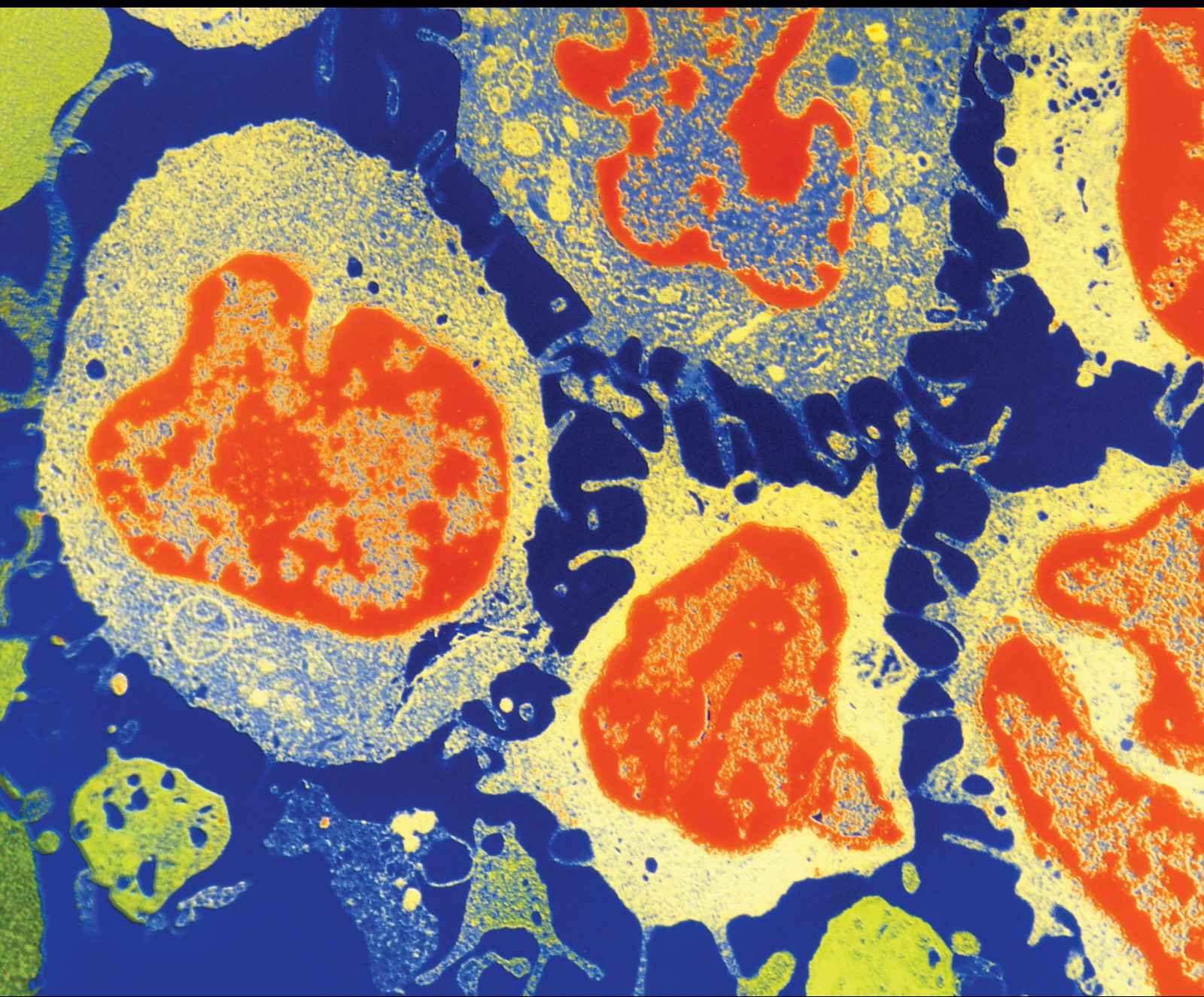

Cancer Metastasis: A Therapeutic Target

Journal of Oncology

Cancer Metastasis: A Therapeutic Target

Lead Guest Editor: Peramaiyan Rajendran
Guest Editors: Wei-Ting Chao, Esaki Shankar, Ganapathy Ekambaram, and Kalayarasan Srinivasan

Editorial Board

Contents

Hindawi
Journal of Oncology
Volume 2019, Article ID 7907282, 2 pages
https://doi.org/10.1155/2019/7907282

Editorial

Cancer Metastasis: A Therapeutic Target

Peramaiyan Rajendran,[1] **Wei-Ting Chao**,[2] **Esaki M. Shankar**,[3] **Ekambaram Ganapathy**,[4] **and Kalayarasan Srinivasan**[5]

[1]*Department of Biological Sciences, College of Science, King Faisal University, Hofouf, Al-Ahsa 31982, Saudi Arabia*
[2]*Department of Life Science, Tunghai University, Taichung, 40704, Taiwan*
[3]*Division of Infection Biology and Medical Microbiology, Department of Life Sciences, Central University of Tamil Nadu, Neelakudi, Thiruvarur 610 005, Tamil Nadu, India*
[4]*Department of Radiation Oncology, Division of Molecular Oncology, University of California at Los Angeles (UCLA), Los Angeles, CA 90095, USA*
[5]*Division of Molecular Radiation Biology, Department of Radiation Oncology, University of Texas Southwestern Medical Center, Dallas, TX, USA*

Correspondence should be addressed to Peramaiyan Rajendran; peramaiyanrajendran@gmail.com

Received 17 June 2019; Accepted 17 June 2019; Published 7 August 2019

Metastasis to vital organs from cancers of the liver, breast, lung, colon, melanoma, and prostate accounts for ~90% of all cancer-related deaths. Investigators have published a wealth of data on basic science and clinical medicine documenting metastases and their prognostic significance, pathobiological mechanisms, therapeutic targets, and diagnostic advances. Most of the work has been dedicated to understand the importance and significance of cancer metastasis and the clinical therapeutic proteins targeted for potential translational implications. Consequently, given that, evidences pertinent to such measures have set the stage for clinicians and basic medical scientists to advance from the bench to the bedside, and the Journal of Oncology has set out to publish a special issue devoted to a topic titled "Cancer Metastasis: A Therapeutic Target." The result is a collection of ten outstanding articles submitted by investigators representing ten countries across North America, Europe, and Asia. In all cases, the methods section of each manuscript included a statement documenting that the clinical investigations were performed following institutional review board approval and/or that informed consents from patients or their legal representatives were secured before setting out for the respective investigations.

S. Sundararajan et al. (2019), based in USA, in the paper titled "Sequential Interventional Management of Osseous Neoplasms via Embolization, Cryoablation, and Osteoplasty," have demonstrated that combination therapy has the potential to transform into an effective mainstay of treatment paradigm in the palliative care of osseous neoplasms to improve the quality of life of individuals. A. Trebinska-Stryjewska et al. (2019), from Poland, in the paper titled "Cytoplasmic HAX1 Is an Independent Risk Factor for Breast Cancer Metastasis," have established that HAX1 localization is important for the prediction of metastatic relapse and that cytoplasmic but not nuclear HAX1 is an independent risk factor for breast cancer metastasis. S. M. Messerli et al. from USA in their article titled "Use of Antimetastatic SOD3-Mimetic Albumin as a Primer in Triple Negative Breast Cancer" support the hypothesis that PNA works through the inhibition of extracellular superoxide/ROS production leading to the conversion of 4T1 cells from a metastatic tumorigenic state to a cytostatic state. Their findings advocate potential future clinical trials using PNA as an antimetastatic SOD3-mimetic drug to increase overall survival in TNBC patients.

A. Bisgin and Colleagues (2019) from Turkey in their article titled "Interaction of CD200 Overexpression on Tumor Cells with CD200R1 Overexpression on Stromal Cells: An Escape from the Host Immune Response in Rectal Cancer

Patients" have clearly shown that tumor-stroma communication through CD200 and its receptor interaction is selected in patients with high risk of relapse. High levels of these molecules support instigation of the far and local metastatic nest that provides solid ground for metastasis. S. H. Kim et al. (2019) from South Korea in the paper titled "The De Ritis and Neutrophil-to-Lymphocyte Ratios May Aid in the Risk Assessment of Patients with Metastatic Renal Cell Carcinoma" have demonstrated that the overall survival and predictive ability were increased when NLR and DRR markers were added to established Heng or mMSKCC risk models in patients with mRCC treated with first-line targeted therapy. E. Dirican and E. Kiliç (2019) from Turkey in the paper titled "A Machine Learning Approach for the Association of ki-67 Scoring with Prognostic Factors" investigated the way of clustering of prognostic factors by ki-67 score using a machine learning approach and multiple correspondence analysis. They have found that low scores of ki-67 correlate with early-stage disease and high scores with advanced disease suggesting that 14% threshold value is crucial for ki-67 score. S. Destek and V. O. Gul in their article titled "S100A4 May Be a Good Prognostic Marker and a Therapeutic Target for Colon Cancer" have established the role of S100A4 in the prognosis of colon cancer and its prognostic significance. Their work provides a unique perspective on the published clinical significance of S100A4 in colon cancer prognosis.

A series of three review papers, one from Portugal titled "Liver Metastases and Histological Growth Patterns: Biological Behavior and Potential Clinical Implications—Another Path to Individualized Medicine?" by R. I. Oliveira et al. (2019), one from China titled "Resection of Liver Metastases: A Treatment Provides a Long-Term Survival Benefit for Patients with Advanced Pancreatic Neuroendocrine Tumors: A Systematic Review and Meta-Analysis" by X. Yu et al. (2019), and one from China as well titled "iRGD, A Promising Peptide for Cancer Imaging and Potential Therapeutic Agent for Various Cancers" by H. Zuo (2019), have clearly examined several diverse therapeutic targets on cancer metastasis. Each work provides a unique perspective on published clinical trials on the importance and therapeutic targets associated with cancer metastases. Uniformly, all authors highlight both the promise and the challenges faced by clinicians and basic medical scientists in the emerging field of cancer metastasis. Their manuscripts identify the critical need for additional prospective, randomized controlled clinical trials evaluating metastasis. In summary, this special issue provides a snapshot of the status of cancer metastasis and clinical trials carried out in the area from across the globe. We hope that the articles published herein will provide a benchmark for future meta-analyses evaluating a far greater body of clinical evidence regarding the safety and efficacy of cancer metastasis therapies, and we sincerely trust that the articles published in this special issue will amuse the audience of the Journal of Oncology that has dedicated itself to ending the menace that indeed is awaiting its end.

Conflicts of Interest

The authors declare that there are no conflicts of interest.

Peramaiyan Rajendran
Wei-Ting Chao
Esaki M. Shankar
Ekambaram Ganapathy
Kalayarasan Srinivasan

Hindawi
Journal of Oncology
Volume 2019, Article ID 9367845, 15 pages
https://doi.org/10.1155/2019/9367845

Review Article

iRGD: A Promising Peptide for Cancer Imaging and a Potential Therapeutic Agent for Various Cancers

Houdong Zuo

Sichuan Key Laboratory of Medical Imaging, Department of Radiology, Affiliated Hospital of North Sichuan Medical College, Nanchong, Sichuan 637000, China

Correspondence should be addressed to Houdong Zuo; zuohoud@163.com

Received 2 August 2018; Revised 4 June 2019; Accepted 11 June 2019; Published 26 June 2019

Guest Editor: Peramaiyan Rajendran

Poor penetration into the tumor parenchyma and the reduced therapeutic efficacy of anticancer drugs and other medications are the major problems in tumor treatment. A new tumor-homing and penetrating peptide, iRGD (CRGDK/RGPD/EC), can be effectively used to combine and deliver imaging agents or anticancer drugs into tumors. The different "vascular zip codes" expressed in different tissues can serve as targets for docking-based (synaptic) delivery of diagnostic and therapeutic molecules. αv-Integrins are abundantly expressed in the tumor vasculature, where they are recognized by peptides containing the RGD integrin recognition motif. The iRGD peptide follows a multistep tumor-targeting process: First, it is proteolytically cleaved to generate the CRGDK fragment by binding to the surface of cells expressing αv integrins ($\alpha v\beta 3$ and $\alpha v\beta 5$). Then, the fragment binds to neuropilin-1 and penetrates the tumor parenchyma more deeply. Compared with conventional RGD peptides, the affinity of iRGD for αv integrins is in the mid to low nanomolar range, and the CRGDK fragment has a stronger affinity for neuropilin-1 than that for αv integrins because of the C-terminal exposure of a conditional C-end Rule (CendR) motif (R/KXXR/K), whose receptor proved to be neuropilin-1. Consequently, these advantages facilitate the transfer of CRGDK fragments from integrins to neuropilin-1 and consequently deeper penetration into the tumor. Due to its specific binding and strong affinity, the iRGD peptide can deliver imaging agents and anticancer drugs into tumors effectively and deeply, which is useful in detecting the tumor, blocking tumor growth, and inhibiting tumor metastasis. This review aims to focus on the role of iRGD in the imaging and treatment of various cancers.

1. Introduction

Cancer is a prominent disease and a leading cause of mortality worldwide [1]. In 2018, 1,735,350 new cancer cases and 609,640 cancer-related deaths were estimated to occur in the United States. Lung and breast cancers are the most frequently diagnosed cancers and the leading causes of cancer-related death in men and women, respectively [1]. Early detection is important for cancer therapy. Currently, magnetic resonance imaging (MRI) and ultrasound (US) are the most reasonable imaging modalities used for the early detection and evaluation of cancer after preoperative chemotherapy or surgery [2]. Cancer imaging is crucial for early detection; therefore, the development of cancer imaging agents that can be effectively delivered to tumor parenchyma is a research hotspot.

The current main therapeutic options for most cancers, such as breast and gastric cancer, are surgical resection and clinical chemotherapy [3, 4]. However, the current challenge of systemic therapy is poor penetration into the tumor parenchyma and the adverse effects of the drugs. In some solid tumors, many drugs can only penetrate 3-5 cell diameters from the blood vessels into the parenchyma and exhibit fewer anticancer effects [5]. The vascular zip codes, which are representative of biochemical signatures in different tumor tissues, may serve as potential targets for docking-based diagnostic and therapeutic delivery [6, 7]. Therefore, cancer-targeted therapies are necessary and significant. The αv integrins ($\alpha v\beta 3$ and $\alpha v\beta 5$) are highly expressed in the cancer vasculature and can bind peptides containing the RGD integrin recognition motif [7]. RGD peptides are a kind of peptide that contain Arg-Gly-Asp sequence, which is widely found in the living body and is the recognition site for integrins and its ligand protein interaction. In tumor blood vessels, two key molecules (neuropilin-1, NRP-1, and neuropilin-2, NRP-2) can regulate tumor tissue

vasculature permeability and enhance permeability through the interaction between the C-end Rule (CendR) motif and neuropilin [8]. NRP involved as a coreceptor of key receptor tyrosine kinases (RTKs) in many signaling pathways is of particular importance for cell survival and cell fate. NRP1 is a 120 kDa and NRP2 is a 112 kDa transmembrane glycoprotein [9]. NRP1 was widely found in neuronal cells and blood vessels of different tissues, especially in arterial vessels, and NRP2 is expressed in neural crest-derived cells [10]. Integrins have been reported to interact with NRPs, because NRPs are versatile in their structure and repertoire of soluble ligands [11]. The interaction between the CendR motif and NRP-1 seems to be a vital factor for penetration of biological barriers. And the R/KXXR/K motif is considered to be as a mediator of cell and tissue penetration [12]. Therefore, the strict requirement for the CendR motif is to be at the C-terminus of the peptide to facilitate cell binding. This motif cannot be activated unless it occupies a C-terminal position in the peptide and this position effect is named the C-end Rule (CendR). In general, the typical characteristics of CendR are as follows: (1) R/KXXR/K recognition motif; (2) requirement for C-terminal exposure of the motif for activity; (3) transition of internal CendR motifs to active, C-terminal ones through proteolytic cleavage; and (4) NRP-1 dependence of the recognition and penetration activities [12].

iRGD is a newly identified peptide. Similar to conventional RGD, iRGD can bind to the surface of cancer cells with high levels of αv integrin expression [13]. iRGD plays a role following a multistep process.

The CRGDK fragment is generated when iRGD is injected intravenously and functions by targeting αv integrins and exposing the CendR motif at the C-terminus to activate the RXXR/K sequence motif. The interaction between the CendR motif and NRPs activates the bulk delivery process, allowing anticancer drugs to penetrate deeply into the tumor tissue through conjugation to or even coadministration with iRGD [14, 15]. Therefore, iRGD can serve as an effective therapeutic target to enhance the efficacy of anticancer drugs. This review aims to highlight the role of iRGD peptide in cancer imaging and therapy.

2. iRGD Peptide

Conventional RGD binds specifically to integrin $\alpha v\beta 3$ on the surface of the tumor vasculature [16] and plays an important role in delivering anticancer drugs, imaging agents, nanoparticles, and virus vectors to blood vessels [13, 14, 17]. The iRGD peptide, with its short amino acid sequence (Arg-Gly-Asp), is a recently identified type of tumor-targeting peptide that was discovered by phage display. This peptide can control the permeability of tumor cells, regulate cellular internalization and extravasation, and promote deeper tissue penetration to improve the imaging sensitivity and therapeutic efficacy [13, 14]. Like the conventional RGD peptide, iRGD (CRGDK/RGPD/EC) can bind to αv integrins that are specifically expressed on the surface of tumor vessels when intravenously injected first [13, 18]. Then, iRGD is cleaved into CRGDK/R by a protease. Because iRGD has a functional sequence, it has affinity for NRP-1, specifically for the active C-end Rule (CendR) motif (R/KXXR/K) exposed at the C-terminus [12]. Tumor tissue penetration is triggered by peptide binding to integrins through the interaction of the CendR motif with NRP-1. This binding process allows the extravasation and penetration of imaging agents or drugs either conjugated to the iRGD peptide or coadministered with iRGD into the target tumor tissues and cells [13, 14, 19].

In general, compared with RGD, the iRGD peptide has the following advantages: First, the affinity of iRGD for αv integrins is in the mid to low nanomolar range. Second, the proteolytically processed CRGDK fragment gains a stronger affinity for neuropilin-1 than its residual affinity for αv integrins because of the C-terminal exposure of the conditional C-end Rule (CendR) motif (R/KXXR/K), whose receptor proved to be neuropilin-1. The above changes facilitate the shift of CRGDK from integrins to neuropilin-1 and the consequent penetration activities. Every phase involved in this multistep process increases the tumor specificity of iRGD conspicuously. Third, iRGD has greater homing biological characteristics possibly owing to the RGD-directed specific homing of the intact peptide [13]. Fourth, the recruitment of iRGD to the cell surface through the iRGD-integrin interaction is likely necessary for the proteolytic cleavage that activates the resulting tumor penetration because protease inhibitors are usually inanimate on cell surfaces but block proteolysis elsewhere [20]. Fifth, the cell penetrating capability of iRGD is far better than that of conventional RGD peptides, possibly because integrins shuttle between the cell surface and intracellular compartments, and some viral pathogens enter into cells utilizing this mechanism [21]. Finally, iRGD has no adverse effect or cytotoxicity on healthy cells [22], which has caused it to gain considerable attention in targeted research.

3. The Process of iRGD Peptide Penetration into Tumors

The phage peptide was first identified by Pasqualini and Ruoslahti in 1996 when a large number of peptides homed to tumor cells were developed [23]. Pasqualini and Ruoslahti discovered new organ-targeting peptide sequences by in vivo screening. They found that some peptides had the ability to regulate the selective localization of phage to brain and kidney vasculature, displaying high selectivity. Then, they synthesized one peptide (CLSSRLDAC) expressed by the brain-localizing phage and demonstrated specific inhibition of homologous phage localization. When the red blood cells were coated with this peptide and injected intravenously, they showed selective localization to the brain. These peptide sequences were first identified targeting endothelial cells, which could be useful in delivering cells, drugs, and genes into the selected tissues in the future [23]. iRGD contains an Arg-Gly-Asp sequence, which can bind to integrins ($\alpha v\beta 3$ and $\alpha v\beta 5$) specifically expressed on the surface of tumor cells. Briefly, iRGD exerts its function following 3 key steps: (1) iRGD peptides bind to integrins ($\alpha v\beta 3$ and $\alpha v\beta 5$); (2) the peptide is proteolytically cleaved in tumors to produce CRGDK/R and expose the activated CendR motif

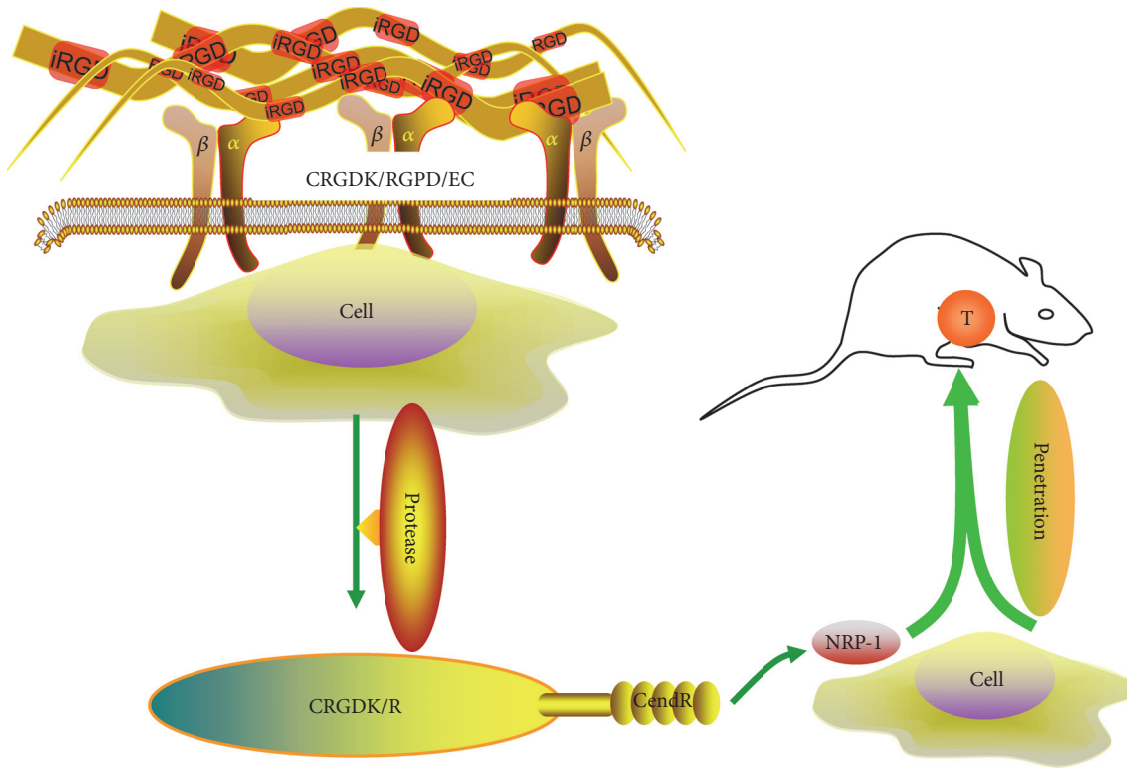

Figure 1: The key steps in the tumor-targeting process of the iRGD peptide. First, iRGD peptides (CRGDK/RGPD/EC) bind to integrins ($\alpha v\beta 3$ and $\alpha v\beta 5$). Second, the peptide is proteolytically cleaved in the tumor to produce CRGDK/R and expose the activated CendR motif (R/KXXR/K) at the C-terminal end. Third, the CendR motif binds to NRP-1 to trigger tumor tissue penetration. T: tumor.

(R/KXXR/K) at the C-terminus; and (3) CendR binds to NRP-1 to trigger tumor tissue penetration (Figure 1).

4. iRGD for Tumor Imaging

Many nanoparticles, imaging agents, compounds, and ligands coupled, conjugated, and modified by iRGD have been widely studied for tumor imaging and detection [13, 17, 24]. Sugahara et al. [13] intravenously injected iRGD peptide linked to superparamagnetic iron oxide (SPIO) nanoworms into mice with 22Rv1 orthotopic xenograft tumors. The iron oxide nanoparticles showed hypointensity on T2-weighted MR images. The vasculature was hypointense, and the iRGD nanoworms elicited hypointense signal regions in the tumor; by contrast, the CRGDC nanoworms lowered only the signal intensity of the tumor vasculature. These findings were confirmed by optical imaging, which indicated that iRGD was more efficient than conventional RGD peptides [13, 17, 25]. Zuo et al. [22] reported that the iRGD peptide enhanced the positive labeling rate of pancreatic cancer cells and cell uptake with superparamagnetic iron oxide (SPIO) and demonstrated the optimal imaging effect with appropriate concentrations. Moncelet et al. [26] found that either E-[c(RGDfK)2] or iRGD internalization increased the signal-to-noise ratio (SNR), cell labeling, and intracellular signals and improved the MRI diagnosis in glioblastoma cells. In 2016, Xin et al. [27] developed a new tumor-targeting MRI contrast agent by conjugating gadolinium-diethylene triamine pentaacetate (Gd-DTPA) to the bispecific recombinant anti-EGFR-iRGD protein (anti-EGFR-iRGD-DTPA-Gd). This new agent had no obvious cytotoxicity to human gastric carcinoma cells and demonstrated higher T1 relaxivity and superior tumor-targeting ability compared with those of Magnevist. The same findings were also observed and verified by in vivo experiments. Ye et al. [28] artificially synthesized two new iRGD peptide analogues (Ac-Cys(IRDye®800CW)-iRGD and DOTA-Cys(IRDye®800CW)-iRGD) and revealed that both analogues showed significant tumor localization assessed with optical imaging in MDA-MB-435 tumor-bearing mice. Cho et al. [29] synthesized a fluorescence-activatable multifunctional monolithic probe based on a cyclic iRGD peptide for tumor imaging, and it remarkably improved the imaging effect with fluorescence contrast between tumor and normal tissues because the background minimized the tumor-specific signal. Yang et al. [30] synthesized an active-tumor-targeting imaging system with a physical method that used a fabricated iRGD to redshift emissive carbon nanodots (iRGD-CDs). iRGD-CDs showed a higher accumulation in 4T1 cells in vitro; in vivo, iRGD-CDs could penetrate and selectively accumulate in tumors, leading to a better tumor imaging efficacy. The following characteristics may account for the better tumor imaging efficacy: (1) iRGD-CDs have a uniform diameter of 3.3 ± 0.57 nm, well-resolved lattice structures with a d spacing value of 0.22 nm, and longer excitation and emission; (2)

iRGD-CDs are stable and do not exhibit obvious attenuation of fluorescence intensity with increases in incubation time; (3) iRGD-CDs have good hemocompatibility and low cytotoxicity; (4) iRGD-CDs could significantly improve the tumor targeting and sensitivity of CDs and could be efficiently delivered to 4T1 tumor tissue; and (5) the iRGD-CD distribution in tumors is much higher than that of the CD group. Przysiecka et al. [31] synthesized $CuInZn_xS_{2+x}$ quantum dots (QD) electrostatically associated with iRGD (iRGD/QD) to investigate the role of iRGD in the transport of nanoparticles to various human cancer cell lines. Their findings revealed the high penetration ability for the iRGD/QD assembly. Imaging experiments showed that iRGD/QD assemblies were distributed evenly throughout the whole HeLa spheroid, and iRGD/QD may serve as a great potential tumor-targeting imaging agent and/or nanocarrier. A new transformable integrin-targeted ultrasound contrast agent, iRGD microbubbles (iRGD-MBs), which incorporate iRGD-lipopeptides, was developed for tumor angiogenesis imaging. iRGD-MBs showed stronger binding specificity towards endothelial cells than the control agent in vitro. In vivo, iRGD-MBs also displayed stronger enhancement within tumors after intravenous injection in mice bearing 4T1 breast tumors [32]. A novel dual-targeted ultrasound contrast agent (iRGD/CCR2 dual-targeted cationic microbubbles, $MB_{iRGD/CCR2}$) was newly prepared by Xu et al. [33]. The data showed that $MB_{iRGD/CCR2}$ had higher binding efficacy with bEnd.3 cells and MCF-7 cells, as well as loading pGPU6/GFP/Neo-shAKT2 plasmid DNA more effectively, and had higher gene transfection efficiency under ultrasound exposure than the control agent. In a recent study, a new theranostic peptide platform (Cy5.5-iRGDC-Pt(IV)) could not only demonstrate an ideal tumor imaging effect but also induce tumor-specific apoptosis resulting in evident tumor suppression by conjugating a fluorescent dye and a cisplatin prodrug on each terminus of cyclic iRGD for simultaneous cancer-targeted imaging and therapy. In addition, the new platform had negligible systemic toxicity [34]. This area is an up-and-coming research hotspot and must be investigated thoroughly.

Previous studies and findings suggested that the iRGD peptide is a potential tumor target for more sensitive visualization and more effective gene therapy.

5. iRGD for Cancer Therapy

The functional mechanism of iRGD is well recognized and illustrated, and its preclinical investigation has been carried out thoroughly. The following substantial studies for cancer therapy in vitro and in vivo regarding different cancers are summarized in detail.

5.1. Breast Cancer. Breast cancer is a leading cause of death among women [1]. To date, there are no ideal treatment options except surgery and chemotherapy; thus, more effective and noninvasive treatment is urgently needed. Since the development of the iRGD peptide, it has been widely and continuously used in the study of breast cancer therapy. Sugahara et al. [13] investigated the efficacy of iRGD-Abraxane in a tumor model using the BT474 human breast cancer cell line. After intravenous injection, iRGD-Abraxane accumulated in the tumor 11-fold more than nontargeted Abraxane and approximately 4-fold more than CRGDC-Abraxane. In addition, significant tumor growth suppression was observed in vivo [13, 14, 34]. In 2013, Liu et al. [35] devised a new strategy to improve anticancer efficiency by conjugating a Dox-loaded crosslinked multilamellar liposomal vesicle (cMLV) to the iRGD peptide. The iRGD peptide facilitated and increased the binding ability and cellular uptake of cMLV in breast cancer cells. They also found that iRGD-conjugated cMLVs (iRGD-cMLVs) delivered into cells were regulated by the clathrin-mediated pathway. These findings suggest that the iRGD peptide can overcome the transport limitation of the targeted payload into the tumor parenchyma and establish tissue-penetrating anticancer drug delivery. The molecular mechanism by which iRGD exerts high-efficiency tissue penetration may be related to the vascular permeabilization induced by the CendR function of iRGD [13].

Another study by Cun et al. [36] developed a novel and scalable complex (iRGD-DOX-AuNPs-GNPs) and a tumor-microenvironment-responsive multistage system (DOX-AuNPs-GNPs) that was pH-sensitive. The data showed that coadministration of iRGD with DOX-AuNPs-GNPs increased cellular uptake, facilitated apoptosis in vitro, and exhibited higher penetration and accumulation resulting in the best antitumor efficiency in 4T1 tumor mice in vivo. The results may be due to the interaction between $\alpha v\beta 3$ and NRP-1 receptor overexpression in 4T1 cells. To potentiate chemotherapy, loaded liposomes modified by nRGD (nRGD-Lipo-Dox) were developed by covalently conjugating the alanine-alanine asparagine "tail" residues to the cyclic tumor-homing peptide iRGD in the 4T1 breast cancer mouse model; nRGD-Lipo-Dox showed a prominent antitumor effect by penetrating and accumulating in the tumor [37]. The use of doxorubicin-loaded low-temperature-sensitive liposomes (LTSL-DOX) modified by iRGD (iRGD-LTSL-DOX) was reported by Deng et al. [38]. iRGD-LTSL-DOX can specifically bind to $\alpha v\beta 3$ on breast cancer cells and release encapsulated DOX under special conditions. In vivo, the results showed that DOX released and rapidly penetrated into tumor tissues after high-intensity focused ultrasound (HIFU) in the 4T1 breast tumor models, leading to enhancement of the drug's anticancer efficacy. Therefore, they concluded that iRGD penetration and the HIFU thermal effect jointly enhanced drug delivery.

iRGD-modified core-shell nanocapsules (iRGD-NCs) loaded with paclitaxel (PTX) were prepared by Jin et al. [39] The nanocapsules had some superior properties, such as increased drug loading, higher drug accumulation in tumors, higher cytotoxicity against cancer cells, longer circulation effects, and significant anticancer effects. First, iRGD-NCs showed a superior anticancer ability because iRGD increased NC accumulation and penetration in tumors. Second, iRGD significantly improved the pharmacokinetics of PTX, prolonged drug circulation in blood, and increased drug bioavailability.

In an in vivo study, Chen et al. [40] developed iRGD-CDD by conjugating Bit1 CDD to iRGD, which resulted

in the compound possessing unique tumor-penetrating and cell-internalizing properties. In orthotopic implantations of MCFA-10CA1a and 4T1 breast cancer cells into mice, iRGD-CDD spread extensively when intratumorally injected and inhibited tumor growth significantly, leading to an average reduction of 77% in tumor volume and eradication of some tumors. They speculated that Bit1 and Bit1-CDD regulated the activities of the antiapoptotic and oncogenic transducing-like enhancer of split (TLE) proteins to mediate cell death. In addition, CendR peptides may deliver CDD into the cytoplasm and take part in protein transduction [40].

A cysteine residue was added to the iRGD peptide (Cys-iRGD) to prolong the cytoplasmic half-life of iRGD compared to that of parental iRGD, as reported by Pang et al. [41] Cys-iRGD accumulation in the tumor was more robust than that of parental iRGD. A new composition (Cys-X-iRGD) was synthesized by increasing the Cys-iRGD via insertion of a GGSGGSGG linker between them. The results demonstrated that Cys-X-iRGD induced more trastuzumab accumulation outside tumor blood vessels significantly than the control agent in 4T1 breast cancer. In addition, this function was regulated by covalent binding of iRGD to plasma albumin through a specific disulfide bond. Some polypeptide hormones modified by iRGD can also change the biological behavior of breast cancer cells and enhance targeted anticancer effects [42]. iRGD conjugated to thymosin alpha 1 (Tα1-iRGD) showed higher binding ability to breast cancer cells and significantly inhibited MCF-7 cell growth. In addition, Tα1-iRGD can enhance anticancer drug efficacy by increasing cell penetration and tumor accumulation. These findings may be related to the preservation of anticancer immunomodulatory activity of Tα1 by enhancing the proliferation of spleen lymphocytes in mouse models. In addition, Tα1-iRGD also considerably induced MCF-7 cell apoptosis, which might be related to the superior effect of Tα1 on upregulating BCL2-associated X protein (Bax), caspase 9 expression, etc. [42]. The authors also produced a new product (TP5-iRGD) by fusing iRGD with the C-terminus of thymopentin (TP5), and it had the same anticancer effect in vitro and in vivo [43].

Kotamraju et al. [44] reported that FAM-X-C(iRGD)REKA extravasated into tumors interior from the blood vessels; however, the CREKA peptide alone homed only to the tumor vasculature in mice bearing MCF10CA1A human breast cancer xenograft tumors. Their findings imply that penetration into a tumor's interior is an internal function of iRGD.

Ma et al. [45] synthesized pH-sensitive fluorocarbon functionalized nanoparticles (SFNs) conjugated to the tumor-penetrating peptide iRGD. SFNs not only overcame their inherent instability but also facilitated dramatic tumor accumulation and penetration in an orthotopic breast cancer mouse model in vivo, resulting in a synergistic effect between iRGD and SFNs and a consequent increase in tumor necrosis or apoptosis, reduction in tumor angiogenesis, and suppression of Ki-67-positive tumor cell proliferation.

In vivo, induction of an antitumor immune response can also be a strategy for breast cancer therapy [46]. Deng et al. [46] found that anticancer drug accumulation in tumors was greatly increased when nanostructured lipid carriers (NLCs) coadministered with iRGD led to significant tumor growth suppression and an increase in immunogenic cell death. Therefore, the antitumor immune response of chemotherapy greatly benefits anticancer efficacy and renders a promising application for tumor therapy.

5.2. Lung Cancer. Numerous anticancer drugs or therapy modalities with iRGD targeting have been applied in lung cancers, including human non-small-cell lung cancer (NSCLC) and Lewis lung carcinoma in animal models. In 2012, Song et al. [47] explored the effect of methoxy poly(ethylene glycol)-block-poly(L-glutamic acid) (mPEG-b-PLG) loaded with cis-diamminedichloroplatinum (cisplatin, CDDP) in combination with iRGD for the treatment of NSCLC. In vivo, mPEG-b-PLG-loaded CDDP coadministered with iRGD exhibited elevated antitumor efficacy, resulting in the reduction of tumor volume and a prolonged survival time by over 30%, which was associated with the reduced toxicity, increased drug concentration in tumor, lower drug dose, and fewer side effects when CDDP was loaded with iRGD. Zhang et al. [48] improved anticancer efficacy of gemcitabine by coadministering it with the iRGD peptide in A549 xenograft mouse models. In vivo, tumor growth slowed and tumor weight decreased with gemcitabine+iRGD. The tumor growth inhibition rate of gemcitabine+iRGD was 86.9%, which was lower than that in the iRGD and gemcitabine groups. In addition, gemcitabine coadministered with iRGD inhibited cell proliferation and induced apoptosis in a human NSCLC-derived A549 cell line. Another study focused on coadministering cetuximab with iRGD in a murine model of human NSCLC [49]. Here, the data showed that cetuximab combined with iRGD could enhance tumor penetration and drug accumulation in tumor tissues, particularly at 3 and 9 h after cetuximab and iRGD administration. Because of the abundant overexpression of $\alpha v\beta 3$, $\alpha v\beta 5$, and NRP-1 in NSCLC cells, the binding and interaction of iRGD with these proteins facilitated the enhancement of anticancer drug effect [48]. Puig-Saus et al. [50] genetically inserted the iRGD peptide in the fiber C-terminus of an oncolytic tumor-retargeted adenovirus called ICOVIR15K to enhance its tumor penetration. The results showed that insertion of iRGD could increase tumor transduction and early adenovirus dissemination through the tumor and enhance anticancer efficacy in lung cancer. Lao et al. [51] revealed that thymosin alpha 1 (Tα1) modified by the iRGD peptide inhibited cell proliferation and enhanced the specificity and potency of Tα1 to the human lung cancer cell line H460. It was reported that Tα1 was able to elevate the expression of histocompatibility complex class I surface molecules and tumor antigens in tumor cells, which indicated the potential of Tα1 for enhanced anticancer activity [52]. In an in vitro experiment with Lewis lung carcinoma (LLC) cells, Solomon et al. [53] developed a tumor spheroid culture model and found that the iRGD peptide coadministered with unmodified liposomes presented higher accumulation and penetration features leading to higher anticancer activity. The authors summarize the following plausible explanations. First, the surface charge of the formulation may contribute

to the high cell-binding ability to the liposomes. Second, the micelles were very small in size, which may be responsible for the higher penetration ability of the DOTAP-liposomes. Third, there might have been a significant loss in the membrane integrity of the cells of the spheroid.

Another difficult problem is drug resistance. The findings by Shen et al. [54] sought to overcome this difficulty. In their study, iPTPNs (iRGD-conjugated D-α-tocopheryl polyethylene glycol 1000 succinate mediated codelivery of paclitaxel and survivin shRNA) were formed, which simultaneously exerted an enhanced permeability and retention effect and an iRGD-mediated active-targeting effect. iPTPNs significantly enhanced the accumulation of PTX and survivin shRNA (shSur) and facilitated cancer cell apoptosis in tumors. The in vivo anticancer efficacy showed that the tumor volume of the iPTPN group (10 mg/kg) decreased dramatically. Therefore, iRGD-mediated PTX and shSur codelivery had the potential for lung cancer resistance reversal.

Some cytokines are also involved in tumor suppression and the selective induction of apoptosis in many human cancer cells, and some cytokines can exhibit enhanced function with the assistance of iRGD. A novel recombinant protein (IL-24-iRGD) was designed by fusing the C-terminal domain of interleukin-24 to the iRGD peptide. The results showed that IL-24-iRGD induced apoptosis and inhibited tumor growth to a significantly greater extent, which had a higher tumor growth inhibition rate (59.1%) than the control treatment (26.2%) [55].

5.3. Prostate Cancer. Prostate cancer is one of the leading causes of death in men, and distant metastasis is frequent in prostate cancer patients [1]. In recent years, many studies have focused on prostate cancer treatment. DOX coinjected with iRGD significantly enhanced penetration and accumulation more than 7-fold in orthotopic 22Rv1 tumors compared to DOX given alone. The efficacy of combination therapy was three times greater than DOX administration alone. A combination of 3 mg/kg DOX and iRGD showed a maximum benefit of DOX activity by inducing tumor growth inhibition based on stronger TUNEL staining, a sign of cell death [14]. De et al. [56] developed a new peptide with higher bioactivity named amphipathic tail-anchoring peptide-iRGD-M8 (ATAP-iRGD-M8), which improved stability and aqueous solubility in cultured cancer cells without conferring cytotoxicity. Because this peptide had a longer half-life in blood circulation due to degradation protection, improved solubility in physiological saline solutions, and the advantage of ATAP, it induced apoptosis independently of Bcl-2 family proteins. In addition, their findings showed significant tumor growth inhibition with intravenous injection of ATAP-iRGD-M8 [56]. Peng et al. [57] reported that a monolayer (2D) and multilayer (3D) of DU-145 prostate cancer cells treated with tumor-penetrating peptide conjugates (P-DOX-PLGLAG-iRGD) accumulated more DOX than control-treated cells did. Meanwhile, P-DOX-PLGLAG-iRGD showed the best penetration ability in 3D multicellular DU-145 tumor cell spheroids. Multifunctional porous silicon (PSi) nanoparticles modified with iRGD enhanced the uptake of nanoparticles by tumor cells in ectopic PC3-MM2 mouse xenograft models. Here, PSi nanoparticles were delivered and distributed in the tumor, leading to efficient tumor growth inhibition with nanoparticle-loaded sorafenib compared to that of free drug due to the fast release of sorafenib from the PSi matrix into the blood after intravenous injection and its limited dissolution rate in blood circulation [58].

Theranostic nanoparticles have also been applied in the treatment of prostate cancer. A polymer nanoparticle (IO@PNP) was synthesized by Herranz-Blanco et al. [59]. IO@PNPs were largely internalized by endothelial (EA.hy926) and metastatic cancer (PC3MM2) cell lines. The internalization rate of iRGD-conjugated IO@PNPs into EA.hy926 cells was moderately increased, but no enhancement was observed with PC3MM2 cells. Poly(ethylene glycol)-*block*-poly(histidine) with pH-responsive and proton-sponge characteristics facilitated rapid lysosomal escape. In addition, IO@PNP-doxorubicin and iRGD showed both intracellular lysosomal escape and efficient transfer of doxorubicin to the nuclei of cells. In summary, the IO@PNP-doxorubicin with the iRGD modification enhanced the anticancer efficacy of DOX by improving the intracellular delivery of DOX encapsulated in IO@PNPs.

5.4. Melanoma. Melanoma is a highly malignant tumor with a high risk of metastasis. Therefore, targeting melanoma therapy has attracted broad attention. Su et al. [60] developed a multifunctional nanogel for melanoma targeting using DOX-encapsulated iRGD-decorated nanogels (NGs), which facilitate drug release from B16 tumor cells because of the maintenance of their thermo- and pH-responsiveness features. The intracellular uptake of DOX-NGs was increased remarkably via iRGD modification in B16 tumor cells. NGs with a pH-responsive function showed controlled DOX release in deep tumors and much fewer side effects from DOX, leading to maximal anticancer efficacy in vivo. A new sterically stabilized liposome (SSL) with DOX-loaded and iRGD-modified (iRGD-SSL-DOX) was applied to B16-F10 cells in vitro and to tumor-bearing mice in vivo because αv integrin receptor and NRP-1 were also overexpressed in B16-F10 cells [61]. All the in vitro and in vivo results showed that tumor-targeting and tumor-penetrating activities of SSL modified with iRGD were much more enhanced than those of the control treatment. The antitumor efficiency against melanoma tumors also increased significantly, which was reflected by the substantial inhibition of tumor growth and reduction in tumor size [62]. Another similar study was performed using a novel liposome modified with iRGD in B16-F10 melanoma, which contained the conjugated linoleic acid-paclitaxel (iRGD-SSL-CLA-PTX). Here, cellular uptake of the drug and CLA-PTX levels after iRGD-SSL-CLA-PTX treatment increased at different time points. The in vivo experiments demonstrated that iRGD-SSL-CLA-PTX greatly suppressed the growth of B16-F10 tumors [63] because the benefits in increasing drug exposure were improved through ligand-modified delivery systems in vitro and the enhanced permeability and retention effect (PRE) [64]. Interestingly, Deng et al. [65] developed a new anticancer synthesis-oligomeric hyaluronic acid-liposome (HA-Lip) for melanoma. When coadministered with iRGD, HA-Lip could

penetrate into the tumor more efficiently because of the enhanced internalization through receptor-mediated endocytosis on tumor cell surfaces. Meanwhile, in the in vivo test, DOX-loaded HA-Lip coadministered with iRGD showed a considerably improved anticancer effect on melanoma. Thymosin alpha 1 (Tα1) modified by the iRGD peptide also inhibited B16F10 cell proliferation and enhanced the targeting and binding affinity in vitro [51].

5.5. Gastric Cancer. Gastric cancer is a common malignant tumor of the digestive system that has a poor prognosis. New molecular-targeted therapies may be a potential strategy for gastric cancers. Thus, gastric cancer-targeted therapy has prevailed since 2015. Sha et al. [66] demonstrated that PTX combined with anti-EGFR-iRGD showed a higher attachment and binding affinity in three human gastric cancer cell lines and inhibited tumor growth in vivo with an approximate tumor volume reduction of 46.66% compared with the control. The improved anti-EGFR-iRGD has significant advantages in solid tumor therapy, especially for the treatment of gastric cancer with various drugs, including DOX, bevacizumab, and PTX, and this effect may be related to the delay of macrophage-mediated drug clearance, which facilitated persistent circulation and enhanced drug delivery into tumors more efficiently [67]. KLA-iRGD, another functional recombinant protein, was constructed [68]. KLA is a peptide that can disrupt mitochondrial membranes, resulting in cell death. iRGD can facilitate KLA function in cell death. KLA-iRGD inhibits tumor growth via activation of the receptor neuropilin-1 and subsequent internalization activity. KLA-iRGD spreads rapidly and extensively in the gastric tumor mass. The recombinant KLA-iRGD protein considerably reduces tumor size and volume, which indicates that it has a higher anticancer efficacy in mice in vivo.

iRGD functionalization potentiated intraperitoneal PTX-loaded pH-sensitive poly(oligoethylene glycol methacrylate)-poly(2-(diisopropylamino)ethyl methacrylate)-polymersomes (POEGMA-PDPA-PS) tumor selectivity and anticancer activity in gastric cancer mouse models. The anticancer efficacy of iRGD-PS-PTX was enhanced greatly compared to that of untargeted PS. Through their study, Dai et al. revealed that the CendR peptide RPARPAR is able to recruit polymersomes to NRP-1 and target polymersomes to cells positive for NRP-1 expression, and PTX-polymersomes targeting CendR peptides showed selective cytotoxicity for NRP-1-positive cells [62]. In addition, under physiological pH conditions, iRGD-polymersomes rapidly disassembled and released PTX after cellular internalization, which may contribute to the increased chemotherapy efficacy [69, 70]. In 2017, some novel targeting methods and treatment modalities were investigated. sTRAIL-iRGD (soluble tumor necrosis factor-related apoptosis-inducing ligand-iRGD), a recombinant protein consisting of sTRAIL fused to an iRGD peptide, was synthesized by Huang et al. [71]. During both in vitro and in vivo studies, sTRAIL-iRGD combined with PTX had significant antitumor efficacy. Repeated treatment with sTRAIL-iRGD-PTX inhibited tumor growth and reduced tumor volume in vivo. sTRAIL was cleaved proteolytically from TRIAIL and retained the characteristics along with the positive effects of iRGD, including apoptosis induction in transformed cancer cells, no negative side effects to the host, and significant anticancer activity.

iRGD could also potentiate the anticancer effect of 5-fluorouracil (5-FU) on gastric cancer cells through NRP1. In vitro, cells treated with 5-FU + iRGD weakened cell viability, proliferation, migration, and invasion. In vivo, the anticancer efficacy of 5-FU was dramatically enhanced with iRGD treatment, resulting in slower tumor growth, but the distinct mechanism by which iRGD regulates 5-FU is still being investigated [72].

Cell immunotherapy is another potential therapy, but it is limited by the poor infiltration of activated lymphocytes into tumors. However, exciting progress in cell immunotherapy has already begun to become integral to cancer treatment strategies [73]. iRGD-modified T cells were able to penetrate into the core of the three-dimensional multicellular sphere when a time-efficient platform that links iRGD to the T cell surface was applied. By contrast, T cells alone could not penetrate the spheres. Meanwhile, iRGD modification could increase T cell numbers in the tumor parenchyma up to 10 times in different tumor models in vivo. Moreover, the iRGD modification had a synergistic effect with programmed death-1 (PD-1) disruption in enhancing the anticancer effect and extending the survival time in mouse models [73].

5.6. Liver Cancer. As early as 2011, studies on hepatocellular carcinoma-targeted therapy with the iRGD peptide began. Poly(ε-caprolactone)-b-poly(N-vinylpyrrolidone) (PCL-b-PVP) copolymers with different PVP block lengths and PTX-loaded nanoparticles that contained 15% drugs and had more than 90% encapsulation efficiency were developed. iRGD-PTX-PCL-PVP showed superior cytotoxicity and cellular uptake of the particles, which indicated that the iRGD peptide contributes to the interaction of the nanoparticles with tumor cells through NRP-1 overexpression on the cell surface. iRGD-PTX-PCL-PVP facilitated the accumulation of nanoparticles at the tumor site because the small nanoparticles (<50 nm) can easily penetrate through the endothelial wall of hepatic cells, leading to enhanced liver uptake [74]. The permeability of the nanoparticles was greatly improved, and the best anticancer efficacy was exhibited in the H22 tumor-bearing mouse models. This effect might be related to the circulatory nanoparticles in vivo, which were trapped in the tumor via the EPR effect or active affinity [75]. Endostatin is a 20 kDa C-terminal fragment, 183 amino acid residues in length, that is derived from collagen XVIII [76] and has been used in cancer treatment for its anticancer activity. iRGD-modified endostatin became much more efficient as a liver cancer therapy. The results indicated that iRGD-modified endostatin inhibited cell proliferation and migration and enhanced endostatin distribution largely in tumors. The antitumor activity and liver cancer growth suppression are due to the neovascularization block by endostatin via iRGD binding to $\alpha_V\beta$ integrins [77]. M-SAL-iRGD for both liver cancer cells and cancer stem cells (CSCs) salinomycin delivery was synthesized by Mao et al. [78]. M-SAL-iRGD showed great superiority with a small size (10 nm) and higher drug encapsulation efficacy

(more than 90%). M-SAL-iRGD enhanced cytotoxicity, greatly targeting M-SAL and salinomycin in both liver cancer cells and CSCs. M-SAL-iRGD showed a greater tissue distribution and anticancer efficacy in liver cancer-bearing mice. The anticancer mechanism of the M-SAL-iRGD is elaborated as follows. First, M-SAL-iRGD accumulates in tumors because of the increasing EPR effect. Second, M-SAL-iRGD binds to $\alpha_V\beta$ integrin and is subsequently proteolytically cleaved into the M-SAL-CRGDK/R motif, which has a higher affinity for NRP-1. Third, NRP-1 binding activates tissue penetration. Finally, after internalization, salinomycin is released from M-SAL-iRGD rapidly in the cytoplasm and kills hepatocellular carcinoma cells and CSCs [78]. iRGD-modified lipid-polymer hybrid NPs with a shell core synthesized for DOX and sorafenib (SOR) codelivery (DOX+SOR/iRGD NPs) were observed by Zhang et al. [79]. DOX+SOR/iRGD NPs showed an increasing synergistic cytotoxicity in cell proliferation and an apoptosis internalization rate in HepG2 cells due to many advantages, such as the synergistic cytotoxicity of drugs, sustainable drug release, enhanced cellular internalization, longer circulation time, and enhanced tumor accumulation. More importantly, DOX+SOR/iRGD NPs showed optimal anticancer activity and apoptosis efficacy in vitro and in vivo mediated by the iRGD interaction with $\alpha_V\beta$ integrin. Schmithals et al. [80] reported that the tumor penetrability of sorafenib and doxorubicin could be considerably enhanced in hepatocellular carcinoma with iRGD through a synergistic effect. They also found that iRGD potentiated the efficiency of drug delivery (approximately threefold) to a specific site in HCC-bearing mouse models. Similar results were observed in a study by Wang et al. [81]. iRGD−PEG-PLA-loaded vandetanib had greatly improved therapeutic efficacy, leading to nearly 60% tumor growth suppression compared to 20 mg/kg vandetanib administration alone. All the above studies suggested that the anticancer effect was enhanced by the interaction of iRGD with $\alpha_V\beta$ integrin expressed on liver cancer cells.

5.7. Pancreatic Cancer. The pancreas is a retroperitoneal organ adjacent to the celiac plexus [82]. Pancreatic cancer is a highly malignant tumor that invades the celiac plexus and metastasizes to other organs [83]. Currently, drug treatments for pancreatic cancer are unsatisfactory. The advent of the iRGD peptide is good for pancreatic cancers because conjugated iRGD can be used directly due to the presence of $\alpha_V\beta$ integrin on the pancreatic cancer cell surface. Targeted therapies for pancreatic cancer have made great strides.

In 2009, a fluorescein-labeled iRGD (FAM-iRGD) was synthesized and added to pancreatic cancer cells (MIA PaCa-2) [13]. FAM-iRGD accumulated in or around tumor vessels and tissues and showed strong fluorescence compared to that in normal tissues, which indicated that FAM-iRGD exhibits strong homing and binding affinity in tumors. For the in vivo tests, FAM-iRGD accumulated and is retained within the tumor because of the increasing permeability in tumor vessels and strong positive expression of neuropilin-1 in tumor cells, which suggests that vascular permeabilization is involved in the molecular mechanism of iRGD-mediated rapid tumor tissue penetration. In pancreatic cancer mouse models with NRP-1 overexpression (BxPC-3 and MIA PaCa-2), gemcitabine coadministered with iRGD showed enhanced tumor penetration and anticancer ability in comparison with gemcitabine alone as confirmed by pancreatic cancer models. These models also revealed that the iRGD effect largely depends on the level of NRP-1 in the tumor, which indicated that the iRGD peptide-mediated effect may be exploitable in some pancreatic cancer patients with high NRP1 expression [84]. Liu et al. [85] developed a multifunctional mesoporous silica nanoparticle (MSNP) designated as a "silicasome", which contains a nonsupported lipid bilayer (LB), to improve the efficacy of pancreatic ductal adenocarcinoma (PDAC) chemotherapy. Silicasome showed a significantly increased drug-loading ability, improved stability in vessels, and reduced drug loss during circulation. Through research and analysis, the transcytosis pathway, EPR effect, nutritional transport pathways, and vascular growth factors may be involved in the molecular mechanism [86, 87]. Another iRGD-nanocage targeting system for pancreatic cancer was described [88]. The iRGD domain was connected to the C-terminal region of heat shock protein (HSP) to form an iRGD-nanocage. An L30-iRGD-nanocage with 30 amino acid linkers exhibited superior binding affinity to pancreatic cancer cells (AsPC-1) and increased cellular uptake, which was related to the length of the linker between the nanocages and the iRGD domain. In addition, OSU03012 (a hydrophobic anticancer drug)-loaded iRGD-nanocages induced AsPC-1 cell death more efficiently in vitro by activating the caspase cascade because of the presence of the iRGD domain; the internalization was accelerated by interactions between the iRGD domain and NRP-1 on the surface of pancreatic cancer cells [89] and by the bystander effect [14]. In a new report in 2017, Tsang et al. [90] found that tumor-targeting peptides (iRGD and cRGD) coupled to U1 adaptors with fluorescence presented targeted tumor localization and highly potent anticancer efficacy (>90%) by targeting two oncogenes (KRAS and MYC) in pancreatic cancer in vivo. Because U1 Adaptor is a new generation gene silencing technology that may serve as a new therapeutic modality for targeting any oncogene [91], U1 Adaptors were translated to target KRAS and MYC, and the adaptors strongly inhibit pancreatic cancer cell proliferation. The iRGD-tumor-penetrating nanocomplexes (iRGD-TPNs) with polyethylene glycol (PEG)-peptide conjugates delivering anti-KRAS siRNA to tumor sites significantly delayed tumor growth in murine models. The significance of iRGD-TPNs is their ability to not only overcome physical barriers to therapy but also achieve knockdown of the gold standard genetic target by leveraging the stroma [92].

Finally, oncolytic adenovirus modified by iRGD by insertion of an iRGD peptide sequence in the fiber C-terminus of ICOVIR15K could also enhance pancreatic cancer (MIA PaCa-2) cell transduction, intratumoral spread, and anticancer efficacy with a great reduction of the tumor volume. The reasonable explanations are as follows: First, the insertion of the iRGD peptide in the fiber C-terminus

of ICOVIR15K boosted the binding and internalization ability of the virus in cells that highly expressed NRP-1. Second, the insertion of iRGD and RPARPAR peptides did not damage the basal characteristics of adenovirus update through integrin receptor-mediated endocytosis. Third, the phenotype of iRGD was additive to the KKTK-to-RGDK fiber shaft modification, which was proven to enhance tumor transduction and anticancer activity [50, 93].

5.8. Glioma. Many functional peptides could enhance the binding affinity to gliomas. MT1-AF7p, a newly identified peptide, showed a prime affinity for membrane type-1 matrix metalloproteinase (MT1-MMP), which is an ideal antiglioblastoma target [94]. Gu et al. developed MT1-AF7p-conjugated nanoparticles (NPs) by employing MT1-MMP modifying paclitaxel-loaded PEG-PLA nanoparticles (MT1-NP-PTX). iRGD coadministration with these nanoparticles significantly enhanced its penetration across the blood-brain tumor barrier (BTB) and increased its accumulation in glioma parenchyma. It also significantly improved the antiglioma effect in mice bearing C6 glioma tumors. This enhanced effect was deemed to benefit from the transcytosis mediated by MT1-AF7p and iRGD-facilitated NP extravasation and tumor penetration [95]. More importantly, the MT1-AF7p peptide may contribute to increasing NP penetration into the glioma itself [87]. Wang et al. [96] produced an iRGD-PPCD conjugate to investigate its effect on glioma. The results indicated that the iRGD-mediated PPCD delivery system possessed a higher penetrating ability and superiority because the enhanced cellular internalization of the conjugate was activated by $\alpha_V\beta$ integrins on the C6 cell surface. After systemic administration in vivo, iRGD-mediated PPCD demonstrated potent penetration ability, higher accumulation in tumors leading to tumor vascular density, and a reduction in the average vascular diameter. The underlying mechanisms for the enhancement of tumor accumulation and penetration are summarized as follows: (1) the conjugate is long-circulating and has an applicable size; (2) iRGD peptides coupled to PPCD activate tumor-targeted properties to further improve the accumulation; and (3) the penetration of cells and tissues for iRGD-mediated PPCD is activated by proteolytic cleavage to expose the cryptic CendR, which binds to NRP-1 on the cell surface [87]. In a recent study, chitosan surface-modified poly(lactide-coglycolide) nanoparticles (PLGA/CS NPs) loaded with carmustine (BCNU) and its sensitizer (O^6-benzylguanine, BG) were prepared [97]. iRGD-modified NPs or iRGD coadministration with NPs showed significant enhancement of tumor penetration, accumulation, and antitumor activity. In addition, the median survival time of iRGD NPs or iRGD+NPs was prolonged in mice bearing F98 gliomas. The potential mechanisms of the iRGD-mediated PLGA/CS NP system with enhanced efficacy are similar to those identified in the study by Wang et al. [96]. Another explanation is also significant: the BG was released from the CS shell of NPs and then depleted O^6-methylguanine-DNA-methyltransferase, so the tumor cell sensitivity to BCNU increased, which was released later from the PLGA core [97].

5.9. Cervical Cancer. The applications of iRGD in cervical cancer therapy have also been investigated in recent years. A-PTX-SF-NPs were synthesized using PTX-SF-NPs joined to anti-EGFR-iRGD because it was a simple method and showed better anticancer activity. Furthermore, there was a high number of carboxyl groups on the PTX-SF-NP surface, which could combine with the recombinant protein through carbodiimide [98]. A-PTX-SF-NPs had a small size, penetrated the tumor tissues easily, and showed increased cytotoxicity towards the tumor cells. In HeLa tumor-bearing nude mice, A-PTX-SF-NPs exhibited better tumor-targeting and anticancer efficacy in vivo, and an EPR effect was obtained [99].

Mesoporous silica nanoparticles (MSNs) conjugated with iRGD, a novel tumor-targeting delivery system loaded with combretastatin A4 (CA4) and doxorubicin (DOX), were used to improve antiangiogenesis activity and chemotherapy efficacy [100]. MSNs-iRGD target $\alpha_2\beta_3$ integrin receptors expressed in cervical cancer cells and vasculature cells. MSNs-iRGD loaded with CA4 and DOX could accumulate at the targeted tumor site due to the prolonged blood circulation, which resulted in better targeting to the vessel wall. CA4 is first released to disrupt the tumor vasculature and reduce the tumor blood supply; then the impaired tumor vasculatures would promote the penetration of the drug delivery system. Finally, the chemotherapy drug DOX was released into the circulation to promote apoptosis of cancer cells. Thus, the anticancer efficacy was enhanced significantly in vivo.

5.10. Colorectal Cancer. The effect of polymersomes, polysaccharide nanoparticles, and anticancer drugs with iRGD was also observed in colorectal cancer therapy through a CendR motif binding to NRP-1 [69, 101–103]. Due to the internalization of iRGD and NPR-1, tumor cell penetration and tissue accumulation were enhanced. Intraperitoneally administered iRGD-polymersomes showed higher tumor-specific accumulation and penetration in mice bearing colon cancer tumors comprising CT26 cells. iRGD-polymersomes loaded with PTX potentiated the tumor growth and metastasis inhibition effects in vivo, and the results indicated that the combination of direct penetration and circulation-mediated homing with iRGD was involved, which facilitated payload delivery to the targeted tumor sites [69]. Sugahara et al. [102] investigated the function of iRGD in improving tumor-targeting penetration of intraperitoneal compounds and enhancing intraperitoneal chemotherapy (IPC) in mice bearing human colon cancer tumors. The data showed that intratumoral entry of dextran and DOX was enhanced by approximately 300% and 250%, respectively, after intraperitoneal coinjection with iRGD. Meanwhile, bulky peritoneal tumor growth was suppressed, and systemic drug toxicity decreased when using intraperitoneal iRGD/doxorubicin combination therapy depending on the CendR-mediated transtumoral bulk transport system, which implied that intraperitoneal iRGD combined with IPC could be a simple yet effective approach to treating colorectal cancer and peritoneal carcinomatosis due to higher intratumoral drug accumulation even in the presence of ascites.

Doxorubicin-loaded polysaccharide nanoparticles (Dex-SA-DOX-CDDP NPs) coadministered with iRGD can efficiently inhibit tumor growth in both subcutaneous transplantation colorectal carcinoma and primary colorectal carcinoma with CT26 murine colon carcinoma cell lines due to the prolonged circulation, enhanced tumor localization, and accumulation in the tumor via the EPR effect [86, 101].

Ma et al. [103] devised a new strategy (PEGylated camptothecin-loaded poly(lactic acid/glycolic acid) nanoparticles, iRGD-PEG-NPs) to enhance drug tumor accumulation and targeted delivery for colon cancer therapy with iRGD modification and a camptothecin (CPT) payload. They found that this new nanoparticle loaded with CPT had enhanced tumor accumulation, induced apoptosis, and efficiently downregulated *Bcl-2* mRNA expression, which was deemed to promote apoptosis and inhibit tumor growth in orthotopic colon tumors in mice in vivo. The possible reasons for the improved anticancer efficacy may be the following: (1) NPs have an appropriate size with an average diameter less than 280 nm, which results in the optimally enhanced permeability and retention effect and the avoidance of uptake by the reticuloendothelial system or rapid renal clearance [104]. (2) iRGD-PEG-NPs enter cells via receptor-mediated endocytosis to enhance the cellular uptake efficiency of NPs and enhance the cytotoxicity of CPT-loaded NPs. (3) iRGD-PEG-NPs have excellent hemocompatibility, which facilitates chemotherapeutic efficacy.

5.11. Ovarian Cancer. The synergistic effect of ovarian cancer therapy with iRGD was less studied. The expression of αv integrins and NRP-1 on the surface of ovarian cancer cell facilitates the function of iRGD. Fluorescein-iRGD (FAM-iRGD) efficiently penetrated IGROV-1 xenograft tumors with 30 mm thickness, which indicated promising prospects for iRGD in delivering drugs into human ovarian tumors [102]. An urgent challenge for ovarian cancer therapy is to overcome multidrug resistance (MDR). Zhang et al. [105] developed a new codelivery system (PTX+TET/iRGD LPNs) with iRGD-modified lipid-polymer hybrid nanosystems (LPNs) coupled to paclitaxel (PTX) and tetrandrine (TET) at a precise ratio (1/1 molar ratio) to overcome MDR. They found that the delivery system conferred higher anticancer drug load capacity, stable properties, and redox-sensitive drug release profiles. In their study, they designed a coloaded LPN profile to release drugs in sequential order. TET was released first in cells, and then PTX was released in the cytoplasm. This ingenious design improves the anticancer efficacy. Owing to these superior properties, when treated with PTX+TET/iRGD LPNs, A2780 ovarian cancer cells showed much more PTX accumulation. In addition, PTX+TET/iRGD LPNs exerted significant cytotoxicity to A2780/PTX cells, enhanced reactive oxygen species (ROS) production, and induced apoptosis. These findings demonstrate the important role of iRGD in ovarian cancer therapy.

6. iRGD in Inhibiting Tumor Metastasis

Tumor metastasis is another leading cause of death in cancer patients [1]. Therefore, many studies also focus on improving drug resistance and enhancing anticancer efficacy. The iRGD peptide itself had no effect on tumors or metastatic lesions; however, iRGD exerted its inhibitory function on tumor metastasis by delivering drugs to the tumor and by targeting integrins expressed on the cancer cell surface.

In 2015, Sugahara et al. [102] revealed that iRGD peptide coadministered with anticancer drugs via intraperitoneal injection could improve the therapeutic index and inhibit human peritoneal metastasis explants. In another study, Sugahara et al. [18] showed that the iRGD peptide inhibited cancer cell attachment to fibronectin and inhibited cancer cell migration in vitro through interactions with NRP-1. iRGD possessed chemorepulsive properties and inhibited prostate and pancreatic cancer metastasis in nude mouse models bearing GFP-PC-3 and LM-PmC tumors. Hamilton et al. [106] reported that iRGD-iron oxide nanoworms significantly inhibited breast cancer brain metastasis and significantly affected tumor progression in the early stages of metastasis. These findings were verified in two different models using MDA-MB-231 and 4T1 cell lines in vivo. The antimetastatic activity of iRGD may be regulated by NRP binding, which has been shown to inhibit tumor growth and metastasis [107]. In addition, iRGD peptide coated onto NPs extended the half-life of the peptide in the circulation, resulting in a prolonged time of activity at the target site [108]. Ni et al. [109] found that iRGD conjugated to PTX nanocrystallites (in the form of nanodots and nanoparticles) can endow nanocrystallites with a much higher drug-loading capacity, superior monodispersibility, and specific tumor-targeting ability, subsequently leading to cancer stem cell elimination and restricting breast cancer growth and metastasis in murine models. Li et al. reported that doxorubicin-loaded cisplatin crosslinked polysaccharide-based nanoparticles (Dex-SA-DOX-CDDP NPs) combined with iRGD can synergistically and efficiently suppress primary breast tumor growth and inhibit the metastasis of 4T1 murine orthotopic mammary carcinoma because of the prolonged circulation and enhanced tumor localization and accumulation of the anticancer drug in tumors via the EPR effect [101]. In 2016, Qifan et al. [110] showed that iRGD administration activated neuropilin-1 on the tumor cell surface and facilitated the internalization of the procytotoxic peptide (m(KLA)-iRGD) into 4T1 tumor cells. Then, apoptosis was rapidly triggered by m(KLA)-iRGD through the mitochondrial-induced apoptotic pathway and the death receptor pathway in NRP1+/$\alpha v\beta 3$/Cathepsin B+ tumor cells. Finally, after the m(KLA)-iRGD peptide was intravenously administered at an appropriate dose, lung metastasis was completely blocked. All these findings indicate the important functions of iRGD in inhibiting tumor metastasis.

7. Conclusion

In summary, the biofunctional iRGD peptide can facilitate tumor imaging as well as cancer and metastasis therapy through interactions with integrins expressed on the tumor cell surface; these intrinsic characteristics render it a promising prospect in tumor imaging and therapy.

Because of the targeting features of iRGD, some imaging agents, polysomes, anticancer drugs, immune modulators, and cytokines can be modified with or conjugated to iRGD to penetrate tumors more deeply and effectively, leading to much more satisfactory imaging and enhanced antitumor efficacy. The function and effect of the iRGD peptide have been tested and confirmed in vitro and in vivo by an immense number of concrete studies. Therefore, the iRGD peptide serves as a potential and promising target for improving imaging and therapeutic efficacy in humans.

Abbreviations

iRGD: Internalizing Arg-Gly-Asp peptide
NRP-1: Neuropilin-1
MRI: Magnetic resonance imaging
EGFR: Epidermal growth factor receptor
NP: Nanoparticle
QD: Quantum dot
MB: Microbubble
CCR2: C-C chemokine receptor type 2
DOX: Doxorubicin
HIFU: High-intensity focused ultrasound
CDD: Cell death domain
BCL-2: B-cell lymphoma 2
PTX: Paclitaxel
sTRAIL: Soluble tumor necrosis factor (TNF)-related apoptosis-inducing ligand (TRAIL)
iPTPNs: iRGD-conjugated D-α-tocopheryl polyethylene glycol 1000 succinate mediated codelivery of paclitaxel and survivin shRNA
M-SAL: Salinomycin-loaded DSPE-PEG2000 nanomicelles
DSPE-PEG2000: 1,2-Distearoyl-*sn*-glycero-3-phosphoethanolamine-*N*-[methoxypolyethylene glycol)-2000] (ammonium salt)
SOR: Sorafenib
PEG-PLA: Poly(ethylene glycol)-poly(lactic acid)
PPCD: PEGylated polyamidoamine (PAMAM) dendrimer-cis-aconityl-doxorubicin
PLGA/CS NPs: Chitosan surface-modified poly(lactide-co-glycolide) nanoparticles
PTX-SF-NPs: PTX-loaded silk fibroin nanoparticles
EPR: Enhanced permeability and retention
MDR: Multidrug resistance
Dex-SA-DOX-CDDP NPs: Succinic acid decorated dextran doxorubicin-loaded cisplatin (CDDP) crosslinked polysaccharide-based nanoparticles.

Conflicts of Interest

There are no conflicts of interest in this work.

Acknowledgments

This review was supported by grants from the Nature Science Foundation of China (Grant no. 81701756) and from Sichuan Provincial Department of Education (no. 18ZB0215). The manuscript was edited by American Journal Experts.

References

[1] R. L. Siegel, K. D. Miller, and A. Jemal, "Cancer statistics, 2018," *CA: A Cancer Journal for Clinicians*, vol. 68, no. 1, pp. 7–30, 2018.

[2] M. Iwase, M. Sawaki, M. Hattori et al., "Assessing residual cancer cells using MRI and US after preoperative chemotherapy in primary breast cancer to omit surgery," *Breast Cancer*, vol. 25, no. 5, pp. 583–589, 2018.

[3] H. Kaise, F. Shimizu, K. Akazawa et al., "Prediction of pathological response to neoadjuvant chemotherapy in breast cancer patients by imaging," *Journal of Surgical Research*, vol. 225, pp. 175–180, 2018.

[4] S. H. Jang, Y. J. Jung, M. G. Kim, and S. J. Kwon, "The prognostic significance of compliance with postoperative adjuvant chemotherapy in patients with stage III gastric cancer: An observational study," *Gastric Cancer*, vol. 18, no. 1, pp. 48–57, 2018.

[5] T. W. Hambley and W. N. Hait, "Is anticancer drug development heading in the right direction?" *Cancer Research*, vol. 69, no. 4, pp. 1259–1262, 2009.

[6] E. Ruoslahti, "Specialization of tumour vasculature," *Nature Reviews Cancer*, vol. 2, no. 2, pp. 83–90, 2002.

[7] E. Ruoslahti and D. Rajotte, "An address system in the vasculature of normal tissues and tumors," *Annual Review of Immunology*, vol. 18, pp. 813–827, 2000.

[8] G. J. Prud'homme and Y. Glinka, "Neuropilins are multifunctional coreceptors involved in tumor initiation, growth, metastasis and immunity," *Oncotarget* , vol. 3, no. 9, pp. 921–939, 2012.

[9] S. Niland and J. A. Eble, "Neuropilins in the context of tumor vasculature," *International Journal of Molecular Sciences*, vol. 20, no. 3, p. 639, 2019.

[10] Y. Herzog, C. Kalcheim, N. Kahane, R. Reshef, and G. Neufeld, "Differential expression of neuropilin-1 and neuropilin-2 in arteries and veins," *Mechanisms of Development*, vol. 109, no. 1, pp. 115–119, 2001.

[11] U. Yaqoob, S. Cao, U. Shergill et al., "Neuropilin-1 stimulates tumor growth by increasing fibronectin fibril assembly in the tumor microenvironment," *Cancer Research*, vol. 72, no. 16, pp. 4047–4059, 2012.

[12] T. Teesalu, K. N. Sugahara, V. R. Kotamraju, and E. Ruoslahti, "C-end rule peptides mediate neuropilin-1-dependent cell, vascular, and tissue penetration," *Proceedings of the National Acadamy of Sciences of the United States of America*, vol. 106, no. 38, pp. 16157–16162, 2009.

[13] K. N. Sugahara, T. Teesalu, P. P. Karmali et al., "Tissue-penetrating delivery of compounds and nanoparticles into tumors," *Cancer Cell*, vol. 16, no. 6, pp. 510–520, 2009.

[14] K. N. Sugahara, T. Teesalu, P. Prakash Karmali et al., "Coadministration of a tumor-penetrating peptide enhances the efficacy of cancer drugs," *Science*, vol. 328, no. 5981, pp. 1031–1035, 2010.

[15] T. Teesalu, K. N. Sugahara, and E. Ruoslahti, "Tumor-penetrating peptides," *Frontiers in Oncology*, vol. 3, Article ID 00216, 2013.

[16] P.-H. Wu, Y. Onodera, Y. Ichikawa et al., "Targeting integrins with RGD-conjugated gold nanoparticles in radiotherapy decreases the invasive activity of breast cancer cells," *International Journal of Nanomedicine*, vol. 12, pp. 5069–5085, 2017.

[17] E. A. Murphy, B. K. Majeti, L. A. Barnes et al., "Nanoparticle-mediated drug delivery to tumor vasculature suppresses metastasis," *Proceedings of the National Acadamy of Sciences of the United States of America*, vol. 105, no. 27, pp. 9343–9348, 2008.

[18] K. N. Sugahara, G. B. Braun, T. H. De Mendoza et al., "Tumor-penetrating iRGD peptide inhibits metastasis," *Molecular Cancer Therapeutics*, vol. 14, no. 1, pp. 120–128, 2015.

[19] Y. Wang, Y. Xie, J. Li et al., "Tumor-penetrating nanoparticles for enhanced anticancer activity of combined photodynamic and hypoxia-activated therapy," *ACS Nano*, vol. 11, no. 2, pp. 2227–2238, 2017.

[20] S. W. Hall, J. E. Humphries, and S. L. Gonias, "Inhibition of cell surface receptor-bound plasmin by alpha 2-antiplasmin and alpha 2-macroglobulin," *Journal of Biological Chemistry*, vol. 266, no. 19, pp. 12329–12336, 1991.

[21] T. Pellinen and J. Ivaska, "Integrin traffic," *Journal of Cell Science*, vol. 119, no. 18, pp. 3723–3731, 2006.

[22] H. D. Zuo, W. W. Yao, T. W. Chen et al., "The effect of superparamagnetic iron oxide with iRGD peptide on the labeling of pancreatic cancer cells *in vitro*: a preliminary study," *BioMed Research International*, vol. 2014, Article ID 852352, 8 pages, 2014.

[23] R. Pasqualini and E. Ruoslahti, "Organ targeting in vivo using phage display peptide libraries," *Nature*, vol. 380, no. 6572, pp. 364–366, 1996.

[24] D. A. Sipkins, D. A. Cheresh, M. R. Kazemi, L. M. Nevin, M. D. Bednarski, and K. C. P. Li, "Detection of tumor angiogenesis *in vivo* by $\alpha_v\beta_3$-targeted magnetic resonance imaging," *Nature Medicine*, vol. 4, no. 5, pp. 623–626, 1998.

[25] R. Pasqualini, E. Koivunen, and E. Ruoslahti, "αv integrins as receptors for tumor targeting by circulating ligands," *Nature Biotechnology*, vol. 15, no. 6, pp. 542–546, 1997.

[26] D. Moncelet, V. Bouchaud, P. Mellet et al., "Cellular density effect on RGD ligand internalization in glioblastoma for MRI application," *PLoS ONE*, vol. 8, no. 12, Article ID e82777, 2013.

[27] X. Xin, H. Sha, J. Shen, B. Zhang, B. Zhu, and B. Liu, "Coupling Gd-DTPA with a bispecific,recombinant protein anti-EGFR-iRGD complex improves tumor targeting in MRI," *Oncology Reports*, vol. 35, no. 6, pp. 3227–3235, 2016.

[28] Y. Ye, L. Zhu, Y. Ma, G. Niu, and X. Chen, "Synthesis and evaluation of new iRGD peptide analogs for tumor optical imaging," *Bioorganic & Medicinal Chemistry Letters*, vol. 21, no. 4, pp. 1146–1150, 2011.

[29] H.-J. Cho, S.-J. Lee, S.-J. Park et al., "Activatable iRGD-based peptide monolith: Targeting, internalization, and fluorescence activation for precise tumor imaging," *Journal of Controlled Release*, vol. 237, pp. 177–184, 2016.

[30] Y. Yang, X. Wang, G. Liao et al., "iRGD-decorated red shift emissive carbon nanodots for tumor targeting fluorescence imaging," *Journal of Colloid and Interface Science*, vol. 509, pp. 515–521, 2018.

[31] Ł. Przysiecka, M. Michalska, G. Nowaczyk et al., "iRGD peptide as effective transporter of CuInZnxS2 + x quantum dots into human cancer cells," *Colloids and Surfaces B: Biointerfaces*, vol. 146, pp. 9–18, 2016.

[32] F. Yan, X. Xu, Y. Chen et al., "A Lipopeptide-Based αvβ3 Integrin-Targeted Ultrasound Contrast Agent for Molecular Imaging of Tumor Angiogenesis," *Ultrasound in Medicine & Biology*, vol. 41, no. 10, pp. 2765–2773, 2015.

[33] J. Xu, X. Zeng, Y. Liu et al., "A novel dual-targeted ultrasound contrast agent provides improvement of gene delivery efficiency in vitro," *Tumor Biology*, vol. 37, no. 7, pp. 8609–8619, 2016.

[34] H. Cho, S. Park, Y. Lee, and S. Kim, "Theranostic iRGD peptide containing cisplatin prodrug: Dual-cargo tumor penetration for improved imaging and therapy," *Journal of Controlled Release*, vol. 300, pp. 73–80, 2019.

[35] Y. Liu, M. Ji, M. K. Wong et al., "Enhanced therapeutic efficacy of iRGD-conjugated crosslinked multilayer liposomes for drug delivery," *BioMed Research International*, vol. 2013, Article ID 378380, 11 pages, 2013.

[36] X. Cun, J. Chen, S. Ruan et al., "A novel strategy through combining iRGD peptide with tumor-microenvironment-responsive and multistage nanoparticles for deep tumor penetration," *ACS Applied Materials & Interfaces*, vol. 7, no. 49, pp. 27458–27466, 2015.

[37] X. Song, Z. Wan, T. Chen et al., "Development of a multi-target peptide for potentiating chemotherapy by modulating tumor microenvironment," *Biomaterials*, vol. 108, pp. 44–56, 2016.

[38] Z. Deng, Y. Xiao, M. Pan et al., "Hyperthermia-triggered drug delivery from iRGD-modified temperature-sensitive liposomes enhances the anti-tumor efficacy using high intensity focused ultrasound," *Journal of Controlled Release*, vol. 243, pp. 333–341, 2016.

[39] Z. Jin, Y. Lv, H. Cao et al., "Core-shell nanocarriers with high paclitaxel loading for passive and active targeting," *Scientific Reports*, vol. 6, Article ID 27559, 2016.

[40] R. Chen, G. B. Braun, X. Luo, K. N. Sugahara, T. Teesalu, and E. Ruoslahti, "Application of a proapoptotic peptide to intratumorally spreading cancer therapy," *Cancer Research*, vol. 73, no. 4, pp. 1352–1361, 2013.

[41] H.-B. Pang, G. B. Braun, Z.-G. She et al., "A free cysteine prolongs the half-life of a homing peptide and improves its tumor-penetrating activity," *Journal of Controlled Release*, vol. 175, no. 1, pp. 48–53, 2014.

[42] X. Lao, B. Li, M. Liu et al., "A modified thymosin alpha 1 inhibits the growth of breast cancer both in vitro and in vivo: suppressment of cell proliferation, inducible cell apoptosis and enhancement of targeted anticancer effects," *Apoptosis*, vol. 20, no. 10, article no. 1151, pp. 1307–1320, 2015.

[43] X. Lao, B. Li, M. Liu, J. Chen, X. Gao, and H. Zheng, "Increased antitumor activity of tumor-specific peptide modified thymopentin," *Biochimie*, vol. 107, pp. 277–285, 2014.

[44] V. R. Kotamraju, S. Sharma, P. Kolhar, L. Agemy, J. Pavlovich, and E. Ruoslahti, "Increasing tumor accessibility with conjugatable disulfide-bridged tumor-penetrating peptides for cancer diagnosis and treatment," *Breast Cancer: Basic and Clinical Research*, vol. 9, pp. 79–87, 2015.

[45] S. Ma, J. Zhou, Y. Zhang et al., "Highly stable fluorinated nanocarriers with iRGD for overcoming the stability dilemma and enhancing tumor penetration in an orthotopic breast cancer," *ACS Applied Materials & Interfaces*, vol. 8, no. 42, pp. 28468–28479, 2016.

[46] C. Deng, M. Jia, G. Wei et al., "Inducing optimal antitumor immune response through coadministering iRGD with pirarubicin loaded nanostructured lipid carriers for breast cancer therapy," *Molecular Pharmaceutics*, vol. 14, no. 1, pp. 296–309, 2017.

[47] W. Song, M. Li, Z. Tang et al., "Methoxypoly(ethylene glycol)-block-Poly(L-glutamic acid)-loaded cisplatin and a combination with irgd for the treatment of non-small-cell lung cancers," *Macromolecular Bioscience*, vol. 12, no. 11, pp. 1514–1523, 2012.

[48] Q. Zhang, Y. Zhang, K. Li, H. Wang, H. Li, and J. Zheng, "A novel strategy to improve the therapeutic efficacy of gemcitabine for non-small cell lung cancer by the tumor-penetrating peptide iRGD," *PLoS ONE*, vol. 10, no. 6, Article ID e0129865, 2015.

[49] Y. Zhang, J. Yang, M. Ding et al., "Tumor-penetration and antitumor efficacy of cetuximab are enhanced by co-administered irgd in a murine model of human NSCLC," *Oncology Letters*, vol. 12, no. 5, pp. 3241–3249, 2016.

[50] C. Puig-Saus, L. A. Rojas, E. Laborda et al., "IRGD tumor-penetrating peptide-modified oncolytic adenovirus shows enhanced tumor transduction, intratumoral dissemination and antitumor efficacy," *Gene Therapy*, vol. 21, no. 8, pp. 767–774, 2014.

[51] X. Lao, M. Liu, J. Chen, and H. Zheng, "A tumor-penetrating peptide modification enhances the antitumor activity of thymosin alpha 1," *PLoS ONE*, vol. 8, no. 8, Article ID e72242, 2013.

[52] E. Garaci, F. Pica, A. Serafino et al., "Thymosin α1 and cancer: action on immune effector and tumor target cells," *Annals of the New York Academy of Sciences*, vol. 1269, no. 1, pp. 26–33, 2012.

[53] M. A. Solomon, J. Lemera, and G. G. M. D'Souza, "Development of an in vitro tumor spheroid culture model amenable to high-throughput testing of potential anticancer nanotherapeutics," *Journal of Liposome Research*, vol. 26, no. 3, pp. 246–260, 2016.

[54] J. Shen, Q. Meng, H. Sui et al., "IRGD conjugated TPGS mediates codelivery of paclitaxel and survivin shRNA for the reversal of lung cancer resistance," *Molecular Pharmaceutics*, vol. 11, no. 8, pp. 2579–2591, 2014.

[55] J. Yang, J. Yang, Y. Wei et al., "Modification of IL-24 by tumor penetrating peptide iRGD enhanced its antitumor efficacy against non-small cell lung cancer," *International Immunopharmacology*, vol. 70, pp. 125–134, 2019.

[56] G. De, J.-K. Ko, T. Tan, H. Zhu, H. Li, and J. Ma, "Amphipathic tail-anchoring peptide is a promising therapeutic agent for prostate cancer treatment," *Oncotarget* , vol. 5, no. 17, pp. 7734–7747, 2014.

[57] Z.-H. Peng and J. Kopeček, "Enhancing accumulation and penetration of HPMA copolymer-doxorubicin conjugates in 2d and 3d prostate cancer cells via irgd conjugation with an MMP-2 Cleavable Spacer," *Journal of the American Chemical Society*, vol. 137, no. 21, pp. 6726–6729, 2015.

[58] C.-F. Wang, M. P. Sarparanta, E. M. Mäkilä et al., "Multifunctional porous silicon nanoparticles for cancer theranostics," *Biomaterials*, vol. 48, pp. 108–118, 2015.

[59] B. Herranz-Blanco, M. Shahbazi, A. R. Correia et al., "pH-Switch nanoprecipitation of polymeric nanoparticles for multimodal cancer targeting and intracellular triggered delivery of doxorubicin," *Advanced Healthcare Materials*, vol. 5, no. 15, pp. 1904–1916, 2016.

[60] S. Su, H. Wang, X. Liu, Y. Wu, and G. Nie, "IRGD-coupled responsive fluorescent nanogel for targeted drug delivery," *Biomaterials*, vol. 34, no. 13, pp. 3523–3533, 2013.

[61] K.-F. Yu, W.-Q. Zhang, L.-M. Luo et al., "The antitumor activity of a doxorubicin loaded, iRGD-modified sterically-stabilized liposome on B16-F10 melanoma cells: in vitro and in vivo evaluation," *International Journal of Nanomedicine*, vol. 8, pp. 2473–2485, 2013.

[62] W. Dai, Y. Fan, H. Zhang, X. Wang, Q. Zhang, and X. Wang, "A comprehensive study of iRGD-modified liposomes with improved chemotherapeutic efficacy on B16 melanoma," *Drug Delivery*, vol. 22, no. 1, pp. 10–20, 2015.

[63] R. Du, T. Zhong, W.-Q. Zhang et al., "Antitumor effect of iRGD-modified liposomes containing conjugated linoleic acid-paclitaxel (CLA-PTX) on B16-F10 melanoma," *International Journal of Nanomedicine*, vol. 9, no. 1, pp. 3091–3105, 2014.

[64] R. van der Meel, L. J. C. Vehmeijer, R. J. Kok, G. Storm, and E. V. B. van Gaal, "Ligand-targeted particulate nanomedicines undergoing clinical evaluation: current status," *Advanced Drug Delivery Reviews*, vol. 65, no. 10, pp. 1284–1298, 2013.

[65] C. Deng, Q. Zhang, Y. Fu, X. Sun, T. Gong, and Z. Zhang, "Coadministration of oligomeric hyaluronic acid-modified liposomes with tumor-penetrating peptide-iRGD enhances the antitumor efficacy of doxorubicin against melanoma," *ACS Applied Materials & Interfaces*, vol. 9, no. 2, pp. 1280–1292, 2017.

[66] H. Sha, R. Li, X. Bian et al., "A tumor-penetrating recombinant protein anti-EGFR-iRGD enhance efficacy of paclitaxel in 3D multicellular spheroids and gastric cancer in vivo," *European Journal of Pharmaceutical Sciences*, vol. 77, pp. 60–72, 2015.

[67] H. Sha, Z. Zou, K. Xin et al., "Tumor-penetrating peptide fused EGFR single-domain antibody enhances cancer drug penetration into 3D multicellular spheroids and facilitates effective gastric cancer therapy," *Journal of Controlled Release*, vol. 200, pp. 188–200, 2015.

[68] Y. Huang, X. Li, H. Sha et al., "Tumor-penetrating peptide fused to a pro-Apoptotic peptide facilitates effective gastric cancer therapy," *Oncology Reports*, vol. 37, no. 4, pp. 2063–2070, 2017.

[69] L. Simón-Gracia, H. Hunt, P. Scodeller et al., "iRGD peptide conjugation potentiates intraperitoneal tumor delivery of paclitaxel with polymersomes," *Biomaterials*, vol. 104, pp. 247–257, 2016.

[70] L. Simón-Gracia, H. Hunt, P. D. Scodeller et al., "Paclitaxel-loaded polymersomes for enhanced intraperitoneal chemotherapy," *Molecular Cancer Therapeutics*, vol. 15, no. 4, pp. 670–679, 2016.

[71] Y. Huang, X. Li, H. Sha et al., "sTRAIL-iRGD is a promising therapeutic agent for gastric cancer treatment," *Scientific Reports*, vol. 7, no. 1, article 579, 2017.

[72] L. Zhang, Y. Xing, Q. Gao, X. Sun, D. Zhang, and G. Cao, "Combination of NRP1-mediated iRGD with 5-fluorouracil suppresses proliferation, migration and invasion of gastric cancer cells," *Biomedicine & Pharmacotherapy*, vol. 93, pp. 1136–1143, 2017.

[73] N. Ding, Z. Zou, H. Sha et al., "iRGD synergizes with PD-1 knockout immunotherapy by enhancing lymphocyte infiltration in gastric cancer," *Nature Communications*, vol. 10, no. 1, article 1336, 2019.

[74] C. Wu, S. J. Hansen, Q. Hou et al., "Design of highly emissive polymer dot bioconjugates for in vivo tumor targeting," *Angewandte Chemie International Edition*, vol. 50, no. 15, pp. 3430–3434, 2011.

[75] Z. Zhu, C. Xie, Q. Liu et al., "The effect of hydrophilic chain length and iRGD on drug delivery from poly(ε-caprolactone)-poly(N-vinylpyrrolidone) nanoparticles," *Biomaterials*, vol. 32, no. 35, pp. 9525–9535, 2011.

[76] J. Folkman, "Antiangiogenesis in cancer therapy—endostatin and its mechanisms of action," *Experimental Cell Research*, vol. 312, no. 5, pp. 594–607, 2006.

[77] H.-T. Zhang, H.-C. Li, Z.-W. Li, and C.-H. Guo, "A tumor-penetrating peptide modification enhances the antitumor activity of endostatin in vivo," *Anti-Cancer Drugs*, vol. 22, no. 5, pp. 409–415, 2011.

[78] X. Mao, J. Liu, Z. Gong et al., "IRGD-conjugated DSPE-PEG2000 nanomicelles for targeted delivery of salinomycin for treatment of both liver cancer cells and cancer stem cells," *Nanomedicine*, vol. 10, no. 17, pp. 2677–2695, 2015.

[79] J. Zhang, J. Hu, H. F. Chan, M. Skibba, G. Liang, and M. Chen, "iRGD decorated lipid-polymer hybrid nanoparticles for targeted co-delivery of doxorubicin and sorafenib to enhance anti-hepatocellular carcinoma efficacy," *Nanomedicine: Nanotechnology, Biology and Medicine*, vol. 12, no. 5, pp. 1303–1311, 2016.

[80] C. Schmithals, V. Köberle, H. Korkusuz et al., "Improving drug penetrability with iRGD leverages the therapeutic response to sorafenib and doxorubicin in hepatocellular carcinoma," *Cancer Research*, vol. 75, no. 15, pp. 3147–3154, 2015.

[81] J. Wang, H. Wang, J. Li et al., "IRGD-decorated polymeric nanoparticles for the efficient delivery of vandetanib to hepatocellular carcinoma: preparation and in vitro and in vivo evaluation," *ACS Applied Materials & Interfaces*, vol. 8, no. 30, pp. 19228–19237, 2016.

[82] H. D. Zuo, X. M. Zhang, C. J. Li et al., "CT and MR imaging patterns for pancreatic carcinoma invading the extrapancreatic neural plexus (Part I): anatomy, imaging of the extrapancreatic nerve," *World Journal of Radiology*, vol. 4, no. 2, pp. 36–43, 2012.

[83] H. D. Zuo, W. Tang, X. M. Zhang et al., "CT and MR imaging patterns for pancreatic carcinoma invading the extrapancreatic neural plexus (Part II): Imaging of pancreatic carcinoma nerve invasion," *World Journal of Radiology*, vol. 4, no. 1, pp. 13–20, 2012.

[84] Y. Akashi, T. Oda, Y. Ohara et al., "Anticancer effects of gemcitabine are enhanced by co-administered iRGD peptide in murine pancreatic cancer models that overexpressed neuropilin-1," *British Journal of Cancer*, vol. 110, no. 6, pp. 1481–1487, 2014.

[85] X. Liu, P. Lin, I. Perrett et al., "Tumor-penetrating peptide enhances transcytosis of silicasome-based chemotherapy for pancreatic cancer," *The Journal of Clinical Investigation*, vol. 127, no. 5, pp. 2007–2018, 2017.

[86] L. M. Ellis, "The role of neuropilins in cancer," *Molecular Cancer Therapeutics*, vol. 5, no. 5, pp. 1099–1107, 2006.

[87] Y. Glinka and G. J. Prud'homme, "Neuropilin-1 is a receptor for transforming growth factor beta-1, activates its latent form, and promotes regulatory T cell activity," *Journal of Leukocyte Biology*, vol. 84, no. 1, pp. 302–310, 2008.

[88] M. Murata, S. Narahara, T. Kawano et al., "Design and function of engineered protein nanocages as a drug delivery system for targeting pancreatic cancer cells via neuropilin-1," *Molecular Pharmaceutics*, vol. 12, no. 5, pp. 1422–1430, 2015.

[89] E. Ruoslahti, S. N. Bhatia, and M. J. Sailor, "Targeting of drugs and nanoparticles to tumors," *The Journal of Cell Biology*, vol. 188, no. 6, pp. 759–768, 2010.

[90] A. T. Tsang, C. Dudgeon, L. Yi et al., "U1 adaptors suppress the KRAS-MYC oncogenic axis in human pancreatic cancer xenografts," *Molecular Cancer Therapeutics*, vol. 16, no. 8, pp. 1445–1455, 2017.

[91] R. Goraczniak, M. A. Behlke, and S. I. Gunderson, "Gene silencing by synthetic U1 Adaptors," *Nature Biotechnology*, vol. 27, no. 3, pp. 257–263, 2009.

[92] J. H. Lo, L. Hao, M. D. Muzumdar et al., "iRGD-guided tumor-penetrating nanocomplexes for therapeutic sirna delivery to pancreatic cancer," *Molecular Cancer Therapeutics*, vol. 17, no. 11, pp. 2377–2388, 2018.

[93] J. J. Rojas, M. Gimenez-Alejandre, R. Gil-Hoyos, M. Cascallo, and R. Alemany, "Improved systemic antitumor therapy with oncolytic adenoviruses by replacing the fiber shaft HSG-binding domain with RGD," *Gene Therapy*, vol. 19, no. 4, pp. 453–457, 2012.

[94] L. Zhu, H. Wang, L. Wang et al., "High-affinity peptide against MT1-MMP for in vivo tumor imaging," *Journal of Controlled Release*, vol. 150, no. 3, pp. 248–255, 2011.

[95] G. Gu, X. Gao, Q. Hu et al., "The influence of the penetrating peptide iRGD on the effect of paclitaxel-loaded MT1-AF7p-conjugated nanoparticles on glioma cells," *Biomaterials*, vol. 34, no. 21, pp. 5138–5148, 2013.

[96] K. Wang, X. Zhang, Y. Liu, C. Liu, B. Jiang, and Y. Jiang, "Tumor penetrability and anti-angiogenesis using iRGD-mediated delivery of doxorubicin-polymer conjugates," *Biomaterials*, vol. 35, no. 30, pp. 8735–8747, 2014.

[97] C. Liu, S. Yao, X. Li, F. Wang, and Y. Jiang, "iRGD-mediated core-shell nanoparticles loading carmustine and O6-benzylguanine for glioma therapy," *Journal of Drug Targeting*, vol. 25, no. 3, pp. 235–246, 2017.

[98] X. Wang and D. L. Kaplan, "Functionalization of silk fibroin with neutravidin and biotin," *Macromolecular Bioscience*, vol. 11, no. 1, pp. 100–110, 2011.

[99] X. Bian, P. Wu, H. Sha et al., "Anti-EGFR-iRGD recombinant protein conjugated silk fibroin nanoparticles for enhanced tumor targeting and antitumor efficiency," *Onco Targets and Therapy*, vol. 9, pp. 3153–3162, 2016.

[100] X. Li, M. Wu, L. Pan, and J. Shi, "Tumor vascular-targeted co-delivery of anti-angiogenesis and chemotherapeutic agents by mesoporous silica nanoparticle-based drug delivery system for synergetic therapy of tumor," *International Journal of Nanomedicine*, vol. 11, pp. 93–105, 2015.

[101] M. Li, Z. Tang, D. Zhang et al., "Doxorubicin-loaded polysaccharide nanoparticles suppress the growth of murine colorectal carcinoma and inhibit the metastasis of murine mammary carcinoma in rodent models," *Biomaterials*, vol. 51, pp. 161–172, 2015.

[102] K. N. Sugahara, P. Scodeller, G. B. Braun et al., "A tumor-penetrating peptide enhances circulation-independent targeting of peritoneal carcinomatosis," *Journal of Controlled Release*, vol. 212, pp. 59–69, 2015.

[103] L. Ma, Q. Chen, P. Ma et al., "IRGD-functionalized PEGylated nanoparticles for enhanced colon tumor accumulation and targeted drug delivery," *Nanomedicine*, vol. 12, no. 16, pp. 1991–2006, 2017.

[104] J. S. Suk, Q. Xu, N. Kim, J. Hanes, and L. M. Ensign, "PEGylation as a strategy for improving nanoparticle-based drug and gene delivery," *Advanced Drug Delivery Reviews*, vol. 99, pp. 28–51, 2016.

[105] J. Zhang, L. Wang, H. Fai Chan et al., "Co-delivery of paclitaxel and tetrandrine via iRGD peptide conjugated lipid-polymer hybrid nanoparticles overcome multidrug resistance in cancer cells," *Scientific Reports*, vol. 7, no. 1, article 46057, 2017.

[106] A. M. Hamilton, S. Aidoudi-Ahmed, S. Sharma et al., "Nanoparticles coated with the tumor-penetrating peptide iRGD reduce experimental breast cancer metastasis in the brain," *Journal of Molecular Medicine*, vol. 93, no. 9, pp. 991–1001, 2015.

[107] C. Grandclement and C. Borg, "Neuropilins: A new target for cancer therapy," *Cancers*, vol. 3, no. 2, pp. 1899–1928, 2011.

[108] E. Ruoslahti, "Peptides as targeting elements and tissue penetration devices for nanoparticles," *Advanced Materials*, vol. 24, no. 28, pp. 3747–3756, 2012.

[109] D. Ni, H. Ding, S. Liu et al., "Superior intratumoral penetration of paclitaxel nanodots strengthens tumor restriction and metastasis prevention," *Small*, vol. 11, no. 21, pp. 2518–2526, 2015.

[110] W. Qifan, N. Fen, X. Ying, F. Xinwei, D. Jun, and Z. Ge, "iRGD-targeted delivery of a pro-apoptotic peptide activated by cathepsin B inhibits tumor growth and metastasis in mice," *Tumor Biology*, vol. 37, no. 8, pp. 10643–10652, 2016.

Hindawi
Journal of Oncology
Volume 2019, Article ID 5247837, 6 pages
https://doi.org/10.1155/2019/5247837

Research Article

Sequential Interventional Management of Osseous Neoplasms via Embolization, Cryoablation, and Osteoplasty

Sri Hari Sundararajan,[1] **Steven Calamita**,[2] **Peter Girgis**,[3] **Gregory Ngo**,[3] **Srirajkumar Ranganathan**,[4,5] **Marisa Giglio**,[6] **Vyacheslav Gendel**,[7] **Sharad Goyal**,[8] **John Nosher**,[3] **and Sudipta Roychowdhury**[3]

[1]*Department of Radiology, Weill Cornell Medical College, 525 East 68th Street, New York, NY 10065, USA*
[2]*Department of Radiology, Dartmouth-Hitchcock Medical Center, One Medical Center Drive, Lebanon, NH 03756, USA*
[3]*Department of Radiology, Rutgers-Robert Wood Johnson Medical School, 1 Robert Wood Johnson Place, New Brunswick, NJ 08901, USA*
[4]*Northwestern University Feinberg School of Medicine, Chicago, IL, USA*
[5]*DePaul University - Lincoln Park Campus, 2400 N Sheffield Ave, Chicago, IL 60614, USA*
[6]*Penn State College of Medicine, 500 University Drive, Hershey, PA 17033, USA*
[7]*Department of Radiology, Northwell Lenox Hill Hospital, 100 E 77th St, New York, NY 10075, USA*
[8]*Rutgers-Cancer Institute of New Jersey, Department of Radiation Oncology, 195 Little Albany St, New Brunswick, NJ 08901, USA*

Correspondence should be addressed to Sri Hari Sundararajan; srihari.sundararajan@univrad.com

Received 2 August 2018; Accepted 26 March 2019; Published 14 April 2019

Guest Editor: Peramaiyan Rajendran

The purpose of this study is to determine if sequential interventional therapy can become a mainstay option in providing palliation from fastidious osseous neoplasms in patients with pain refractory to oral analgesia and radiotherapy. This retrospective monocentric study was approved by our institutional review board. Between July 2012 and August 2014, we reviewed 15 patients (6 women, 9 men; age range of 36-81 years) who underwent embolization followed by cryoablation, with or without osteoplasty. Patient demographics and tumor characteristics, including primary histology and the location of metastasis, were included in our review. Pain intensity at baseline, after radiotherapy, and after sequential interventional therapy was reviewed using the hospital electronic medical record. The use of oral analgesia and procedural complications was also noted. Data was then assessed for normality and a two-tailed Student's *t*-test was performed on mean pain scores for difference phases of treatment. While radiotherapy offers pain relief with a mean pain score of 7.25 ±1.5 ($p = <.0001$), sequential interventional therapy results in better comfort as demonstrated by a mean pain score of 3.9 ± 2.6 ($p = .0015$). Moreover, all patients who reported oral analgesic use at presentation reported a decrease in their requirement after sequential interventional therapy. Embolization and cryoablation were performed in all patients, while osteoplasty was indicated in 6 cases. There was no difference in postprocedural pain intensity between patients who required osteoplasty and patients who did not ($p = 0.7514$). There were no complications observed during treatment. This retrospective study shows that sequential intervention with transarterial embolization, cryoablation, and osteoplasty is both safe and efficacious for bone pain refractory to the current standard of care. We demonstrated that this combination therapy has the potential to become an effective mainstay treatment paradigm in the palliative care of osseous neoplasm to improve quality of life.

1. Introduction

Both primary malignant and metastatic osseous neoplasms are a significant cause of cancer morbidity and mortality [1]. Metastatic osseous neoplasms are more prevalent, with primary tumors most frequently originating from breast, prostate, and kidney cancer. Metastases are associated with fracture, spinal cord compression, and hypercalcemia, with pain as the cardinal symptom affecting up to 80% of patients [2]. Both primary and metastatic osseous neoplasms can

Table 1: Patient and tumor characteristics.

Characteristic	Datum
No. of patients (female/male) n=15	6/9
Mean age, y (+/- SD)	62 (13)
Range	36-81
Previous RT	14/15 (93%)
Oral analgesics at presentation	13/15 (87%)
Tumor type histology (n=15)	
Lung	4 (26%)
Urothelial	3 (20%)
Renal	2 (13%)
Pancreas	1 (7%)
Breast	1 (7%)
Osteosarcoma	1 (7%)
Endometrial	1 (7%)
Colorectal	1 (7%)
Other∗	1 (7%)
Tumor Location (n=16)	
Sacrum	8 (50%)
Scapula	3 (19%)
Ilium	3 (19%)
Ischium	3 (19%)
Embolization and cryoablation only	6/15 (40%)
Embolization, cryoablation, and osteoplasty	9/15 (60%)
Patients with one metastasis†	14/15 (93%)
Patients with two metastases†	1/15 (7%)

∗Primary adenocarcinoma of unknown origin.
† considers only metastases that were treated with ST, not total metastases.

be difficult to treat, given their ability to alter weight-bearing mechanics and their propensity to invade adjacent neurovascular bundles. Tumor burden and associated pain can prove difficult to manage despite comprehensive medical management due to radiotherapy (RT) resistance, maximization of analgesia, and noncandidacy for surgery. In fact, 20-30% of patients treated with external beam radiation therapy do not experience primary pain relief [3]. Minimally invasive treatment options have been well described and are preferred, particularly in patients with metastatic disease and low 5-year survival rates [4]. Multicenter studies have demonstrated that radiofrequency (RF) ablation is efficacious for pain relief in patients with osseous metastases [5]. However, a significant limitation of RF ablation is the inability of intraprocedural visualization of the ablation zone, thereby increasing the complication rate. Cryoablation allows for greater control of the ablation margin because a low-attenuation ice ball is identifiable on computed tomography (CT) monitoring. This allows cryoablation to be performed in close proximity to critical structures, as observed with spinal metastases. Thus, the efficacy and safety of image-guided percutaneous cryoablation for painful osseous neoplasms have been well established [6, 7]. However, recurrence of disease or incomplete alleviation of symptoms can occur despite the above treatment [4]. Transarterial embolization has been used to decrease hemorrhage associated with both surgical and minimally invasive interventions [8]. In addition, embolization has been used in cases in which ablation would compromise neurovascular structures [9]. We hypothesize that a treatment paradigm of sequential therapy (ST) with arterial embolization, cryoablation, and osteoplasty will demonstrate significant improvement in pain and improved quality of life with minimal complications.

2. Materials and Methods

2.1. Study Design. This retrospective monocentric study was approved by the institutional review board. All patients who underwent the paradigm of embolization, cryoablation, and osteoplasty received thorough informed consent at the time of procedure. Consent included explaining the risks versus benefits of undergoing their treatments, as well as collection of images and permission for publishing their deidentified imaging and clinical information. All patients were referred to our interventional radiologists and triaged on the basis of their clinical exam and diagnostic imaging. Fifteen patients' medical records from July 2012 to August 2014 from our institution were reviewed and deemed eligible based on our inclusion criteria. Patient's demographics and tumor characteristics are provided in Table 1. The mean age was 62 and the most common location of metastasis was the sacrum. With the exception of one patient, all subjects underwent

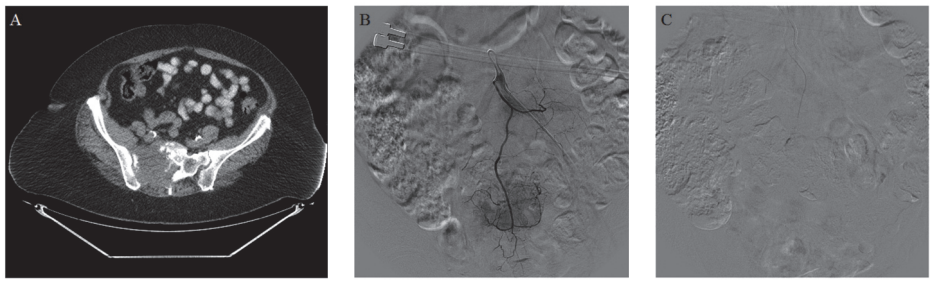

(a) (b) (c)

Figure 1: (a) Axial CT demonstrating osseous neoplasm in right sacroiliac wing in 72-year-old female patient. (b) Selective angiography of median sacral artery showing tumor blush and tumor vascularity. (c) Embolization of medical sacral artery with 300 micron PVA particles with diminished vascular supply.

prior radiation therapy ranging from one to three cycles. The patient's primary neoplasm, location of metastasis, and whether they underwent RT were noted. Both the initial pain scores and pain scores after RT were documented. Patients who underwent interventional sequential therapy were followed up between one and eight weeks and their pain scores after ST were documented. Analgesia reduction was determined by chart review with any noted reduction qualifying as a positive finding. Complications were assessed by the interventional radiology team both at the time of the procedure and during follow-up.

2.2. Inclusion/Exclusion Criteria. Inclusion criteria included men and women of 19-81 years of ages with primary or secondary osseous neoplasms and inoperable tumor burden who have pretreatment CT or magnetic resonance (MR) imaging charactering the extent of disease. Subjects may or may not have undergone treatment of the underlying condition. Patient must have received sequential embolization and cryoablation. Patients may or may not have been treated with osteoplasty. Subjects must have undergone follow-up imaging in one to three months following treatment to assess effects. Exclusion criteria include absence of any of the above.

2.3. Methods of Intervention. Cryoablation with preprocedural angiographic embolization was offered as a means of decreasing patient pain. Postablation osteoplasty was offered for improved stabilization in select patients. Informed consent was obtained after explaining the risks and benefits of the procedures, as well as explaining the procedures that would be performed for palliative measures. The discussed risks included bleeding, infection, potential injury to nonpathological bone, and regional organ damage. The patient, prior to pursuing treatment, understood these risks. Data related to the procedures was recorded under an IRB-approved protocol

All procedures were performed under general anesthesia with total intravenous anesthesia (TIVA) in conjunction with succinylcholine administered by a trained anesthesiologist. A certified intraoperative neural monitoring specialist was present in the room at all times. A neurologist oversaw monitoring remotely. Cryoablation and osteoplasty typically follow one to two days after embolization. Angiographic embolization was performed prior to cryoablation to decrease tumor perfusion. Vessels were selected based on the location of the neoplasm. The internal and external iliac vessels were targeted for iliac and ischial lesions. The lateral/median sacral, gluteal, and iliolumbar vessels were targeted for sacral lesions. The thoracoacromial and circumflex humeral vessels were targeted for scapular lesions. Sodium Brevital 3 mg (JHP Pharmaceuticals, New Jersey) was injected prior to embolization to assess if changes in recorded transcranial motor evoked potentials (TcMEPs) were visualized. Waveforms remained stable after Brevital injection, following which embolization was performed using 300 to 500 micron polyvinyl alcohol (PVA) particles (Boston Scientific, Massachusetts). Postangiography images showed significantly diminished tumor vascularity (Figure 1).

The patients were then brought back within two days to undergo cryoablation. The patients were placed in the appropriate position and prepped and draped in a sterile fashion. Bilateral 10-guage bone biopsy needles serving as introducers were inserted into the osseous lesion. 15 mm cryoablation probes were inserted through each introducer away from adjacent neurovascular structures. Real-time temperature monitoring was accomplished with a temperature probe. Once positioning was verified, a single freeze-thaw-freeze cycle was performed for 10, 8, and 10 minutes, respectively. This resulted in formation of ovoid ice balls within the boundaries of the lesion (Figure 2). While the measured temperature of the cryoablation probe central zone reached -40°C, the temperature probe in surrounding normal bone never decreased below 34°C. Osteoplasty was then performed on the same day with injection of methyl-methacrylate into both 10-guage needles. The lesions were filled with cement under rapid CT guidance to verify no cement extravasation (Figure 2). The needles were subsequently removed and adequate hemostasis was achieved using manual compression. The primary and secondary outcomes were pain evaluation and oral analgesic usage, respectively.

2.4. Statistics. This was a single-arm retrospective study in which patients were their own controls. Primary endpoints

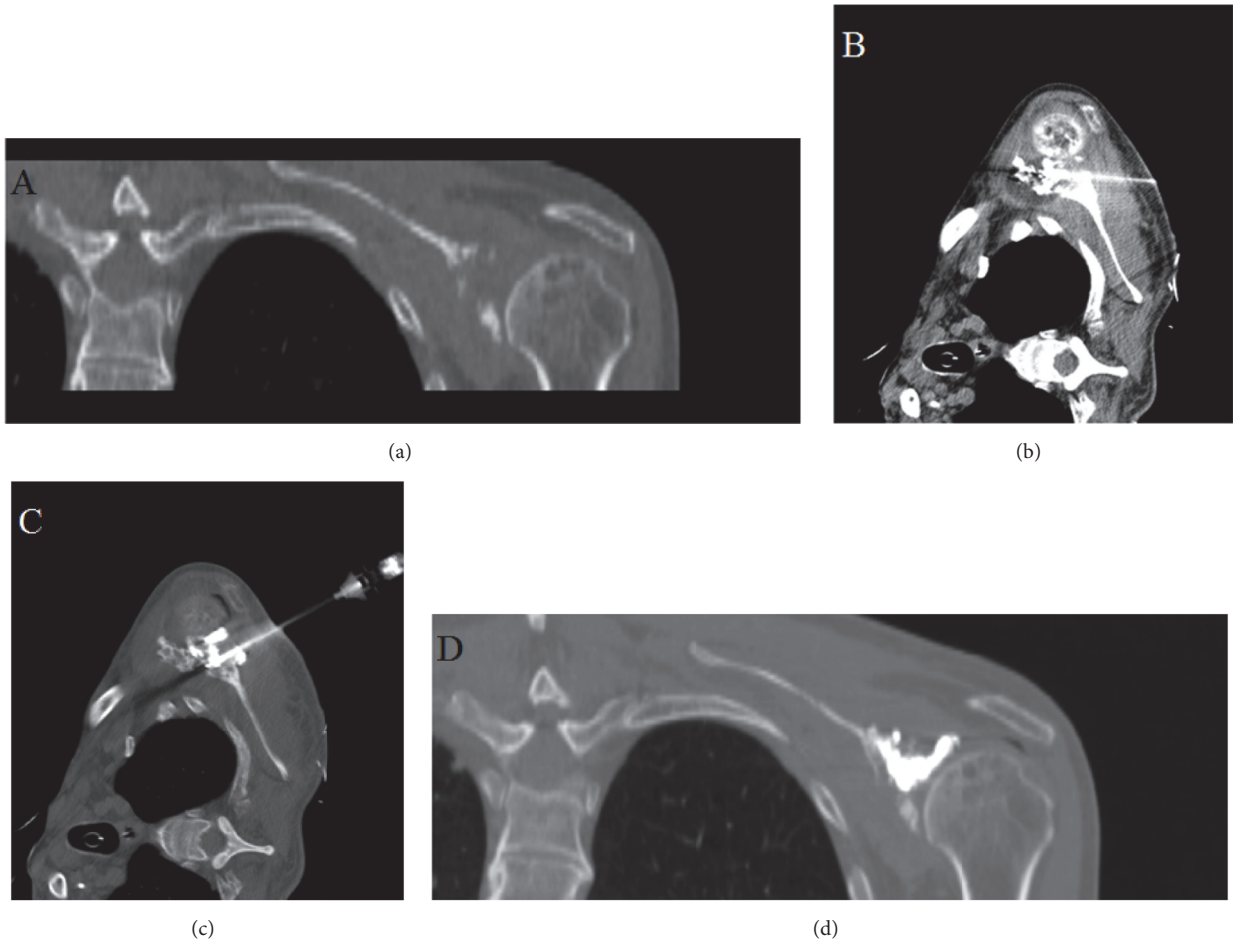

Figure 2: (a) Coronal CT demonstrating osteosarcoma of scapula in 69-year-old male patient. (b) Cryoablation probes inserted through scapula with ovoid intralesional ice ball formation. (c) Axial CT demonstrating cement injection into ablation cavity. (d) Postosteoplasty image illustrating bony reconstruction.

were pain at baseline, pain after RT, and pain after ST. Pain was measured using the numeric rating scale (NRS-11) [10]. Secondary endpoints were the percentage of patients with a reduction in analgesic use following treatment and any reported complications. Data were tested for Gaussian distribution with D'Agostino-Pearson omnibus normality test. A two-tailed Student's *t*-test was performed comparing mean pain scores at baseline and after RT and mean pain scores after RT and after ST. For patients with no reported post-ST pain scores, their baseline and post-RT scores were still included in our analysis. We also assessed mean pain scores between patients who received osteoplasty and patients who did not receive osteoplasty using Mann-Whitney *U* test. Data are presented as mean ± SD and differences were considered statistically significant at $p<0.05$. Statistical tests were performed using GraphPad Prism 7.0 software.

3. Results

Between July 2012 and August 2014, nine patients underwent embolization, cryoablation, and osteoplasty. Six patients underwent embolization and cryoablation only. Fourteen patients were treated with RT prior. Postprocedural pain was assessed between one and eight weeks, with an average of 3 weeks. All patients had documented baseline and post-RT pain scores. Twelve of fifteen patients (80%) had documented NRS-11 pain score at follow-up. Technical success was achieved in all procedures. Symptomatic neoplasms were fully embolized with stasis achieved in tumor feeding vessels. Cryoablation was performed with visualization of the ice ball on CT. No complications occurred at any point during the embolization, cryoablation, or osteoplasty.

Figure 3 shows pain scores charted throughout the different phases of care for each patient. Treatment correlates significantly with primary pain relief. Mean pain at baseline was 8.7 ± 1.1. Patients reported pain reduction after RT with mean pain scores of 7.25 ±1.5 ($p =<0.0001$). After ST, mean pain scores were further reduced to 3.9 ± 2.6 ($p=0.0015$). All patients who were using oral analgesics reported decrease use (13/13, 100%). Osteoplasty was performed in seven cases when indicated. Patients without large bony defects and who at the time were judged not to benefit from the procedure did not undergo osteoplasty. Figure 4 shows pain scores in a

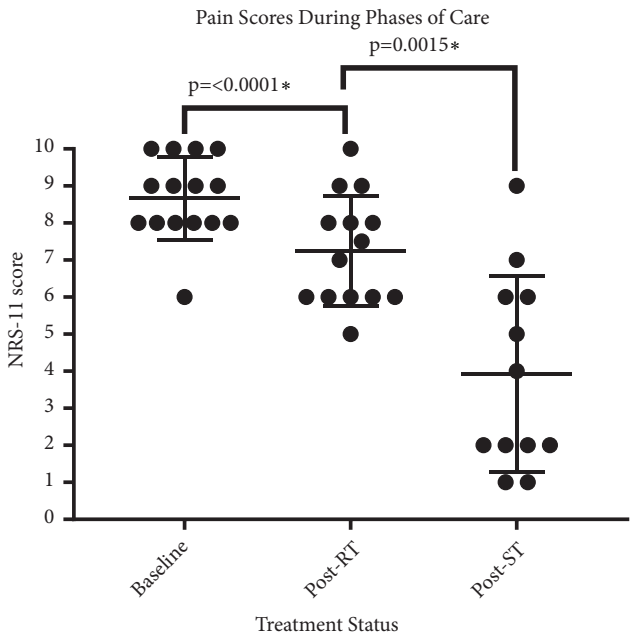

Figure 3: Patient reported NRS-11 pain scores throughout phases of care. Mean pain at baseline was 8.7 ± 1.1. Mean pain after RT was 7.25 ±1.5 (p =<0.0001). Mean pain after ST was 3.9 ± 2.6 (p=0.0015). Statistical significance was set to $p < 0.05$.

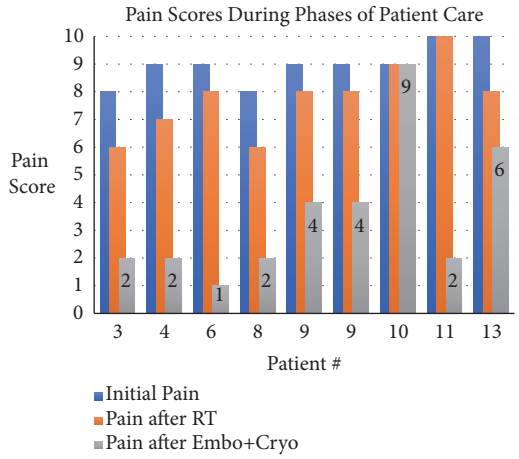

Figure 4: Patient #3 (unknown primary), patient #4 (lung primary), patient #6 (endometrial primary), patient #8 (renal primary), patient #9 (pancreatic primary), patient #10 (osteosarcoma primary), patient #11 (lung primary), and patient #13 (urothelial primary).

color-coded bar graph for a subset of patients with different primary neoplasms treated with ST.

There was no difference in postprocedural pain scores between patients who required osteoplasty and patients who did not (p = 0.7514). One patient did not report postprocedural pain improvements. This patient did, however, report lifestyle improvements with the ability to lay on the side of the tumor.

4. Discussion

Minimally invasive treatment options for both primary and metastatic osseous neoplasms have been developed and tested over the past decade [3]. Studies have assessed the efficacy of various ablative techniques, embolization, and osteoplasty as standalone treatments. Yet, when the condition to be treated is multifactorial, so too should the treatment regimen. As no single procedure is uniformly superior to another, incorporation of several effective treatment options based on the clinical symptomatology, histopathological grading, and staging and the radiologic-defined anatomic extent of disease may provide justification for the proposed treatment paradigm. For example, it has been established that transarterial embolization before cryoablation reduces postprocedural related hemorrhage [11, 12]. In addition, embolization allows for the treatment of tumors located near neurovascular structures in which the full margin cannot be covered by cryoablation alone. Other ablative procedures such as radiofrequency ablation have also been studied and proven to be efficacious. However, due to lack of visualization of the ablation zone, it may be less useful near high-risk neurovascular structures. Given this limitation, cryoablation has become a more important procedure in part due to better control of the ablation zone [13]. Mechanistically, cryoablation achieves tissue death via rapid freezing which results in intracellular ice formation and cellular destruction as osmotic pressures rise and cells dehydrate. Recent research suggests that, in addition to physical cell death, cryoablation results in the activation of apoptosis cascades and the modulation of host immune system function to bypass cancer cell's defensive capabilities [14]. Therefore, cryoablation may have an anticancer effect due to its effects on the microenvironment. Finally, osteoplasty may be performed, particularly in cases of osteolytic disease. Osteoplasty has a role as the ablative procedures do not provide support to the bony structure and may result in incomplete pain relief and reduced stability [15].

Clinically, bone pain is managed with a spectrum of analgesics beginning with nonsteroidal anti-inflammatory drugs and culminating in opiate therapy. Adjuvant therapies such as RT and nerve blocks are also common. Studies suggest that the pathophysiology of bone pain is multifactorial. Cancer cells and the associated stroma express receptor activator of nuclear factor κ-B ligand (RANKL) which interacts with osteoclast expressed RANK resulting in bone resorption. This process involves an acidic area adjacent to the bone that results in upregulation of specific ion channels, such as transient receptor potential cation channel subfamily V member 1 (TrpV1) [16], which results in cancer bone pain through sensitization and activation of nerve fibers. Endogenous substances such as formaldehyde and osteoblast derived insulin-like growth factor I have been shown to activate TrpV1 receptors as well. Additionally, osteoclastic resorption distorts bone architecture resulting in microfractures which also contribute to pain. In addition to RANKL expression, tumor cells and stroma can directly secrete prostaglandins, proteases, and endothelins which have also been associated with increased pain perception [17]. Therefore, the aforementioned antitumor effects of cryoablation may be

further explained by decreasing the production of algogenic substances occurring after tumor death.

Our study results suggest that sequential embolization, cryoablation, and osteoplasty are effective and yield a statistically significant improvement in pain control without complications. This subjective reduction in reported pain scores was confirmed with a uniform reduction in postprocedural oral analgesics in all patients. We have demonstrated that these procedures are safe and efficient and have a role in patients who are symptomatic despite both maximal medical treatment and RT. The pain relief observed is primarily related to cryoablation. Embolization prior to cryoablation provides hemostatic control and allows for targeted therapy of extraosseous disease and osseous sites not amenable to safe cryoablation. Limitations to this study are primarily related to a retrospective design. We were only able to identify 15 patients who underwent ST. This small sample size limited our statistical power. In addition, the histology studied may not be representative of the general population. For example, the primary tumor dictates the characteristics of the metastasis (osteolytic versus osteoblastic), which can impact treatment decisions and outcomes. In addition, we had to rely on chart review to obtain postprocedural pain scores, which were not always quantified. Further studies should be prospectively designed and include a larger sample size with more varied pathology and longer patient follow-up to assess recurrence.

5. Conclusions

In summary, ST of painful osseous neoplasms with transarterial embolization, cryoablation, and osteoplasty results in a dramatic reduction in reported pain and analgesic use without complications. We demonstrated that this combination has the potential to become a mainstay paradigm in the palliative care of osseous neoplasm for patients otherwise resistant to radiotherapy. We suggest that a multidisciplinary team implementing optimal medication, RT, and interventional procedures can provide comprehensive management of these patients and improve their quality of life.

Data Availability

The data used to support the findings of this study are included within the article and the data sources are available from the corresponding author upon request.

Disclosure

The authors declare that there was no specific funding for this research. This research was performed as part of the authors' employment by Robert Wood Johnson University Hospital.

Conflicts of Interest

The authors declare that there are no conflicts of interest regarding the publication of this paper.

References

[1] R. Siegel, D. Naishadham, and A. Jemal, "Cancer statistics, 2013," *CA: A Cancer Journal for Clinicians*, vol. 63, no. 1, pp. 11–30, 2013.

[2] N. A. Janjan, R. Payne, T. Gillis et al., "Presenting symptoms in patients referred to a multidisciplinary clinic for bone metastases," *Journal of Pain and Symptom Management*, vol. 16, no. 3, pp. 171–178, 1998.

[3] M. R. Callstrom, J. W. Charboneau, M. P. Goetz et al., "Image-guided ablation of painful metastatic bone tumors: a new and effective approach to a difficult problem," *Skeletal Radiology*, vol. 35, no. 1, pp. 1–15, 2006.

[4] H. Yang, L. Zhu, N. A. Ebraheim et al., "Analysis of risk factors for recurrence after the resection of sacral chordoma combined with embolization," *The Spine Journal*, vol. 9, no. 12, pp. 972–980, 2009.

[5] M. P. Goetz, "Percutaneous image-guided radiofrequency ablation of painful metastases involving bone: a multicenter study," *Journal of Clinical Oncology*, vol. 22, no. 2, pp. 300–306, 2004.

[6] M. R. Callstrom, D. E. Dupuy, S. B. Solomon et al., "Percutaneous image-guided cryoablation of painful metastases involving bone," *Cancer*, vol. 119, no. 5, pp. 1033–1041, 2013.

[7] A. Tomasian, A. Wallace, B. Northrup, T. J. Hillen, and J. W. Jennings, "Spine cryoablation: pain palliation and local tumor control for vertebral metastases," *American Journal of Neuroradiology*, vol. 37, no. 1, pp. 189–195, 2016.

[8] N. Kumar, B. Tan, A. S. Zaw et al., "The role of preoperative vascular embolization in surgery for metastatic spinal tumours," *European Spine Journal*, vol. 25, no. 12, pp. 3962–3970, 2016.

[9] P. P. Barton, R. E. Waneck, F. J. Karnel, P. Ritschl, J. Kramer, and G. L. Lechner, "Embolization of bone metastases," *Journal of Vascular and Interventional Radiology*, vol. 7, no. 1, pp. 81–88, 1996.

[10] A. Williamson and B. Hoggart, "Pain: a review of three commonly used pain rating scales," *Journal of Clinical Nursing*, vol. 14, no. 7, pp. 798–804, 2005.

[11] D. A. Woodrum, T. D. Atwell, M. A. Farrell, J. C. Andrews, J. W. Charboneau, and M. R. Callstrom, "Role of intraarterial embolization before cryoablation of large renal tumors: a pilot study," *Journal of Vascular and Interventional Radiology*, vol. 21, no. 6, pp. 930–936, 2010.

[12] J. M. Miller, P. Julien, A. Wachsman, R. J. Van Allan, and M. L. Friedman, "The role of embolization in reducing the complications of cryoablation in renal cell carcinoma," *Clinical Radiology*, vol. 69, no. 10, pp. 1045–1049, 2014.

[13] M. R. Callstrom and A. N. Kurup, "Percutaneous ablation for bone and soft tissue metastases-why cryoablation?" *Skeletal Radiology*, vol. 38, no. 9, pp. 835–839, 2009.

[14] J. G. Baust, J. C. Bischof, S. Jiang-Hughes et al., "Re-purposing cryoablation: a combinatorial 'therapy' for the destruction of tissue," *Prostate Cancer and Prostatic Diseases*, vol. 18, no. 2, pp. 87–95, 2015.

[15] G. C. Anselmetti, "Osteoplasty: percutaneous bone cement injection beyond the spine," *Seminars in Interventional Radiology*, vol. 27, no. 2, pp. 199–208, 2010.

[16] P. Mantyh, "Bone cancer pain: causes, consequences, and therapeutic opportunities," *Pain*, vol. 154, supplement 1, pp. S54–S62, 2013.

[17] P. W. O'Donnell and D. R. Clohisy, "Biology of bone cancer pain," *Metastatic Bone Disease*, pp. 37–44, 2015.

Hindawi
Journal of Oncology
Volume 2019, Article ID 6375025, 13 pages
https://doi.org/10.1155/2019/6375025

Research Article

Cytoplasmic HAX1 Is an Independent Risk Factor for Breast Cancer Metastasis

Alicja Trebinska-Stryjewska, Lukasz Szafron, Alina Rembiszewska, Maciej Wakula, Sylwia Tabor, Renata Sienkiewicz, Joanna Owczarek, Anna Balcerak, Anna Felisiak-Golabek, and Ewa A. Grzybowska

Maria Sklodowska-Curie Memorial Cancer Center and Institute of Oncology, Roentgena 5, 02-781 Warsaw, Poland

Correspondence should be addressed to Ewa A. Grzybowska; ewag@coi.waw.pl

Received 31 July 2018; Revised 20 February 2019; Accepted 7 March 2019; Published 10 April 2019

Guest Editor: Peramaiyan Rajendran

HAX1 is an antiapoptotic factor involved in the regulation of cell migration and calcium homeostasis, overexpressed in several cancers, including breast cancer. It has been suggested that HAX1 is also implicated in metastasis. Herein we report the results of meta-analysis of *HAX1* expression, based on publicly available data, which confirms its significant overexpression in breast cancer and demonstrates copy number gain and prognostic value of *HAX1* overexpression for metastatic relapse in ER+ tumors. IHC analysis reported here also reveals its significant overexpression in breast cancer samples from primary tumors, indicating significantly higher HAX1 protein levels in a group of patients who developed distant metastases in a disease course. Moreover, we demonstrate that HAX1 localization is important for the prediction of metastatic relapse and that cytoplasmic but not nuclear HAX1 is an independent risk factor for breast cancer metastasis.

1. Introduction

Breast cancer is the most common neoplasm and the primary cause of cancer death in women [1]. Breast cancer mortality is almost exclusively due to metastatic disease [2, 3]. The current 5-year survival for primary breast cancer is quite high (80-92%), but, despite the advances in diagnosis and treatment of early breast cancer patients, about 20-40% experience distant organ metastases, for which the prognosis is significantly worse [4–7]. Breast cancer is heterogeneous disease and a probability to develop metastases depends not only on histopathological parameters (lymph node status, histologic grade, and tumor size) but also on molecular subtypes defined roughly as basal-like, normal-like, HER2–enriched, and luminal A and luminal B, each of which has a different prognosis and a pattern of recurrence. For luminal cancers (estrogen and/or progesterone receptor positive) the prognosis is better due to a very effective adjuvant endocrine therapy and the fact that the metastases appear late, often many years after initial diagnosis. Disseminated tumor cells could stay dormant for as long as 20 years but eventually may start to proliferate. Late recurrences were observed in as much as 50% of these cancers [4]. Basal cancers tend to metastasize early (with a peak about 2-3 years after diagnosis) and frequently [8, 9], but typically there is no recurrence after 5 years in this subtype. Distinct pattern of metastatic relapse in basal and luminal subtypes suggests different routes for metastasis.

Better molecular characteristic of the primary tumor is crucial for a good prediction of the clinical outcome. Genetic tests such as MammaPrint (for luminal and basal cancers) [10] and Oncotype DX (luminal cancers only) [11] were developed as a diagnostic tool to predict risk of breast cancer metastasis, based on mRNA expression signature of selected gene sets (70 and 21 genes, resp.). Quantification of the risk of recurrence is especially important for selecting a subset of luminal patients who may benefit from additional chemotherapy and sparing those who would not.

Two other factors have both prognostic and predictive values in breast cancer and are commonly used in risk-assessment: urokinase plasminogen activator protein (uPA)

and its inhibitor (PAI-1). ELISA-based assay, developed to assess the levels of both proteins in breast cancer tissues, allows to stratify the patients with node-negative disease into a low-risk group, with a good prognosis without adjuvant chemotherapy and a high-risk group, with high expression of both markers, who may benefit from chemotherapy [12, 13].

Additionally, to monitor a response to the treatment and to assess the probability of metastasis, several blood-based biomarkers have been developed, including Human Epidermal Growth Factor Receptor 2 (HER2), Cancer Antigen 15-3 (CA 15-3, MUC1), and Carcinoembryonic Antigen (CEA) [14].

Herein we assessed the potential of HAX1 expression level in primary tumor samples as an independent prognostic factor for breast cancer metastasis. HAX1 was first characterized in 1997 as an antiapoptotic factor [15] and several reports confirm its involvement in the regulation of apoptosis [16–18]. Additionally, HAX1 was implicated in the regulation of cell motility [19–21] and calcium homeostasis [22].

HAX1 overexpression was reported in several cancers [23–25], including breast cancer [26, 27], and its role in metastasis was suggested in some reports [20, 28]. Sheng and Ni [28] reported that higher HAX1 expression was related to a lower 10-year survival rate in breast cancer patients.

In this report we present data analysis which confirms significant HAX1 overexpression in breast cancer samples, coinciding with high amplification of the *HAX1* gene. Moreover, the analyses reveal significant difference between HAX1 levels in primary tumor samples between nonmetastatic and metastatic groups of patients, indicating that HAX1 may represent an independent risk factor for breast cancer metastasis. Additionally, it was demonstrated that IHC assay which takes into account protein localization may predict clinical outcome more precisely and with a higher strength than mRNA-based estimations.

2. Materials and Methods

2.1. Study Group. Formalin-fixed, paraffin-embedded (FFPE) tissue samples were collected from breast cancer patients receiving surgical intervention at the Maria Sklodowska-Curie Institute, Oncology Center, between January 2007 and May 2007, after informed consent. The study was approved by Ethics Committee from the Maria Sklodowska-Curie Institute, Oncology Center, Warsaw, in accordance with the guidelines of the Helsinki Declaration of 1975, revised in 1983. Clinical data and histology reports for each patient were reviewed by two clinicians and a pathologist, respectively. De-identified patients data were accessed using MedStream Designer platform (Transition Technologies S.A.). Patients were retrospectively analyzed and divided into two groups: with and without distant metastases within the follow-up period of 9 years. Inclusion criteria for the study were as follows: invasive breast cancer stages I-III, the absence of distant metastasis at the time of surgery, and the presence of tumor tissue in FFPE confirmed by a pathologist. Exclusion criteria were as follows: previous history of breast cancer, previous or simultaneous history of any other malignances, and neoadjuvant chemotherapy. A total of 46 patients who met the inclusion and exclusion criteria were selected: 23 consecutive patients with distant metastases and 23 consecutive patients without distant metastases within the follow-up period (comparative group). Assuming a power of 80%, α=0.05, and normal distribution of data, a number of patients tested would allow to detect a difference of at least 0.43 between group means (with a common standard deviation equal to 0.5) when analyzed with Mann-Whitney U test.

Patients' age at the time of diagnosis, estrogen receptor (ER) status, progesterone receptor (PGR) status, HER status, tumor size (pTNM scale), node status (pTNM scale), clinical stage (AJCC Anatomic Stage Group), histological grade (Nottingham Histologic Score system), histology, and molecular subtype (based on routine immunohistochemical evaluation of ER, PGR, HER2 and Ki-67) were recorded. Patients' characteristics are shown in Table S1.

2.2. Follow-Up and Outcomes. Patients' records were tracked from the time of surgery until May 2016. Information about clinical outcomes (distant metastases confirmed by imaging or histologic evidence, death from any cause) was retrieved from clinical records and The National Cancer Registry in Poland. Distant relapse-free survival (DRFS) was defined according to STEEP system [34] as the time from surgical intervention until the time of distant recurrence, death from any cause, or the last follow-up. Complete events in DRFS analysis were distant metastasis or death, whichever came first. Overall survival (OS) was defined as the time from surgery to the last follow-up (censored event) or to the time of death from any cause (complete event).

2.3. Immunohistochemistry. Immunohistochemical staining with a monoclonal mouse anti-HAX1 antibody (BD Biosciences) or a control mouse IgG of the same subclass was performed as described previously [27] on a set of representative slides from formalin-fixed, paraffin-embedded breast tumors. HAX-1 expression was scored manually according to Ball et al. [35]. It was evaluated independently for nuclear and cytoplasmic staining. Light microscopy evaluation at 400x magnification was used to count 100 tumor cells within areas of the strongest staining. Each nucleus and cytoplasm in a given field was assigned to an intensity category of 0 (absent), 1 (weak), 2 (moderate), or 3 (strong). The percentage of cells in each intensity category was determined as N0, N1, N2, and N3, respectively. A distribution score (ID score) was then calculated as

$$\mathrm{ID} = \frac{(/\mathrm{N0} * 0/ + /\mathrm{N1} * 1/ + /\mathrm{N2} * 2/ + /\mathrm{N3} * 3/)}{100}. \quad (1)$$

The ID score therefore ranged from 0 (absent staining in all cells) to a maximum 3 (100% cells having a staining intensity of 3). The values of total HAX1 staining were obtained by adding nuclear and cytoplasmic ID scores for each sample.

2.4. Immunofluorescence. MCF7 (ATCC), MDA-MB-231 (ATCC), and HeLa (ATCC) human cell lines were used in the experiments. All cell lines were authenticated by Eurofins Genomics (Germany). Cells were grown in Dulbecco's

Modified Eagle Medium supplemented with 10% fetal bovine serum (Thermo Fisher Scientific). Immunofluorescence was performed as described previously [36] with primary anti-HAX1 antibody (rabbit, 1:100, Thermo Fisher Scientific) and secondary goat anti-rabbit Alexa Fluor 594 antibody (1:500, Thermo Fisher Scientific). Cells were observed using the Zeiss LSM 800 confocal microscope. Images represent single Z-stacks. Colocalization was quantified using ImageJ JACoP plugin [37], for 3-5 independent fields of vision and approximately 25-60 cells per field.

2.5. Database Gene Expression Analysis. *HAX1* gene expression in primary breast cancer compared to normal breast tissue was analyzed using the Oncomine™ Platform (Thermo Fisher, Ann Arbor, MI) [38, 39]. *HAX1* expression (RNAseq) in breast cancer in relation to phenotypic variables was explored in TCGA-BRCA cohort (data generated by the TCGA Research Network: http://cancergenome.nih.gov/) using Xena Functional Genomics Explorer (https://xena-browser.net/, 2018) and in a set of microarray data using bcGenExMiner (http://bcgenex.centregauducheau.fr, 2018) [33].

2.6. Database Copy Number Variation and Mutation Analysis. Genomic alterations (mutations, gene amplification, and/or deletion) of *HAX1* gene in breast cancer were assessed using cBioPortal for Cancer Genomics (http://www.cbioportal.org/index.do, 2018) [40, 41]. The following cohorts of invasive breast carcinoma were included: Breast Cancer (METABRIC) [29, 42], Breast Invasive Carcinoma (British Columbia) [43], Breast Invasive Carcinoma (Broad) [44], Breast Invasive Carcinoma (Sanger) [45], Breast Invasive Carcinoma (TCGA, PanCancer Atlas) [30], Mutational profiles of metastatic breast cancer (France) [46], and the Metastatic Breast Cancer Project (Provisional, April 2018). The other cohorts were excluded from the analysis due to patients overlapping or the difference in sample type (xenografts instead of primary tumor). Groups with shallow deletion (possibly heterozygous deletion), diploid status, gain, or high-level amplification of *HAX1* gene generated by GISTIC algorithm [47] were compared for mRNA expression in METABRIC and TCGA cohorts. For the latter, *HAX1* mRNA levels were also correlated with log2 copy number values using Pearson's correlation coefficient.

HAX1 copy number variation in primary breast cancer in comparison to normal tissues was also analyzed on the Oncomine Platform using the following threshold values: p-value 0.05, fold change 'all', and gene rank 'top 5%.'

2.7. Database Survival and Prognostic Analysis. Survival analyses of patients stratified according to *HAX1* expression were performed using KM Plotter (http://kmplot.com/analysis/, 2018) [48]. HAX1 expression levels based on Affymetrix probe ID 201145_at in 35 cohorts of breast cancer patients deposited in GEO database (Gene Expression Omnibus, NCBI) were used. The general settings were as follows: patients split by median or by best cut-off; follow-up threshold: all; probe set options: only JetSet best probe set; quality control: removing redundant samples and excluding biased arrays.

Survival analysis of patients with metastatic relapse information was also performed using Breast Cancer Gene-Expression Miner v4.1 (bcGenExMiner v4.1) [33]. Patients were split into two groups according to gene's expression median and Kaplan-Meier survival curves were plotted for each group. Breast Cancer Gene-Expression Miner v4.1 was also used in targeted prognostic analysis of *HAX1* gene expression for all patients with metastatic relapse information. The results summarize univariate Cox scores (hazard ratios, p-values) for each cohort fulfilling the chosen criteria and all of these cohorts pooled together. The results were presented in forest plot. Additionally, multivariate Cox scores (adjusted on NPI/AOL) were calculated for *HAX1*.

2.8. Statistical Analysis. Statistical analysis was performed using SAS Enterprise Guide 7.11 (Copyright ©2015 by SAS Institute Inc., Cary, NC, USA) and Stata software (StataCorp., College Station, TX, StataCorp LP.). GraphPad Prism version 6.07 for Windows (GraphPad Software, La Jolla, California USA, www.graphpad.com) was used to visualize data. O'Brien-Castelloe approximation (SAS Enterprise Guide 7.11) was employed for statistical power and sample size analysis for Mann-Whitney U test. Baseline demographics, tumor characteristics, and types of treatment were compared between the group of patients with distant metastases and the comparative group using the Mann-Whitney U test for continuous and ordinal variables and by Pearson's chi-squared test for categorical variables. The Shapiro-Wilk W test was used to determine whether HAX1 protein levels measured by immunohistochemistry were normally distributed. The associations between HAX1 immunoreactivity and progression, along with clinicopathological parameters, ER, PGR, and HER2 status, were assessed using the Mann-Whitney U test or Kruskal-Wallis test, depending on whether the nominal variable had two or more categories. If significant, the Kruskal-Wallis test was followed by pairwise comparisons using the Mann-Whitney U test. Receiver operating characteristic (ROC) curve analysis was performed to determine the overall test performance and to calculate possible cutoff points for HAX1 protein levels. Optimal cutoff values were calculated using the nearest to (0,1) method and the maximum value of the Youden index. Kaplan-Meier survival analyses were carried out for overall survival (OS) and distant relapse-free survival (DRFS). The log-rank test was used to evaluate the equality of survivor function for groups with lower and higher HAX1 expression categorized according to values obtained in the ROC curve analysis. The Cox proportional hazards model was used for univariate and multivariate analyses of patient survival depending on HAX1 expression, categorized as described above. In the multivariate survival analyses, HAX1 levels were assessed along with the following variables: PGR expression (categorization: positive vs. negative), clinical stage (I vs. II vs. III), histological grade (1 vs. 2 vs. 3), and molecular subtype (luminal vs. others). Hazard ratios (HR) with 95% confidence intervals and p-values were reported (Table 1). *HAX1* gene expression retrieved from databases was compared in different subgroups using Student's t-test and one-way Welch's or Fisher's ANOVA followed by post-hoc Tukey-Kramer test. All tests used in this

Table 1: Multivariate Cox regression analysis of HAX1 levels in human breast cancers.

Evaluation of HAX1 levels in the cell nuclei		
Variable name	*OS (23/46)*[1]	*DRFS (28/46)*[1]
	HR (95% CI), p	HR (95% CI), p
HAX1 (≤1.05 vs. >1.05)	NS	NS
Histological grade (2 vs. 1)	6.06E+8 (2.26E+8-1.63E+9), <0.001	NS
Clinical stage (III vs. I)	3.171 (1.017-9.884), 0.047	NS
Evaluation of HAX1 levels in the cytoplasm		
Variable name	*OS (23/46)*	*DRFS (28/46)*
	HR (95% CI), p	HR (95% CI), p
HAX1 (≤1.02 vs. >1.02)	NS	*2.832 (1.207-6.644), 0.017*
Histological grade (2 vs. 1)	4.86E+8 (1.74E+8-1.36E+9), <0.001	NS
Evaluation of HAX1 levels in both of the nuclei and the cytoplasm		
Variable name	*OS (23/46)*	*DRFS (28/46)*
	HR (95% CI), p	HR (95% CI), p
HAX1 (≤2.06 vs. >2.06)	NS	*4.249 (1.404-12.86), 0.010*
Histological grade (2 vs. 1)	3.44E+8 (1.17E+8-1.01E+9), <0.001	NS

The multivariate analysis of prognosis was carried out using the Cox proportional hazards model. [1]Values before and after a slash (/) stand for the number of complete observations versus all observations, respectively. Only the results with p-values <0.05 are shown and those with p-values <0.05 for HAX1 expression are highlighted in italic type. HR and CI stand for the hazard ratio and confidence interval, respectively. OS: overall survival; DRFS: distant recurrence-free survival; NS: a nonsignificant result (p ≥0.05).

study were two-tailed and the significance level (alpha) was always set to 0.05.

3. Results

3.1. HAX1 Is Significantly Overexpressed in the Majority of Analyzed Datasets of Breast Cancer Primary Tumor Samples. *HAX1* overexpression in primary breast cancer in comparison to normal breast tissues was identified at mRNA [26, 27] and protein level [27]. To further confirm this observation we performed analysis on breast cancer cohorts using the Oncomine Platform [38, 39] and taking into account invasive breast cancer samples (ductal and lobular). *HAX1* gene expression in invasive primary tumor was significantly elevated compared to normal tissue in 16 out of 19 analyses (Figure 1(a), legend in Figure S1). Detailed analyses for ductal and lobular carcinoma in selected datasets confirmed these conclusions (Figures 1(b)–1(e)).

HAX1 expression in breast cancer in relation to phenotypic variables was assessed in a set of microarray data using Breast Cancer Gene-Expression Miner v4.1 (bcGenExMiner) [33]. This analysis revealed that *HAX1* expression correlates positively with grade (Figure 1(f)), confirming our previous results, obtained on a small group of patients [27]. It was also observed that *HAX1* expression differs significantly in molecular subtypes of breast cancer, with the highest expression in basal and luminal B subtypes, associated with more aggressive neoplasm (Figure 1(g)).

3.2. HAX1 Gene Copy Number Is Altered in Breast Cancer Patients. Analysis of *HAX1* gene in 7 cohorts of invasive breast carcinoma patients using cBioPortal for Cancer Genomics [40, 41] revealed *HAX1* altered status in 15% (549/3655) of sequenced cases. Only three patients had mutations in *HAX1* sequence, one truncating E59X and two missense mutations, E39K and P259A. Majority of the identified alterations comprised of high-level gene amplification which was detected in all 4 cohorts containing copy number variation data [29, 30, 42, 46] and ranged from 5.16% to 21.06% of all cases (average 16.01%) (Figure 2(a)). Additionally, low-level *HAX1* gene gain was identified in 36.81% to 63.86% cases (average 45.92%) whereas shallow deletion (possibly heterozygous deletion) was present in only 0% to 3.76% of patients (average 1.49%). Additionally, log-2 *HAX1* gene copy number units were compared between blood, breast, and invasive ductal and invasive lobular carcinoma in TCGA-BRCA cohort using the Oncomine Platform and were found to be elevated for both invasive ductal carcinoma (fold change: 1.273, p=9.26E-135, gene rank: top 1%, Figure 2(b)) and invasive lobular carcinoma (fold change: 1.297, p=1.13E-22, gene rank: top 2%, Figure 2(c)).

Two cohorts analyzed using cBioPortal, METABRIC [29], and TCGA-BRCA [30] contained gene expression information so it was possible to relate *HAX1* gene copy number with *HAX1* mRNA level. In both cohorts mRNA expression differed significantly between putative groups with diploid DNA content and *HAX1* gene gain or amplification (Figures 2(d) and 2(e)). In TCGA cohort HAX1 log2 copy number values showed a moderate positive correlation with mRNA expression (Pearson's r=0.656, p<0.0001, Figure 2(f)).

3.3. HAX1 Overexpression Is Associated with Cancer Relapse and Has Prognostic Impact on ER+ Subset. Survival analyses of breast cancer patients stratified according to *HAX1* expression were performed using KM Plotter and microarray data from 35 breast cancer cohorts from GEO (Gene Expression Omnibus, NCBI). RFS (relapse-free survival) analysis including 3,951 patients showed a statistically significant difference

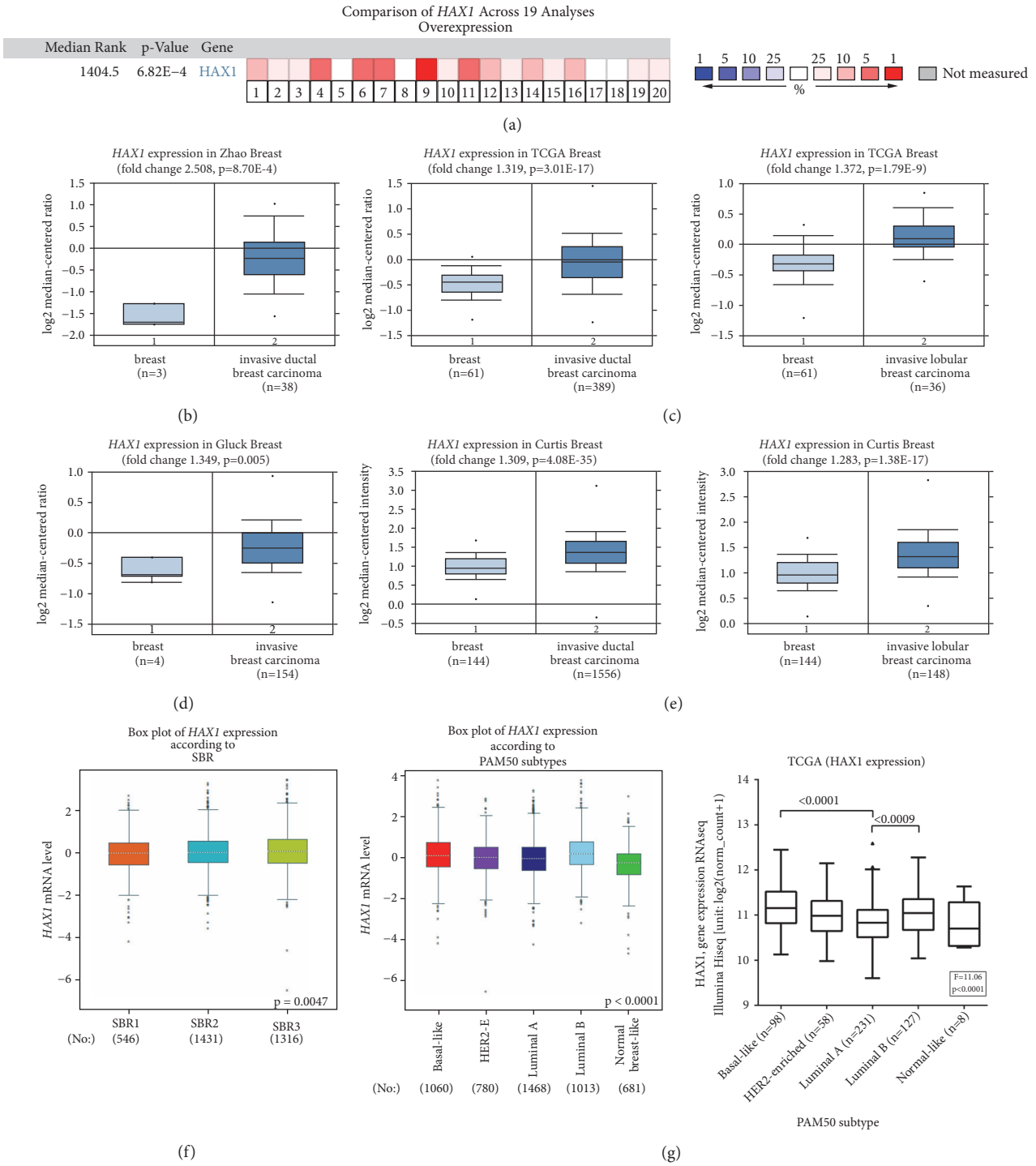

Figure 1: HAX1 is overexpressed in primary breast tumor in comparison to normal breast tissue. (a-e) *HAX1* expression in invasive breast cancer (ductal and lobular) in comparison to normal breast tissue assessed in publicly available datasets on the Oncomine Platform. (a) Comparison of *HAX1* overexpression across 19 analyses. Dataset legend in Figure S1. (b-e) *HAX1* overexpression in selected datasets [29–32]. Differences between groups were assessed by Student's t-test and results with p-values <0.05 were considered significant. (f) *HAX1* expression in breast cancer samples stratified according to grade (Scarff-Bloom-Richardson grade, SBR) analyzed using bcGenExMiner. (g) *HAX1* expression in breast cancer samples stratified according to molecular subtype (PAM50 classification) in a set of microarray data analyzed using bcGenExMiner [33] (left panel) or RNAseq TCGA-BRCA data (right panel). Differences between groups in (f) and (g) were assessed by Welch's or Fisher's ANOVA followed by post-hoc Tukey-Kramer test.

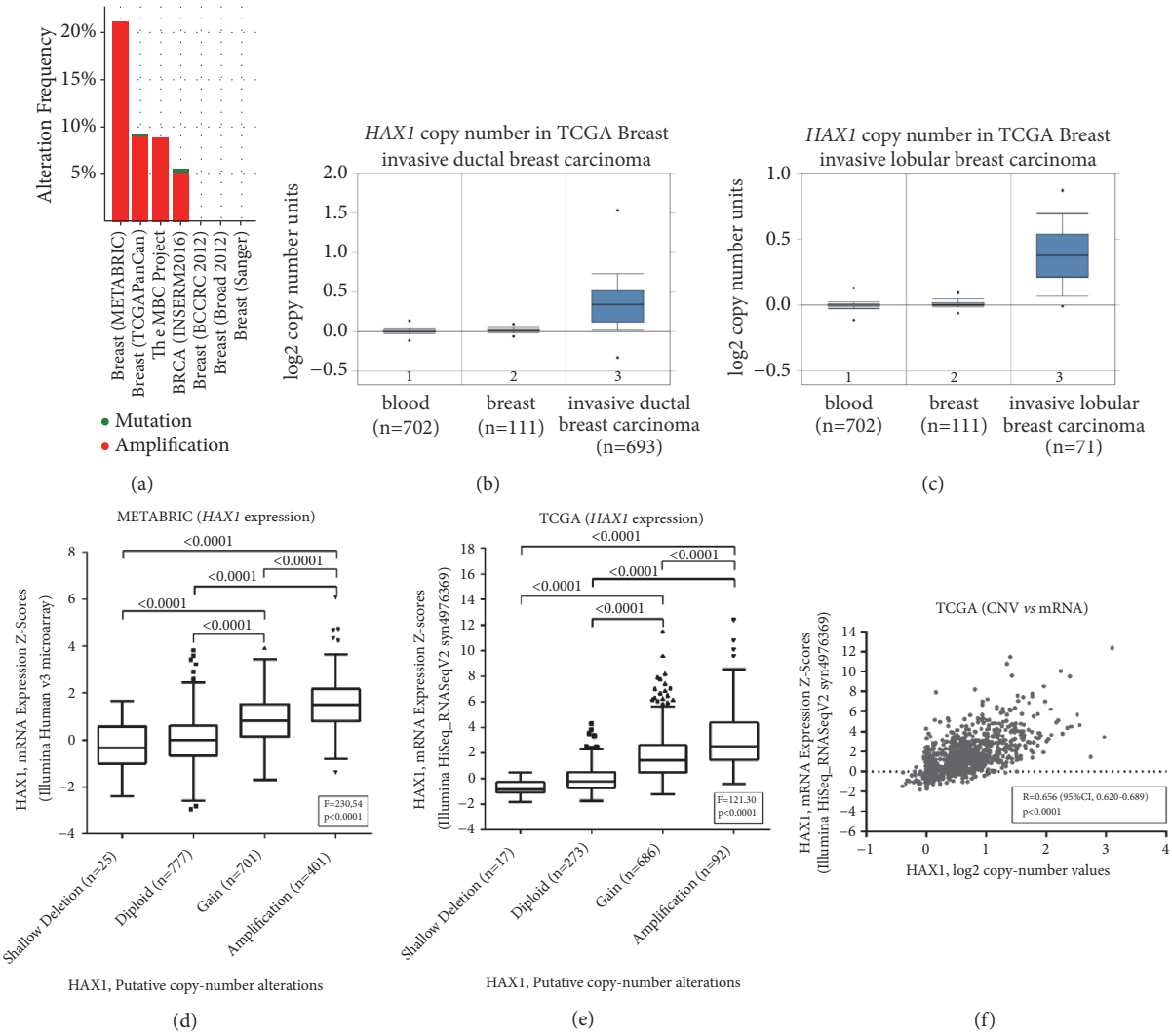

FIGURE 2: *HAX1* gene copy number is altered in breast cancer patients. (a) Alterations in *HAX1* gene analyzed in 7 cohorts of invasive breast carcinoma patients using cBioPortal for Cancer Genomics. (b-c) *HAX1* gene copy number in TCGA-BRCA data from the Oncomine Platform for (b) invasive ductal carcinoma and (c) invasive lobular carcinoma compared to blood and normal breast tissue. (d-e) Comparison of *HAX1* expression in primary breast cancer samples in relation to DNA copy number in (d) METABRIC cohort [29] and (e) TCGA-BRCA cohort [30]. Differences between groups were assessed by Fisher's ANOVA followed by post-hoc Tukey-Kramer test. (f) Correlation of *HAX1* expression and log2 copy number values in TCGA-BRCA cohort (Pearson's correlation coefficient).

in survival, favoring patients with lower *HAX1* expression regardless of whether patients were split by median (HR=1.37, 95% CI, 1.22-1.52, log-rank p=2.2E-08, Figure 3(a)) or best cutoff value (HR=1.42, 95% CI, 1.27-1.58, log-rank p=3.6E-10, FDR=1%). OS (overall survival) analysis in 1,402 patients also indicated statistically significant more favorable prognosis for patients with lower *HAX1* expression, but only if patients were split by best cutoff value (HR=1.41, 95%CI, 1.12-1.77, log-rank p=0.0034) and at the expense of false discovery rate (FDR=50%) (Figure S2A).

In breast cancer ER status is one of the most important prognostic and predictive factors. Therefore, RFS analysis was performed using KM Plotter on subgroups of breast cancer patients with different ER status, using median value of *HAX1* expression to avoid high values of FDR. Statistical significance was detected for ER+ (n=2,061) but not ER- (n=801) subgroup of patients (HR=1.18, 95% CI, 1.00-1.39, log-rank p=0.044 and HR=1.12, 95% CI, 0.89-1.40, log-rank p=0.33, resp., Figure 3(a)).

Prognostic analysis was carried out using bcGenExMiner [33]. Targeted prognostic analysis for *HAX1* in a group of ER-positive patients with metastatic relapse information (n = 2,822) revealed statistical significance (HR=1.15, p-value=0.0008) for *HAX1* expression level in the pooled cohort (Figure 3(b), left panel). Additionally, to evaluate independent prognostic impact of *HAX1* in ER+ patients relative to the well-established breast cancer prognostic indexes, including Nottingham Prognostic Index (NPI) [49] and Adjuvant! Online (AOL) [50], adjusted Cox proportional hazards model was used, revealing statistical significance for

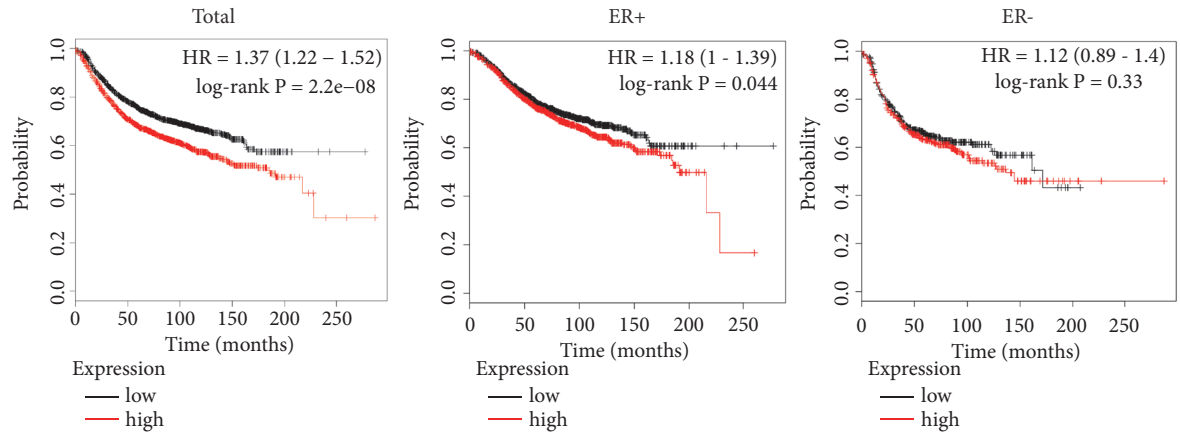

(a)

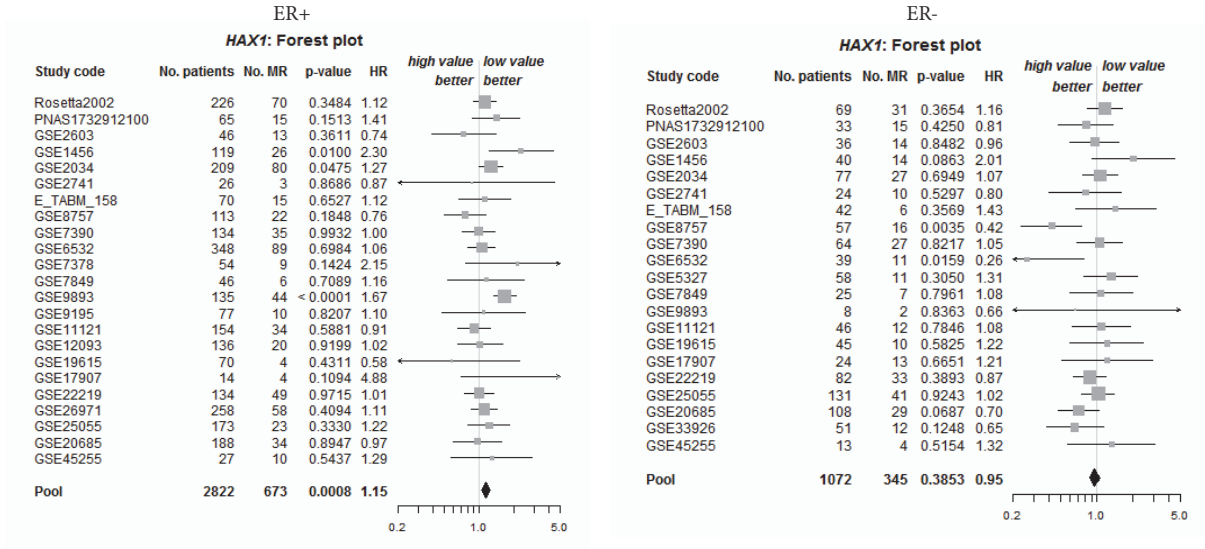

(b)

Figure 3: *HAX1* overexpression is higher in patients with breast cancer relapse and has prognostic impact on ER+ subset of patients. (a) RFS analysis for total number of patients and subsets with different ER status (left: ER+; right: ER-). Patients were split into groups with high and low *HAX1* expression (based on microarray data, split by median). Kaplan-Meier estimates were generated in KM Plotter online tool for all data available for 2017 (merged datasets). Probability of cancer relapse is plotted against time. (b) Forest plots estimating prognostic impact of *HAX1* expression in ER+ (n = 2,822) and ER- (n = 1,072) subsets of patients with metastatic relapse information (bcGenExMiner). Values in columns represent summarized univariate Cox scores (p-values, hazard ratios) for each cohort fulfilling the chosen criteria and for pooled cohorts. MR: metastatic relapse.

HAX1 expression adjusted on AOL (HR 1.27, 95% CI 1.06-1.52, p-value: 0.0108, 12 cohorts, 382 patients, 101 metastases).

The same analysis performed for patients with negative ER status (n=1,072) revealed the lack of statistical significance (p-value=0.3853 for the pooled cohort) and even the tendency for better prognosis associated with HAX1 overexpression (Figure 3(b), right panel).

Prognostic analysis performed for *HAX1* expression regardless of ER status (n=3,924) indicated significance, but bordering on the 0.05 threshold (HR=1.07, 95% CI, 1.00-1.14, p-value: 0.0432, Figure S2B). Additionally, KM curves for metastatic relapse-free survival (MRFS) were plotted in bcGenExMiner for each group of patients with metastatic relapse information (all patients, ER+, ER-), and the results were consistent with the previous RFS analyses, showing significant difference for ER+ group of patients and the lack of significance in ER- group of patients (Figure S2C).

3.4. Cytoplasmic HAX1 Levels Are Significantly Higher in the Primary Tumor of Breast Cancer Patients Who Experience Distant Metastasis during the Disease Course. 46 breast cancer patients who were free of distant metastasis at the time of surgery and received no neoadjuvant therapy were retrospectively analyzed for HAX1 protein levels (cytoplasmic and nuclear) in primary tumors by immunohistochemistry. Half of the analyzed group developed distant metastasis during a follow-up period of 9 years. Cytoplasmic HAX1 protein levels were significantly elevated (p=0.0003) in the group of patients

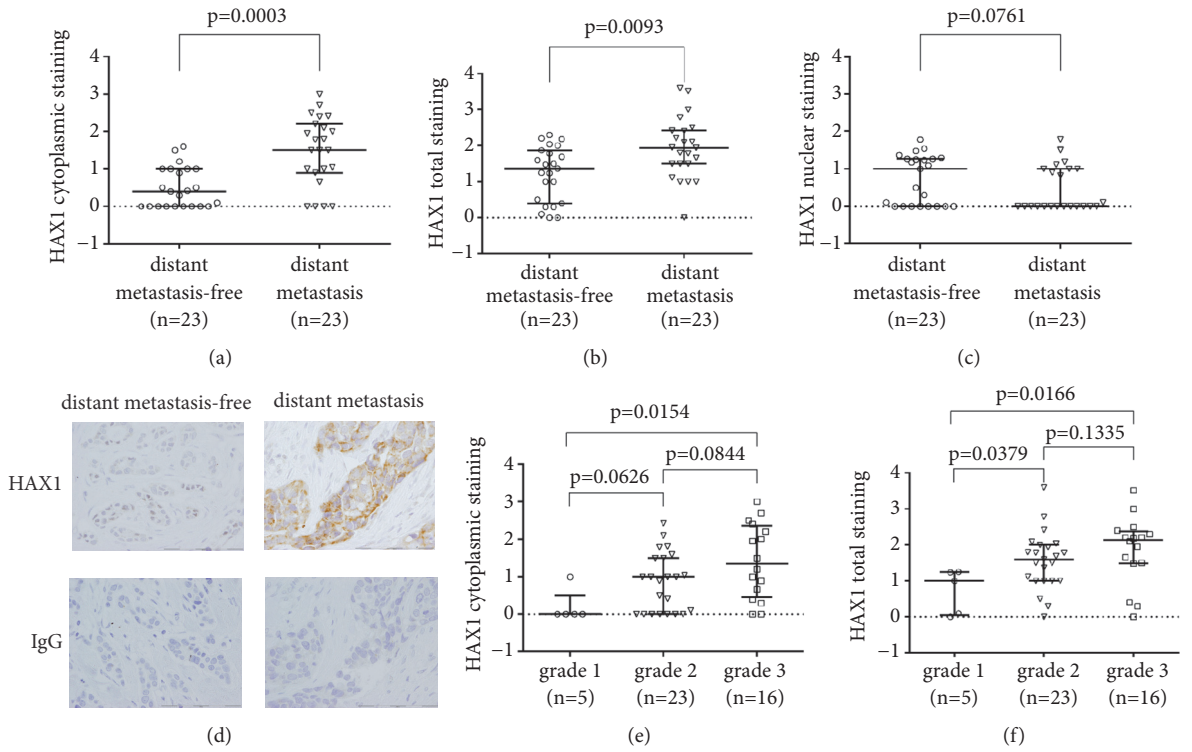

Figure 4: HAX1 protein level in primary tumors stratified according to selected clinical and histological factors (presence of distant metastases, tumor grade). (a-d) HAX1 protein levels in the primary tumor were quantified from IHC data in distant metastasis-free versus distant metastasis group for (a) cytoplasmic, (b) total, and (c) nuclear HAX1 staining. (d) Representative images of HAX1 IHC and negative isotype control for patients from metastasis-free versus distant metastasis group. ×40 objective, bar: 100 μm. (e) Cytoplasmic and (f) total HAX1 staining in breast cancers stratified according to tumor grade (grades 1-3). Results for individual patients and median and interquartile range for each group are shown. Differences in HAX1 protein levels between groups were assessed by the Mann-Whitney U test and results with p-values <0.05 were considered significant.

with distant metastasis (median 1.50, mean±SD 1.48±0.92, 95% CI of the mean 1.08-1.87) compared to the group with no distant metastasis (median 0.40, mean±SD 0.50±0.54, 95% CI of the mean 0.26-0.73) (Figure 4(a)). Total HAX1 staining was also higher in the distant metastasis patient group, although the effect was less prominent (metastasis: median 1.94, mean±SD 1.93±0.85, 95% CI of the mean 1.56-2.29 vs. metastasis-free: median 1.37, mean±SD 1.22±0.76, 95% CI of the mean 0.89-1.55, p=0.0093) (Figure 4(b)). The opposite effect, albeit not statistically significant, was observed for nuclear HAX1 levels (metastasis: median 0.00, mean±SD 0.45±0.60, 95% CI of the mean 0.19-0.71 vs. metastasis-free: median 1.00, mean±SD 0.73±0.66, 95% CI of the mean 0.44-1.01, p=0.0761) (Figure 4(c)). Representative images of the typical staining in metastasis-free and metastatic groups are presented in Figure 4(d).

The two analyzed groups were well matched, as patients' clinicopathological parameters and treatment did not differ significantly except for PGR status (Table S1). Analyses of HAX1 protein levels in groups stratified according to known prognostic factors showed that the values of the cytoplasmic and total HAX1 signal were positively associated with tumor grade (Figures 4(e) and 4(f), resp.), but not other prognostic factors.

3.5. High Cytoplasmic and Total HAX1 Protein Levels in Breast Cancer Cells Are Risk Factors for Distant Metastasis and Death. To ascertain if HAX1 protein levels in primary tumor can be used as a prognostic factor in breast cancer, we analyzed follow-up patient data and recorded time to distant recurrence and/or time to death from any cause for all 46 patients. The total follow-up time was 9 years; 61% of the patients had been followed for a minimum of 5 years. 23 patients developed distant metastasis. 23 out of 46 patients were still alive at the end of the follow-up period (18 in a group with no distant metastasis and 5 in a group with distant metastasis).

Receiver operating characteristic (ROC) analysis was performed to define the best cutoff value of the HAX1 signal and to measure the overall test performance which would use HAX1 protein levels to predict breast cancer metastasis. The analysis was done separately for cytoplasmic, total, and nuclear HAX1 immunohistochemical staining (Figures 5(a)–5(c)). The highest value of area under the curve (AUC) was obtained for cytoplasmic HAX1: 0.7977 (95% CI 0.6628-0.9327, p=0.0005) (Figure 5(a)). The best cutoff points for cytoplasmic, nuclear, and total HAX1 were, respectively, 1.02 (sensitivity 0.65 and specificity 0.87), 1.05 (sensitivity 0.82 and specificity 0.48), and 1.49 (sensitivity 0.78 and specificity 0.57).

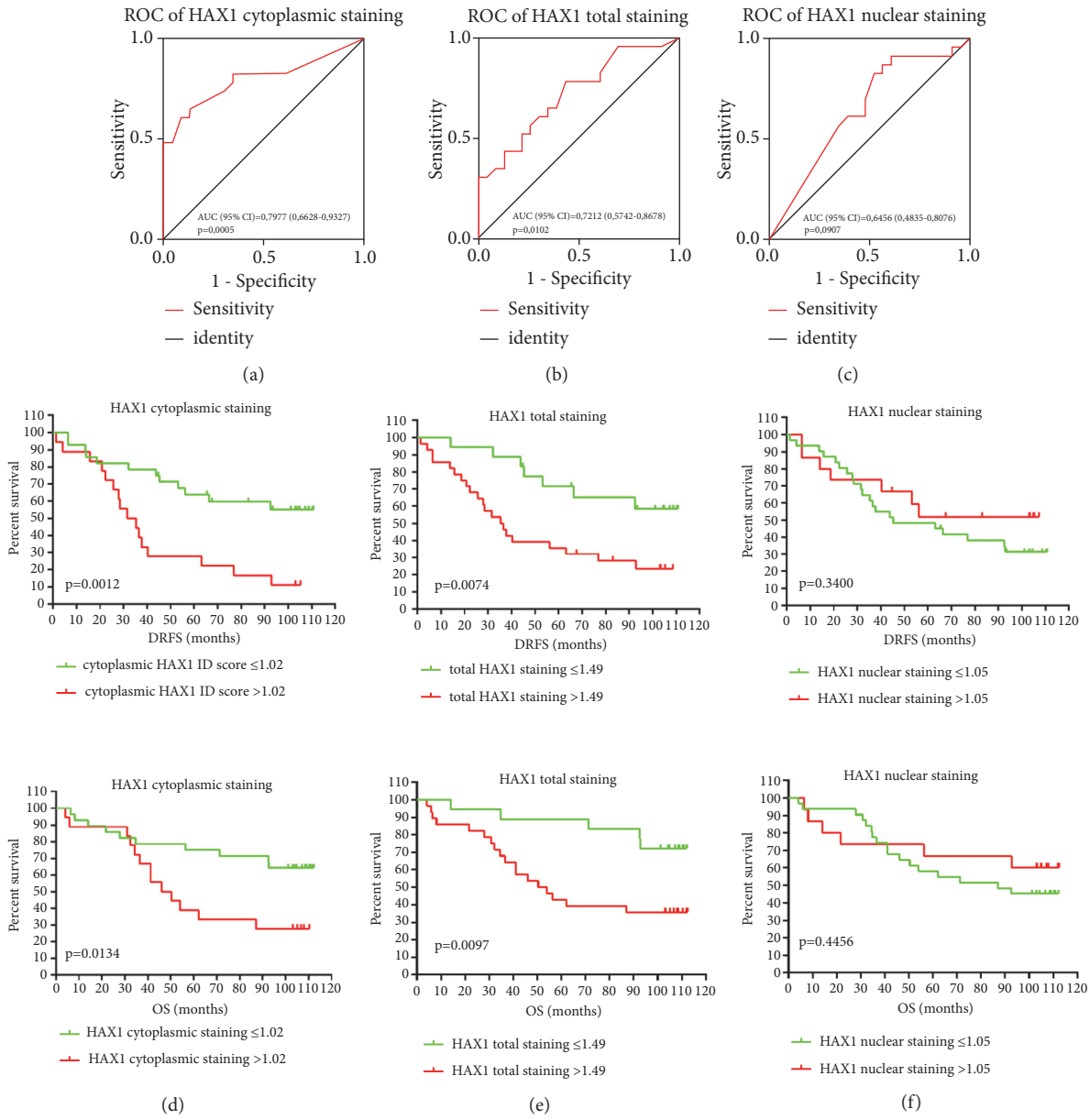

FIGURE 5: HAX1 protein level in primary tumor is a risk factor for breast cancer progression. (a-c) Receiver operating characteristic analysis for (a) cytoplasmic, (b) total, and (c) nuclear HAX1 protein levels was performed to define the best cutoff values for subsequent survival analysis. Area under curve (AUC) with 95% CI and p-values for each ROC curve are shown. (d-f) Kaplan-Meier survival estimates for distant recurrence-free survival (DRFS) and overall survival (OS) in breast cancer patients according to proposed cutoff values of (d) cytoplasmic HAX1 protein levels ≤1.02 (n=28) versus >1.02 (n=18), (e) total HAX1 protein levels ≤1.49 (n=18) versus >1.49 (n=28), and (f) nuclear HAX1 protein levels ≤1.05 (n=31) versus >1.05 (n=15). The log-rank test was used to evaluate the equality of survivor function for groups with lower and higher HAX1 expression and p-values <0.05 were considered significant.

Cutoff points estimated from ROC curves were used in subsequent survival analyses by the Kaplan-Meier method. The log-rank test showed a significant difference favoring, for both distant recurrence-free survival (DRFS) and overall survival (OS), patients with a cytoplasmic HAX1 ID score of ≤1.02 (p=0.0012 and p=0.0134, resp., Figure 5(d)). 43% of patients in the group with cytoplasmic HAX1 protein levels ≤1.02 experienced distant metastasis/death within 9 years compared to 89% of patients in the group with cytoplasmic HAX1 protein levels >1.02. Overall survival analysis showed that, at the end of follow-up, 64% of patients were still alive in the group with a cytoplasmic HAX1 of ≤1.02 compared to 28% of patients in the group with cytoplasmic HAX1 >1.02. Similar results were observed for total HAX1 protein levels. Patients with total HAX1 protein levels ≤1.49 showed significantly increased DRFS and OS compared to the group with a total

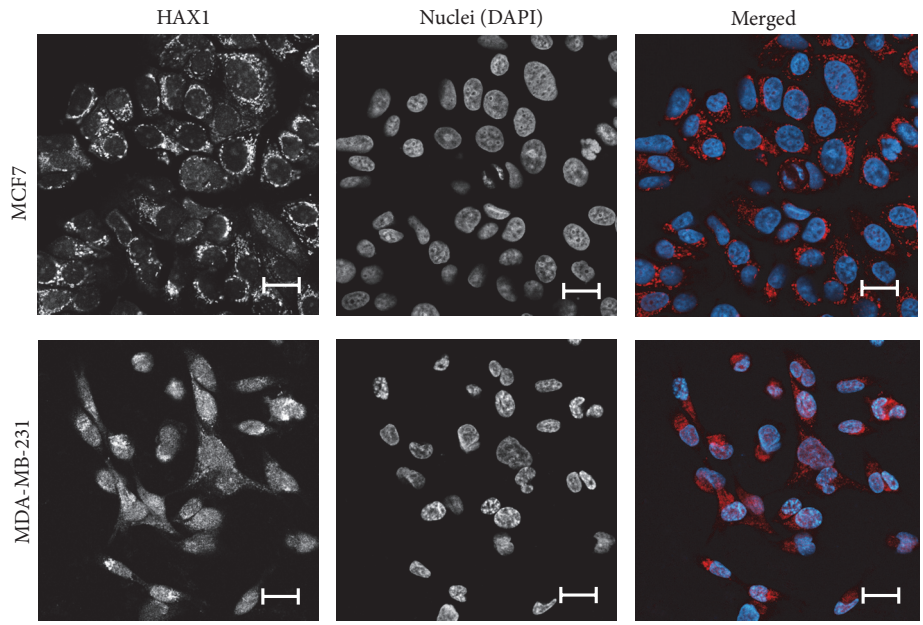

Figure 6: HAX1 localization in breast cancer cell lines of different characteristics. Endogenous staining of HAX1 (red) and nuclei (DAPI, blue) in MCF7, luminal-like epithelial cells and MDA-MB-231, basal-like cells after epithelial-mesenchymal transition. Bar: 20 μm.

HAX1 protein level of >1.49 (p=0.0074 and p=0.0097, resp., Figure 5(e)). Nuclear HAX1 staining showed no prognostic value for neither DRFS nor OS (Figure 5(f)).

Overall survival (OS) and distant recurrence-free survival (DRFS) for 46 breast cancer patients were also evaluated by 3 different univariate and multivariate analyzes, in which the HAX1 protein expression, either cytoplasmic, nuclear, or cumulative, was assessed by IHC (Table 1). We found out that elevated HAX1 levels in the cytoplasm emerged as an independent, negative prognostic factor, associated with an increased risk of distant metastasis (HR 2.832, 95% CI 1.207-6.644, p=0.017). Correspondingly, the results obtained for cumulative expression of HAX1 also showed its adverse effect on DRFS (HR 4.249, 95% CI 1.404-12.86, p=0.010). HAX1 nuclear expression had no impact on survival.

3.6. HAX1 Localization Varies among Breast Cancer Cell Lines. Endogenous HAX1 protein was detected by immunofluorescence in luminal-like MCF7 and basal-like MDA-MB-231 cell lines, revealing significant differences. In MCF7 cells HAX1 staining was mostly cytoplasmic, while in MDA-MB-231 HAX1 was also detected in the nuclei (Figure 6). Nuclear colocalization was calculated using ImageJ JACoP, showing a significant shift of Pearson's correlation coefficient (PCC) and two Mander's overlap coefficients (M1, M2) from 0.101 (PCC), 0.207 (M1), and 0.116 (M2) in MCF7 cells to 0.467 (PCC), 0.377 (M1), and 0.592 (M2) in MDA-MB-231 cells, respectively (p-values for PCC, M1, and M2: 0.0105, 0.0328, and 0.0181, resp.).

4. Discussion

Advancing on our previous study [27], in which we demonstrated *HAX1* overexpression in breast cancer and its differential localization (cytoplasmic and nuclear), we expanded our analysis to assess its effect on metastasis. Database analysis on large group of patients confirmed *HAX1* overexpression in breast cancer samples, which tallies with the previous study by Luo et al. [26]. The analysis revealed also the correlation of HAX1 overexpression with tumor grade, which is consistent with our previous [27] and current IHC results. Additionally, *HAX1* overexpression was shown to correlate with gene amplification. Although there were several studies reporting *HAX1* overexpression in different types of malignancies, we showed for the first time that high *HAX1* mRNA levels in cancer cells could be a consequence of gene amplification, at least in breast cancer. Detailed analysis of *HAX1* expression in molecular subtypes demonstrated that the highest overexpression was observed in basal and luminal B subtypes, which are more aggressive.

Database analysis of *HAX1* expression in correlation to metastasis revealed its significant prognostic value for luminal (ER+) subset while for ER-, despite high overexpression in basal cancers, the expression level had no prognostic value. This apparent paradox can be resolved on the basis of cellular localization.

Our previous IHC analysis [27] indicated two different localizations of HAX1 protein in breast cancer tumor samples: cytoplasmic and nuclear. Nuclear localization of HAX1 was also reported in cell lines [36] and rat tests [51]. Different localization may translate into different functionality and different impact on tumor progression, as in case of Aurora A kinase, where nuclear protein acquires kinase-independent transactivating function, which enhances breast cancer stem cell phenotype [52]. Thus, in this report, we have analyzed HAX1 protein levels in the primary tumor of breast cancer patients divided into metastatic and nonmetastatic groups. IHC analysis enabled us to differentiate between cytoplasmic and nuclear localization of HAX1. Overall, our results

demonstrated that HAX1 protein level is significantly higher in metastatic group of patients, but this effect can be observed only for evaluations concerning cytoplasmic and total HAX1, while for nuclear localization it does not exist and the trend is even opposite (less HAX1 in metastatic group). Clearly, the results for total HAX1 levels are influenced by the cytoplasmic subset, for which the difference is huge.

Thus, our evaluation of HAX1 protein levels and localization in the samples from metastatic versus nonmetastatic groups of patients indicates a positive relationship between HAX1 cytoplasmic expression and the occurrence of a secondary tumor at distant locations in the course of the disease (opposite to the relations observed for Aurora A). High cytoplasmic HAX1 level is associated negatively with progression-free survival and overall survival. Similar results were obtained for total HAX1; however, ROC curve analysis indicated a higher ability to identify patients at risk of progression when using cytoplasmic, not total HAX1 levels.

Accordingly, the experimental immunofluorescence results showing that HAX1 localization is more cytoplasmic in luminal-like than basal-like cell lines can explain the apparent difference in HAX1 prognostic value for ER+ and ER- subsets. It seems plausible that, in basal cells, despite the high HAX1 expression, nuclear localization of HAX1 prevents its prometastatic action, by assuming different functionality or simply by sequestering cytoplasmic HAX1. Alternatively, it seems plausible that nuclear HAX1 can block and/or sequester in inactive complexes some nuclear factor(s), specific to luminal cancers, whose action is linked to metastasis, probably by the regulation of transcription. Thus, nuclear HAX1 would have protective effect (restricted to luminal-like cells), which would not be present in cells with cytoplasmic HAX1. Of note, HAX1 was shown to bind directly estrogen receptor [53], which is a prometastatic factor. Estrogen responsiveness is one of the main factors differentiating between the two cell lines used in experiments. However, since luminal patients are treated with anti-estrogen therapy, some other factors may be involved. Further research should explain specific molecular mechanisms of function for cytoplasmic and nuclear HAX1, which contribute to metastasis.

5. Conclusions

Overall, presented results indicate *HAX1* overexpression, copy number gain, and prognostic impact on metastatic breast cancer. Moreover, cytoplasmic but not nuclear HAX1 demonstrated to be an independent, negative prognostic factor for breast cancer metastasis.

Multigene tests like MammaPrint and Oncotype DX have a proved prognostic value, but they rely on expression on mRNA level, which does not always accurately correspond to protein level and does not consider the factor of protein localization. It is possible that for some markers establishing the level of localized protein provides more accurate prediction than mRNA profiling. Further analysis is required to confirm its prognostic value in the clinic, but assessing HAX1 protein levels and localization in primary tumor samples may become a useful tool for estimating the probability of luminal breast cancer dissemination.

Data Availability

The data used to support the findings of this study are available from the corresponding author upon request.

Conflicts of Interest

The authors declare no conflicts of interest.

Funding

This work was supported by the Polish National Science Center Grants Nos. 2011/01/B/NZ1/03674, 2014/14/M/NZ1/00437, and 2016/21/B/NZ2/03473. MedStream Designer (Transition Technologies S.A.) purchase was financed by ONKO.SYS project (Grant No. POIG.02.03.00-14-084/13) from the Polish National Centre for Research and Development.

Acknowledgments

We would like to thank Maria Zwierko, PhD for providing patients' data from The National Cancer Registry in Poland.

Supplementary Materials

Table S1: clinical and pathological characteristics of breast cancer patients. Figure S1: dataset legend to Oncomine meta-analysis of *HAX1* expression in breast cancer (ductal and lobular). Figure S2: *HAX1* overexpression is associated with metastatic relapse and survival (additional data). *(Supplementary Materials)*

References

[1] F. Bray, J. Ferlay, I. Soerjomataram et al., "Global cancer statistics 2018: GLOBOCAN estimates of incidence and mortality worldwide for 36 cancers in 185 countries," *CA: A Cancer Journal for Clinicians*, vol. 68, no. 6, Article ID 30207593, pp. 394–424, 2018.

[2] C. L. Chaffer and R. A. Weinberg, "A perspective on cancer cell metastasis," *Science*, vol. 331, no. 6024, pp. 1559–1564, 2011.

[3] F. Cardoso, A. Costa, L. Norton et al., "1st International consensus guidelines for advanced breast cancer (ABC 1)," *Breast*, vol. 21, no. 3, Article ID 22425534, pp. 242-52, 2012.

[4] X. H. Zhang, M. Giuliano, M. V. Trivedi, R. Schiff, and C. K. Osborne, "Metastasis dormancy in estrogen receptor-positive breast cancer," *Clinical Cancer Research*, vol. 19, no. 23, Article ID 24298069, pp. 6389–6397, 2013.

[5] Z. H. Li, P. H. Hu, J. H. Tu et al., "Luminal B breast cancer: patterns of recurrence and clinical outcome," *Oncotarget*, vol. 7, no. 40, Article ID 27542253, pp. 65024–65033, 2016.

[6] R. L. Siegel, K. D. Miller, and A. Jemal, "Cancer statistics, 2015," *CA: A Cancer Journal for Clinicians*, vol. 65, no. 1, Article ID 25559415, pp. 5–29, 2015.

[7] J. Ferlay, I. Soerjomataram, R. Dikshit et al., "Cancer incidence and mortality worldwide: sources, methods and major patterns

in GLOBOCAN 2012," *International Journal of Cancer*, vol. 136, no. 5, Article ID 25220842, pp. E359–86, 2014.

[8] F. Bertucci, P. Finetti, and D. Birnbaum, "Basal breast cancer: A complex and deadly molecular subtype," *Current Molecular Medicine*, vol. 12, no. 1, Article ID 22082486, pp. 96–110, 2012.

[9] H. Kennecke, R. Yerushalmi, R. Woods et al., "Metastatic behavior of breast cancer subtypes," *Journal of Clinical Oncology*, vol. 28, no. 20, Article ID 20498394, pp. 3271–3277, 2010.

[10] M. J. van de Vijver, Y. D. He, L. J. van't Veer et al., "A gene-expression signature as a predictor of survival in breast cancer," *The New England Journal of Medicine*, vol. 347, no. 25, Article ID 12490681, pp. 1999–2009, 2002.

[11] S. Paik, S. Shak, G. Tang et al., "A multigene assay to predict recurrence of tamoxifen-treated, node-negative breast cancer," *The New England Journal of Medicine*, vol. 351, no. 27, Article ID 15591335, pp. 2817–2826, 2004.

[12] V. R. Jacobs, R. E. Kates, E. Kantelhardt et al., "Health economic impact of risk group selection according to ASCO-recommended biomarkers uPA/PAI-1 in node-negative primary breast cancer," *Breast Cancer Research and Treatment*, vol. 138, no. 3, pp. 839–850, 2013.

[13] F. Janicke, A. Prechtl, C. Thomssen et al., "Randomized adjuvant chemotherapy trial in high-risk, lymph node-negative breast cancer patients identified by urokinase-type plasminogen activator and plasminogen activator inhibitor type 1," *JNCI: Journal of the National Cancer Institute*, vol. 93, no. 12, Article ID 11416112, pp. 913-20, 2001.

[14] R. Molina, J. M. Augé, J. M. Escudero et al., "Evaluation of tumor markers (HER-2/neu oncoprotein, CEA, and CA 15.3) in patients with locoregional breast cancer: prognostic value," *Tumor Biology*, vol. 31, no. 3, Article ID 20361287, pp. 171–180, 2010.

[15] Y. Suzuki, C. Demoliere, D. Kitamura et al., "HAX-1, a novel intracellular protein, localized on mitochondria, directly associates with HS1, a substrate of Src family tyrosine kinases," *The Journal of Immunology*, vol. 158, no. 6, Article ID 9058808, pp. 2736-44, 1997.

[16] Y. Han, Y. Chen, Z. Liu et al., "Overexpression of HAX-1 protects cardiac myocytes from apoptosis through caspase-9 inhibition," *Circulation Research*, vol. 99, no. 4, Article ID 16857965, pp. 415–423, 2006.

[17] L. Cilenti, M. M. Soundarapandian, G. A. Kyriazis et al., "Regulation of HAX-1 anti-apoptotic protein by Omi/HtrA2 protease during cell death," *The Journal of Biological Chemistry*, vol. 279, no. 48, pp. 50295–50301, 2004.

[18] T. V. Sharp, H. W. Wang, A. Koumi et al., "K15 protein of Kaposi's sarcoma-associated herpesvirus is latently expressed and binds to HAX-1, a protein with antiapoptotic function," *Journal of Virology*, vol. 76, no. 2, Article ID 11752170, pp. 802–816, 2002.

[19] P. J. Cavnar, E. Berthier, D. J. Beebe, and A. Huttenlocher, "Hax1 regulates neutrophil adhesion and motility through RhoA," *The Journal of Cell Biology*, vol. 193, no. 3, Article ID 21518791, pp. 465–473, 2011.

[20] A. G. Ramsay, M. D. Keppler, M. Jazayeri et al., "HS1-associated protein X-1 regulates carcinoma cell migration and invasion via clathrin-mediated endocytosis of integrin $\alpha v\beta 6$," *Cancer Research*, vol. 67, no. 11, Article ID 17545607, pp. 5275–5284, 2007.

[21] V. Radhika, D. Onesime, J. H. Ha, and N. Dhanasekaran, "Gα13 stimulates cell migration through cortactin-interacting protein Hax-1," *The Journal of Biological Chemistry*, vol. 279, no. 47, Article ID 15339924, pp. 49406–49413, 2004.

[22] E. Vafiadaki, D. A. Arvanitis, S. N. Pagakis et al., "The anti-apoptotic protein HAX-1 interacts with SERCA2 and regulates Its protein levels to promote cell survival," *Molecular Biology of the Cell (MBoC)*, vol. 20, no. 1, Article ID 18971376, pp. 306–318, 2009.

[23] X. Li, J. Jiang, R. Yang et al., "Expression of HAX-1 in colorectal cancer and its role in cancer cell growth," *Molecular Medicine Reports*, vol. 12, no. 3, Article ID 26062578, pp. 4071–4078, 2015.

[24] X. Li, T. Li, B. You et al., "Expression and function of HAX-1 in human cutaneous squamous cell carcinoma," *Journal of Cancer*, vol. 6, no. 4, Article ID 25767605, pp. 351–359, 2015.

[25] H. Wu, J. Chen, Q. Wang et al., "Abnormal expression of HAX1 is associated with cellular proliferation and migration in human hypopharyngeal squamous cell carcinoma," *Molecular Medicine Reports*, vol. 16, no. 4, Article ID 28791389, pp. 4664–4670, 2017.

[26] J. Hu, Z. Li, X. Li et al., "hSav1 interacts with HAX1 and attenuates its anti-apoptotic effects in MCF-7 breast cancer cells," *International Journal of Molecular Medicine*, vol. 28, no. 3, Article ID 21567072, pp. 349–355, 2011.

[27] A. Trebinska, A. Rembiszewska, K. Ciosek et al., "HAX-1 overexpression, splicing and cellular localization in tumors," *BMC Cancer*, vol. 10, no. 76, Article ID 20196840, 2010.

[28] C. Sheng and Q. Ni, "Expression of HAX1 and Ki-67 in breast cancer and its correlations with patient's clinicopathological characteristics and prognosis," *International Journal of Clinical and Experimental Medicine*, vol. 8, no. 11, Article ID 26885017, pp. 4–10, 2090.

[29] C. Curtis, S. P. Shah, S. F. Chin et al., "The genomic and transcriptomic architecture of 2, 000 breast tumours reveals novel subgroups," *Nature*, vol. 486, no. 7403, Article ID 22522925, pp. 346–352, 2012.

[30] N. Cancer Genome Atlas, "Comprehensive molecular portraits of human breast tumours," *Nature*, vol. 490, no. 7418, Article ID 23000897, pp. 61–70, 2012.

[31] S. Gluck, J. S. Ross, M. Royce et al., "TP53 genomics predict higher clinical and pathologic tumor response in operable early-stage breast cancer treated with docetaxel-capecitabine +/- trastuzumab," *Breast Cancer Research and Treatment*, vol. 132, Article ID 21373875, pp. 781–791, 2012.

[32] H. Zhao, A. Langerod, Y. Ji et al., "Different gene expression patterns in invasive lobular and ductal carcinomas of the breast," *Molecular Biology of the Cell (MBoC)*, vol. 15, no. 6, Article ID 15034139, pp. 2523–2536, 2004.

[33] P. Jézéquel, M. Campone, W. Gouraud et al., "bc-GenExMiner: an easy-to-use online platform for gene prognostic analyses in breast cancer," *Breast Cancer Research and Treatment*, vol. 131, no. 3, Article ID 21452023, pp. 765–775, 2012.

[34] C. A. Hudis, W. E. Barlow, J. P. Costantino et al., "Proposal for standardized definitions for efficacy end points in adjuvant breast cancer trials: the STEEP system," *Journal of Clinical Oncology*, vol. 25, no. 15, Article ID 17513820, pp. 2127–2132, 2007.

[35] E. Ball, J. Bond, B. Franc et al., "An immunohistochemical study of p16(INK4a) expression in multistep thyroid tumourigenesis," *European Journal of Cancer*, vol. 43, no. 1, Article ID 17046239, pp. 194–201, 2007.

[36] E. A. Grzybowska, V. Zayat, R. Konopiński et al., "HAX-1 is a nucleocytoplasmic shuttling protein with a possible role in mRNA processing," *FEBS Journal*, vol. 280, no. 1, Article ID 23164465, pp. 256–272, 2013.

[37] S. Bolte and F. P. Cordelières, "A guided tour into subcellular colocalization analysis in light microscopy," *Journal of Microscopy*, vol. 224, no. 3, pp. 213–232, 2006.

[38] D. R. Rhodes, J. Yu, K. Shanker et al., "ONCOMINE, a cancer microarray database and integrated data-mining platform," *Neoplasia*, vol. 6, no. 1, Article ID 15068665, pp. 1–6, 2004.

[39] D. R. Rhodes, S. Kalyana-Sundaram, V. Mahavisno et al., "Oncomine 3.0: genes, pathways, and networks in a collection of 18,000 cancer gene expression profiles," *Neoplasia*, vol. 9, no. 2, Article ID 17356713, pp. 166–180, 2007.

[40] J. Gao, B. A. Aksoy, U. Dogrusoz et al., "Integrative analysis of complex cancer genomics and clinical profiles using the cBioPortal," *Science Signaling*, vol. 6, no. 269, Article ID 23550210, 2013.

[41] E. Cerami, J. Gao, U. Dogrusoz et al., "The cBio cancer genomics portal: an open platform for exploring multidimensional cancer genomics data," *Cancer Discovery*, vol. 2, no. 5, Article ID 22588877, pp. 401–404, 2012.

[42] B. Pereira, S. F. Chin, O. M. Rueda et al., "The somatic mutation profiles of 2, 433 breast cancers refines their genomic and transcriptomic landscapes," *Nature Communications*, Article ID 27161491, 2016.

[43] S. P. Shah, A. Roth, R. Goya et al., "The clonal and mutational evolution spectrum of primary triple-negative breast cancers," *Nature*, vol. 486, no. 7403, Article ID 22495314, pp. 395–399, 2012.

[44] S. Banerji, K. Cibulskis, C. Rangel-Escareno et al., "Sequence analysis of mutations and translocations across breast cancer subtypes," *Nature*, vol. 486, no. 7403, Article ID 22722202, pp. 405–409, 2012.

[45] P. J. Stephens, P. S. Tarpey, H. Davies et al., "The landscape of cancer genes and mutational processes in breast cancer," *Nature*, vol. 486, no. 7403, Article ID 22722201, pp. 400–404, 2012.

[46] C. Lefebvre, T. Bachelot, T. Filleron et al., "Mutational profile of metastatic breast cancers: a retrospective analysis," *PLoS Med*, vol. 13, no. 2, Article ID e1002201, 2016.

[47] R. Beroukhim, G. Getz, L. Nghiemphu et al., "Assessing the significance of chromosomal aberrations in cancer: methodology and application to glioma," in *Proceedings of the National Academy of Sciences of USA*, vol. 104, pp. 20007-12, 2007 Dec 11.

[48] B. Gyorffy, A. Lanczky, A. C. Eklund et al., "An online survival analysis tool to rapidly assess the effect of 22,277 genes on breast cancer prognosis using microarray data of 1,809 patients," *Breast Cancer Research and Treatment*, vol. 123, no. 3, Article ID 20020197, pp. 725–731, 2010.

[49] M. H. Galea, R. W. Blamey, C. E. Elston, and I. O. Ellis, "The Nottingham prognostic index in primary breast cancer," *Breast Cancer Research and Treatment*, vol. 22, no. 3, pp. 207–219, 1992.

[50] P. M. Ravdin, L. A. Siminoff, G. J. Davis et al., "Computer program to assist in making decisions about adjuvant therapy for women with early breast cancer," *Journal of Clinical Oncology*, vol. 19, no. 4, Article ID 11181660, pp. 980–991, 2001.

[51] E. Sarnowska, E. A. Grzybowska, K. Sobczak et al., "Hairpin structure within the 3'UTR of DNA polymerase beta mRNA acts as a post-transcriptional regulatory element and interacts with Hax-1," *Nucleic Acids Research*, vol. 35, no. 16, Article ID 17704138, pp. 5499–5510, 2007.

[52] F. Zheng, C. Yue, G. Li et al., "Nuclear AURKA acquires kinase-independent transactivating function to enhance breast cancer stem cell phenotype," *Nature Communications*, vol. 7, no. 10180, Article ID 26782714, 2016.

[53] M. P. Walker, M. Zhang, T. P. Le, P. Wu, M. Lainé, and G. L. Greene, "RAC3 is a pro-migratory co-activator of ERα," *Oncogene*, vol. 30, no. 17, pp. 1984–1994, 2011.

Hindawi
Journal of Oncology
Volume 2019, Article ID 3253696, 11 pages
https://doi.org/10.1155/2019/3253696

Research Article

Use of Antimetastatic SOD3-Mimetic Albumin as a Primer in Triple Negative Breast Cancer

Shanta M. Messerli,[1] Amanda M. Schaefer,[1] Yongxian Zhuang,[1] Bohdan J. Soltys,[2] Noah Keime,[1] Jenny Jin,[1] Li Ma,[3] Carleton J. C. Hsia,[2] and W. Keith Miskimins[1]

[1]*Cancer Biology and Immunotherapies, Sanford Research, Sioux Falls, 57104 SD, USA*
[2]*AntiRadical Therapeutics LLC, Sioux Falls, 57104 SD, USA*
[3]*Department of Physics, Georgia Southern University, Statesboro, GA 30460, USA*

Correspondence should be addressed to Carleton J. C. Hsia; cjchsia@yahoo.com
and W. Keith Miskimins; keith.miskimins@sanfordhealth.org

Received 8 September 2018; Accepted 30 December 2018; Published 28 February 2019

Guest Editor: Wei-Ting Chao

Of the deaths attributed to cancer, 90% are due to metastasis. Treatments that prevent or cure metastasis remain elusive. Low expression of extracellular superoxide dismutase (EcSOD or SOD3) has been associated with poor outcomes and increased metastatic potential in multiple types of cancer. Here, we characterize the antimetastatic therapeutic mechanisms of a macromolecular extracellular SOD3-mimetic polynitroxyl albumin (PNA, also known as VACNO). PNA is macromolecular human serum albumin conjugated with multiple nitroxide groups and acts as an SOD-mimetic. Here we show that PNA works as a SOD3-mimetic in a highly metastatic 4T1 mouse model of triple negative breast cancer (TNBC). *In vitro*, PNA dose dependently inhibited 4T1 proliferation, colony formation, and reactive oxygen species (ROS) formation. *In vivo*, PNA enhanced reperfusion time in the hypoxic cores of 4T1 tumors as measured by ultrasound imaging. Furthermore, PNA enhanced ultrasound signal intensity within the cores of the 4T1 tumors, indicating PNA can increase blood flow and blood volume within the hypoxic cores of tumors. Lung metastasis from 4T1 flank tumor was inhibited by PNA in the presence or absence of doxorubicin, a chemotherapy agent that produces superoxide and promotes metastasis. In a separate study, PNA increased the survival of mice with 4T1 flank tumors when used in conjunction with three standard chemotherapy drugs (paclitaxel, doxorubicin, and cyclophosphamide), as compared to treatment with chemotherapy alone. In this study, PNA-increased survival was also correlated with reduction of lung metastasis. These results support the hypothesis that PNA works through the inhibition of extracellular superoxide/ROS production leading to the conversion of 4T1 cells from a metastatic tumorigenic state to a cytostatic state. These findings support future clinical trials of PNA as an antimetastatic SOD3-mimetic drug to increase overall survival in TNBC patients.

1. Introduction

The development of antimetastatic drugs is urgently needed to reduce cancer-related deaths caused by metastasis [1]. In humans, metastasis accounts for up to 90% of all cancer-related deaths [2]. For breast cancer, triple negative breast cancer (TNBC) has the greatest chance of developing distant metastases, despite existing systemic therapy with radiation, chemotherapy, and immunotherapy [3]. As there are no currently available targeted therapies for this aggressive disease, we hypothesized that a new treatment which targets the overproduction of extracellular superoxide and its related reactive oxygen species (ROS) may have a major impact on survival of these patients [4, 5]. Due to the inadequacy of a single therapy to effectively eliminate tumors and prevent aggressive regrowth, alternative therapies that target the broader tumor microenvironment (TME) are also warranted. In this study, we examine the efficacy of PNA, an extracellular superoxide dismutase (EcSOD or SOD3) mimetic that was originally developed for ischemic stroke [6, 7]. In stroke, PNA is expected to increase the Golden Hour for treatment via its remarkable ability to treat both ischemic and hemorrhagic stroke safely without neuroimaging before thrombolytic therapy. PNA works by enhancing blood flow without oxidative

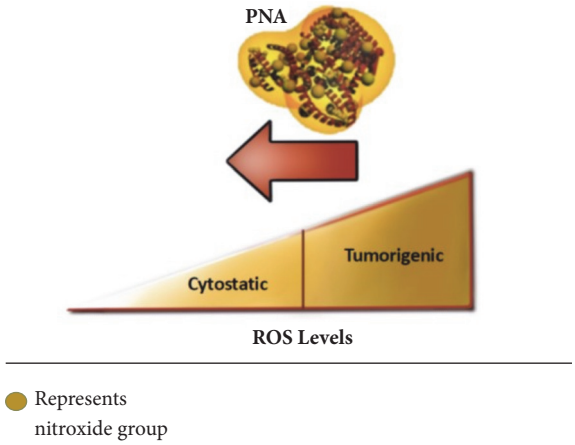

Figure 1: PNA is a human serum albumin that has been modified with multiple caged nitroxide groups. The nitroxide groups exhibit antioxidant activity and have the ability to catalytically remove superoxide in the vasculature and intracellular spaces. Tumors display elevated levels of reactive oxygen species that promote growth and metastasis. PNA is expected to reduce tumor ROS, leading to inhibitory effects on tumor growth, metabolism, and metastasis.

stress and serving as a neuroprotectant [8]. PNA is human serum albumin (HSA) that has been modified with multiple caged nitric oxide groups (Figure 1). With albumin as the carrier, PNA is distributed in the intravascular and lymph compartments to intercept metastasizing cancer cells. PNA targets the vasculature of the TME leading to the restoration of blood flow to the hypoxic tumor core, presumably through the removal of superoxide in the intravascular space. This TME activity is facilitated by the nitroxide groups that exhibit superoxide mimetic activities [6, 7, 9]. Thus, PNA has been demonstrated to catalytically dismutate superoxide in the vasculature and increase the bioavailability of endogenous nitric oxide (NO), leading to improved blood flow. Improved blood flow in tumors has been shown to reverse tumor hypoxia [10], leading to inhibitory effects on tumor growth, metabolism, and metastasis.

The design of PNA, consisting of a novel combination of a HSA and nitroxide as a metal-free superoxide dismutase (SOD3) mimetic, has advantages over small molecular weight and membrane permeable nitroxide that mimics SOD1, SOD2, and SOD3, in cancer therapy. Albumin has a number of characteristics that make it an attractive drug vehicle or *primer*, including the ability of the protein to carry hydrophobic drugs, such as paclitaxel, through the blood and deliver them directly to cancer cells [11]. With HSA as the carrier of the nitroxides, PNA is targeted to the vasculature to increase blood flow and is in equilibrium with the lymph system [7, 9]. The SOD3 mimetic activity of PNA can break down ROS, such as superoxide, and alter the ROS balance within cancer cells and the tumor microenvironment. ROS have been shown to be involved in several cellular processes including proliferation, growth, migration, and apoptosis [12]. In cancer cells, ROS plays a pivotal role in many signaling pathways involved in carcinogenesis and metastasis [13]. For example, increased extracellular superoxide radical has been associated with increased prostate cancer cell invasion [14]. Therefore, we hypothesize that the SOD mimetic activity of the nitroxide groups on PNA will reduce the metastatic phenotype of the tumors, as well as decrease the formation of new cancer cells.

The cores of tumors are often chronically hypoxic, which is closely associated with a negative prognosis and a metastatic phenotype which is more resistant to cancer therapy [15, 16]. By targeting the hypoxic core of primary and metastatic sites, PNA may act to enhance blood flow and improve the therapeutic effects of standard chemotherapy, radiotherapy, and/or immunotherapy.

Recently, it was discovered that deficiency in EcSOD or SOD3 is involved in metastasis of multiple cancer types including TNBC and pancreatic cancer [4]. It is also established that, in the tumorigenic state, the levels of superoxide radicals in the TME are elevated [17–20]. Therefore, a SOD3 mimetic, like PNA, may be suitable as a targeted therapy to replace the deficient SOD3 in cancer cells. The data reported here provides support for this hypothesis in a highly metastatic mouse 4T1 TNBC model.

In this study we demonstrate that PNA inhibits metastasis leading to improved overall survival in a highly metastatic murine model of TNBC. The mechanisms involved in this process are as follows: (1) removal of superoxide and its related ROS of cancer cells; (2) improvement in blood flow to the tumor hypoxic core; (3) reversal of metastasis induced by the superoxide producing chemotherapeutic drug, e.g., doxorubicin; (4) extension of survival when used conjunctively with three standard conjunctive chemotherapeutic drugs with concomitant inhibition of metastasis to the lung.

2. Materials and Methods

2.1. Cell Culture. The mouse mammary carcinoma line 4T1 was purchased from ATCC and used within 5 passages. Cells were cultured in DMEM with 10% fetal bovine serum (FBS), penicillin/streptomycin solution, and amphotericin and incubated at 37°C in 5% CO2. For the SYTOX® Green (ThermoScientific) cell proliferation assay, 4T1 cells were plated in 96-well plates and allowed to attach overnight before being treated with HSA or PNA at indicated concentrations in triplicate. After 72 hr of treatment, cells were stained with 20 μM SYTOX® Green for 15 min. and dead cells' fluorescence was measured in a Spectromax M5 plate reader (Molecular Devices) at excitation/emission 485/530 with a 515 emission cutoff. Then the cells were permeabilized by addition of 6 % Triton-X for 30 min, and total cell fluorescence was measured at excitation/emission 485/530 with a 515-emission cutoff. Data is representative of three independent experiments.

For the colony assays, 4T1 cells were plated at 250 cells per well in a Corning® 6-well plate. After 24 hours, the cells were treated in triplicate with the indicated concentration of PNA or HSA. After 5 days of treatment, cells were washed with PBS and fixed with 70% ethanol for 5 minutes. Colonies were washed again with PBS and then stained with Coomassie Blue [40% methanol, 12% glacial acetic acid, and 0.24% Coomassie Blue]. This was followed by another wash, and then the plates

were imaged using an AlphaImager System. Colony number and size were analyzed using AlphaImager System image analysis software (AlphaInnotech, Santa Clara, CA).

2.2. Flow Cytometry. The production of ROS was detected by using the dye 2',7'-dichlorofluorescein diacetate (DCF-DA), a cell-permeant indicator for reactive oxygen species. DCF is used as a qualitative marker for cellular oxidant stress rather than a marker for specific ROS [21]. 4T1 cells were treated with PNA or HSA at concentrations ranging from 30 to 120 μM for 16-18 hours and then stained with DCF-DA (10 μM). DCF fluorescence was measured using BD C sampler software on the Accuri C6 Flow Cytometer (BD Biosciences).

2.3. Polynitroxyl Albumin. Polynitroxylated albumin (PNA, aka Vascular Albumin with Caged Nitric Oxide or VACNO) is a drug product prepared as a sterile, nonpyrogenic preparation in saline solution. Each 100 mL PNA contains 20 g of injectable-grade human serum albumin (HSA) and 2.5 g of 4-(2-acetamido)-2,2,6,6-tetramethyl-1-piperidinyloxy (AcTPO) covalently attached to the albumin molecules with added stabilizers, including 0.08 moles of sodium caprylate and 0.08 moles of sodium acetyltryptophanate per gram of albumin.

2.4. Mouse Studies. Balb/c mice (Jackson Laboratory) between 4 and 6 weeks of age were maintained in a barrier facility on high efficiency particulate air (HEPA)-filtered racks. The animals were fed with autoclaved laboratory rodent diet (Envigo diet 2918). All animal studies were approved by the Sanford Institutional Animal Care and Use Committee and conducted in accordance with the principles and procedures outlined in the NIH Guide for the Care and Use of Animals.

4T1 cells (5 X 10^4) were injected subcutaneously into the hind limb of female Balb/c mice. In the first *in vivo* experiment examining how PNA affects metastasis, 60 mice were randomly divided into the following groups: PNA (12.5 ml/kg), control HSA (10%), doxorubicin (4 mg/kg, Sigma Aldrich), and doxorubicin (4 mg/kg) plus PNA (12.5 ml/kg). When tumors became palpable (4 days), intraperitoneal (i.p.) injections with PNA, control HSA, doxorubicin, or PNA plus doxorubicin were performed. PNA and HSA treatments were performed three times a week.

In the second *in vivo* 4T1 experiment, 50,000 4T1 cells were subcutaneously injected into Balb/c mice, and 45 mice were divided into the following groups: (1) control chemotherapy group (15 mice), (2) chemotherapy plus PNA delivered intraperitoneally (i.p.) (15 mice), and (3) chemotherapy plus PNA delivered intravenously (i.v.) (15 mice). When tumors became palpable (4 days), the groups received the following treatments: in weeks 1-2, control group received HSA combined with paclitaxel (60 mg/kg), paclitaxel (60 mg/kg) plus PNA delivered i.p., and paclitaxel plus PNA delivered i.v. and in weeks 3-4, the control group received HSA plus doxorubicin (4mg/kg) plus cyclophosphamide (100mg/kg). The experimental groups received doxorubicin, cyclophosphamide (100 mg/kg) and PNA delivered i.p. and doxorubicin, cyclophosphamide, and PNA delivered i.v. The paclitaxel, doxorubicin, and cyclophosphamide were administered once a week, and PNA and has were delivered 3 times a week.

Lung metastasis was quantified in 4T1 mice through injection of India ink into whole lungs via the trachea following sacrifice of the animals as described [22, 23]. The number of visible metastases was manually counted using a dissecting microscope (Nikon SMZ1000).

Quantification of necrotic areas of primary tumor sections was performed using stereology methodology. At the time of sacrifice, primary tumors were harvested, fixed in 10% buffered formalin, and paraffin embedded (FFPE). Tumors were sectioned to 5 μm. Hematoxylin and Eosin (H & E) staining was performed, and analysis of live and dead tissue on tumor sections was performed using Stereo Investigator software (version 10, Micro Bright Field; Williston, VT) by outlining areas of karyolysis indicated by reduced number of nuclei and increased eosin staining. Briefly, the tumor area was outlined, and a grid of counting frames was applied to systematically quantify across the entire tumor section. The area of live tumor tissue versus nonviable was calculated using the area fraction fractionator probe. Counting frames of 200 μm by 200 μm were placed over the tumor section with an average of 50 counting frames per tumor. Tumor tissue was defined as viable or necrotic and the corresponding area of each was calculated using the software package.

2.5. Ultrasound Measurement of Tumor Perfusion. The day prior to ultrasound imaging, a depilatory cream (Nair) was applied to skin on the tumor and surrounding regions to prevent interference with the ultrasound transducer. On the day of imaging, animals were anesthetized with 1.5% isoflurane in oxygen, placed on a heated stage, and restrained using surgical tape. Anesthesia was maintained during imaging using 1.5% isoflurane in oxygen administered via nose cone. Warmed ultrasound gel (Parker Laboratories) was applied to the depilated skin and ultrasound images were captured (Vevo2100; Visual Sonics).

To measure tumor vascularity, Color Doppler imaging was performed on 4T1 tumors 14 days after injection. Tumors had been treated starting 4 days after initiation with PNA or control HSA 3 times per week as described above. Color Doppler imaging was performed across the entire tumor using serial scans. After image-acquisition, the tumor was outlined on the serial scans and the volume was calculated and percent of vascularity within the outlined tumor was calculated by manufacturer's software (Visual Sonics).

To calculate tumor perfusion time following administration of PNA, a microbubble contrast agent (Vevo MicroMarker; Visual Sonics) was used. Tumors had been treated starting 4 days after initiation with PNA or control HSA 3 times per week as described above. Tumor perfusion studies were performed 16 days after tumor initiation. The following procedures were performed in addition to those mentioned above: a 27-gauge butterfly needle connected to a catheter was inserted via tail vein for intravenous injection of the microbubbles contrast agent. The microbubble contrast agent was prepared according to manufacturer instructions and a bolus injection of 50 μL was delivered via tail vein catheter flushed with 20-30 μL of saline. Perfusion of the

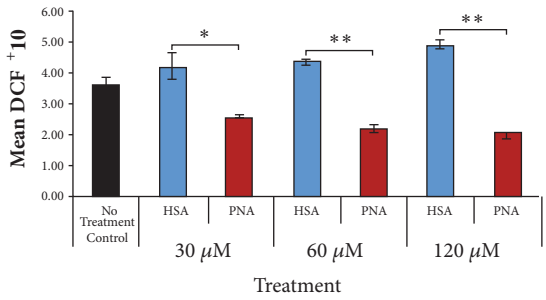

Figure 2: *Treatment with PNA reduces intracellular reactive oxygen species.* 4T1 cells were treated with PNA or corresponding concentration of control HSA for 16-18 hours and then stained with 2',7'-dichlorofluorescein diacetate and measured via flow cytometry. In the presence of reactive oxygen species (ROS), the dye is converted to the fluorescent molecule 2',7'-dichlorofluorescein (DCF) (n=3 for each group; data is representative of three independent experiments; $* = p < 0.05$, $** = p < 0.01$ versus HSA).

tumor microvasculature was calculated using manufacturer software (VevoCQ; Visual Sonics). A baseline perfusion prior to administration of PNA or control HSA was obtained. Following baseline acquisition, PNA (12.5 mL/kg) or control HSA (10%) were delivered via tail vein injection. Thirty minutes after drug injection, a second dose of microbubbles was administered and tumor perfusion was calculated as described above. Tumor perfusion following drug delivery was calculated by taking the 30-minute perfusion time minus the baseline perfusion time.

Statistics. Data is expressed as means ±SEM. P values were determined by paired student's t-tests.

3. Results

3.1. PNA Reduces Reactive Oxygen Species. The key property of PNA is its antioxidant activity, which is mediated by catalytic dismutation of superoxide and related ROS. We hypothesized that PNA treatment of tumor cells would reduce cellular ROS levels, leading to changes in growth and survival. To test this, cultured 4T1 cells were treated with PNA (30-120 μM) for 24 hours. Control cultures received the same concentrations of HSA, the protein component of PNA. Cellular ROS levels were estimated by staining cells with DCF-DA. At each concentration, 4T1 cells treated with PNA had significantly reduced ROS as compared to the corresponding control HSA treatment (Figure 2). Thus, PNA potentially shifts 4T1 cancer cells from a tumorigenic to a cytostatic state (see Figure 1).

3.2. PNA Treatment of Tumor-Bearing Animals Shows Reduced Tumor Perfusion Time and Increased Relative Blood Volume Compared to Control in a Breast Cancer Mouse Model. Our previous studies show that PNA promotes blood flow in animal models of cerebral ischemia, leading to significant reductions in infarct size [6, 7]. Similar findings have been found in cardiac ischemia reperfusion models [24]. This activity is mediated by dismutation of superoxide in blood vessels, preventing the formation of peroxynitrite and allowing the restoration of endogenous nitric oxide in the vasculature. We have recently reported that the restoration of blood flow by PNA in acute hypoxia arising in ischemia stroke also restores blood flow in chronic hypoxia in solid tumors [22]. PNA was shown to promote blood flow and drug delivery to hypoxic flank tumors in a xenograft tumor model using electron paramagnetic resonance (EPR) measurements [22]. To confirm that PNA is also effective in opening up the 4T1 TNBC flank hypoxic tumor core, we tested whether PNA increased tumor blood flow using ultrasound bursting and imaging techniques. Figure 3(a) shows ultrasound measurements demonstrating that PNA increased the perfusion rate of the hypoxic core of 4T1 flank tumors compared to the tail vein infusion of HSA. Figure 3(b) shows the reperfusion kinetics of the microbubble burst by the ultrasound. Figures 3(c) and 3(d) illustrate the difference of the perfusion volume of the flank tumor detected by the microbubble technique from tail vein infusion of HSA versus PNA, respectively. These ultrasound measurements together with the EPR measurements independently validated that the SOD3-mimetic activity PNA improves blood flow within the hypoxic core of two types of solid tumors.

3.3. PNA Is Cytotoxic and Inhibits Cancer Cell Proliferation in TNBC. It is well known that elevated levels of ROS are protumorigenic through activation of signaling pathways that promote cell proliferation, cell survival, and oncogenic transcriptional programs [12–14]. Since PNA reduces cancer cell ROS in 4T1 cells (Figure 2), we predicted that PNA would also reduce proliferation of 4T1 cells. In order to examine this hypothesis, PNA was tested *in vitro* in 4T1 mouse TNBC cell cultures. In this dose response study, cells were exposed for 72 hr to 30 μM, 60 μM, and 120 μM of PNA or corresponding concentrations of control HSA. Live and dead cell numbers were determined using a SYTOX® Green assay, and live cell number was then extrapolated from this data (Figure 4). PNA compared to HSA significantly reduced the number of live cells in a dose dependent manner (n=3 for each group, $**=p<0.001$; $***=p<0.0001$).

The effect of PNA on cell proliferation and survival was further examined in colony formation assays. 4T1 cells were studied for their ability to form colonies within 5 days in the presence of varying doses of PNA and HSA as in Figure 4. In Figure 5, colonies were stained and imaged, and the number and size of the colonies were quantified. There was a significant dose dependent decrease in the number (Figures 5(a) and 5(b), left panel) and size of colonies (Figures 5(a) and 5(b), right panel) in response to PNA compared to control HSA at concentrations ranging from 30 to 120 μM ($p < 0.001$). Results from Figures 4 and 5 suggest that PNA inhibited proliferation and colony formation of 4T1 cells by reducing the superoxide and ROS levels.

3.4. Small Molecule, Membrane Permeable Nitroxide Compound Affects 4T1 Growth and Survival Differently Compared to PNA. Macromolecular PNA is primarily extracellular and, therefore, is an EcSOD/SOD3 mimetic. TEMPOL (4-hydroxy-2,2,6,6-tetramethylpiperidine-N-oxyl), on the other hand, is a small molecule nitroxide that is membrane

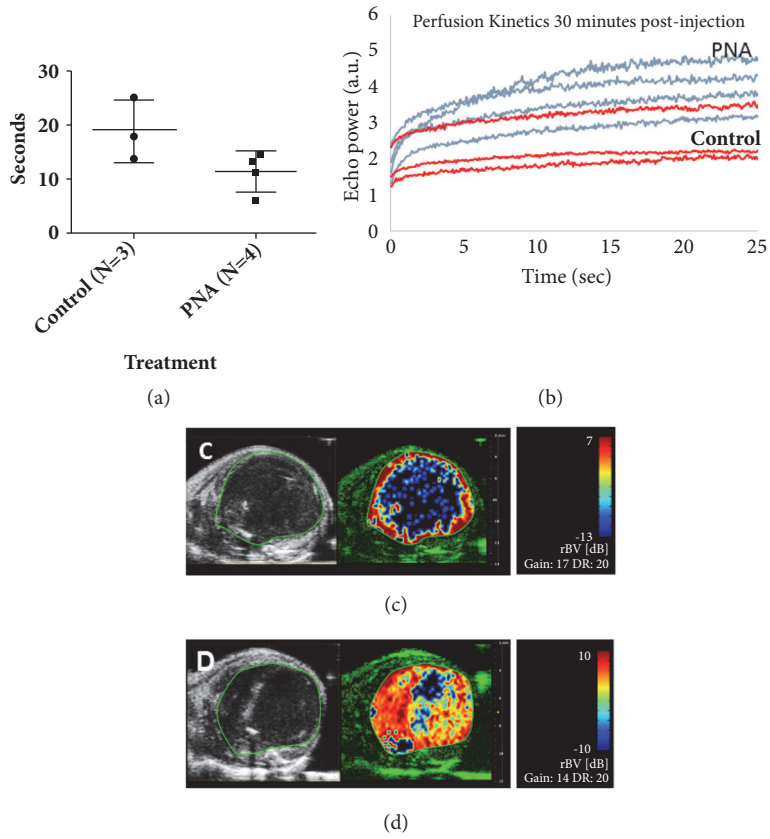

Figure 3: *PNA treated tumors have reduced tumor perfusion time and increased relative blood volume in the metastatic TNBC 4T1 model.* Ultrasound imaging was used to visualize tumor microvasculature. The contrast agent was administered intravenously, images were acquired, and perfusion time was calculated with manufacturer software. PNA or HSA control was administered intravenously. And after 30 minutes, a second dose of contrast agent was administered, and perfusion time was calculated. (a) PNA treated tumors have reduced tumor perfusion time compared to HSA control. Tumor perfusion time was calculated by taking the 30-minute perfusion time minus the baseline perfusion time. (b) The kinetics of perfusion as measured by echo power versus time indicate PNA treated tumors have higher echo power at peak perfusion time compared to HSA control, indicating increased blood flow within the tumor. (c) Tumors were outlined in ultrasound B-mode (left panel). Parametric imaging of relative blood volume is shown 30 minutes after drug injection at the time of peak perfusion (right panel). HSA treated tumors show little to no signal intensity in the core of the tumor. (d) PNA treated tumors show greater relative blood volume within the tumor core.

permeable, reaching all cellular compartments. A dose response study showed that TEMPOL significantly inhibits the 4T1 colony size, at concentrations ranging from 18 to 180 μM, suggesting cytostatic effects on the cancer cells (Figure 6(a)). However, the TEMPOL did not significantly reduce colony number (Figure 6(b)), suggesting a lack of cytotoxic effects on the cancer cells. These results indicate that PNA and small molecule, membrane permeable nitroxides have differences in their specificities and therapeutic indices.

Effects of PNA on 4T1 tumors in vivo. In vivo, 4T1 cells establish rapidly growing tumors that metastasize to lung, liver, bone, and brain [25]. Thus, they are a useful model of human TNBC. Subcutaneous 4T1 tumors were developed in Balb/c mice and treated with PNA or HSA as a control. Tumors from PNA treated mice were not significantly different in size from those of HSA treated animals. However, histological examination of tumors from both groups showed that PNA treated tumors had less live tissue and more necrotic (dead) tissue than the HSA treated controls (Figure 7(a)). The difference between control and PNA treated groups was approaching significance ($p = 0.0705$) but suggested that PNA is having a direct effect on primary tumors as well as on metastasis.

3.5. PNA Reduces Lung Metastasis from 4T1 Primary Tumors. Subcutaneous or orthotopic 4T1 tumors rapidly metastasize to distant tissues in a pattern similar to human TNBC, including metastasizing to the lung [25, 26]. We found that PNA reduced lung metastasis as compared to control HSA treatment but not to a level of significance (Figure 7(b), $p=0.056$). However, we found that there is a dramatic increase in metastasis to the lung induced by a superoxide producing chemotherapy drug doxorubicin (Figure 7(c)). Remarkably, in the presence of PNA and doxorubicin the lung metastasis was nearly abolished (Figure 7(c), paired two-tailed t test, $p=0.038$). This provides strong rationale for combining PNA with other drugs used in adjuvant or neoadjuvant therapy. In this regard, mice bearing 4T1 tumors were subjected to

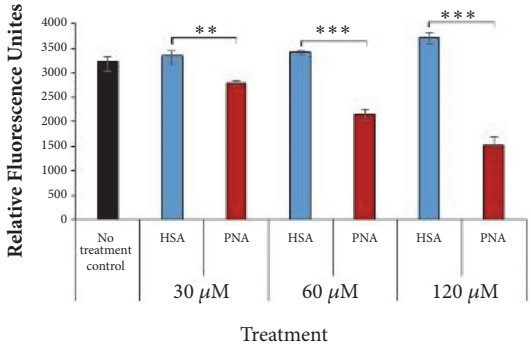

Figure 4: *PNA treatment significantly reduces live cell number.* 4T1 cells were plated and treated the following day with PNA (red bars) or HAS (blue bars), and control (black bar) was media only. After 72 hr, cells were stained with SYTOX® Green and fluorescence was measured. Percent of dead cells and percent of live cells were calculated using fluorescence values. Live cells' fluorescence is shown. Results indicate PNA, compared to HSA, reduces live cell numbers at concentrations ranging from 30 to 120 μM PNA (n=3 for each group; $**=p<0.01$, $***= p<0.001$).

a chemotherapy regimen including paclitaxel, doxorubicin, and cyclophosphamide, with or without PNA (Figure 8(a)). This regimen is similar to that in the I-SPY 2 clinical trials for breast cancer [27]. In this study, PNA again significantly decreased the number of lung metastases (paired t test with $p<0.01$). Furthermore, PNA enhanced overall survival of mice against chemotherapy-mediated toxicity in the 4T1 mouse model (Figure 8(b)). Statistical analysis using the Log-Rank (Mantel-Cox) test indicates a statistical difference between PNA and chemotherapy treated mice compared to HSA and chemotherapy treated mice, with $p<0.0013$. Together, these data demonstrate that PNA reduces metastasis in this triple negative breast cancer model and that this correlates with longer survival times. Thus, this indicates PNA conjunctive therapy with standard chemotherapeutic agents improves survival of 4T1 tumor bearing mice corresponding to a reduction in toxicity of the chemotherapeutic agent and a reduction in lung metastasis.

4. Discussion

Our findings demonstrate that the SOD3-mimetic activity of an extracellular albumin-based macromolecular nitroxide, PNA, converts cancer cells from a tumorigenic state to a cytostatic state by reducing superoxide and ROS levels (see Figure 1). Earlier we reported that PNA works as an SOD3 mimetic to alter the hypoxic state of a solid tumor through blood flow enhancement [28]. In this report we established that the same therapeutic mechanism for PNA also works in the 4T1 TNBC model. We were able to confirm that this action of PNA occurs within 30 minutes of i.v. infusion with two independent biophysical methods (EPR and ultrasound).

Our data suggest that PNA is cytotoxic to murine 4T1 TNBC cells as well as inhibiting their proliferation. In colony forming assays, PNA reduced the number of colonies, suggesting an effect of PNA on the clonogenic survival capacity of cells. PNA also reduced the size of the colonies, indicating reduced ability of the cancer cells to proliferate. More importantly, we have demonstrated that PNA inhibits metastasis, particularly that induced by chemotherapeutic drugs such as doxorubicin, leading to enhanced survival (Figures 7 and 8). We discuss below the significance of the current results for future preclinical and clinical studies that can guide the development of PNA as a *primer* used in conjunction with standard cancer therapies. Thus, our preclinical studies may be relevant to neoadjuvant treatment and to clinical trials such as the I-SPY2 trials [27].

Two key aspects of PNA facilitate its biological activities. First, it catalyzes the dismutation of superoxide by virtue of the multiple covalently attached nitroxide groups. Second, it is based on a macromolecule carrier, HSA, which is capable of targeting extracellular compartments. These properties of PNA are expected to create an essentially superoxide-free milieu within the vasculature and within the tumor microenvironment. In the vasculature, elimination of superoxide prevents the formation of peroxynitrite through its reaction with NO. This allows the restoration of endogenous NO to promote blood flow to the metastasized solid tumor. This is supported by our published studies that demonstrate PNA mediation of increased blood flow and prevention of ischemic reperfusion injury in models of stroke, myocardial infarction, and sickle cell disease [6, 29].

Enhanced blood flow, as shown here and in our previous study [28], is likely to have a number of effects on solid tumors. It is expected to increase oxygen delivery to tumor cells, which would likely reverse hypoxia leading to inactivation of hypoxia inducible factor 1α. This in turn would alter tumor metabolism and growth, as well as several aspects of metastasis including angiogenesis, migration, invasion, and intravasation [30].

PNA reduces cellular ROS in 4T1 breast cancer cell cultures and we have shown that this corresponds to reduced cell proliferation and survival. Because PNA is based on HSA, it is expected to target extracellular spaces within the tumor microenvironment. We did not observe reduced 4T1 tumor sizes in mice treated with PNA. However, the tumors did have reduced amount of live tissue (Figure 7(a)) and increased areas of noncellular or necrotic tissue (not shown), indicating that the drug was directly acting on the tumor. PNA in the extravascular spaces within the tumor microenvironment is expected to reduce tumor superoxide and ROS levels and this may directly lead to interference with metastasis. For example, ROS are able to directly activate matrix metalloproteinases (MMPs) [31]. MMPs are key effectors of tumor invasion and metastasis through degradation of extracellular matrix components. Therefore, PNA may directly interfere with metastasis by blocking MMP activation by eliminating superoxide within the tumor microenvironment. This proposed mechanism may also relate to the effects of doxorubicin and other chemotherapy reagents on metastasis. For example, we found that doxorubicin increases the number of lung metastases compared to control mice, and this was reversed by PNA. This is consistent with other studies showing doxorubicin-induced increases in metastasis in mouse models and human patients [32, 33]. Many chemotherapy

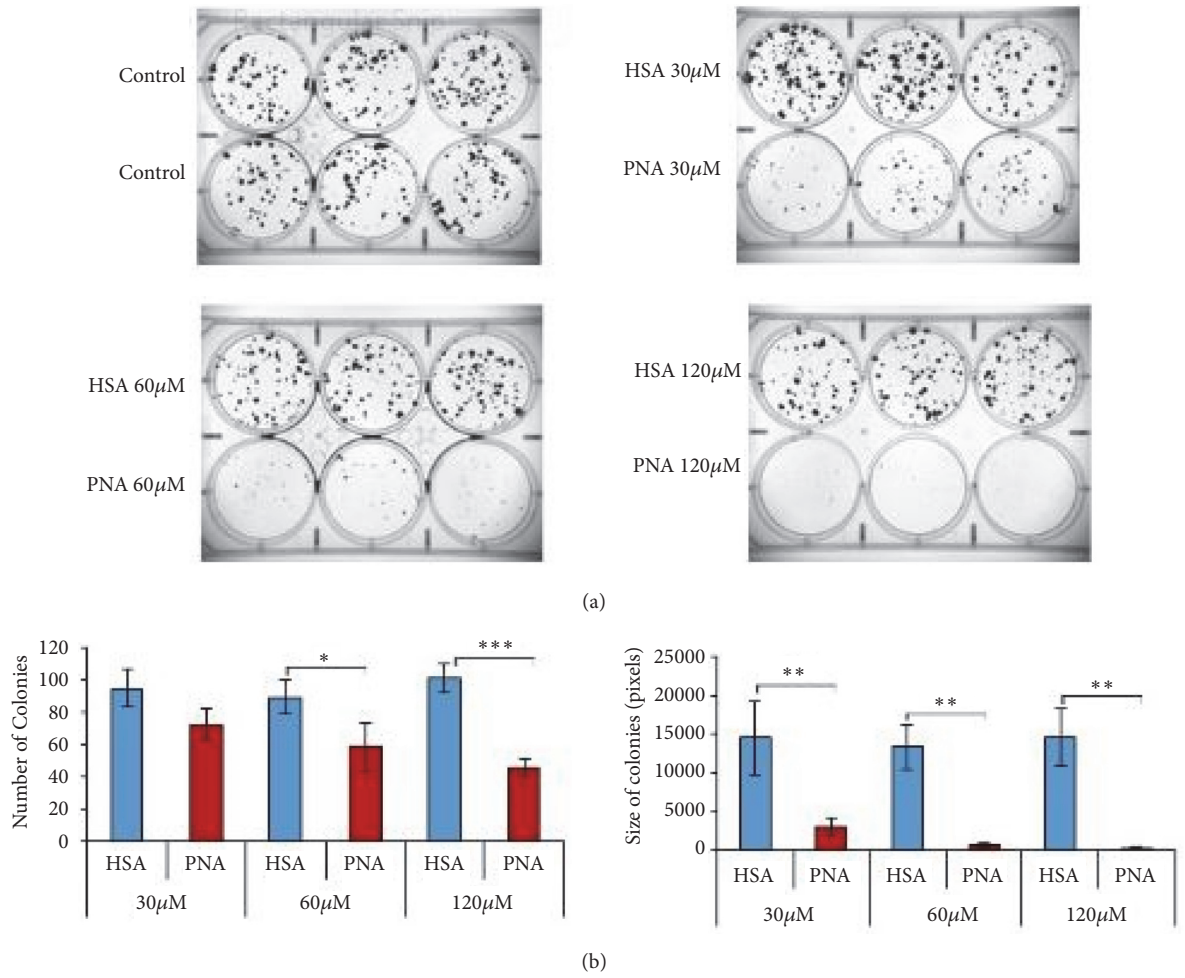

Figure 5: *PNA treatment significantly reduces TNBC cancer cell proliferation*. Colony forming assays were performed in PNA treated 4T1 cell cultures. Cells were plated at low density and then treated with the indicated concentration of PNA (red bars) or HSA (blue bars) as a control. PNA significantly reduces number of colonies compared to HSA treatments (a) and size of colonies (b). n=3 per group; data is representative of three independent experiments (∗ = $p < 0.05$, ∗∗ = $p < 0.01$, and ∗ ∗ ∗ = $p < 0.001$ versus HSA).

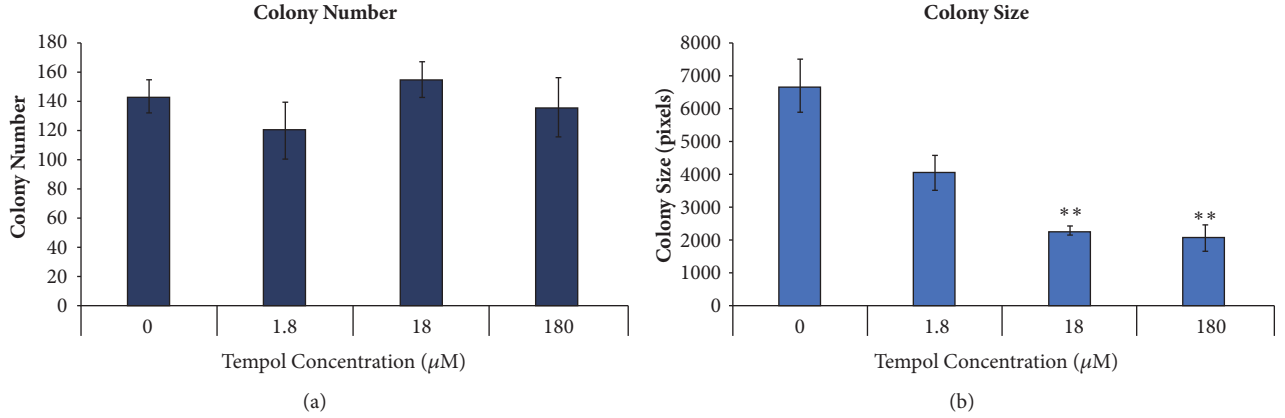

Figure 6: *TEMPOL produces significant decreases in colony size but not colony number.* 4T1 cells were plated at low cell number and treated the following day with TEMPOL at varying concentrations, and the control was DMEM alone. After 5 days, cells were fixed, stained, and imaged using Alpha Imager software. (a) Colony number was counted and (b) total colony size was measured using Alpha Imager software. Data shown suggests that TEMPOL alone inhibits cellular proliferation at concentrations ranging from 18 to 180 μM, according to a two-tailed t test, with $p < 0.001$, but is not significantly cytotoxic at the concentrations shown.

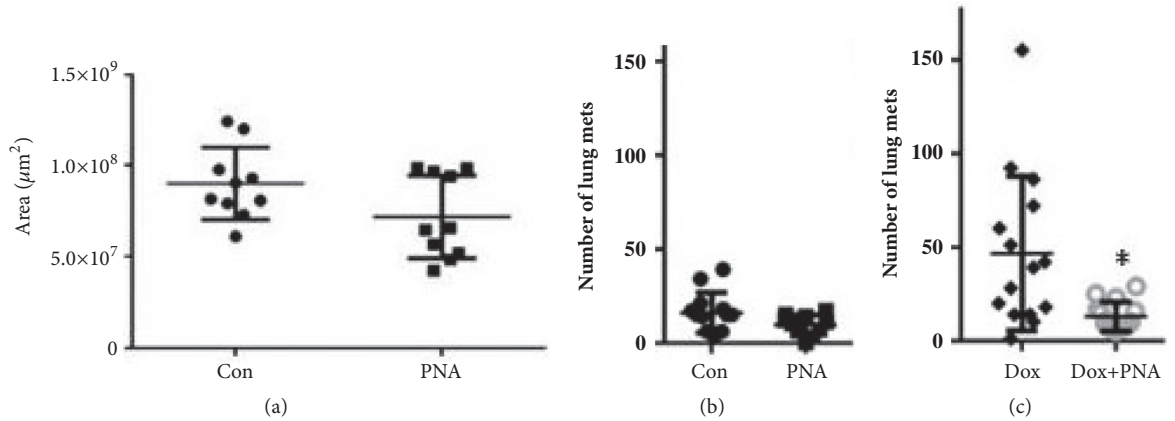

Figure 7: *Live tumor area and number of metastatic lung nodules decreases with PNA treatment while survival increases with PNA treatment.* (a) Subcutaneous 4T1 tumors are treated with HSA (control) or PNA. Tumors sections were stained by H&E and live tissue area was determined by stereology. (b) Tumor bearing mice were treated with or without PNA and after 3 weeks lungs were harvested for counting lung metastatic nodules. (c) 4T1 tumor bearing mice were treated with doxorubicin in the presence or absence of PNA. PNA combined with doxorubicin compared to doxorubicin alone significantly reduces lung metastasis, according to a paired two-tailed t test, $p < 0.05$ (∗).

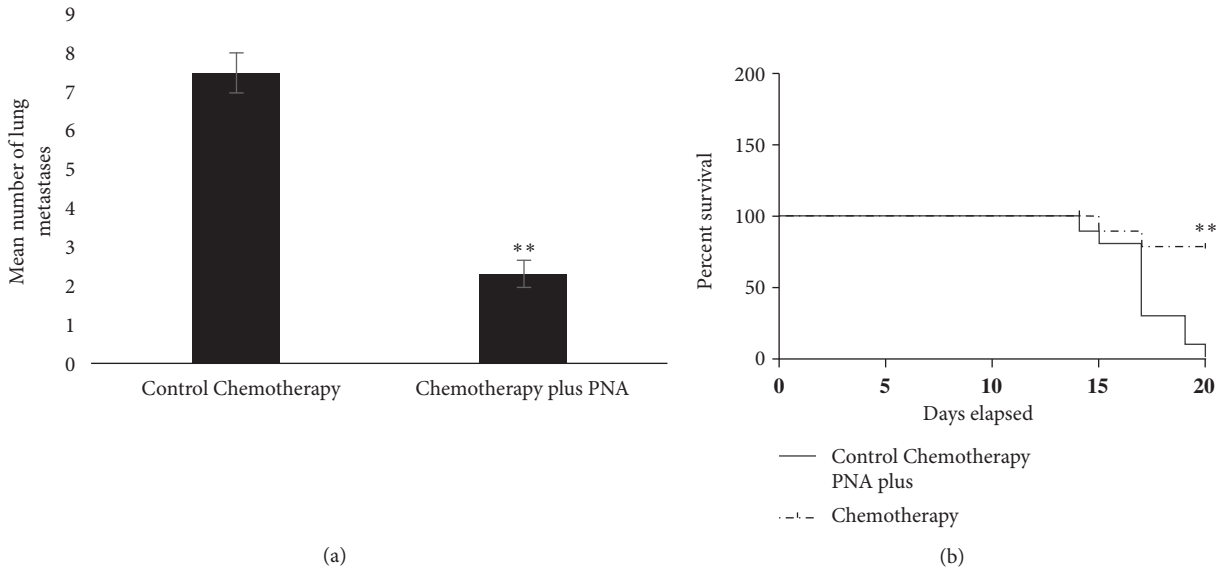

Figure 8: *PNA treatment combined with chemotherapy reduces lung metastasis and enhances survival of mice carrying 4T1 tumors compared to chemotherapy treatment alone.* (a) Tumor bearing mice were treated with a chemotherapy regimen, with and without PNA, and after 3 weeks lungs were harvested for counting metastatic lung nodules. PNA in the presence of chemotherapy significantly reduced lung metastases compared to chemotherapy alone, according to a paired two-tailed t test, $p > 0.01$. (b) PNA combined with chemotherapy significantly increased overall survival of mice compared to chemotherapy alone, according to the Log-Rank (Mantel-Cox) test, with p value =.0013 (∗∗).

agents, including doxorubicin, increase tumor superoxide and ROS, which is associated with the process of metastasis. We show that PNA eliminates the increase in metastasis associated with chemotherapy. This is most likely related to the ability of PNA to eliminate superoxide and ROS in the tumor microenvironment.

Since our experimental design has been to inject PNA into the intraperitoneal cavity, the subsequent biodistribution of PNA warrants consideration. The overall biodistribution of PNA in our studies is expected to be similar to endogenous serum albumin since PNA consists of macromolecular human serum albumin conjugated with multiple nitroxide groups to provide the SOD mimetic activity. Endogenous albumin is mainly synthesized in the liver, enters the circulation, and occurs predominantly in the extravascular space in tissues such as skin, gut, muscle, and other fluids such as cerebrospinal fluid. A substantial amount of albumin is also found within the intravascular space, but only a very small amount is thought to exist intracellularly [34–36]. In our studies, after injection into the intraperitoneal space, PNA is expected to enter the circulation via the lymphatic system and be distributed similarly to endogenous albumin. Imaging studies confirm that fluorescent albumin injected into the intraperitoneal space distributes maximally to the spleen, livers, lungs, and other organs within 3 hrs of injection; levels subsequently decline [37]. Endogenous albumin cycles

through the lymphatic system approximately 28 times during its lifetime (Peters, 1996; Evans, 2002) and injected PNA is expected to behave similarly. More importantly, PNA is not expected to accumulate significantly intracellularly in vivo, similar to endogenous albumin. Thus, the activity of PNA is most similar to ecSOD/SOD3, which is also localized extracellularly.

The intraperitoneal administration of PNA may have two effects. First, PNA would remove extracellular superoxide in all bodily compartments working as EcSOD/SOD3 with minimal effect on the intracellular superoxide levels controlled by SOD1 and SOD2. In contrast a low molecular weight nitroxide chemical like TEMPOL would dismutate both intracellular and extracellular superoxide because it readily crosses membranes and accumulates within cells (Figure 6). Second, it has been known for over four decades that the lymphatics are the first site of metastasis for most solid cancers and there has been a concerted effort in trying to target cancer therapeutics to the lymphatic system (e.g., see [38]). Accumulation of PNA in the lymph nodes and surrounding lymphatics is a possibility and may affect immune cells and metastasis. The possible immunodulatory effects on metastasis by PNA will be evaluated in future studies.

As a macromolecule with multiple nitroxide groups, PNA acts as an SOD3 mimetic. SOD3 (aka EcSOD) is secreted from cells and is found either free in the extracellular space or adhered to the surface of cells. SOD3 expression is frequently diminished in breast and other types of cancer, which contributes to metastasis [4]. Furthermore, low expression of SOD3 in breast cancer is associated with reduced relapse free survival in all types of breast cancer [4]. Overexpression of SOD3 in a human breast cancer xenograft or in the 4T1 syngeneic model led to reduced lung metastasis and longer survival [39, 40].

Taken together, PNA appears to be capable of acting as an SOD3 mimetic to alter the oxidative state within solid tumors, inhibiting their ability to metastasize (see Figure 1). We speculate that elimination of superoxide within the tumor microenvironment directly reverses ROS stimulated metastasis by preventing activation of MMPs, reducing invasion, and inhibiting cancer cell proliferation. PNA enhancement of blood flow is expected to reverse solid tumor hypoxia leading to changes in tumor metabolism and hypoxia-dependent metastatic events. Another potential outcome of increased blood flow in tumors is to act as a *primer* to improve drug delivery to tumors to enhance the therapeutic index of chemotherapy and immunotherapy. An additional advantage of PNA treatment of cancer may be attributable to its ability to protect normal tissues from oxidative stress and inflammatory injuries leading to better quality of life. We have previously demonstrated the ability of PNA to prevent ischemic reperfusion injury, to reduce inflammatory injuries, and to protect normal tissue from ionizing radiation [7, 29]. In the present TNBC studies, we have observed that PNA prevents weight loss promoted by the chemotherapy drug doxorubicin (not shown), suggesting that PNA has protective effects in normal tissues. Ongoing studies are exploring this aspect of PNA as well as the detailed mechanism by which it inhibits metastasis, as well as its effectiveness in other types of solid tumors. As a novel SOD mimetic drug, PNA would be ideally suited for evaluation in trials like the I-SPY 2 platform [27] and FDA breakthrough therapy designation (BTD) to bring PNA from bench to bedside in 3-5 years.

5. Conclusions

PNA reduces ROS in TNBC, is cytotoxic, and is cytostatic to mouse TNBC breast cancer cells in a dose dependent manner. PNA combined with doxorubicin, compared to doxorubicin alone, significantly reduces lung metastasis in a mouse model of breast cancer. Furthermore, PNA reduces metastasis and enhances survival of mice against chemotherapy-mediated toxicity in a 4T1 mouse breast cancer model. These *in vitro* and *in vivo* experimental findings suggest PNA is a promising cancer therapeutic. The antimetastatic mechanism of the SOD3-mimetic PNA on a murine TNBC 4T1 mouse model has been established. If the same antimetastatic mechanisms can be established with a human TNBC mouse model, these preclinical efficacy data will guide a Phase 1b clinical protocol design in recurrent TNBC patients. In addition, PNA could be tested in trials like the I-SPY2 fast track clinical trial protocol to select and graduate new drug candidates through FDA breakthrough therapy designation (BTD).

Data Availability

The data used to support the findings of this study are included within the article.

Conflicts of Interest

Shanta M. Messerli, Amanda M. Schaefer, Yongxian Zhuang, Noah Keime, Jenny Jin, Li Ma, Bohdan J. Soltys, and W. Keith Miskimins declare no conflicts of interest. Carleton J. C. Hsia is sole proprietor with AntiRadical Therapeutics.

Acknowledgments

This research was supported by the National Institutes of Cancer (1R01CA180033-04; W. Keith Miskimins), the National Institute of General Medical Sciences (CoBRE Grant P20GM103548; W. Keith Miskimins), the COBRE P20GM103548P20 Pilot grant (Project lead-Shanta M. Messerli), Sanford Research, and project seed funds from the state of South Dakota.

References

[1] M. Mark Taketo, "Reflections on the spread of metastasis to cancer prevention," *Cancer Prevention Research*, vol. 4, no. 3, pp. 324–328, 2011.

[2] T. N. Seyfried and L. C. Huysentruyt, "On the origin of cancer metastasis," *Critical Reviews in Oncogenesis*, vol. 18, no. 1-2, pp. 43–73, 2013.

[3] D. P. Saraiva, M. Guadalupe Cabral, A. Jacinto, and S. Braga, "How many diseases is triple negative breast cancer: The

protagonism of the immune microenvironment," *ESMO Open*, vol. 2, no. 4, Article ID e000208, 2017.

[4] B. Griess, E. Tom, F. Domann, and M. Teoh-Fitzgerald, "Extracellular superoxide dismutase and its role in cancer," *Free Radical Biology & Medicine*, vol. 112, pp. 464–479, 2017.

[5] W. Li, L. Cao, L. Han, Q. Xu, and Q. Ma, "Superoxide dismutase promotes the epithelial-mesenchymal transition of pancreatic cancer cells via activation of the H_2O_2/ERK/NF-kappaB axi," *International Journal of Oncology*, vol. 46, no. 6, pp. 2613–2620, 2015.

[6] C. Beaulieu, E. Busch, J. Röther, A. de Crespigny, C. J. Hsia, and M. E. Moseley, "Polynitroxyl albumin reduces infarct size in transient focal cerebral ischemia in the rat: potential mechanisms studied by magnetic resonance imaging," *Journal of Cerebral Blood Flow & Metabolism*, vol. 18, no. 9, pp. 1022–1031, 2016.

[7] T. Sugawara, F. Yu, L. Ma, C. J. C. Hsia, and P. H. Chan, "Delayed treatment with polynitroxyl albumin reduces infarct size after stroke in rats," *NeuroReport*, vol. 12, no. 16, pp. 3609–3612, 2001.

[8] M. D. Manole, P. M. Kochanek, L. M. Foley et al., "Polynitroxyl albumin and albumin therapy after pediatric asphyxial cardiac arrest: Effects on cerebral blood flow and neurologic outcome," *Journal of Cerebral Blood Flow & Metabolism*, vol. 32, no. 3, pp. 560–569, 2012.

[9] P. Kuppusamy, P. Wang, J. L. Zweier et al., "Electron paramagnetic resonance imaging of rat heart with nitroxide and polynitroxyl-albumin," *Biochemistry*, vol. 35, no. 22, pp. 7051–7057, 1996.

[10] D. Fukumura and R. K. Jain, "Tumor microvasculature and microenvironment: targets for anti-angiogenesis and normalization," *Microvascular Research*, vol. 74, no. 2-3, pp. 72–84, 2007.

[11] G. Stehle, H. Sinn, A. Wunder et al., "Plasma protein (albumin) catabolism by the tumor itself - Implications for tumor metabolism and the genesis of cachexia," *Critical Review in Oncology/Hematology*, vol. 26, no. 2, pp. 77–100, 1997.

[12] K. Brieger, S. Schiavone, F. J. Miller Jr., and K.-H. Krause, "Reactive oxygen species: from health to disease," *Swiss Medical Weekly*, vol. 142, Article ID w13659, 2012.

[13] P. Storz, "Reactive oxygen species in tumor progression," *Frontiers in Bioscience*, vol. 10, no. 2, pp. 1881–1896, 2005.

[14] L. Chaiswing, W. Zhong, J. J. Cullen, L. W. Oberley, and T. D. Oberley, "Extracellular redox state regulates features associated with prostate cancer cell invasion," *Cancer Research*, vol. 68, no. 14, pp. 5820–5826, 2008.

[15] D. R. Grimes, C. Kelly, K. Bloch, and M. Partridge, "A method for estimating the oxygen consumption rate in multicellular tumour spheroids," *Journal of the Royal Society Interface*, vol. 11, no. 92, Article ID 20131124, 2014.

[16] J. Zhang, J. Zhang, S. Xu et al., "Hypoxia-Induced TPM2 methylation is associated with chemoresistance and poor prognosis in breast cancer," *Cellular Physiology and Biochemistry*, vol. 45, no. 2, pp. 692–705, 2018.

[17] P. A. Cerutti, "Prooxidant states and tumor promotion," *Science*, vol. 227, no. 4685, pp. 375–381, 1985.

[18] J. A. Cook, D. Gius, D. A. Wink, M. C. Krishna, A. Russo, and J. B. Mitchell, "Oxidative stress, redox, and the tumor microenvironment," *Seminars in Radiation Oncology*, vol. 14, no. 3, pp. 259–266, 2004.

[19] A. J. Montero and J. Jassem, "Cellular redox pathways as a therapeutic target in the treatment of cancer," *Drugs*, vol. 71, no. 11, pp. 1385–1396, 2011.

[20] J. G. Wilkes, M. S. Alexander, and J. J. Cullen, "Superoxide dismutases in pancreatic cancer," *Antioxidants*, vol. 6, no. 3, 2017.

[21] X. Chen, Z. Zhong, Z. Xu, L. Chen, and Y. Wang, "2′,7′-Dichlorodihydrofluorescein as a fluorescent probe for reactive oxygen species measurement: Forty years of application and controversy," *Free Radical Research*, vol. 44, no. 6, pp. 587–604, 2010.

[22] P. M. Anderson, B. R. Blazar, F. H. Bach, and A. C. Ochoa, "Anti-CD3 + IL-2-stimulated murine killer cells. In vitro generation and in vivo antitumor activity," *The Journal of Immunology*, vol. 142, no. 4, pp. 1383–1394, 1989.

[23] S. Miretti, I. Roato, R. Taulli et al., "A mouse model of pulmonary metastasis from spontaneous osteosarcoma monitored in vivo by luciferase imaging," *PLoS ONE*, vol. 3, no. 3, Article ID e1828, 2008.

[24] H. Li, L. Ma, C. J. C. Hsia, J. L. Zweier, and P. Kuppusamy, "Polynitroxyl-albumin (PNA) enhances myocardial infarction therapeutic effect of Tempol in rat hearts subjected to regional ischemia-reperfusion," *Free Radical Biology & Medicine*, vol. 32, no. 8, pp. 712–719, 2002.

[25] F. R. Miller, B. E. Miller, and G. H. Heppner, "Characterization of metastatic heterogeneity among subpopulations of a single mouse mammary tumor: heterogeneity in phenotypic stability," *Invasion and Metastasis*, vol. 3, no. 1, pp. 22–31, 1983.

[26] C. J. Aslakson, J. W. Rak, B. E. Miller, and F. R. Miller, "Differential influence of organ site on three subpopulations of a single mouse mammary tumor at two distinct steps in metastasis," *International Journal of Cancer*, vol. 47, no. 3, pp. 466–472, 1991.

[27] A. DeMichele, D. A. Berry, J. Zujewski et al., "Developing safety criteria for introducing new agents into neoadjuvant trials," *Clinical Cancer Research*, vol. 19, no. 11, pp. 2817–2823, 2013.

[28] C. J. Hsia and W. K. Miskimins, "Can macromolecular nitroxide work as extracellular superoxide dismutase mimetic in cancer and stroke therapy?" *Cell Biochemistry and Biophysics*, vol. 76, no. 4, pp. 443-444, 2018.

[29] H. Mahaseth, G. M. Vercellotti, T. E. Welch et al., "Polynitroxyl albumin inhibits inflammation and vasoocclusion in transgenic sickle mice," *Journal of Laboratory and Clinical Medicine*, vol. 145, no. 4, pp. 204–211, 2005.

[30] A. R. Nobre, D. Entenberg, Y. Wang, J. Condeelis, and J. A. Aguirre-Ghiso, "The different routes to metastasis via hypoxia-regulated programs," *Trends in Cell Biology*, vol. 28, no. 11, pp. 941–956, 2018.

[31] K. K. Nelson and J. A. Melendez, "Mitochondrial redox control of matrix metalloproteinases," *Free Radical Biology & Medicine*, vol. 37, no. 6, pp. 768–784, 2004.

[32] G. S. Karagiannis, J. M. Pastoriza, Y. Wang et al., "Neoadjuvant chemotherapy induces breast cancer metastasis through a TMEM-mediated mechanism," *Science Translational Medicine*, vol. 9, no. 397, 2017.

[33] D. Vyas, G. Laput, and A. K. Vyas, "Chemotherapy-enhanced inflammation may lead to the failure of therapy and metastasis," *OncoTargets and Therapy*, vol. 7, pp. 1015–1023, 2014.

[34] T. W. Evans, "Review article: albumin as a drug—biological effects of albumin unrelated to oncotic pressure," *Alimentary Pharmacology and Therapeutics*, vol. 16, 5, pp. 6–11, 2002.

[35] A. M. Merlot, D. S. Kalinowski, and D. R. Richardson, "Unraveling the mysteries of serum albumin-more than just a serum protein," *Frontiers in Physiology*, vol. 5, article 299, 2014.

[36] T. Peters, *All about Albumin: Biochemistry, Genetics, and Medical Applicatins*, Academic Press Limited, San Diego, Calif, USA, 1996.

[37] G. Kijanka, M. Prokopowicz, H. Schellekens, and V. Brinks, "Influence of aggregation and route of injection on the biodistribution of mouse serum albumin," *PLoS ONE*, vol. 9, no. 1, Article ID e85281, 2014.

[38] Y. Xie, T. R. Bagby, M. S. Cohen, and M. L. Forrest, "Drug delivery to the lymphatic system: Importance in future cancer diagnosis and therapies," *Expert Opinion on Drug Delivery*, vol. 6, no. 8, pp. 785–792, 2009.

[39] M. L. T. Teoh, M. P. Fitzgerald, L. W. Oberley, and F. E. Domann, "Overexpression of extracellular superoxide dismutase attenuates heparanase expression and inhibits breast carcinoma cell growth and invasion," *Cancer Research*, vol. 69, no. 15, pp. 6355–6363, 2009.

[40] M. L. Teoh-Fitzgerald, M. P. Fitzgerald, W. Zhong, R. W. Askeland, and F. E. Domann, "Epigenetic reprogramming governs EcSOD expression during human mammary epithelial cell differentiation, tumorigenesis and metastasis," *Oncogene*, vol. 33, no. 3, pp. 358–368, 2014.

Hindawi
Journal of Oncology
Volume 2019, Article ID 6280347, 6 pages
https://doi.org/10.1155/2019/6280347

Review Article

Liver Metastases and Histological Growth Patterns: Biological Behavior and Potential Clinical Implications—Another Path to Individualized Medicine?

Rui Caetano Oliveira,[1,2,3] **Henrique Alexandrino**,[3,4,5] **Maria Augusta Cipriano**,[1] **and José Guilherme Tralhão**[2,3,4,5]

[1]*Pathology Department, Centro Hospitalar e Univeristário de Coimbra, 3000-075, Coimbra, Portugal*
[2]*Biophysics Institute, Faculty of Medicine, University of Coimbra, 3000-548 Coimbra, Portugal*
[3]*Coimbra Institute for Clinical and Biomedical Research (iCBR) area of Environment Genetics and Oncobiology (CIMAGO), Faculty of Medicine, University of Coimbra, 3000-548 Coimbra, Portugal*
[4]*Surgery Department, Centro Hospitalar e Universitário de Coimbra, 3000-075, Coimbra, Portugal*
[5]*Faculty of Medicine, University of Coimbra, 3000-548, Coimbra, Portugal*

Correspondence should be addressed to Rui Caetano Oliveira; ruipedrocoliveira@hotmail.com

Received 3 August 2018; Revised 24 December 2018; Accepted 12 February 2019; Published 25 February 2019

Academic Editor: Akira Hara

Colorectal cancer is a major health burden and despite the recent advances in healthcare and screening programs, a great percentage of patients already present metastases once their disease is found. In those cases, liver surgery has an essential role, but even with neoadjuvant chemotherapy there is a high rate of intrahepatic recurrence. New prognostic factors are needed in order to decide the best surgical approach considering the biological behavior of the tumors in order to tailor the used therapies, moving towards individualized medicine/treatment. However, the majority of the factors described in literature are expensive, time consuming, and difficult to apply on a daily basis. Histological growth patterns have emerged over the past few years as a reproducible characteristic, an easy to apply one, and with very low costs since it only needs the standard Haematoxylin and Eosin stained slides of observation. In this article, we provide a review of the histological growth patterns of liver metastases and their prognostic significance, biological meaning, and therapeutic importance.

1. Introduction

The liver is a common site for metastatic dissemination and in some regions of the globe, namely, Europe, secondary liver tumors are far more common than primary [1] ones. Regarding metastatic disease the adenocarcinomas are predominant, and colorectal carcinoma is the most prevalent place of origin, having a high mortality [2].

In the past few years major advances regarding treatment strategies of colorectal cancer liver metastases (CRCLM), such as more effective chemotherapy regimens, portal vein embolization and staged hepatectomies (including Associating Liver Partition and Portal Vein Ligation for Staged Hepatectomy, ALPSS), and one-stage ultrasound-guided parenchymal preserving resections, all have contributed to extend the limits of oncological resectability [3, 4]. In selected cases, liver transplantation has also been used successfully [5]. However, regardless of the curative intent, intrahepatic recurrence has been reported in more than 50% of the cases, even with adjuvant chemotherapy [6]. Several retrospective studies have identified these patients' cohorts with poor prognostic factors such as tumor size, number of lesions, and tumor progression after chemotherapy or shorter interval from primary tumor surgery [7]. Nevertheless, none of these are absolute contraindications for hepatic surgery and do not represent the tumor-host interaction that will be required for

individualized medicine/treatment. More aggressive hepatic surgeries did not show improved survival [8] rates and neoadjuvant chemotherapy is associated with increased postoperative morbidity [9]. New prognostic and biomarkers are thus of paramount importance.

2. The Detailed Study of CRCLM and Its Importance

Recently, histological growth patterns (GP) have been identified as a practical and reproducible factor of prognosis, easily assessed by Haematoxylin and Eosin (H&E) stained slides by an experienced pathologist. They are defined as expansive (when tumor growth compresses the hepatocytes), desmoplastic (with presence of fibrous tissue in the periphery of the tumor), and replacement (when tumor infiltrates the hepatocytes without architectural changes) (Figures 1 and 2). Our group and others have demonstrated that a pushing growth pattern is related to a worse prognosis [10] while a desmoplastic growth pattern is associated with a more favorable outcome [11]. What is particularly interesting about the GP is that the information is readily available on routine H&E pathological examination and does not require lengthy or expensive ancillary studies. This may be particularly important in low-resource settings.

The correct analysis and consequent accurate classification of the CRCLM growth pattern implies a detailed gross examination with adequate sampling with at least one sample per tumor centimeter, similar to the sampling used for tumor regression grade assessment, for all the lesions [12, 13]; in our institution we perform full sampling of all lesions with size inferior to 3cm.

Other studies have attempted to identify the characteristics that allow for a better or worse prognosis for overall survival such as tumor thickness at the tumor-normal interface [14, 15] and study of the tumor infiltrating lymphocytes and its composition [16, 17]. However, this type of evaluation is complicated, time consuming, and requires special software.

3. Why Are There Different Growth Patterns?

The reason for this behavior has not been fully understood yet. However, it can represent the complexity of tumor/host interactions, with the pushing pattern described by some authors as more angiogenic [18] and the desmoplastic as an inflammatory response of the host; it is also probably related to the response to chemotherapy [19].

The thick band of stroma present in the desmoplastic growth pattern, enriched with collagen, may act as an obstacle to tumor expansion, representing an improved host response with dense lymphocytic infiltration, increase in collagen type IV and integrin blockade, reducing the infiltration of nontumoral parenchyma, therefore demonstrating a more favorable characteristic [10, 20].

The pushing pattern displays biologic properties with increased levels of endothelial cell proliferation fraction [18, 21] and upregulation of vascular factors, such as basic fibroblast growth factor (bFGF) and vascular endothelial growth factor (VEGF) [22], sometimes in a similar mode as in the primary colorectal cancer [23]. The pushing pattern is also characterized by a hypoxic environment, a well-known factor of aggressiveness, and resistance to therapy [24, 25].

The information gained by studying the molecular mechanisms underlying the complex tumor/host interactions associated with the distinct GPs may aid in the selection of new therapeutic targets. Growth receptor blockade (with anti-EGFR antibodies) and antiangiogenic agents (with anti-VEGF antibodies) have already demonstrated excellent results in the treatment of advanced metastatic disease.

Several studies have addressed the relation of GPs and angiogenesis capacity, and the recent discovery mechanism of vessel cooption vascularization of tumors has explained a possible resistance to antiangiogenic agents. This led to the suggestion of a combined therapeutic as possible approach and linked this biological behavior to a specific GP [26].

Other mechanisms of tumoral survival, such as evading the host immune response, epithelial-mesenchymal transition, or hypoxia-resisting factors, may serve as targets for molecular therapies in the near future, namely, immunotherapy [27, 28] and cell cycle inhibitors [29, 30].

By reflecting the tumor-host interaction, the GP of liver metastases can influence overall and disease-free survival. Although GP could influence patient management, being a histopathological characteristic, the GP can only be known after surgical resection. However, imaging techniques could potentially detect different types of growth patterns before surgery.

Due to the simplicity of this biological characteristic, other studies have assessed this biological behavior in liver metastases of nonintestinal carcinomas, such as breast cancer [31] and uveal melanoma [32], but in these cases there is a predominance of the replacement pattern and consequently a worse prognosis.

4. Can we Predict the Growth Pattern before Surgery?

The different prognoses of the colorectal cancer liver metastases (CRCLM) may represent a new prognostic characteristic that may be related to the primary tumor properties and may be predicted by preoperative imaging, allowing individualized patient care.

The radiological response pattern to chemotherapy, particularly with antiangiogenic drugs, has been previously reported as having implications in the prognosis. In a cohort of 209 patients with CRCLM undergoing hepatectomy after neoadjuvant chemotherapy, the presence of a sharply defined border on preoperative computed tomography (CT) was associated with improved overall and disease-free survival [33]. However, the tumor-hepatic tissue interface was not assessed in this study and thus it remains to be answered whether this radiologic pattern corresponded to a distinct histological GP.

More accurate in tissue analysis than CT, Magnetic Resonance imaging (MRI) could provide important answers in this regard, especially with the use of hepatospecific contrast agents. In fact, the relative tumor enhancement

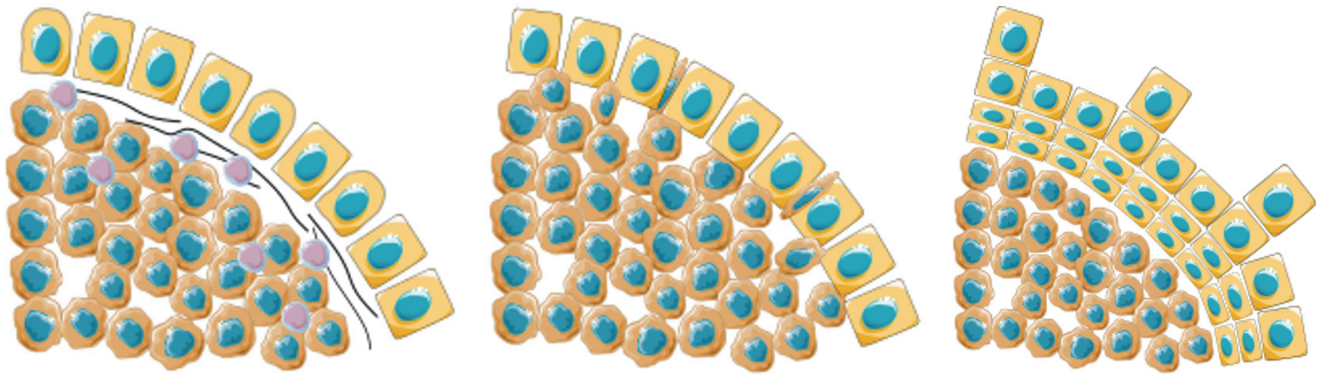

(a) (b) (c)

Figure 1: Schematic representation of the Growth Patterns of Colorectal Liver Metastases, adapted from Temido MJ (2018) Clinical and Pathological Factors of Prognosis after Hepatectomy for Gastric Cancer Liver Metastases. Is desmoplastic growth the key to longer survival? Master Thesis in Medicine, with permission. (a) Desmoplastic Growth Pattern: the tumor is separated from the liver parenchyma by a band of fibrous tissue, which contains tumor infiltrating lymphocytes; (b) Replacement Growth Pattern: the tumor permeates between the liver hepatocytes, without disruption of the normal architecture; (c) Pushing Growth Pattern: the tumor expands and compresses the surrounding hepatocytes.

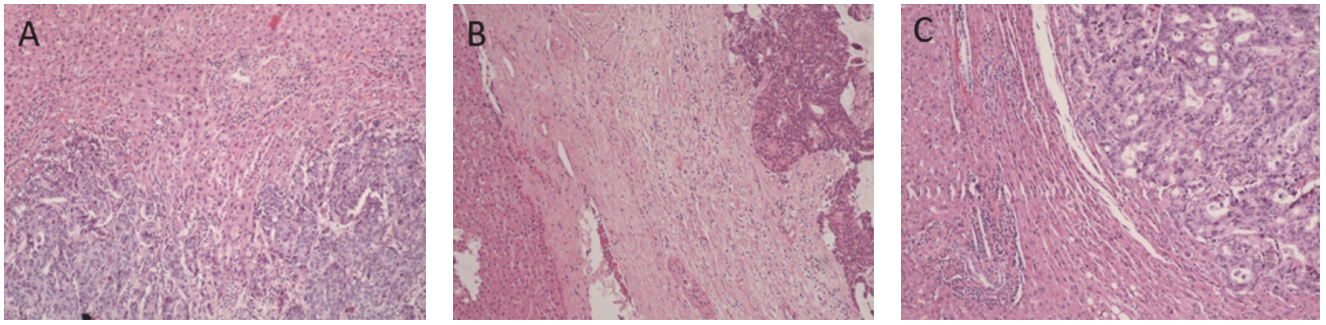

(a) (b) (c)

Figure 2: Haematoxylin & Eosin (H&E) evaluation of the Colorectal Liver Metastasis Growth Patterns, adapted from Falcão, D. et al. Histopathologic patterns as markers of prognosis in patients undergoing hepatectomy for colorectal cancer liver metastases: Pushing growth as an independent risk factor for decreased survival. Eur. J. Surg. Oncol. (2018). doi:10.1016/j.ejso.2018.03.02, with permission. (a) Replacement Growth Pattern: the tumor permeates between the liver hepatocytes, without disruption of the normal architecture, H&E 100x; (b) Desmoplastic Growth Pattern: the tumor is separated from the liver parenchyma by a band of fibrous tissue, which contains tumor infiltrating lymphocytes, H&E 100x; (c) Pushing Growth Pattern: the tumor expands and compresses the surrounding hepatocytes, H&E 100x.

by gadoxetic acid (a contrast agent used in hepatobiliary imaging) can accurately predict the response to chemotherapy in treatment-naïve patients with CRCLM [34]. Moreover, quantitative texture analysis in MRI, using radiomics, can also potentially detect microstructural changes in the liver parenchyma. In one study using an animal model of CRCLM, micrometastases were detected by radiomics before histopathological expression [35]. Hopefully this can also be used in the analysis of tumor-host tissue interface. Further studies will still have to be conducted.

One may raise the question about patients with several metastases; in our study [11], the majority of the CRCLM presented the same GP. It would be a very interesting study to see if in patients submitted to second and third hepatectomy the GP remained the same; some studies have assessed this and it seems that there is maintenance of GP [36]. This would allow better selection of patients for second and third hepatectomy.

5. Implications of CRCLM Growth Pattern in Treatment

Advances in imaging could detect distinct GPs, thus impacting patient management. This could lead to a tailoring of the therapy, both in the choice and duration of chemotherapy and in the use of resection and other locoregional techniques.

In fact, there are two distinct currents of thought in the scientific literature regarding the surgical management of CRCLM [4]: on the one hand, proponents of radical, R0 resections, even if requiring major or extended hepatectomies associated with parenchyma-modulating strategies, such as portal vein embolization or the Associating Liver

Partition and Portal Vein Ligation for Staged Hepatectomy (ALLPS) [37, 38] and, on the other hand, proponents of a parenchymal-sparing, radical but conservative approach, whereby metastases are resected leaving the liver's vascular and biliary structures intact, even if at the cost of R1 resection [39]. However, colorectal cancer liver metastasis is a heterogeneous disease and different patients might present different growth patterns, possibly representing distinct tumor-host interactions. We speculate whether a R1 resection might still be curative in a patient with desmoplastic growth pattern, but not in a patient with pushing growth pattern. This, however, remains unproven.

Moreover, knowledge of the GP could also influence the choice and duration of chemotherapy regimens. Although beneficial, preoperative chemotherapy in CRCLM can cause hepatotoxicity and increase postoperative morbidity [9, 40–42] Although evidence for this is scant, in our previous study we found that patients treated with a combination of oxaliplatin and 5-fluoruracil (FOLFOX) were more likely to present a pushing GP on the pathological analysis of the resected specimen [11], in which way this information aid in the choice of chemotherapy is still unknown.

Histological GPs are indeed a powerful tool, but in the past, they were described using several designations, thus raising barriers for worldwide harmonisation [43]. The recent development of a consensus should provide this parameter with enough strength and reproducibility for daily clinical use [44].

Concerning the surgical approach, literature is not unanimous regarding the perfect approach to synchronous CRCLM: some advocate the colorectal surgery first [45], others advocate a liver first approach [46], and finally are those who perform a synchronous resection [47, 48]. Nevertheless, no single strategy gains unanimity among surgeons [45].

The possibility of predicting the GP of CRCLM in preoperatory evaluation may allow for an individualized treatment algorithm for each patient. Particular imaging features of the metastatic disease could also expand this information. In this way, neoadjuvant chemotherapy, known to be more effective on the secondary tumor than on the primary [49] one, could be adequately selected, in both the choice of the agents and the duration. In addition, timing and extent of surgical resection could also be selected according to the risk of intrahepatic recurrence.

6. Conclusion

We hope that further investigation into GPs can help clinicians to choose therapies in a multimodal perspective, not only in cases of CRCLM but also in other indications, such as gastric or breast cancer liver metastases. The consistent report of the CRCLM GP in pathology reports according to the correct consensus [44] should be a powerful and consistent characteristic for behavior prediction. In the near future, we envision that imaging may provide important answers regarding GPs, and this knowledge may help the selection of the right therapy for each patient.

Conflicts of Interest

The authors declare that they have no conflicts of interest.

References

[1] B. A. Centeno, "Pathology of liver metastases," *Cancer Control*, vol. 13, no. 1, pp. 13–26, 2006.

[2] K. Kawada, S. Hasegawa, T. Murakami et al., "Molecular mechanisms of liver metastasis," *International Journal of Clinical Oncology*, vol. 16, no. 5, pp. 464–472, 2011.

[3] R. P. Jones, N. Kokudo, G. Folprecht et al., "Colorectal liver metastases: a critical review of state of the art," *Liver Cancer*, vol. 6, no. 1, pp. 66–71, 2017.

[4] G. Torzilli, R. Adam, L. Viganò et al., "Surgery of colorectal liver metastases: pushing the limits," *Liver Cancer*, vol. 6, no. 1, pp. 80–89, 2017.

[5] M. Hagness et al., "Liver transplantation for nonresectable liver metastases from colorectal cancer," *Annals of Surgery*, vol. 257, pp. 800–806, 2013.

[6] R. P. Jones, R. Jackson, D. F. J. Dunne et al., "Systematic review and meta-analysis of follow-up after hepatectomy for colorectal liver metastases," *British Journal of Surgery*, vol. 99, no. 4, pp. 477–486, 2012.

[7] K. U. Jang, C. W. Kim, K.-H. Kim et al., "Prognostic factors in terms of the number of metastatic nodules in patients with colorectal cancer liver metastases," *Annals of Coloproctology*, vol. 32, no. 3, pp. 92–100, 2016.

[8] Y. Mise, T. A. Aloia, K. W. Brudvik, L. Schwarz, J.-N. Vauthey, and C. Conrad, "Parenchymal-sparing hepatectomy in colorectal liver metastasis improves salvageability and survival," *Annals of Surgery*, vol. 263, no. 1, pp. 146–152, 2016.

[9] J. Martins, H. Alexandrino, R. Oliveira et al., "Sinusoidal dilation increases the risk of complications in hepatectomy for CRCLM – Protective effect of bevacizumab and diabetes mellitus, serum gamma-glutamyltranspeptidase as predictive factor," *European Journal of Surgical Oncology (EJSO)*, vol. 42, no. 5, pp. 713–721, 2016.

[10] P. B. Vermeulen, C. Colpaert, R. Salgado et al., "Liver metastases from colorectal adenocarcinomas grow in three patterns with different angiogenesis and desmoplasia," *The Journal of Pathology*, vol. 195, no. 3, pp. 336–342, 2001.

[11] D. Falcão, H. Alexandrino, R. Caetano Oliveira et al., "Histopathologic patterns as markers of prognosis in patients undergoing hepatectomy for colorectal cancer liver metastases – Pushing growth as an independent risk factor for decreased survival," *European Journal of Surgical Oncology*, vol. 44, no. 8, pp. 1212–1219, 2018.

[12] L. Rubbia-Brandt, E. Giostra, C. Brezault et al., "Importance of histological tumor response assessment in predicting the outcome in patients with colorectal liver metastases treated with neo-adjuvant chemotherapy followed by liver surgery," *Annals of Oncology*, vol. 18, no. 2, pp. 299–304, 2007.

[13] G. M. Fonseca, P. Herman, S. F. Faraj et al., "Pathological factors and prognosis of resected liver metastases of colorectal carcinoma: implications and proposal for a pathological reporting protocol," *Histopathology*, vol. 72, no. 3, pp. 377–390, 2018.

[14] D. M. Maru, S. Kopetz, P. Boonsirikamchai et al., "Tumor thickness at the tumor-normal interface: a novel pathologic indicator of chemotherapy response in hepatic colorectal metastases," *The American Journal of Surgical Pathology*, vol. 34, no. 9, pp. 1287–1294, 2010.

[15] M. Abengózar, M. J. Fernández-Aceñero, S. Chaves, and A. Celdrán, "Prognostic utility of tumor thickness at the tumor-normal interface in chemotherapy-treated hepatic colorectal metastasis," *Pathology - Research and Practice*, vol. 208, no. 4, pp. 235–239, 2012.

[16] S. C. Katz, V. Pillarisetty, Z. M. Bamboat et al., "T cell infiltrate predicts long-term survival following resection of colorectal cancer liver metastases," *Annals of Surgical Oncology*, vol. 16, no. 9, pp. 2524–2530, 2009.

[17] P. Wagner, M. Koch, D. Nummer et al., "Detection and functional analysis of tumor infiltrating T-lymphocytes (TIL) in liver metastases from colorectal cancer," *Annals of Surgical Oncology*, vol. 15, no. 8, pp. 2310–2317, 2008.

[18] R. L. Eefsen, G. G. Van den Eynden, G. Høyer-Hansen et al., "Histopathological growth pattern, proteolysis and angiogenesis in chemonaive patients resected for multiple colorectal liver metastases," *Journal of Oncology*, vol. 2012, Article ID 907971, 12 pages, 2012.

[19] R. L. Eefsen, L. Engelholm, W. Alpizar-Alpizar et al., "Inflammation and uPAR-expression in colorectal liver metastases in relation to growth pattern and neo-adjuvant therapy," *Cancer Microenvironment*, vol. 8, no. 2, pp. 93–100, 2015.

[20] K. Nielsen, H. C. Rolff, R. L. Eefsen, and B. Vainer, "The morphological growth patterns of colorectal liver metastases are prognostic for overall survival," *Modern Pathology*, vol. 27, no. 12, pp. 1641–1648, 2014.

[21] F. Stessels, G. van den Eynden, I. van der Auwera et al., "Breast adenocarcinoma liver metastases, in contrast to colorectal cancer liver metastases, display a non-angiogenic growth pattern that preserves the stroma and lacks hypoxia," *British Journal of Cancer*, vol. 90, no. 7, pp. 1429–1436, 2004.

[22] B. Döme, M. J. C. Hendrix, S. Paku, J. Tóvári, and J. Tímár, "Alternative vascularization mechanisms in cancer," *The American Journal of Pathology*, vol. 170, no. 1, pp. 1–15, 2007.

[23] G. G. Van Den Eynden, A. W. Majeed, M. Illemann et al., "The multifaceted role of the microenvironment in liver metastasis: biology and clinical implications," *Cancer Research*, vol. 73, no. 7, pp. 2031–2043, 2013.

[24] E. B. Rankin and A. J. Giaccia, "Hypoxic control of metastasis," *Science*, vol. 352, no. 6282, pp. 175–180, 2016.

[25] B. Muz, P. de la Puente, F. Azab, and A. K. Azab, "The role of hypoxia in cancer progression, angiogenesis, metastasis, and resistance to therapy," *Hypoxia*, vol. 3, no. 83, 2015.

[26] S. Frentzas et al., "Vessel co-option mediates resistance to anti-angiogenic therapy in liver metastases," *Nature Medicine*, vol. 22, Article ID 12941302, pp. 1294–1302, 2016.

[27] P. Boland and W. Ma, "Immunotherapy for colorectal cancer," *Cancers* , vol. 9, no. 5, p. 50, 2017.

[28] B. Bashir and A. E. Snook, "Immunotherapy regimens for metastatic colorectal carcinomas," *Human Vaccines & Immunotherapeutics*, vol. 14, pp. 250–254, 2018.

[29] P. Hou, T. Jiang, F. Chen et al., "KIF4A facilitates cell proliferation via induction of p21-mediated cell cycle progression and promotes metastasis in colorectal cancer," *Cell Death & Disease*, vol. 9, no. 5, 2018.

[30] W. Huang, Y. Kuo, H. Kuo et al., "CIL-102-induced cell cycle arrest and apoptosis in colorectal cancer cells via upregulation of p21 and GADD45," *PLoS ONE*, vol. 12, Article ID e0168989, 2017.

[31] R. Ma, Y. Feng, S. Lin et al., "Mechanisms involved in breast cancer liver metastasis," *Journal of Translational Medicine*, vol. 13, no. 64, 2015.

[32] R. Barnhill, P. Vermeulen, S. Daelemans et al., "Replacement and desmoplastic histopathological growth patterns: A pilot study of prediction of outcome in patients with uveal melanoma liver metastases," *The Journal of Pathology: Clinical Research*, vol. 4, no. 4, pp. 227–240, 2018.

[33] J. Shindoh, E. M. Loyer, S. Kopetz et al., "Optimal morphologic response to preoperative chemotherapy: An alternate outcome end point before resection of hepatic colorectal metastases," *Journal of Clinical Oncology*, vol. 30, no. 36, pp. 4566–4572, 2012.

[34] S. Murata, S. Matsushima, Y. Sato et al., "Predicting chemotherapeutic response for colorectal liver metastases using relative tumor enhancement of gadoxetic acid disodium-enhanced magnetic resonance imaging," *Abdominal Radiology*, vol. 43, no. 12, pp. 3301–3306, 2018.

[35] A. S. Becker, M. A. Schneider, M. C. Wurnig, M. Wagner, P. A. Clavien, and A. Boss, "Radiomics of liver MRI predict metastases in mice," *European Radiology Experimental*, vol. 2, no. 11, 2018.

[36] M. A. C. Machado, F. F. Makdissi, R. C. Surjan, T. Basseres, and E. Schadde, "Transition from open to laparoscopic ALPPS for patients with very small FLR: the initial experience," *HPB*, vol. 19, no. 1, pp. 59–66, 2017.

[37] E. Schadde, V. Ardiles, K. Slankamenac et al., "ALPPS offers a better chance of complete resection in patients with primarily unresectable liver tumors compared with conventional-staged hepatectomies: results of a multicenter analysis," *World Journal of Surgery*, vol. 38, no. 6, pp. 1510–1519, 2014.

[38] M. Narita, E. Oussoultzoglou, D. Jaeck et al., "Two-stage hepatectomy for multiple bilobar colorectal liver metastases," *British Journal of Surgery*, vol. 98, no. 10, pp. 1463–1475, 2011.

[39] G. Torzilli, F. Procopio, F. Botea et al., "One-stage ultrasonographically guided hepatectomy for multiple bilobar colorectal metastases: A feasible and effective alternative to the 2-stage approach," *Surgery*, vol. 146, no. 1, pp. 60–71, 2009.

[40] B. Nordlinger, E. Van Cutsem, P. Rougier et al., "Does chemotherapy prior to liver resection increase the potential for cure in patients with metastatic colorectal cancer? A report from the European Colorectal Metastases Treatment Group," *European Journal of Cancer*, vol. 43, no. 14, pp. 2037–2045, 2007.

[41] L. Rubbia-Brandt, V. Audard, P. Sartoretti et al., "Severe hepatic sinusoidal obstruction associated with oxaliplatin-based chemotherapy in patients with metastatic colorectal cancer," *Annals of Oncology*, vol. 15, no. 3, pp. 460–466, 2004.

[42] T. Aloia, M. Sebagh, M. Plasse et al., "Liver histology and surgical outcomes after preoperative chemotherapy with fluorouracil plus oxaliplatin in colorectal cancer liver metastases," *Journal of Clinical Oncology*, vol. 24, no. 31, pp. 4983–4990, 2006.

[43] C. Fernández Moro, B. Bozóky, and M. Gerling, "Growth patterns of colorectal cancer liver metastases and their impact on prognosis: a systematic review," *BMJ Open Gastroenterol*, vol. 5, Article ID e000217, 2018.

[44] P. van Dam, E. P. van der Stok, L. Teuwen et al., "International consensus guidelines for scoring the histopathological growth patterns of liver metastasis," *British Journal of Cancer*, vol. 117, no. 10, pp. 1427–1441, 2017.

[45] M. Baltatzis, A. K. C. Chan, S. Jegatheeswaran, J. M. Mason, and A. K. Siriwardena, "Colorectal cancer with synchronous hepatic metastases: Systematic review of reports comparing synchronous surgery with sequential bowel-first or liver-first approaches," *European Journal of Surgical Oncology*, vol. 42, no. 2, pp. 159–165, 2016.

[46] H. Salvador-Rosés, S. López-Ben, M. Casellas-Robert et al., "Oncological strategies for locally advanced rectal cancer with synchronous liver metastases, interval strategy versus rectum first strategy: a comparison of short-term outcomes," *Clinical and Translational Oncology*, vol. 20, no. 8, pp. 1018–1025, 2018.

[47] J. S. Abelson, F. Michelassi, T. Sun et al., "Simultaneous resection for synchronous colorectal liver metastasis: the new standard of care?" *Journal of Gastrointestinal Surgery*, vol. 21, no. 6, pp. 975–982, 2017.

[48] J. Waisberg and I. G. Ivankovics, "Liver-first approach of colorectal cancer with synchronous hepatic metastases: A reverse strategy," *World Journal of Hepatology*, vol. 7, no. 11, pp. 1444–1449, 2015.

[49] P. Gervaz, L. Rubbia-Brandt, A. Andres et al., "Neoadjuvant chemotherapy in patients with stage IV colorectal cancer: A comparison of histological response in liver metastases, primary tumors, and regional Lymph nodes," *Annals of Surgical Oncology*, vol. 17, no. 10, pp. 2714–2719, 2010.

Hindawi
Journal of Oncology
Volume 2019, Article ID 5689464, 7 pages
https://doi.org/10.1155/2019/5689464

Research Article

Interaction of CD200 Overexpression on Tumor Cells with CD200R1 Overexpression on Stromal Cells: An Escape from the Host Immune Response in Rectal Cancer Patients

Atil Bisgin,[1,2] **Wen-Jian Meng**,[1] **Gunnar Adell**,[1] **and Xiao-Feng Sun**[1]

[1]*Department of Oncology and Department of Clinical and Experimental Medicine, Linköping University, Linköping, Sweden*
[2]*Medical Genetics Department of Balcali Clinics and Hospital, Faculty of Medicine, Cukurova University, Adana, Turkey*

Correspondence should be addressed to Atil Bisgin; abisgin@yahoo.com

Received 8 July 2018; Accepted 29 November 2018; Published 21 January 2019

Guest Editor: Ganapathy Ekambaram

CD200 imparts an immunoregulatory signal through its receptor, CD200R1, leading to the suppression of tumor specific immunity. The mechanism of CD200:CD200R1 signaling pathway is still uncertain. Our aim was to investigate the expression and localization of CD200 and its receptor CD200R1 and their clinical significance in rectal cancer patients. We examined the immunohistochemical expressions and localizations of CD200 and CD200R1 in 140 rectal cancer patients. Among the patients, 79 underwent the preoperative radiotherapy and the others were untreated prior to the surgery. In addition, 121 matched normal rectal mucosa samples were evaluated. The results of immunohistochemical analysis showed a strikingly high level of CD200 in tumor cells ($p=0.001$) and CD200R1 expression in normal mucosal epithelium and stromal cells. Importantly, CD200R1 was overexpressed in stromal cells of the metastatic cancer patients compared to patients without metastases ($p=0.002$). More than that, 87% of metastatic patients had a phenotype of upregulated CD200 in tumor cells accompanied by overexpressed CD200R1 in stromal cells. In addition, low levels of CD200 were correlated with improved overall survival in untreated patients. We showed that tumor-stroma communication through CD200 and its receptor interaction is selected in patients with high risk of relapse. High levels of these molecules support instigation of the far and local metastatic nest that provides solid ground for metastasis. Our current data also disclose a mechanism by which CD200:CD200R1 affects tumor progression and may strengthen the feasibility of targeting CD200 or CD200R1 as anticancer strategy.

1. Introduction

Cancer progression is a multistep process including the most critical steps; tumor invasion and metastasis that are the major causes of cancer deaths and the obstacles to the successful treatment [1]. Many studies focused on identifying the progression and metastasis controlling genes [2, 3]. However, cancer metastasis is also dependent on the stromal compartment not exclusively regulated by intrinsic genes in cancer cells. Many studies have shown the interaction of cancer cells and stromal cells. CD200:CD200R1 signaling is one of the pivotal members of inflammatory signaling that has been shown recently [4].

CD200 is a membrane glycoprotein that widely expressed multiple cells/tissues [5, 6]. Its distinctive expression was subsequently studied by a number of different groups, confirming that high expression of CD200 was an independent prognostic factor and predicting reduced overall survival in a number of hematological malignancies, including multiple myeloma, acute myeloid leukemia (AML), and chronic lymphocytic leukemia (CLL) [7–9]. So the question has arisen, given this role as a prognostic factor in human blood malignancies, as how CD200 is involved in cancer. A hypothetical model suggested that the overexpression of CD200 is associated with inhibition of tumor-specific immunity by switching the cytokine profiles from T-helper 1 cells (Th1) to T-helper 2 cells. There are also most recent studies showing that CD200 expression controls two other pathways; one is a regulatory T cell expansion and disease progression in acute myeloid leukemia (AML) and chronic lymphocytic

Table 1

Characteristic	Rectal Cancer RT Group n = 61 (%)	Normal RT Group n = 55 (%)	Rectal Cancer Untreated n = 79 (%)	Normal Untreated n = 66 (%)
Sex				
Male	36 (59)	27 (49)	45 (56)	33 (50)
Female	25 (41)	28 (51)	34 (44)	33 (50)
Age (years)	62.6	61.7	63.4	62.7
TNM				
I + II + III	56 (91)		74 (94)	
IV	5 (9)		5 (6)	
Differentiation Grade				
Good	5 (8)		4 (5)	
Moderate	36 (59)		59 (75)	
Poor	20 (33)		16 (20)	
Metastasis				
No	41 (67)		49 (62)	
Yes	20 (33)		30 (38)	
Recurrence				
No	45 (74)		61 (77)	
Yes	16 (26)		18 (23)	

Patient characteristics. Rectal cancer RT group: rectal cancer patients underwent preoperative radiotherapy. Rectal cancer untreated: rectal cancer patients without any treatment prior to the operation. Normal RT group: normal rectal mucosa from rectal cancer RT group. Normal untreated: normal rectal mucosa from rectal cancer untreated group.

leukemia (CLL); other one is the checkpoint blockade that augments cytotoxicity of cytokine-induced killer cells against human myeloid leukemia blasts [10, 11]. This mechanism may take part in loss of antitumor control and results in immunocompromised tumor environment [8, 12].

In vitro and in vivo studies showed that CD200-expressing tumor cells can suppress T-cell responses [8, 12, 13]. On the other hand, CD200 is also a ligand for a structurally similar receptor CD200R1 that imparts an immunoregulatory signal [14]. This interaction is one of the most important immunological checkpoints: leading to the suppression immune responses [15]. The most recent in vitro studies suggest that blocking this CD200:CD200R1 interaction enhances Th1 responses and that is how the CD200-expressing cancer cells survive immune therapy or a natural immune response [8, 16, 17].

As a member of immune inhibitory receptors CD200R1 has another important role for the maintenance of immune tolerance and its expression is more restricted on myeloid and lymphoid lineages of cells. Tumor cells mostly use these immune inhibitory receptors for their benefits. Through this endogenous inhibitory pathway, CD200:CD200R1 interaction may also be featured in tumor progression, outgrowth, and/or metastasis. This idea was confirmed in one member of epithelial tumors, in skin carcinogenesis [18–20].

We set our study on molecular screening of tissue samples from rectal cancer patients. In this scenario, we investigated the expression and localization of CD200 and its receptor CD200R1 to identify a molecular marker useful for determining prognosis through routine clinical assessment with clinicopathological findings.

2. Material and Methods

2.1. Clinical Assessment of Rectal Cancer Patients. Paraffin-embedded tissues from rectal cancer patients were evaluated for our study. The study was approved by the local committee on ethics. Demographic and clinical data of the patients are given in Table 1.

There were two rectal cancer patients' groups: first group underwent the preoperative radiotherapy treatment as named "RT group" and second which is the patients without any treatment prior to the surgery was named "untreated group". The mean age at the time of diagnosis was 62.6 years in RT group and 63.4 in untreated group. All patients were pathologically staged according to the American Joint Committee on Cancer, also known as the TNM system. Most individuals had earlier stages: 56 of Stages I, II, and III (91%) and 5 cases of Stage IV (9%) in RT group and 74 cases of Stages I, II, and III (94%) and 5 cases of Stage IV (6%) in untreated group. Patients were also categorized by the differentiation grade from poor to good. Using this grading system by pathologists; in RT Group 20 cases had poor differentiation (33%), 36 cases had moderate differentiation (59%), and 5 cases had good differentiation (11%), while 16 patients with poor differentiation, 59 with moderate differentiation, and 4 with good differentiation were classified in untreated group.

Additionally, since the proliferation of cancer cells is thought to be a key feature of progression, Ki-67 expression pattern was added into the clinicopathological findings to assess the proliferative activity that had been previously reported by our group [21].

2.2. Immunohistochemistry. All primary antibodies used for CD200:CD200R1 immunohistochemistry were obtained from AbCam (anti-CD200/OX2 antibody [OX-104], ab33363; anti-CD200R antibody [OX-108], ab17225). Since CD200 and its receptor CD200R1 were predominantly expressed on myeloid and lymphoid cells, samples of lymphoid tissues and lymph node sections were included as positive controls to optimize the primary antibody titers. Negative controls were stained only with the appropriate secondary antibody.

Immunohistochemical analysis was carried out according to the antibody staining protocol in tissue microarray slides (TMAs). Benign and malignant tissues were stained using the above-stated primary antibodies. The slides were counterstained with hematoxylin and then coverslipped.

2.3. Analysis of Immunohistochemical Staining for CD200 and CD200R1 Expressions. Immunohistochemical analysis of TMAs was performed by 2 independent, dedicated clinicians without any prior knowledge of the paired specimens and clinical data. Sections from normal rectal mucosal samples and primary tumor samples that were prepared from the resection of the tumor by surgery were analyzed. Primary tumor samples were assessed into two regions and analyzed separately for the tumoral and stromal area around the tumor. Both intensity and marker distribution (percentage of the positively stained cells) were used for the semiquantitative scoring. Intensity was scored as 0 for negative, 1 for weak, 2 for moderate, and 3 for strong. The distribution was also similarly scored as follows: $0 \leq 10\%$; 1 = 10% to 45%; 2 = 46% to 70%; 3 = 71% to 85%; and $4 \geq 85\%$. The final immunostaining score was then calculated by adding both intensity and marker distribution scores.

2.4. Statistical Analysis. Statistica v.10 software for Windows was used for the statistical analyses. Statistical differences were evaluated when the probability level is less than 5% ($p<0.05$). The standard errors of the means are shown as error bars in the figures. Since the normal distribution was not detected by Kolmogorov-Smirnov test, comparison of each two groups was conducted by Mann-Whitney *U* tests. Spearman Rho analyses were revealed for the correlation analysis between CD200:CD200R1 profile and clinical findings.

3. Results and Discussion

3.1. Expressions of CD200:CD200R1 for Immunohistochemical Analysis and Confirmation for Scoring of Rectal Cancer Specimens. Optimization of the primary antibody concentrations of CD200 and its receptor CD200R1 was performed using lymph node sections regardless of disease before the analyses. While primary antibodies generated a well staining pattern on node sections in 1:200 dilution for CD200 and 1:50 dilution for CD200R1, lymph node sections that were treated with the secondary antibody alone as a negative control did not yield any staining (data not shown). These results support that the CD200 and CD200R1 expression on paraffin-embedded rectal cancer tissue samples could be detected by immunohistochemical staining protocol and then scored.

3.2. Rectal Cancer Tissues Displayed Increased CD200 Expression Compared with Normal Rectal Mucosa. Total of 140 paraffin-embedded tissues of rectal cancer patients were analyzed for determining the CD200 and CD200R1 expression by immunohistochemistry. Seventy-nine of 140 are the samples from untreated group and 61 of 140 are from patients that underwent radiotherapy treatment prior to the surgery. In addition, 121 normal rectal epithelial mucosa samples from the distant area were stained and then scored. Fifty-five of 121 were from preoperative radiotherapy given patients and the rest were from the untreated group of patients. Representative immunohistochemical staining images are shown in Figure 1(a), and Figure 1(b) shows the comparison of the both normal mucosa and rectal cancer groups. In patients with rectal cancer in independence of the radiotherapy given or not, overexpression of CD200 was detected in contrast to normal mucosa samples (Suppl. Table 1). The expression levels difference was statistically significant ($p = 0.001$).

3.3. Overexpression of CD200 Represents Similar Profiles to Those of Rectal Cancer Patients with or without Preoperative Radiotherapy. To compare CD200 and CD200R1 expression profiles of rectal cancer patients depending of the preoperative treatment modality, two groups; one underwent preoperative radiotherapy and the other without any treatment, were assessed. Patients displayed higher levels of CD200 and this high CD200 expression was similar in both groups (Figure 1(b)). The difference did not reveal any statistical difference ($p = 0.597$).

3.4. The Significance of CD200 Expression on Normal Mucosa in Connection with Survival. The main outcome of developing different treatment protocols and all is overall survival. Based on our long period followed-up rectal cancer patients' data, the low levels of CD200 expression in normal epithelium (score ≤ 3) related to long survival (more than 5 years) in untreated rectal patients group according to the implemented correlation and survival test ($p = 0.020$) (data not shown).

3.5. CD200R1 Expression Profiles in Rectal Cancer Patients. Representative immunohistochemical staining for CD200R1 images of rectal cancer is shown in Figure 2(a), and Figure 2(b) shows the comparison of the all groups including normal mucosa and rectal cancer groups whom one group without any treatment and the other underwent preoperative radiotherapy. There was a distinctive CD200R1 expression profile, and no difference was noted between the groups after the statistical evaluation as follows; $p = 0.434$ in between normal mucosa and preoperative radiotherapy gorup; $p = 0.482$ in between normal mucosa and untreated group; and $p = 0.570$ in between two groups.

3.6. Overexpression of CD200R1 in Stromal Cells of Rectal Cancer Patients Correlated with the High Recurrence Risk and Metastasis. The main clinical parameter for the patients is the recurrence risk and metastasis. Based on this parameter, among all 140 patients 50 cases had metastasis and 34 cases had recurrences. In more details, 20 of 50 and 16 of 34

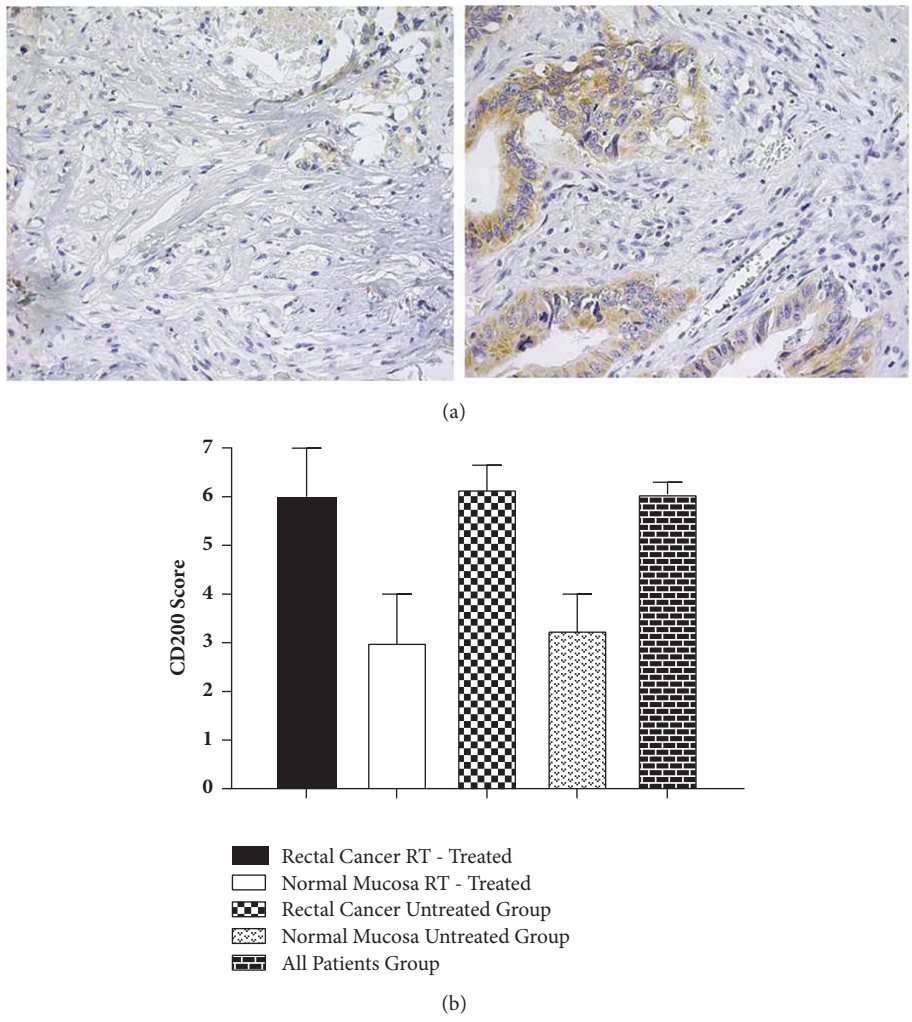

Figure 1: (a) Immunohistochemical staining of CD200 in total 140 rectal cancer patients. Representative images (magnification x 60) are provided from different patients with low (on the left) and high scorings (on the right). Brown precipitate indicates positive staining. (b) Semiquantitative scoring of CD200 immunohistochemical staining in patients with rectal cancer and normal mucosa. Scoring was performed as described in the section of Materials and Methods.

underwent preoperative radiotherapy and 30 of 50 and 18 of 34 were untreated rectal cancer patients. Interestingly, when we put all together, the high recurrence risk and metastasis group, CD200R1 was overexpressed in stromal cells of these patients compared to the no recurrence and nonmetastatic group. The correlation test was used to reveal any correlation. The overexpressed CD200R1 is correlated with high recurrence risk and the metastasis in rectal cancer patients in independent of preoperative radiotherapy (Suppl. Tables 2 and 3).

3.7. High Scores of CD200 in Tumor Cells Together with CD200R1 in Stromal Cells Related to Metastatic Pattern. Finally, we investigated evidence for a correlation between CD200:CD200R1 expression profile and the metastasis risk. Interestingly upregulated CD200 expression is when only associated with CD200R1 overexpression strongly correlated with metastatic pattern of rectal cancer patients (Suppl. Table 4A). These high expression levels of over 6 in IHC scoring were shown in 87% rectal cancer patients with metastasis. A correlation between CD200 and its receptor CD200R1 expression was investigated using Spearman Rho Correlation analysis. This increased expression of CD200 on tumor cells was not correlated with CD200R1 expression on tumor or stromal cells (Suppl. Table 4B).

3.8. Proliferative Activity of Rectal Cancer Patients. Proliferative activity was assessed in terms of the Ki-67 IHC staining in our groups' previous reported study [21]. Among the tissue sections analyzed, rectal cancer cells exhibited a wide range of Ki-67 expression that was ranged from 0 to 86 percent positivity, reflecting a variation in proliferative activity. However, neither clinical variables nor CD200:CD200R1 had any relation to Ki-67 expression.

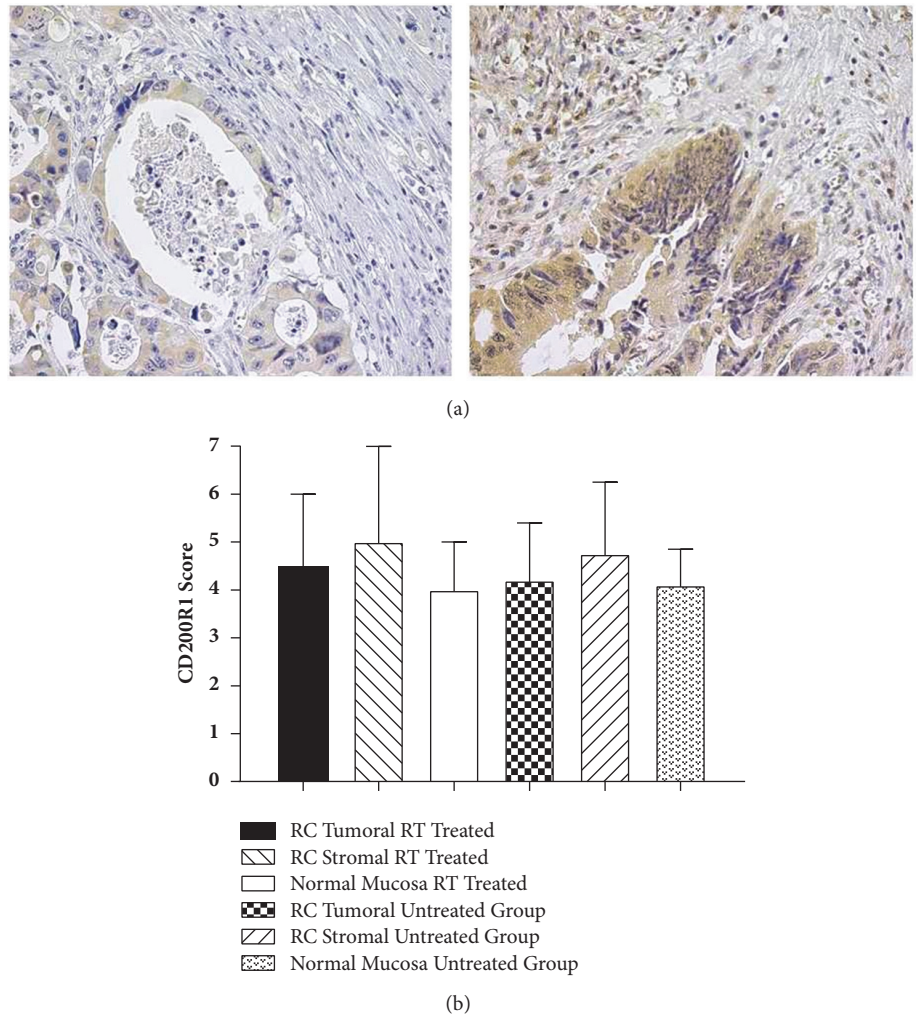

Figure 2: (a) Immunohıstochemical staining of CD200R1 in total 140 rectal cancer patients. Representative images including both the tumoral and stromal regions (magnification x 60) are provided from different patients with low and high scorings. Brown precipitate indicates positive staining. (b) Semiquantitative scoring of CD200R1 immunohistochemical staining in patients with rectal cancer tumoral expression and stromal expression and normal mucosa. Scoring was performed as described in the section of Materials and Methods.

4. Conclusions

Colorectal cancer is the second leading cause of cancer-related mortality and metastatic pattern still remains incurable [22]. Most recent studies have focused on the contribution of tumor microenvironment to the progression of tumors including colorectal cancer. A major contributor to the tumor microenvironment is inflammation and inflammatory mediators that are adept in supporting tumor cell growth, survival, and metastasis [23].

An important immunological checkpoint is CD200:CD200R1 signaling pathway that controls inflammation, immune tolerance, and antitumor immune responses [18]. Several studies in hematologic tumors suggested the CD200 overexpression as a prognostic factor, while some others showed the expression in solid malignancies [7, 9, 16, 19]. According to all published data, it has been proposed that CD200 expression plays a role in the ability to escape the immune system. More speculative most recently published findings were CD200:CD200R1 signaling suppressing antitumor responses and regulating the metastatic growth [20].

Tumor metastasis is a complex multistep process in which cell migration and invasion are important steps. Our most important finding was the correlation between metastatic pattern and high expression patterns of CD200 on tumor cells together with CD200R1 expression on stromal cells. These findings suggest a potential role of stromal cells and the interaction to the tumor cells. This cell-cell and ligand-receptor interaction might be one of the important steps of metastasis and oncogenesis.

Another most important fundamental in oncogenesis is the cellular proliferation, to maintain tissue homeostasis. For that reason, we assessed the relationship between expression patterns of tumor cell proliferation marker Ki-67 and CD200:CD200R1. There are some discrepancies in the literature that some reported no relation between

Ki-67 immunoreactivity and various clinicopathological and prognostic variables in cases with colorectal carcinomas; on the other hand some of them reported its relation to histologic grade and pathological stage [21, 24, 25]. Still, Ki-67 is the most reliable and reproducible marker. In our study, there was no correlation between CD200:CD200R1 and Ki-67 but CD200:CD200R1 expression patterns were related to metastasis and recurrence. The results thus supporting the hypothesis that metastasis in rectal cancers has a linkage with host related stromal cells not only with tumor cells itself, neither may not regulated by only the proliferative activity that was assessed by Ki-67 staining.

On the basis of our findings, we propose not only the upregulation of CD200 on tumor cells, but also CD200R1 overexpression on stromal cells in terms of the interaction between CD200 and its receptor CD200R1, which are the hallmark of metastatic rectal cancer and potentially responsible for supporting the survival of CD200 expressing tumor cells.

CD200:CD200R1 interaction and the mechanism still remain significant unknowns. However, the immune inhibitory receptors/pathways already become important therapeutic targets to strengthen antitumor responses in cancer treatment during the last few years. Most recent studies confirmed the increase in chemotherapy activity within the synergy of CD200 (or CD200R) blockade to cure and to produce immune resistance to metastasis of metastatic breast cancer in mice models [11]. Moreover, there are ongoing clinical trials against the inhibitory receptors including CTLA4, PD-1, and an antibody currently being evaluated where blocks CD200:CD200R1 (Alexion Pharmaceuticals, NCT00648739) have yielded promising results [26]. Our findings also suggest the extension of the therapeutic use of CD200:CD200R1 blockers to rectal cancer patients that might lead to the more effective treatment modalities.

Another revealed data of our study was CD200 expression on normal mucosa cells that had also an aspect of its relation to survival. However, this correlation is only limited in the untreated group. There might be 2 main explanations of this correlation in untreated group but not in preoperative radiotherapy patients. The fact that CD200 overexpression is a predictor of poor prognosis in a number of hematologic malignancies supports our data. Because of its immunosuppressive effect, low expression of CD200 attenuates the inflammation and the inflammation might enhance the survival of patients according to the antitumor effect. Second since the radiotherapy has an effect on normal tissue homeostasis, it may also affect the immune response, the repertoire, and future immune reactions to the tumor via the field effect.

Collectively, all these results highlight the strong contribution that tumor cells and stromal cells communication defined the metastatic outcome of rectal cancer patients. Particularly, our analysis implicates CD200 and CD200R1 have an effect on survival and metastasis. Because of the long follow-up time together with the different treatment modalities used and other clinical data in our large study group, we determined the correlations and clinical importance of CD200:CD200R1 receptor profile and their location of expression in rectal cancer patients.

In conclusion, we have identified CD200 and its receptor CD200R1 expression profiles and their location in tumor and tumor surrounding is, for the first time, demonstrated in rectal cancer patients. We have also combined the expression pattern in relation to clinical status and treatment. In summary, we showed that cross talk between tumor and stroma might support metastasis-specific functions. These results also point the CD200:CD200R1 expression profile might be useful to follow up rectal cancer progression by virtue of their connection to recurrence risk, metastasis, and survival depending on the treatment modality, whereas rectal cancer patients appear to be targets for adjuvant therapies directed at interrupting CD200:CD200R1 immunoregulatory axis.

Data Availability

The data used to support the findings of this study are included within the article.

Conflicts of Interest

The authors declare that there are no conflicts of interest regarding the publication of this paper.

Acknowledgments

This work was supported by the grants from the Swedish Cancer Foundation, Swedish Research Council, The Health Research Council in the South-East of Sweden, and Swedish Lions Research Foundation. We thank Birgitta Holmlund for providing the tissue sections and TMA slides. Moreover, this study had been presented as an abstract in Proceedings of the 105th Annual Meeting of the American Association for Cancer Research, 2014.

Supplementary Materials

Supplementary Table 1. Immunohistochemical scoring of CD200 in rectal cancer tissues compared to the benign epithelium (p=0.001). Supplementary Table 2. Comparative analysis of CD200R1 expression in cases with recurrence and without recurrence. Scoring was assessed on the stromal region of primary tumor samples. Supplementary Table 3. Comparative analysis of CD200R1 expression on stromal region of primary tumor sections. Cases compared between with or without lymph node metastasis. Supplementary Table 4. (A) The expression pattern of CD200 and CD200R1 in metastatic versus nonmetastatic rectal cancer patients. (B) Spearman Rho correlation analysis of CD200 and its receptor CD200R1. Correlation considered as significant at the 0.01 and 0.05 levels (2- tailed). *(Supplementary Materials)*

References

[1] P. S. Steeg, "Metastasis suppressors alter the signal transduction of cancer cells," *Nature Reviews Cancer*, vol. 3, no. 1, pp. 55–63, 2003.

[2] C. Chang, J. Shih, Y. Jeng et al., "Connective Tissue Growth Factor and Its Role in Lung Adenocarcinoma Invasion and Metastasis," *JNCI: Journal of the National Cancer Institute*, vol. 96, no. 5, pp. 364–375, 2004.

[3] S. Gnosa, Y.-M. Shen, C.-J. Wang et al., "Expression of AEG-1 mRNA and protein in colorectal cancer patients and colon cancer cell lines," *Journal of Translational Medicine*, vol. 10, no. 1, article no. 109, 2012.

[4] L. M. Coussens and Z. Werb, "Inflammation and cancer," *Nature*, vol. 420, no. 6917, pp. 860–867, 2002.

[5] A. N. Barclay and H. A. Ward, "Purification and Chemical Characterisation of Membrane Glycoproteins from Rat Thymocytes and Brain, Recognised by Monoclonal Antibody MRC OX 2," *European Journal of Biochemistry*, vol. 129, no. 2, pp. 447–458, 1982.

[6] D. A. Clark, A. Keil, Z. Chen, U. Markert, J. Manuel, and R. M. Gorczynski, "Placental trophoblast from successful human pregnancies expresses the tolerance signaling molecule, CD200 (OX-2)," *American Journal of Reproductive Immunology*, vol. 50, no. 3, pp. 187–195, 2003.

[7] A. Tonks, R. Hills, P. White et al., "CD200 as a prognostic factor in acute myeloid leukaemia," *Leukemia*, vol. 21, no. 3, pp. 566–568, 2007.

[8] J. R. McWhirter, A. Kretz-Rommel, A. Saven et al., "Antibodies selected from combinatorial libraries block a tumor antigen that plays a key role in immunomodulation," *Proceedings of the National Acadamy of Sciences of the United States of America*, vol. 103, no. 4, pp. 1041–1046, 2006.

[9] J. Moreaux, D. Hose, T. Reme et al., "CD200 is a new prognostic factor in multiple myeloma," *Blood*, vol. 108, no. 13, pp. 4194–4197, 2006.

[10] A. Memarian, M. Nourizadeh, F. Masoumi et al., "Upregulation of CD200 is associated with Foxp3$^+$ regulatory T cell expansion and disease progression in acute myeloid leukemia," *Tumor Biology*, vol. 34, no. 1, pp. 531–542, 2013.

[11] S. L. Poh and Y. C. Linn, "Immune checkpoint inhibitors enhance cytotoxicity of cytokine-induced killer cells against human myeloid leukaemic blasts," *Cancer Immunology, Immunotherapy*, vol. 65, no. 5, pp. 525–536, 2016.

[12] A. Kretz-Rommel, F. Qin, N. Dakappagari et al., "CD200 expression on tumor cells suppresses antitumor immunity: new approaches to cancer immunotherapy," *The Journal of Immunology*, vol. 178, no. 9, pp. 5595–5605, 2007.

[13] C. P. Pallasch, S. Ulbrich, R. Brinker, M. Hallek, R. A. Uger, and C.-M. Wendtner, "Disruption of T cell suppression in chronic lymphocytic leukemia by CD200 blockade," *Leukemia Research*, vol. 33, no. 3, pp. 460–464, 2009.

[14] G. J. Wright, H. Cherwinski, M. Foster-Cuevas et al., "Characterization of the CD200 receptor family in mice and humans and their interactions with CD200," *The Journal of Immunology*, vol. 171, no. 6, pp. 3034–3046, 2003.

[15] E. S. K. Rijkers, T. de Ruiter, A. Baridi, H. Veninga, R. M. Hoek, and L. Meyaard, "The inhibitory CD200R is differentially expressed on human and mouse T and B lymphocytes," *Molecular Immunology*, vol. 45, no. 4, pp. 1126–1135, 2008.

[16] A. Podnos, D. A. Clark, N. Erin, K. Yu, and R. M. Gorczynski, "Further evidence for a role of tumor CD200 expression in breast cancer metastasis: Decreased metastasis in CD200R1KO mice or using CD200-silenced EMT6," *Breast Cancer Research and Treatment*, vol. 136, no. 1, pp. 117–127, 2012.

[17] R. M. Gorczynski, D. A. Clark, N. Erin, and I. Khatri, "Role of CD200 expression in regulation of metastasis of EMT6 tumor cells in mice," *Breast Cancer Research and Treatment*, vol. 130, no. 1, pp. 49–60, 2011.

[18] T. P. Rygiel and L. Meyaard, "CD200R signaling in tumor tolerance and inflammation: a tricky balance," *Current Opinion in Immunology*, vol. 24, no. 2, pp. 233–238, 2012.

[19] M. Stumpfova, D. Ratner, E. B. Desciak, Y. D. Eliezri, and D. M. Owens, "The immunosuppressive surface ligand CD200 augments the metastatic capacity of squamous cell carcinoma," *Cancer Research*, vol. 70, no. 7, pp. 2962–2972, 2010.

[20] T. P. Rygiel, G. Karnam, G. Goverse et al., "CD200-CD200R signaling suppresses anti-tumor responses independently of CD200 expression on the tumor," *Oncogene*, vol. 31, no. 24, pp. 2979–2988, 2012.

[21] G. Adell, H. Zhang, A. Jansson, X.-F. Sun, O. Stål, and B. Nordenskjöld, "Decreased tumor cell proliferation as an indicator of the effect of preoperative radiotherapy of rectal cancer," *International Journal of Radiation Oncology * Biology * Physics*, vol. 50, no. 3, pp. 659–663, 2001.

[22] E. P. Whitlock, J. S. Lin, E. Liles, T. L. Beil, and R. Fu, "Screening for colorectal cancer: a targeted, updated systematic review for the U.S. Preventive Services Task Force," *Annals of Internal Medicine*, vol. 149, no. 9, pp. 638–658, 2008.

[23] A. Mantovani, P. Allavena, A. Sica, and F. Balkwill, "Cancer-related inflammation," *Nature*, vol. 454, no. 7203, pp. 436–444, 2008.

[24] H. Ishida, S. Sadahiro, T. Suzuki et al., "Proliferative, infiltrative, and metastatic activities in colorectal tumors assessed by MIB-1 antibody.," *Oncology Reports*, vol. 10, no. 6, pp. 1741–1745, 2003.

[25] H. Petrowsky, I. Sturm, O. Graubitz et al., "Relevance of Ki-67 antigen expression and K-ras mutation in colorectal liver metastases," *European Journal of Surgical Oncology*, vol. 27, no. 1, pp. 80–87, 2001.

[26] D. Rangachari and J. R. Brahmer, "Targeting the immune system in the treatment of non-small-cell lung cancer," *Current Treatment Options in Oncology*, vol. 14, no. 4, pp. 580–594, 2013.

Hindawi
Journal of Oncology
Volume 2018, Article ID 1953571, 8 pages
https://doi.org/10.1155/2018/1953571

Research Article

The De Ritis and Neutrophil-to-Lymphocyte Ratios May Aid in the Risk Assessment of Patients with Metastatic Renal Cell Carcinoma

Sung Han Kim,[1] **Eun Young Park**,[2] **Jungnam Joo**,[2] **and Jinsoo Chung**[1]

[1]*Department of Urology, Center for Prostate Cancer, National Cancer Center, Goyang, Republic of Korea*
[2]*Biometrics Research Branch, Research Institute and Hospital, National Cancer Center, Goyang, Republic of Korea*

Correspondence should be addressed to Jinsoo Chung; cjs5225@ncc.re.kr

Received 3 August 2018; Accepted 14 October 2018; Published 18 December 2018

Guest Editor: Peramaiyan Rajendran

Purpose. This study aimed to determine whether baseline blood inflammatory markers can predict progression-free survival (PFS) and overall survival (OS) in patients with metastatic renal cell carcinoma (mRCC). *Methods*. The study included 158 patients with mRCC treated with first-line targeted therapy between 2002 and 2016. A multivariable cox proportional hazards model identified inflammatory factors that predict PFS and OS. Using bootstrap method, new prognostic model compared with Heng and modified MSKCC risk model (mMSKCC). The effect of inflammatory factors were investigated by comparing increased C-index adding significant inflammatory factors to Heng and mMSKCC model. *Results*. On multivariable analysis, nephrectomy (HR 0.48), NLR (HR 1.04), were significant risk factors for PFS; nephrectomy (HR 0.38), hemoglobin (HR 1.71), alkaline phosphatase (HR 1.73), NLR (HR 1.01) and DRR (HR 1.34), were significant factors for OS ($p<0.05$). Our new model that incorporated NLR and DRR had higher (though insignificant) predictability (C-index=0.610) than mMSKCC risk model (C-index=0.569) in PFS and significantly better predictability (C-index=0.727) than Heng and mMSKCC risk model (C-index, 0.661, 0.612, respectively) in OS. Adding inflammatory factors to the Heng criteria (C-index, 0.697 for OS) and MSKCC (0.691 for OS) tended to improve their predictive abilities. *Conclusions*. The NLR and DRR may increase predictive ability compared to the established Heng and mMSKCC risk models in mRCC.

1. Introduction

Patients with metastatic renal cell carcinoma (mRCC) generally show poor prognoses; the 5-year survival rate is 8–20% [1–4]. Clinicians use several prognostic models to stratify patients and determine optimal therapeutic strategies; these include the International Metastatic Renal Cell Carcinoma Database Consortium (IMDC, also known as Heng) Model [5] and Memorial Sloan-Kettering Cancer Center (MSKCC/Motzer score) model [4]. The Heng prognostic model incorporates the Karnofsky performance status, corrected serum calcium, hemoglobin, time from diagnosis to treatment, platelets, and neutrophils [5], whereas the MSKCC model incorporates lactate dehydrogenase, corrected serum calcium, Karnofsky performance status, hemoglobin, and time from initial diagnosis to commencing therapy [6]. However, both models have been cited for their shortcomings and inaccuracies in predicting mRCC prognosis.

Recent scientific improvements have allowed for more thorough examinations of the pathophysiologies of various cancers, including RCC. Such advances have elucidated the importance of the tumor microenvironment, including the host inflammatory immune response and cellular turnover metabolism, in carcinogenesis and tumor progression, especially in RCC [7, 8]. Tumors tend to create microenvironments that promote inflammatory cell proliferation and produce a greater amount of immune response mediators [9]. Laboratory markers of systemic inflammation are among the many prognostic biomarkers identified in RCC, irrespective of the localized or metastatic state of the tumor. C-reactive protein [10], neutrophil-to-lymphocyte ratio (NLR) [11], lymphocyte-to-monocyte ratio [12], and

platelet-to-lymphocyte ratio (PLR) [13] have been identified as independent prognostic variables in treatment-naïve patients with RCC [2, 5]. Additionally, recent studies showed that the De Ritis ratio (DRR), which is the ratio of aspartate transaminase (AST) to alanine transaminase (ALT), is indicative of cellular metabolism and cancer cell turnover [14].

The assessment of blood-based markers of inflammatory and metabolic responses in patients with cancer provides a simple and cost-effective evaluation method in clinical practice. Therefore, we investigated the prognostic value of systemic inflammatory markers as well as AST/ALT-related parameters and evaluated those that may be useful in improving survival stratification offered by the current Heng and MSKCC risk models in patients with mRCC treated with targeted therapy.

2. Materials and Methods

2.1. Ethical Statements. This retrospective study was approved by the Institutional Review Board of the National Cancer Center (No. NCC2015-0087), which waived the requirement for written informed consent. Patient data were anonymized and deidentified prior to analysis. Study procedures were performed in accordance with the guidelines of the Declaration of Helsinki.

2.2. Study Design and Patients. Between June 2002 and January 2016, 158 consecutive patients with mRCC treated with first-line vascular endothelial growth factor-targeted therapy (sorafenib, sunitinib, pazopanib, or axitinib) were retrospectively extracted from the prospectively collected kidney cancer database, in which all baseline demographics and clinical and laboratory data, including systemic inflammatory marker information, were prospectively collected. All RCC diagnoses were based on the histological analyses of specimens obtained at nephrectomy, renal biopsies, and/or biopsies acquired from metastatic sites.

2.3. Response Assessment. Therapy was administered until disease progression, unacceptable toxicity, or cessation upon the directive of the physician (J.C.). Responses were evaluated using the Response Assessment Criteria in Solid Tumors version 1.1. Progressive disease was defined as a 20% increase in the sum of the products of all measurable lesions, appearance of any new lesions, or reappearance of any lesion that had previously disappeared.

2.4. Statistical Analysis. The baseline clinical and inflammatory factors were summarized in Table 1. Progression-free survival (PFS) duration was defined to date of initiation of therapy to date of progression of disease and overall survival (OS) duration was defined to date of initiation of therapy to date of death or last follow up date, respectively. The multivariable Cox proportional hazards model was used to examine the effect of inflammatory factors on prognosis of patients. Each clinical and inflammatory factors with p-value ≤0.15 in univariable analysis were included into multivariable model. Inflammatory factors were used by itself (neutrophil, lymphocyte, ALT, AST) or ratios (NLR, DRR). The final model was proposed using backward selection with an elimination criterion of p-value > 0.05. To compare the predictive ability of new prognostic model with Heng and mMSKCC risk models, 2000 bootstrap samples were used to calculate the C-index of each model. The mean and 95% confidence intervals of difference of C-index were presented. In addition, the C-index of model adding significant inflammatory factors to Heng and mMSKCC risk model was compared to previously that of Heng and mMSKCC risk model. All statistical results were presented as hazard ratio (HR) with 95% confidence intervals. P<0.05 was considered statistically significant. All analyses were performed using R project (version 3.3.3) and SAS version 9.4 (SAS Institute Inc., Cary, NC, USA).

2.5. Dichotomization of Inflammatory Variables. We individually examined the impact of baseline markers of systemic inflammation (hemoglobin, platelets, neutrophils, lymphocytes, LDH, corrected Ca, albumin, alkaline phosphatase, AST, ALT) on PFS and OS. These markers were analyzed as categorical variables. Dichotomization of these variables was based on the upper (platelets, neutrophils, LDH, corrected Ca, alkaline phosphatase, AST, ALT) or lower (hemoglobin, albumin and lymphocytes) ranges of normal measurements. No widely accepted cut-off points for NLR, and DRR were previously adopted [15, 16]; therefore, we analyzed these variables as continuous variables.

3. Results

3.1. Baseline Characteristics. The mean patient age (when commencing treatment) and treatment duration were 58.6 (standard deviation [SD] 10.6) years and median treatment duration was 4.8 months. Metachronous mRCC (61.4%) and male sex (78.5%) were dominant, and 89 of 158 patients (56.3%) had a history of nephrectomy. The baseline proportions of the favorable, intermediate, and poor risk groups according to the MSKCC criteria were 12.2%, 70.8%, and 17%, respectively; those according to the Heng criteria were 10.6%, 71.2%, and 18.2%, respectively. The progression rate was 81.7% after first-line targeted therapy. The patients' baseline data are described in Table 1.

3.2. Significant Prognostic Risk Factors for PFS and OS. Univariable analysis showed that metachronous type (hazard ratio [HR] 0.64), nephrectomy (0.48), DFI≤ 1(1.76), Heng (2.00, 2.84), Platelet (1.95), Albumin (1.78), NLR (1.03), AST (2.56) were significantly associated with PFS (p<0.05). More factors were significant in OS univariable analysis, with metachronous type (0.48), nephrectomy (0.34), DFI≤ 1 (2.04), mMSKCC (1.77, 2.83), Heng (3.11, 6.46), Liver mets (1.92), Hb (2.04), Platelet (2.51), Neutrophil (2.17), Lymphocyte (1.71), Albumin (3.77), Alkaline phosphatase (1.83), NLR (1.06), AST (3.60) and DRR (1.39). In multivariable analysis, nephrectomy (HR 0.48) and NLR (HR 1.04) were associated with PFS(p<0.05) (Table 2).

Table 1: Comparison of baseline clinicopathological demographics among treatment groups (N=158).

Variables	N (%) or mean±sd or median (min-max)
Age (miss=1, years)	58.62±10.64
Gender, Male/Female	124 (78.5)/34 (21.5)
Metastatic type, Synchronous/Metachronous	97 (61.4)/61 (38.6)
Body mass index (miss=13)	23.70±3.27
KPS (miss=19), KPS >80	127 (91.4)
KPS ≤80	12 (8.6)
Nephrectomy	89 (56.3)
ECOG baseline (miss=1) 0/1+2+3/unknown	75 (47.8)/64 (40.8)/18 (11.5)
Underlying disease, Diabetes (miss=1)	37 (23.6)
Hypertension (miss=1)	73 (46.5)
Cerebrovascular disease	6 (3.8)
Cardiac disease	4 (2.5)
Duration from the first-line treatment (months)	4.8 (1.0-70.4)
Disease free interval (months)	2.0 (0.0-240.0)
Disease free interval≤1 year	106 (67.1)
MSKCC new (miss=52) favorable/intermediate/poor	13 (12.3)/75 (70.8)/18 (17)
Heng new (miss=26) favorable/intermediate/poor	14 (10.6)/94 (71.2)/24 (18.2)
Metastatic Organ, Lung metastasis	113 (71.5)
Liver metastasis (miss=1)	33 (21)
Lymph node metastasis	69 (43.7)
Bone metastasis (miss=1)	54 (34.4)
Brain metastasis (miss=5)	18 (11.8)
Number of metastatic organs (miss=6)	2.20±0.96
Baseline laboratory parameters	
Leukocyte (miss=4) ≥10	29 (18.8)
Hemoglobin (miss=4) M<13, F<11.5	90 (58.4)
Platelet (miss=4) ≥400K	19 (12.3)
Neutrophil (miss=6) <7500/	124 (81.6)
Neutrophil lymphocyte ratio	2.68 (0.77-39.2)
Lymphocyte (miss=4) ≥1500	94 (61)
LDH (miss=41) ≥300	13 (11.1)
Corrected Calcium (miss=9) ≥10	11 (7.4)
Albumin (miss=10) <3.5	23 (15.5)
Alkaline phosphatase (miss=14) ≥104	50 (34.7)
AST (miss=10) ≥40	12 (8.1)
ALT (miss=10)≥40)	18 (12.2)
De Retis ratio	1.38±0.92
Creatinine (miss=7) ≥0.9	134 (88.7)
Targeted agents TKI (miss=1), sunitinib, sorafenib, pazopanib	105 (66.9)/21 (13.4)/31 (19.8)
First line treatment result continue/PD/AE/unknown	9 (5.7)/129 (81.7)/11 (7)/9 (5.7)
Survival (%)	17.70%
Progression (%)	98.10%

KPS, Karnofsky performance status score; ECOG, Eastern Cooperative Oncology Group performance status; MSKCC, Memorial Sloan Kettering Cancer Center; LDH, lactate dehydrogenase; AST, aspartate transaminase; ALT, alanine transaminase.

Multivariable models using inflammatory factors as ratio (NLR, DRR) were better predictive ability. Nephrectomy (HR, 0.48) and NLR (1.04) were significant prognostic factors in PFS and nephrectomy (HR 0.38), Hb (1.71), alkaline phosphatase (1.73), NLR (1.07) and DRR (1.34) were also significant factors in OS ($p<0.05$) (Table 3).

3.3. Modeling New Prognostic Risk Criteria for PFS. Two new risk models were created using significant risk factors for PFS, including treatment itself or ratio (Table 4). Model A used inflammatory factors itself (neutrophil, lymphocyte, ALT, AST), and model B used ratio (NLR, DRR). The model consisted of nephrectomy and AST (Model A: C-index 0.594)

Table 2: Univariate and multivariate analyses of the new prognostic factors for progression-free survival.

Variables		Univariable		Multivariable model 1		Multivariable model 2	
	N (event)	HR (95% CI)	p-value	HR (95% CI)	p-value	HR (95% CI)	p-value
Age ≥55 years	101 (76)	0.79 (0.56-1.13)	0.204				
Female gender	34 (28)	1.07 (0.69-1.65)	0.770				
Metachronous type	61 (50)	0.64 (0.44-0.92)	0.015				
Nephrectomy	89 (72)	0.48 (0.33-0.70)	<.001	0.48 (0.32-0.71)	<.001	0.48 (0.33-0.71)	<.001
Body mass index	145 (121)	0.98 (0.92-1.04)	0.500				
KPS≤80	12 (11)	1.10 (0.59-2.08)	0.760				
DFI≤1year	106 (87)	1.76 (1.20-2.58)	0.004				
mMSKCC, favorable	48 (42)	1	(0.287)				
intermediate	74 (59)	1.38 (0.92-2.06)	0.121				
poor	12 (10)	1.34 (0.66-2.71)	0.415				
Heng, favorable	14 (12)	1	(0.021)				
intermediate	94 (77)	2.00 (1.08-3.73)	0.029				
poor	24 (20)	2.84 (1.36-5.92)	0.006				
Lung metastasis	113 (93)	0.79 (0.53-1.16)	0.228				
Liver metastasis	33 (26)	1.23 (0.79-1.90)	0.366				
Bone metastasis	54 (47)	0.92 (0.64-1.32)	0.652				
Brain metastasis	18 (16)	1.30 (0.77-2.22)	0.329				
Hb, M<13, F<11.5	90 (70)	1.30 (0.91-1.86)	0.148				
Platelet ≥400K	19 (15)	1.95 (1.12-3.39)	0.018				
Neutrophil ≥7500	28 (21)	1.60 (0.99-2.57)	0.054				
Lymphocyte≥1500	60 (47)	1.37 (0.95-1.98)	0.097				
NLR	152 (125)	1.03 (1.00-1.06)	0.026			1.04 (1.00-1.07)	0.029
LDH ≥300	13 (12)	1.72 (0.93-3.19)	0.084				
Corrected Calcium ≥10	11 (9)	0.93 (0.46-1.85)	0.832				
Albumin <3.5	23 (16)	1.78 (1.04-3.07)	0.037				
Alkaline phosphatase ≥104	50 (42)	1.40 (0.96-2.07)	0.085				
AST≥40	12 (11)	2.56 (1.36-4.84)	0.004	1.96 (1.03-3.76)	0.042		
ALT≥40	18 (15)	1.26 (0.73-2.18)	0.399				
De Retis ratio	148 (122)	1.19 (0.97-1.45)	0.096				

KPS, Karnofsky performance status score; DFI, disease-free interval; Hb, hemoglobin; NLR, neutrophil-to-lymphocyte ratio; LDH, lactate dehydrogenase; AST, aspartate transaminase; ALT, alanine transaminase; HR, hazard ratio; CI, confidence interval.
Multivariable model 1 (uni p-value ≤0.15 without LDH) used with metachronous type, nephrectomy, DFI<1, Hb, platelet, neutrophil, lymphocyte, albumin, Alkaline phosphatase, AST.
Multivariable model 2 (uni p-value ≤0.15 without LDH) used with metachronous type, nephrectomy, DFI<1, Hb, platelet, albumin, Alkaline phosphatase, NLR, de retis ratio.

or nephrectomy and NLR (Model B: C-index 0.610) show no significant differences (mean difference 0.017, 95% CI -0.021 to 0.057) using 2000 bootstrap samples. When comparing the 2 models with the Heng and mMSKCC risk models, 2 models did not show better predictive ability than Heng or mMSKCC risk models. To investigate the effect of inflammatory factors, the models with adding significant inflammatory factor were analyzed. No significant increases in C-index by adding inflammatory factors to established Heng or mMSKCC risk models (p>0.05).

3.4. Modeling New Prognostic Risk Criteria for OS. The same methods were applied to derive new OS prediction models. Model A included nephrectomy, liver metastasis, hemoglobin, neutrophil, and alkaline phosphatase, which were significant factors for OS multivariate analysis (Table 3). Model B incorporated nephrectomy, hemoglobin, NLR, alkaline phosphatase, and DRR. Models A and B had Harrell's C-indices of 0.708 and 0.727, respectively, with no significant difference (the mean difference was 0.02, 95% CI -0.011 to 0.058, Table 5). Compared to the Heng (C-index, 0.661) risk model, Model B was significantly better predictive ability (mean difference was -0.055, 95% CI -0.112 to -0.004). Compared to the mMSKCC (C-index, 0.612) risk models, Model A and B showed significantly better predictive ability (mean difference was -0.097, 95% CI -0.153 to -0.043, mean difference was -0.117, 95% CI -0.174, -0.066, respectively).

There were no significant increases of predictive ability in models with adding inflammatory factors to Heng risk model. On the other hand, the addition of inflammatory factors to mMSKCC risk model showed significant increases

Table 3: Univariate and multivariate analyses of overall survival using the new prognostic factors.

Variables		Univariable		Multivariable 1		Multivariable 2	
	N (event)	HR (95% CI)	p-value	HR (95% CI)	p-value	HR (95% CI)	p-value
Age ≥55 years	101 (81)	0.92 (0.64-1.32)	0.635				
Female gender	34 (33)	1.38 (0.92-2.06)	0.117				
Metachronous type	61 (48)	0.48 (0.33-0.69)	<.001				
Nephrectomy	89 (70)	0.34 (0.23-0.50)	<.001	0.37 (0.24-0.55)	<.001	0.38 (0.25-0.56)	<.001
Body mass index	145 (118)	0.96 (0.90-1.02)	0.159				
KPS≤80	12 (10)	1.02 (0.53-1.96)	0.955				
DFI≤1year	106 (88)	2.04 (1.40-2.99)	<.001				
mMSKCC, favorable	48 (33)	1	(0.003)				
intermediate	74 (64)	1.77 (1.16-2.70)	0.009				
poor	12 (12)	2.83 (1.45-5.54)	0.002				
Heng, favorable	14 (7)	1	<.001				
intermediate	94 (79)	3.11 (1.42-6.78)	0.004				
poor	24 (21)	6.46 (2.70-15.46)	<.001				
Lung metastasis	113 (91)	0.76 (0.52-1.11)	0.152				
Liver metastasis	33 (32)	1.92 (1.28-2.89)	0.002	1.88 (1.21-2.94)	0.005		
Bone metastasis	54 (48)	1.12 (0.78-1.61)	0.533				
Brain metastasis	18 (13)	0.98 (0.55-1.75)	0.955				
Hb, M<13, F<11.5	90 (81)	2.04 (1.41-2.94)	<.001	1.83 (1.23-2.71)	0.003	1.71 (1.16-2.51)	0.007
Platelet ≥400	19 (16)	2.51 (1.45-4.34)	0.001				
Neutrophil ≥7500	28 (24)	2.17 (1.37-3.42)	0.001	2.58 (1.55-4.30)	<.001		
Lymphocyte≥1500	60 (53)	1.71 (1.19-2.45)	0.003				
NLR	152 (125)	1.06 (1.03-1.09)	<.001			1.07 (1.04-1.11)	<.001
LDH ≥300	13 (11)	1.37 (0.72-2.58)	0.338				
Corrected Calcium ≥10	11 (11)	1.73 (0.92-3.24)	0.087				
Albumin <3.5	23 (21)	3.77 (2.28-6.22)	<.001				
Alkaline phosphatase≥104	50 (43)	1.83 (1.23-2.70)	0.003	1.63 (1.08-2.45)	0.019	1.73 (1.16-2.58)	0.008
AST≥40	12 (12)	3.60 (1.95-6.65)	<.001				
ALT≥40	101 (81)	0.92 (0.64-1.32)	0.635				
De Retis ratio	34 (33)	1.38 (0.92-2.06)	0.117			1.34 (1.09-1.64)	0.006

KPS, Karnofsky performance score; DFI, disease-free interval; Hb, hemoglobin; NLR, neutrophil-to-lymphocyte ratio; LDH, lactate dehydrogenase; AST, aspartate transaminase; ALT, alanine transaminase; HR, hazard ratio; CI, confidence interval.
Multivariable 1 (uni p-value ≤0.15 without LDH) used with gender, metachronous type, nephrectomy, DFI<1, liver mets, Hb, platelet, neutrophil, Lymphocyte, corrected ca, Alkaline phosphatase, AST.
Multivariable 2 (uni p-value ≤0.15 without LDH) used with gender, metachronous type, nephrectomy, DFI<1, liver mets, Hb, platelet, corrected ca, Alkaline phosphatase, NLR, de retis ratio.

Table 4: Comparison of new risk models for progression-free survival using the Heng and MSKCC risk models with 2000 bootstraps.

Model	Harrell's C index	mean(difference), 95% CI (2.5%, 97.5% of difference)
Model A	0.594	Model B vs A: 0.017 (-0.021, 0.057)
Model B	0.610	
Heng risk model	0.614	Heng vs Model A: 0.034 (-0.030, 0.103)
		Heng vs Model B: -0.009 (-0.081, 0.058)
MSKCC risk model	0.569	mMSKCC vs Model A: -0.025 (-0.106, 0.054)
		mMSKCC vs Model B: -0.042 (-0.127, 0.036)
Heng risk model + DRR	0.639	Heng vs (Heng+DRR): -0.025 (-0.082, 0.013)
Model C = mMSKCC risk model + AST	0.569	mMSKCC vs Model C -0.013 (-0.052, 0.015)
Model D = mMSKCC risk model + NLR + DRR	0.602	mMSKCC vs Model D: -0.046 (-0.117, 0.002)
		Model C vs Model D: -0.033 (-0.102, 0.020)

MSKCC, Memorial Sloan Kettering Cancer Center; AST, aspartate transaminase; NLR, neutrophil-to-lymphocyte ratio; CI, confidence interval.
Model A = Nephrectomy, AST.
Model B = Nephrectomy, NLR.

Table 5: Comparison of new risk models for overall survival using the Heng and MSKCC risk models with 2000 bootstraps.

Model	Harrell's C index	mean(difference), 95% CI (2.5%, 97.5% of difference)
Model A	0.708	Model B vs A: 0.02 (-0.011, 0.058)
Model B	0.727	
Heng risk model	0.661	Heng vs Model A: -0.035 (-0.088, 0.008) Heng vs Model B: -0.055 (-0.112, -0.004)
mMSKCC risk model	0.612	mMSKCC vs Model A: -0.097 (-0.153, -0.043) mMSKCC vs Model B: -0.117 (-0.174, -0.066)
Model C = Heng risk model + AST	0.676	Heng vs (Heng + SGOT): -0.011 (-0.031, 0.004)
Model D = Heng risk model + Alkaline phosphatase + DRR	0.697	Heng vs (Heng + De Ritis ratio): -0.035 (-0.083, 0) (Heng + SGOT) vs (Heng + De Ritis ratio): -0.024 (-0.07, 0.011)
Model E = mMSKCC risk model + Neutrophil + AST	0.658	mMSKCC vs Model E: -0.049 (-0.098, -0.013)
Model F = mMSKCC risk model + NLR + Alkaline phosphatase +DRR	0.691	mMSKCC vs Model F: -0.084 (-0.149, -0.034) Model E vs Model F: -0.034 (-0.092, 0.014)

MSKCC, Memorial Sloan Kettering Cancer Center; AST, aspartate transaminase; NLR, neutrophil-to-lymphocyte ratio; CI, confidence interval.
Model A = Nephrectomy, Liver mets, Hb, Neutrophil, Alkaline phosphatase.
Model B = Nephrectomy, Hb, NLR, Alkaline phosphatase, DRR.

of predictive ability. Incorporating the neutrophil and AST into the mMSKCC risk model and NLR, alkaline phosphatase and DRR into the mMSKCC risk model showed that the C-index increased from 0.612 to 0.658 and 0.691, respectively.

4. Discussion

Development of an accurate prognostic model is important for a patient's risk-oriented treatment strategy in treatment-naive clinical settings. The current Heng and MSKCC models can potentially be improved by incorporating novel prognostic variables or can be replaced with new models with different variables [4, 5]. Our study evaluated the potential for novel prognostic factors to improve the predictive power of the current Heng and MSKCC risk models or to derive a new model entirely; to that end, we achieved a significant improvement in the predictive accuracy of OS. Notably, our new model plus the addition of new prognostic factors to current models reflects the importance of inflammatory factors; moreover, they were based on an Asian population, whereas the original MSKCC and Heng models are mainly based on Western populations and do not incorporate inflammation/immune-related factors. Our study thus offers wider applicability with more precise prognostication of patients of different ethnicities.

A number of factors analyzed in our study have already been shown to significantly predict PFS and OS [13]. The most interesting finding in our study was that the NLR, DRR (or AST) and nephrectomy were significant prognostic factors for both PFS and OS. Our results also reflect the limitation of the current MSKCC and Heng risk models, in which PFS and OS are not always correlated with each other [19].

The prognostic significances of nephrectomy, NLR, and DRR were previously described [14, 20, 21]; however, no study has previously demonstrated their collective implications for PFS and OS. The NLR and nephrectomy are the most common prognostic factors in mRCC; nephrectomy was incorporated into the recently revised Heng risk model [22]. NLR was also proposed as a replacement for the neutrophil count, and our findings demonstrated its superiority.

A partial rationale for our study was that RCC has been closely linked to immune responses in systemic inflammation [9]; moreover, cancerous tissues show a greater rate of aerobic glycolysis than normal tissue (the Warburg effect) [23]. Neutrophils are the major inflammatory component of tumors; circulating neutrophils produce cytokines that stimulate cancer progression [24], while tumor-associated neutrophils and their bone marrow precursors (peripheral neutrophils and myeloid positive suppressor cells) suppress immune T cells [25]. The association of increased neutrophil counts with poor RCC prognosis [1] resulted in elevated neutrophils being considered an independent predictor of poor prognosis in the Heng risk model of clear-cell mRCC [5] and non-mRCC [16] during treatment [21, 26]. The switch from neutrophil count to NLR was based on the idea that the latter is a potential indicator of host immune and neutrophil-dependent tumorigenesis, as well as inflammation induced by T cell function [20]. Patients with an increased NLR exhibit relative lymphocytopenia, which can lead to worse prognosis and an increased potential for tumor progression.

The baseline NLR and its changes during targeted therapy administration may predict outcomes, as early NLR decrease was associated with favorable PFS and OS whereas its increase was associated with unfavorable outcomes [15]. This can assist clinicians in determining whether to maintain treatment with the same therapeutic agent or switch to another (e.g., in patients whose tumors slightly grew on imaging [stable disease status] but with a drop in the NLR). Moreover, as tyrosine kinase inhibitors exert antiangiogenic and immunomodulatory effects such as neutrophil migration and T lymphocyte-dendritic cell cross-talk [27], the implications of NLR changes in mRCC patients receiving such therapies may have greater significance than in the RCC

patient population as a whole. The NLR might also be useful when administering immunotherapeutic regimens [3].

We showed that the pretreatment DRR (or AST) is an independent predictive biomarker for PFS and OS in patients with mRCC treated with targeted therapy. Pathological processes that can lead to a higher proliferative state, tissue damage, and high tumor cell turnover tend to increase AST but not the liver-specific ALT (at least not to the same extent), making the AST/ALT ratio an attractive potential biomarker [28]. AST is expressed in different subcomponents of breast cancer, pancreatic cancer, lung cancer, and cholangiocarcinoma cells [28]. The DRR has already been suggested as an independent prognostic biomarker, including metastasis-free survival and OS after curative nephrectomy [14] for non-mRCC patients and those with mRCC who underwent cytoreductive nephrectomy [29].

Previous studies suggested explanations for the DRR's ability to predict survival in patients with RCC [14, 23]. The AST and ALT levels might be involved in glycolysis in clear-cell RCC. Moreover, von Hippel-Lindau loss, a key trigger of clear-cell RCC, elevates hypoxia-induced factor levels, which is linked to markedly increased glycolysis [30]. Moreover, AST is a critical component of the malate-aspartate shuttle pathway of glycolysis [30].

This study had several limitations, including its retrospective design, single center restrictions, and disproportionally small risk groups. The cut-off levels of NLR and DRR are arbitrary, so there were additional limitations to use as continuous variables. However their prognostic values ought to be sustained in further studies, as no standard guidelines currently exist for NLR cut-off values. Additionally, other inflammatory factors such as C-reactive proteins, interleukin-6, and gamma-glutamyltransferase should be considered in future studies. Finally, our new model does not include biomarkers or genomic information; more specific targets ought to be selected.

5. Conclusion

In overall survival, predictive ability was increased when NLR and DRR markers were added to established Heng or mMSKCC risk models in patients with mRCC treated with first-line targeted therapy. We observed significantly improved predictive ability over the established models, suggesting that our inflammatory factors ought to be incorporated into the Heng and MSKCC risk models.

Data Availability

The datasets used and/or analyzed during the current study are available from the corresponding author (Jinsoo Chung, cjs5225@ncc.re.kr) on reasonable request. The IRB and ethical committee of the National Cancer Center (in Korea) will review the requests because of the patients' information. After the approval of the committee with confirmation of the reasonable requests, the dataset will be freely available. The other contact e-mail besides the corresponding author's e-mail is irb@ncc.re.kr.

Conflicts of Interest

All authors declare that they have no conflicts of interest.

Authors' Contributions

Sung Han Kim wrote the manuscript and collected the dataset; Eun Young Park and Jungnam Joo performed the statistical analyses; and Jung Kwon Kim and Jinsoo Chung designed the study.

Acknowledgments

This study was supported by the National Cancer Center grant (No. NCC 1710290-2).

References

[1] F. Donskov and H. von der Maase, "Impact of immune parameters on long-term survival in metastatic renal cell carcinoma," *Journal of Clinical Oncology*, vol. 24, no. 13, pp. 1997–2005, 2006.

[2] D. Keizman, P. Huang, M. A. Eisenberger et al., "Angiotensin system inhibitors and outcome of sunitinib treatment in patients with metastatic renal cell carcinoma: A retrospective examination," *European Journal of Cancer*, vol. 47, no. 13, pp. 1955–1961, 2011.

[3] R. J. Motzer, B. Escudier, and D. F. McDermott, "Nivolumab versus everolimus in advanced renal-cell carcinoma," *The New England Journal of Medicine*, vol. 373, no. 19, pp. 1803–1813, 2015.

[4] R. J. Motzer, M. Mazumdar, J. Bacik, W. Berg, A. Amsterdam, and J. Ferrara, "Survival and prognostic stratification of 670 patients with advanced renal cell carcinoma," *Journal of Clinical Oncology*, vol. 17, no. 8, pp. 2530–2540, 1999.

[5] D. Y. C. Heng, W. Xie, M. M. Regan et al., "Prognostic factors for overall survival in patients with metastatic renal cell carcinoma treated with vascular endothelial growth factor-targeted agents: results from a large, multicenter study," *Journal of Clinical Oncology*, vol. 27, no. 34, pp. 5794–5799, 2009.

[6] R. J. Motzer, J. Bacik, B. A. Murphy, P. Russo, and M. Mazumdar, "Interferon-alfa as a comparative treatment for clinical trials of new therapies against advanced renal cell carcinoma," *Journal of Clinical Oncology*, vol. 20, no. 1, pp. 289–296, 2002.

[7] F. Colotta, P. Allavena, A. Sica, C. Garlanda, and A. Mantovani, "Cancer-related inflammation, the seventh hallmark of cancer: links to genetic instability," *Carcinogenesis*, vol. 30, no. 7, pp. 1073–1081, 2009.

[8] D. Hanahan and R. A. Weinberg, "Hallmarks of cancer: the next generation," *Cell*, vol. 144, no. 5, pp. 646–674, 2011.

[9] A. Mantovani, P. Allavena, A. Sica, and F. Balkwill, "Cancer-related inflammation," *Nature*, vol. 454, no. 7203, pp. 436–444, 2008.

[10] D.-K. Kim, S. Y. Oh, H.-C. Kwon et al., "Clinical significances of preoperative serum interleukin-6 and C-reactive protein level in operable gastric cancer," *BMC Cancer*, vol. 9, article 155, 2009.

[11] W. Chua, K. A. Charles, V. E. Baracos, and S. J. Clarke, "Neutrophil/lymphocyte ratio predicts chemotherapy outcomes in patients with advanced colorectal cancer," *British Journal of Cancer*, vol. 104, no. 8, pp. 1288–1295, 2011.

[12] F. Balkwill and A. Mantovani, "Inflammation and cancer: back to Virchow?" *The Lancet*, vol. 357, no. 9255, pp. 539–545, 2001.

[13] H.-C. Kwon, S. H. Kim, S. Y. Oh et al., "Clinical significance of preoperative neutrophil-lymphocyte versus platelet-lymphocyte ratio in patients with operable colorectal cancer," *Biomarkers*, vol. 17, no. 3, pp. 216–222, 2012.

[14] H. Lee, S. E. Lee, S.-S. Byun, H. H. Kim, C. Kwak, and S. K. Hong, "De Ritis ratio (aspartate transaminase/alanine transaminase ratio) as a significant prognostic factor after surgical treatment in patients with clear-cell localized renal cell carcinoma: a propensity score-matched study," *BJU International*, vol. 119, no. 2, pp. 261–267, 2017.

[15] A. J. Templeton, J. J. Knox, X. Lin et al., "Change in Neutrophil-to-lymphocyte Ratio in Response to Targeted Therapy for Metastatic Renal Cell Carcinoma as a Prognosticator and Biomarker of Efficacy," *European Urology*, vol. 70, no. 2, pp. 358–364, 2016.

[16] S. S. Byun, E. C. Hwang, S. H. Kang, S. H. Hong, J. Chung, T. G. Kwon et al., "Prognostic Significance of Preoperative Neutrophil-to-Lymphocyte Ratio in Nonmetastatic Renal Cell Carcinoma: A Large, Multicenter Cohort Analysis," *BioMed Research International*, vol. 2016, Article ID 5634148, 8 pages, 2016.

[17] F. E. Harrell Jr., K. L. Lee, and D. B. Mark, "Multivariable prognostic models: issues in developing models, evaluating assumptions and adequacy, and measuring and reducing errors," *Statistics in Medicine*, vol. 15, no. 4, pp. 361–387, 1996.

[18] M. J. Pencina, S. D'Agostino, and R. S. Vasan, "Evaluating the added predictive ability of a new marker: from area under the ROC curve to reclassification and beyond," *Statistics in Medicine*, vol. 27, no. 2, pp. 157–172, 2008.

[19] W.-A. Kwon, I.-C. Cho, A. Yu et al., "Validation of the mskcc and heng risk criteria models for predicting survival in patients with metastatic renal cell carcinoma treated with sunitinib," *Annals of Surgical Oncology*, vol. 20, no. 13, pp. 4397–4404, 2013.

[20] H. Cho, H. W. Hur, S. W. Kim et al., "Pre-treatment neutrophil to lymphocyte ratio is elevated in epithelial ovarian cancer and predicts survival after treatment," *Cancer Immunology, Immunotherapy*, vol. 58, no. 1, pp. 15–23, 2009.

[21] Y. Ohno, J. Nakashima, M. Ohori, T. Hatano, and M. Tachibana, "Pretreatment neutrophil-to-lymphocyte ratio as an independent predictor of recurrence in patients with nonmetastatic renal cell carcinoma," *The Journal of Urology*, vol. 184, no. 3, pp. 873–878, 2010.

[22] D. Y. Heng, W. Xie, M. M. Regan et al., "External validation and comparison with other models of the international metastatic renal-cell carcinoma database consortium prognostic model: a population-based study," *The Lancet Oncology*, vol. 14, no. 2, pp. 141–148, 2013.

[23] P. P. Hsu and D. M. Sabatini, "Cancer cell metabolism: warburg and beyond," *Cell*, vol. 134, no. 5, pp. 703–707, 2008.

[24] Y. H. Kusumanto, W. A. Dam, G. A. P. Hospers, C. Meijer, and N. H. Mulder, "Platelets and granulocytes, in particular the neutrophils, form important compartments for circulating vascular endothelial growth factor," *Angiogenesis*, vol. 6, no. 4, pp. 283–287, 2003.

[25] S. Nagaraj, A. G. Schrum, H. I. Cho, E. Celis, and D. I. Gabrilovich, "Mechanism of T cell tolerance induced by myeloid-derived suppressor cells," *The Journal of Immunology*, vol. 184, no. 6, pp. 3106–3116, 2010.

[26] S. Saroha, R. G. Uzzo, E. R. Plimack, K. Ruth, and T. Al-Saleem, "Lymphopenia is an independent predictor of inferior outcome in clear cell renal carcinoma," *The Journal of Urology*, vol. 189, no. 2, pp. 454–460, 2013.

[27] N. Na, J. Yao, C. Cheng et al., "Meta-analysis of the efficacy of the pretreatment neutrophil-tolymphocyte ratio as a predictor of prognosis in renal carcinoma patients receiving tyrosine kinase inhibitors," *Oncotarget* , vol. 7, no. 28, pp. 44039–44046, 2016.

[28] M. Botros and K. A. Sikaris, "The de ritis ratio: the test of time," *The Clinical Biochemist Reviews*, vol. 34, pp. 117–130, 2013.

[29] H. Ishihara, T. Kondo, K. Yoshida et al., "Evaluation of Preoperative Aspartate Transaminase/Alanine Transaminase Ratio as an Independent Predictive Biomarker in Patients With Metastatic Renal Cell Carcinoma Undergoing Cytoreductive Nephrectomy: A Propensity Score Matching Study," *Clinical Genitourinary Cancer*, vol. 15, no. 5, pp. 598–604, 2017.

[30] W. V. V. Greenhouse and A. L. Lehringer, "Occurrence of the malate-aspartate shuttle in various tumor types," *Cancer Research*, vol. 36, no. 4, pp. 1392–1396, 1976.

Hindawi
Journal of Oncology
Volume 2018, Article ID 6273947, 10 pages
https://doi.org/10.1155/2018/6273947

Review Article

Resection of Liver Metastases: A Treatment Provides a Long-Term Survival Benefit for Patients with Advanced Pancreatic Neuroendocrine Tumors: *A Systematic Review and Meta-Analysis*

Xinzhe Yu,[1,2] **Jichun Gu**,[3] **Haoxuan Wu**,[1] **Deliang Fu**,[3] **Ji Li**,[3] **and Chen Jin**[3]

[1]*Department of Thoracic Surgery, Fudan University Shanghai Cancer Center. 270 Dong-An Rd, Shanghai 200032, China*
[2]*Department of Oncology, Shanghai Medical College, Fudan University, Shanghai, China*
[3]*Pancreatic Surgery Department, Huashan Hospital Affiliated to Fudan University, Shanghai 200040, China*

Correspondence should be addressed to Chen Jin; galleyking@hotmail.com

Received 12 July 2018; Accepted 24 October 2018; Published 14 November 2018

Guest Editor: Wei-Ting Chao

Purpose. Nonsurgical therapies, including biotherapy, chemotherapy, and liver-directed therapy, provided a limit survival benefit for PNET patients with hepatic metastases. With the development of liver resection technique, there was a controversy on whether to perform a liver resection for these patients. *Methods*. A computerized search was made of the Medline/PubMed, EMbase, Cochrane Library, and SinoMed (CBM) before March 2018. A meta-analysis was performed to investigate the differences in the efficacy of liver resection and nonliver resection treatments based on the evaluation of morbidity, 30-day mortality, symptom relief rate, and 1-, 3-, and 5-year survival. Two investigators reviewed all included articles and extracted the data of them. The meta-analysis was performed via Review Manager 5.3 software. *Results*. A total of 13 cohort studies with 1524 patients were included in this meta-analysis. Compared with the nonliver resection group, liver resection group had a longer 1-, 3-, and 5-year survival time and a higher symptom relief with an acceptable mortality and morbidity. *Conclusions*. Liver resection is a safe treatment and could significantly prolong the long-term prognosis for highly selected patients with resectable liver metastases from PNET. Further randomized, controlled trials are needed.

1. Introduction

PNET (pancreatic neuroendocrine tumor), commonly known as islet cell tumors, is a rare malignant neoplasm comprising of <2% pancreatic tumors and its incidence is <1 per 10,000 person per year [1–3]. However, the incidence is increasing recently due to the advancements of imaging and endoscopic technique [4]. In contrast to pancreatic adenocarcinoma, PNET is a kind of relatively indolent tumor [5]. PNET is highly heterogeneous and could be separated with many different subtypes according to secreted hormones [6]. Owing to 50%-80% of PNETs are malignant (except for insulinomas), metastases always turn out during the progression of PNETs and liver is a frequent disseminate site [5, 6] Treatments of hepatic metastases include surgery (hepatic resection), intervention (embolization [HAE] and transcatheter arterial chemoembolization [TACE]), biotherapy (octreotide/interferon and peptide receptor radionuclide therapy [PRRT]), systemic chemotherapy (streptozotocin, 5-fluorouracil, and everolimus), and ablation. Chemoembolization means HAE combined with chemotherapeutic agents [5, 7, 8]. Among these approaches, liver surgery for metastatic disease has provided a potentially curative choice for patients with colorectal cancer [9]. With the safety enhancement of liver surgical techniques, hepatic resection is becoming an optimal option for PNET patients with liver metastases [10]. This meta-analysis was mainly to evaluate overall survival outcomes and postoperative symptom relief from PNET patients with liver metastases between liver resection and nonliver resection groups.

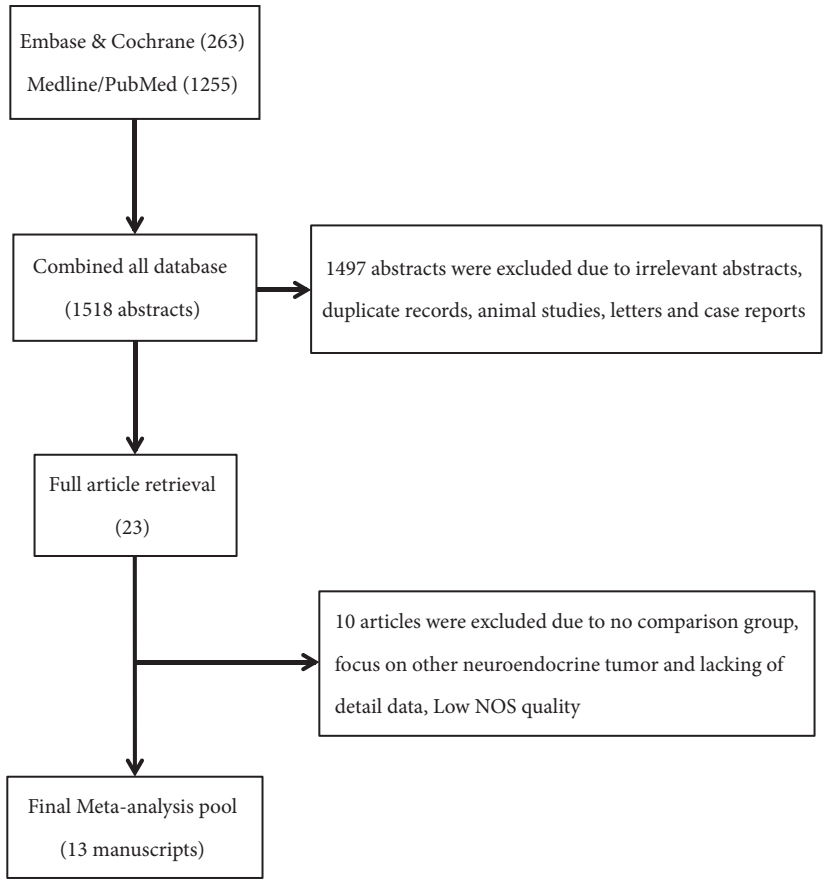

Figure 1: PRISMA Flowchart describing literature search history.

2. Materials and Methods

2.1. Search Strategy. A computerized search was made of the Medline/PubMed, EMbase, Cochrane Library, and SinoMed (CBM) before March 2018. No language was limited. We used the following keywords: "pancreatic neuroendocrine tumors", "hepatic metastases", "liver metastases", "hepatic metastases resection", "liver metastases resection", "hepatectomy", "hepatic resection", and "liver resection", and we combined these keywords with "AND" "OR". We also searched related references in the retrieved studies and reviewed articles from the database. For details, please see the flowchart of search history in Figure 1.

2.2. Inclusion and Exclusion Criteria. The original studies included in the meta-analysis need to meet the following criteria: (1) cohort or comparative studies of patients with liver metastatic PNET undergoing hepatectomy; (2) at least 10 patients that should be reported; (3) at least 1-year overall survival (OS) data that should be available after hepatic resection; (4) NOS score≥6. Abstracts, letters, animal experiments, reviews without original data, case reports, and studies lacking control groups were excluded.

2.3. Data Extraction. Abstracts of all articles were identified by two reviewers (Xinzhe Yu & Jichun Gu) independently. If there were any discrepancies which could not be solved with discussion between the two authors, a third independent author (Chen Jin) would determine the eligibility and data of the study. We extracted such data from all articles as follows: first author, year of publication, study population characteristics, study design, inclusion and exclusion criteria, resection margin, procedure-related morbidity and mortality, OS, and median follow-up. All of the texts, tables, and figures were reviewed for data extraction. All patients in liver resection group were treated with the resection of primary tumors and liver metastases. Patients in nonliver resection group underwent nonliver resection with or without primary tumors resection.

2.4. Quality Assessment. A quality assessment of retrieved studies in this meta-analysis was carried out in the form of Newcastle-Ottawa Quality Assessment Scale (NOS System) for cohort studies [11]. The aspects of selection, comparability, and follow-up were assessed with every inclusive study. Any study that could obtain a score ≥ 7 may be recognized as high-quality study for inclusion.

2.5. Statistical Analysis. We conducted the meta-analysis following the MOOSE guidelines [12] with the Review Manager 5.3 software. The outcomes of liver resection group versus

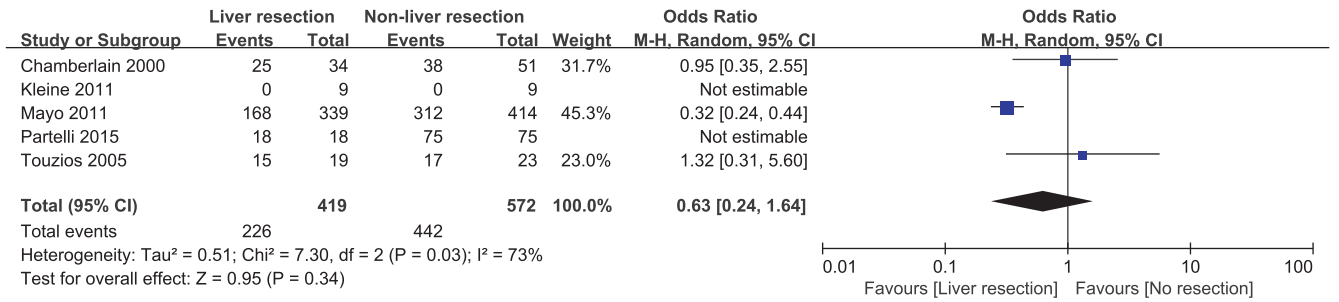

Figure 2: Forest plot for the occurrence time of hepatic metastases (synchronous/metachronous) of liver resection group and nonliver resection group in patients with liver metastases from pancreatic neuroendocrine tumor. There is no significant difference between two groups.

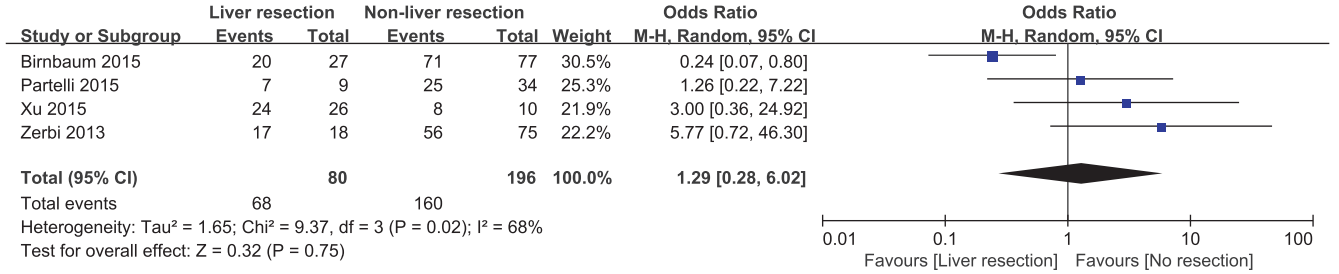

Figure 3: Forest plot for the Grade classification (G1&G2/G3) of liver resection group and nonliver resection group in patients with liver metastases from pancreatic neuroendocrine tumor. There is no significant difference between two groups.

nonliver resection group were pooled with a random-effect or fixed-effect meta-analysis. In addition, heterogeneity among studies was evaluated by I^2 and p value, with significance being set at $p< 0.05$ and $I^2 > 50\%$. A high value for I^2 indicates heterogeneity. If there was substantial heterogeneity, random effects models would be used in analysis. Publication bias was evaluated with a funnel plot.

3. Results

A total of 23 articles were selected for full-text. Among them, 9 studies were recognized as high quality studies because of NOS score ≥7 and 4 studies lacking some of the key data got 6 points, while the rest, 10 studies, were excluded due to NOS scores< 6. In summary, 13 cohort [13–25] studies were included and the details of the included and excluded [26–35] studies were shown in Table 1 and Supporting Table 1. There were 1524 patients in 13 cohort studies included in this meta-analysis, and 616 patients undergoing hepatic resection were divided into liver resection group while other 908 patients were with nonliver resection therapies as the control group. The details of baseline data from these studies were shown in Table 1. Furthermore, a meta-analysis of the site of hepatic metastases (unilobar/bilobar), the grading system (G1&G2/G3), and the occurrence time of hepatic metastases (synchronous/metachronous) was performed, and there is no significant difference on the occurrence time of hepatic metastases and the grading system between two groups (Figure 2: OR=0.63; 95% CI, 0.24, 1.64; p=0.34. Figure 3: OR=1.29; 95% CI, 0.28, 6.02; p=0.75) while the liver resection group have more unilobar hepatic metastases (Figure 4: OR=5.61; 95% CI, 2.87, 10.97; p<0.001).

Then a further literature review of 13 included studies was performed. (Table 2) In general, the median postoperative adjuvant therapy rate is of 42.00% (0%-68.00%). For postoperative outcomes, the morbidity was 33.5% (3.28%-44.44%) and the 30-day mortality was 3.32% (0%-5.30%). For long-term outcomes, compared with nonliver resection group whose median OS was 17 months (17-54.8), liver resection group could be prolonged to 84 months (36-123). Overall, almost all studies have an agreement on the idea that hepatic resection could provide a prognosis benefit for PNET patients with liver metastases and according to the data from these studies, there was no concern about the safety of liver resection.

The median 1-year, 3-year, and 5-year OS rates of all patients in the liver resection group were 92.69%, 76.93%, and 67.54%, respectively, whereas the data of nonliver resection group was 77.31%, 40.94%, and 26.6%. In the retrieved studies, liver resection was not only related to a significant higher 1-year OS rate (OR=3.31; 95% CI, 2.34, 4.67; p<0.001), 3-year OS rate (OR=4.29; 95% CI, 2.71, 6.80; p<0.001), and 5-year OS rate (OR=5.30; 95% CI, 3.24, 8.67; p<0.001) (Table 3) but also created a chance for patients, no matter with functional or nonfunctional PNET, to have a higher symptom relief rate including hormonal symptoms, mechanical symptoms (Figure 5: OR=2.49; 95% CI, 1.03, 6.04; p=0.04). A funnel plot of these 13 studies was used to examine publication bias in the meta-analysis (Figure 6). As shown in Figure 6, this plot

Table 1: Basic study characteristics of included trials.

Author	Year	Country	Time Period	Patient Number	Age		Male/Female ratio	Grade	Hepatic resection (Y/N)	Hepatic Metastases		NOS score
					Liver resection	Non-liver resection		G1/G2/G3		Unilobar/ Bilobar	Synchronous/ Metachronous	
Birnbaum et al	2015	France	1995-2012	118	60 (31-82)	57 (20-83)	62/56	48/43/13	27/91	10/17	27/0	7
Xu et al	2015	China	2008-2013	36	49.9 ± 11.0	56.5 ± 12.5	14/22	6/26/4	26/10	25/11	NR	6
Partelli et al	2015	Italy	2000-2011	93	50 (45-59)	51.5 (43-63)	53/40	21/51/20	18/75	13/80	93/0	7
Zerbi et al	2013	Italy	2004-2007	45	56.9	60.6	26/19	13/19/11	9/36	NR	NR	6
Kleine et al	2011	German	1990-2009	15	55 (20-77)		NR	NR	9/6	NR	15/0	7
Mayo et al	2011	America	1985-2010	753	56 ± 12.6	57 ± 12.8	391/362	NR	339/414	223/530	273/480	8
House et al	2006	America	1988-2003	31	52 (31-71)	41 (31-52)	15/16	NR	26/5	NR	NR	9
Osborne et al	2006	America	2000-2004	120	56 ± 11.6	58 ± 11.1	64/56	NR	61/59	NR	NR	6
Musunuru et al	2006	America	1996-2004	48	56 (27-85)		NR	NR	13/35	14/34	28/20	7
Touzios et al	2005	America	1990-2004	42	58 ± 3	59 ± 3	17/25	NR	19/23	15/27	32/10	6
Solorzano et al	2001	America	1988-1999	100	NR	NR	56/44	NR	20/80	NR	NR	7
Chamberlain et al	2000	America	1992-1998	85	50 (20-79)	54 (23-79)	37/48	NR	34/51	14/71	63/22	7
Chen et al	1998	America	1984-1995	38	54 ± 4	59 ± 3	24/14	NR	15/23	17/21	NR	7

NR indicates no report.

Table 2: All included literatures review.

Study ID	Morbidity	30-day mortality	Postoperative adjuvant therapy Rate	Median OS (m)		Median follow-up (m)	Non-liver resection treatments	Conclusion
				Hepatic resection	Non-liver resection			
Birnbaum 2015	44.00%	5.00%	NR	90	NR	NR	Resection of primary tumors	Resection of liver metastases improve survival
Xu 2015	NR	NR	NR	57.2	54.8	32	Somatostatin analogues and chemotherapy	Resection of liver metastases could not prolong OS but could improve PFS
Partelli 2015	44.44%	NR	68.00%	97	36	41	Somatostatin analogues, PRRT, chemotherapy	Resection of liver metastases improve survival
Zerbi 2013	NR	NR	48.68%	NR	20.5	21	Somatostatin analogues, PRRT, ablation, chemotherapy	Resection of liver metastases could be the first-choice treatment for malignent PNET
Kleine 2011	22.22%	NR	NR	NR	37.8	40	Resection of primary tumors	Resection of liver metastases may prolong OS
Mayo 2011	NR	NR	NR	123	33	26	Intra-arterial therapy and resection of primary tumors	Hepatectomy most benefited those patients with low-volume (<25%) liver metastasis or those with symptomatic high-volume liver metastasis
House 2006	25.00%	0.00%	11.54%	78	17	NR	Somatostatin analogues, chemotherapy, chemoembolization and resection of primary tumors	There is a survival benefit from complete surgical resection of metastatic islet cell tumors originating from the pancreas
Osborne 2006	3.28%	1.64%	65.57%	NR	NR	NR	Somatostatin analogues and chemotherapy, PRRT, embolization	Patients who undergo surgical cytoreduction of symptomatic neuroendocrine hepatic metastases enjoy prolonged survival when compared with their medically treated counterparts

Table 2: Continued.

Study ID	Morbidity	30-day mortality	Postoperative adjuvant therapy Rate	Median OS (m)		Median follow-up (m)	Non-liver resection treatments	Conclusion
				Hepatic resection	Non-liver resection			
Musunuru 2006	NR	NR	8.00%	NR	NR	20	Systemic hormonal and chemotherapy, ablation, hepatic artery embolization	In patients with liver-only neuroendocrine metastases, surgical therapy is associated with improved survival
Touzios 2005	42.00%	5.30%	36.00%	>96	NR	NR	Somatostatin analogues, chemotherapy, PRRT, ablation and resection of primary tumors	Resection has been shown to be an excellent treatment and accumulating data document improved survival with resection of these tumors
Solorzano2001	NR	NR	60.00%	36	21.6	32	Chemotherapy, hepatic artery embolization	Aggressive management should probably be restricted to younger patients with limited extrahepatic disease
Chamberlain 2000	NR	NR	NR	NR	NR	27	Hepatic artery embolization, Somatostatin analogues and chemotherapy and resection of primary tumors	Hepatic resection has a role in the man-agement of patients with NET metastases and may prolong survival
Chen 1998	NR	NR	0.00%	NR	27	27	Chemoembolization, chemotherapy, PRRT and resection of primary tumors	Hepatic resection for metastatic neuroen-docrine tumors may prolong survival

Table 3: Survival outcomes of liver resection group versus nonliver resection group.

Survival outcomes	No. Of studies	No. Of event for liver resection	No. Of event for non-liver resection	OR	95% CI	P Value	Heterogeneity P, I^2	Meta-analysis model
1-year overall survival	13	571/616	702/908	3.31	2.34, 4.67	<0.001	0.55, 0%	Fixed
3-year overall survival	12	467/607	357/872	4.29	2.71, 6.80	<0.001	0.02, 52%	Random
5-year overall survival	12	410/607	232/872	5.30	3.24, 8.67	<0.001	0.02, 53%	Random

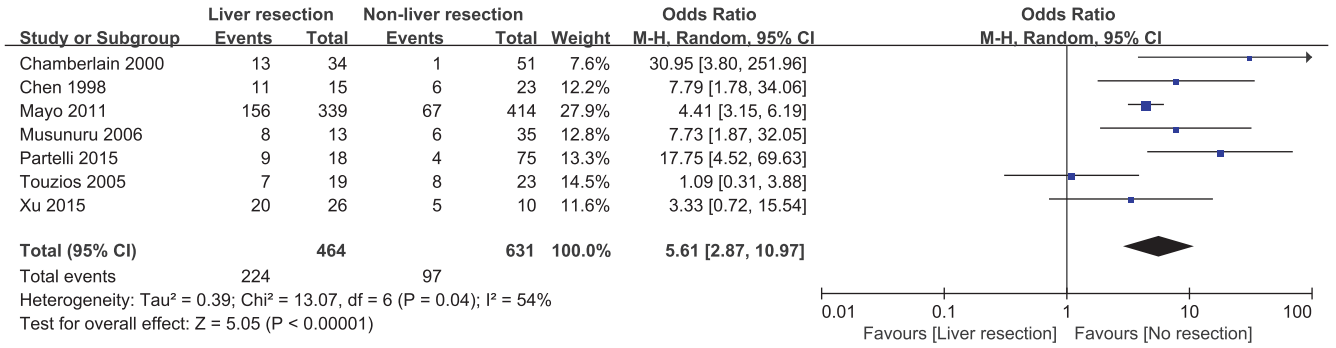

Figure 4: Forest plot for the site of hepatic metastases (unilobar/bilobar) of liver resection group and nonliver resection group in patients with liver metastases from pancreatic neuroendocrine tumor. Liver resection group have more unilobar hepatic metastases.

showed that there was no significant publication bias in this meta-analysis and unpublished data were not evaluated.

4. Discussion

Nowadays, there are various treatments for PNET patients with liver metastases including biotherapy, chemotherapy, and intervention. However, no randomized, controlled studies demonstrated that any of them could prolong the OS [7, 36, 37]. Hepatic resection may be the only treatment, even a curative treatment, to prolong the OS. In this meta-analysis, we are mainly intended to compare the prognosis of hepatic resection group with nonliver resection group in PNET patients with liver metastases. According to the result, liver resection is a safe treatment with a low mortality rate (3.32%) and an acceptable morbidity rate (33.5%). The grading system is related to the proliferation capacity of the tumor measured by Ki-67 staining of the PNET specimens. According to previous studies, patients with G1 and G2 PNET have a better survival compared with G3 [38, 39]. In this meta-analysis, there was no difference between two groups about patients with G1, G2, or G3 (p=0.75). However, we could not further perform a subgroup analysis about the OS of patients with G1, G2, and G3 because of the lack of data. From 13 included cohort studies, liver resection provided a longer median survival, a higher 1-, 3-, and 5-year survival rate and postoperative symptom relief rate. Notably, 13 studies in our pool showed PNET patients with liver metastases undergoing hepatic resection had a median of 67.54% for 5-year survival rate, which is higher than 60% from previous reports [40].

There was one citation retrieved which suggested that 1-, 3-, and 5-year survival rate in liver resection group were lower than nonliver resection group (95, 93, and 87% versus 87, 84, and 66%, p =0.006) because there were no hepatic metastases in nonliver resection group [23]. The rest 12 studies included had a consensus on a prolonged OS and higher 1-, 3-, and 5-year survival rate in liver resection group and, with extending of follow-up duration, the difference was more obvious between the two groups. Although a conclusion that liver resection could prolong the OS for PNET patients with liver metastases was easily acquired, we could not overlook the fact that liver resection group have more unilobar hepatic metastases which means there were more patients with resectable liver metastases. Touzios et al. even suggested that patients with more than 50% liver involvement may not benefit from a liver resection (5-year survival rate: 67% versus 8%, p<0.05) [16]. In another word, liver resection could prolong the OS just for highly selected PNET patients with resectable hepatic metastases.

Due to the decrease of tumor bulk, the symptom relief rate was higher in liver resection group of this meta (p=0.04) [14, 16, 17, 19]. Some authors proposed that liver resection should be attempted if at least 90% of visible tumors could be removed, which means cytoreduction, to relieve symptoms for patients with malignant PNET [7, 41, 42]. Three of included studies (Chamberlain et al., Osborne et al., and Partelli et al.) clarified that cytoreduction could even offer a survival benefit [14, 17, 24]. However, in recent years, some authors consider that 90% debulking threshold is completely made up and advocates that 70% debulking threshold might be a better cut-off value. Morgan et al. discovered that there was no difference in OS between patients who had 100%, >90% or > 70% cytoreduction for all 44 PNET patients with liver metastases (p=0.75) [43]. Although there were small bowel and PNET for all 108 patients, Maxwell et al.

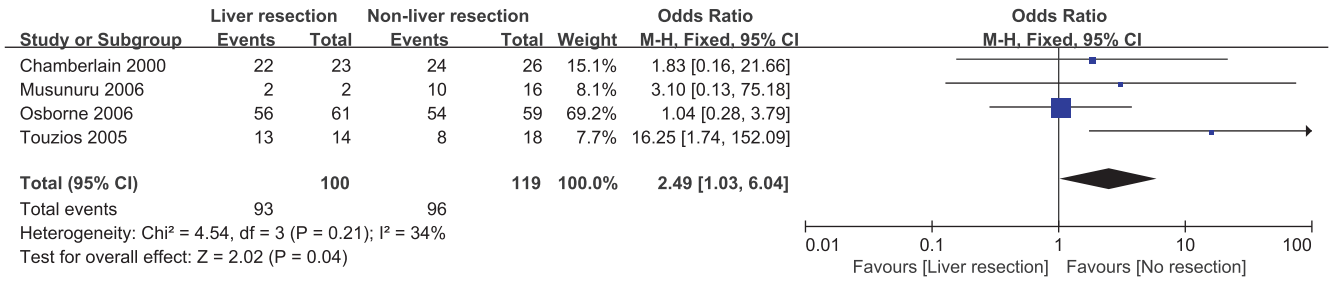

Figure 5: Forest plot for the symptom relief (hormonal symptoms and mechanical symptoms) of liver resection group and nonliver resection group in patients with liver metastases from PNET (functioning or nonfunctioning). Liver resection group have a higher symptom relief rate.

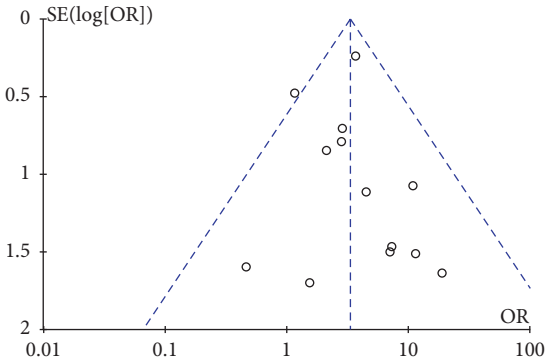

Figure 6: Funnel plot for evaluating publication bias-results from 13 studies.

proposed that patients with greater than 70% debulking had significantly improved OS compared with patients with less than 70% (median OS: not reached vs 6.5 years, p=0.009) [35]. Some included researches carry out liver resection for PNET patients with extrahepatic metastases but did not conduct indepth research on it [14, 16, 21]. Morgan et al. also did the same, yet all deaths in the series were due to liver failure instead of extra-hepatic disease [43]. Thus, 70% debulking threshold might be able to replace 90% for PNET patients with liver metastases and extra-hepatic metastases should not be an obstacle for surgical therapy [44].

Further, some reviews even suggested that the resection of primary tumors should be attempted even if there were metastases because it might decrease the rate of development of liver metastases and extends survival by preventing the development of progressive disease [7, 45, 46]. In this pooled meta-analysis, 7 studies performed resection of primary tumors in nonliver resection group, but we could not perform a subgroup analysis to support the view because of the lack of data [13, 14, 16, 18, 20, 21, 23]. Although we could not draw a conclusion that palliative resection would provide a better prognosis according to these results, we still should attach importance to the role of palliative resection in advanced PNET patients and launch some prospective researches.

Due to the high recurrence rate even after liver resection [38], postoperative adjuvant therapies, including TACE/HAE, systemic chemotherapy, somatostatin analogues, and PRRT, were recommended for PNET patients with hepatic metastases [47]. In this study, the median postoperative adjuvant therapy rate was 42.0% in liver resection group. Although all postoperative adjuvant therapies could relieve the symptoms, their effects on overall survival have not been proved [7, 17, 48–52]. Recently, everolimus (mammalian target of rapamycin [mTOR] inhibitor) yielded a longer progression-free survival (PFS) and a survival benefit of 6.3 months compared with placebo which brought a hope for advanced PNET patients [37, 53].

Our study has some limitations. There were no randomized controlled trials (RCTs) in retrieved studies and the overall level of clinical evidence was relatively low. The heterogeneity of treatment ranging from the sole resection of the primary tumor to multimodal therapy concepts (somatostatin analogues, chemotherapy, TACE/HAE, and resection of the primary tumor) in nonliver resection, and the heterogeneity of patients' characteristics between two groups might be a source of bias.

5. Conclusions

If PNET patients with resectable liver metastases were highly selected, liver surgical resection was an effective and safe treatment to provide a better long-term prognosis including prolonged OS and higher symptom relief. Therefore, there is an urgent need for a further randomized, controlled trial to solve this clinical issue.

Ethical Approval

This article does not contain any studies with human participants or animals performed by any of the authors.

Conflicts of Interest

The authors declare that there are no conflicts of interest regarding the publication of this article.

Authors' Contributions

Xinzhe Yu and Jichun Gu are equal contributors to this manuscript. Xinzhe Yu and Jichun Gu collected and analyzed data and write the manuscript. Ji Li, Deliang Fu, and Haoxuan Wu provided critical revision. Chen Jin designed the study,

determined the eligibility of data, and approved the final version of the manuscript.

Acknowledgments

This work was funded by (1) the National Natural Science Foundation of China (81472221); (2) Key Project of National Health and Planning Commission of the PRC on General Surgery 2012-2014; (3) Key Project of National Health and Planning Commission of the PRC on Oncology 2013-2015; (4) the Research Fund for the Doctoral Program of Higher Education of China (20130071110052 and 20110071110065).

Supplementary Materials

Supporting Table 1: Basic study characteristics of excluded cohort studies. *(Supplementary Materials)*

References

[1] K. Öberg and B. Eriksson, "Endocrine tumours of the pancreas," *Best Practice & Research Clinical Gastroenterology*, vol. 19, no. 5, pp. 753–781, 2005.

[2] T. R. Halfdanarson, K. G. Rabe, J. Rubin, and G. M. Petersen, "Pancreatic neuroendocrine tumors (PNETs): incidence, prognosis and recent trend toward improved survival," *Annals of Oncology*, vol. 19, no. 10, pp. 1727–1733, 2008.

[3] K. Öberg, "Pancreatic endocrine tumors," *Seminars in Oncology*, vol. 37, no. 6, pp. 594–618, 2010.

[4] J. Zhou, L. Enewold, A. Stojadinovic et al., "Incidence rates of exocrine and endocrine pancreatic cancers in the United States," *Cancer Causes & Control*, vol. 21, no. 6, pp. 853–861, 2010.

[5] F. Panzuto, L. Boninsegna, N. Fazio et al., "Metastatic and locally advanced pancreatic endocrine carcinomas: analysis of factors associated with disease progression," *Journal of Clinical Oncology*, vol. 29, no. 17, pp. 2372–2377, 2011.

[6] T. Ito, H. Igarashi, and R. T. Jensen, "Pancreatic neuroendocrine tumors: Clinical features, diagnosis and medical treatment: Advances," *Best Practice & Research Clinical Gastroenterology*, vol. 26, no. 6, pp. 737–753, 2012.

[7] D. C. Metz and R. T. Jensen, "Gastrointestinal neuroendocrine tumors: pancreatic endocrine tumors," *Gastroenterology*, vol. 135, no. 5, pp. 1469–1492, 2008.

[8] R. T. Jensen, G. Cadiot, M. L. Brandi et al., "ENETS consensus guidelines for the management of patients with digestive neuroendocrine neoplasms: Functional pancreatic endocrine tumor syndromes," *Neuroendocrinology*, vol. 95, no. 2, pp. 98–119, 2012.

[9] S. McNally and R. Parks, "Surgery for Colorectal Liver Metastases," *Digestive Surgery*, vol. 30, no. 4-6, pp. 337–347, 2013.

[10] K. S. Gurusamy, R. Ramamoorthy, D. Sharma, and B. R. Davidson, "Liver resection versus other treatments for neuroendocrine tumours in patients with resectable liver metastases," *Cochrane Database of Systematic Reviews*, no. 2, 2009.

[11] A. Stang, "Critical evaluation of the Newcastle-Ottawa scale for the assessment of the quality of nonrandomized studies in meta-analyses," *European Journal of Epidemiology*, vol. 25, no. 9, pp. 603–605, 2010.

[12] D. F. Stroup, J. A. Berlin, S. C. Morton et al., "Meta-analysis of observational studies in epidemiology: a proposal for reporting," *Journal of the American Medical Association*, vol. 283, no. 15, pp. 2008–2012, 2000.

[13] H. Chen, J. M. Hardacre, A. Uzar, J. L. Cameron, and M. A. Choti, "Isolated liver metastases from neuroendocrine tumors: Does resection prolong survival?" *Journal of the American College of Surgeons*, vol. 187, no. 1, pp. 88–93, 1998.

[14] R. S. Chamberlain, D. Canes, K. T. Brown et al., "Hepatic neuroendocrine metastases: Does intervention alter outcomes?" *Journal of the American College of Surgeons*, vol. 190, no. 4, pp. 432–445, 2000.

[15] C. C. Solorzano, J. E. Lee, P. W. T. Pisters et al., "Nonfunctioning islet cell carcinoma of the pancreas: survival results in a contemporary series of 163 patients," *Surgery*, vol. 130, no. 6, pp. 1078–1085, 2001.

[16] J. G. Touzios, J. M. Kiely, S. C. Pitt et al., "Neuroendocrine hepatic metastases: Does aggressive management improve survival?" *Annals of Surgery*, vol. 241, no. 5, pp. 776–785, 2005.

[17] D. A. Osborne, E. E. Zervos, J. Strosberg et al., "Improved outcome with cytoreduction versus embolization for symptomatic hepatic metastases of carcinoid and neuroendocrine tumors," *Annals of Surgical Oncology*, vol. 13, no. 4, pp. 572–581, 2006.

[18] M. G. House, J. L. Cameron, K. D. Lillemoe et al., "Differences in survival for patients with resectable versus unresectable metastases from pancreatic islet cell cancer," *Journal of Gastrointestinal Surgery*, vol. 10, no. 1, pp. 138–145, 2006.

[19] S. Musunuru, H. Chen, S. Rajpal et al., "Metastatic neuroendocrine hepatic tumors: Resection improves survival," *JAMA Surgery*, vol. 141, no. 10, pp. 1000–1004, 2006.

[20] M. Kleine, H. Schrem, F. W. R. Vondran, T. Krech, J. Klempnauer, and H. Bektas, "Extended surgery for advanced pancreatic endocrine tumours," *British Journal of Surgery*, vol. 99, no. 1, pp. 88–94, 2012.

[21] S. C. Mayo, M. C. De Jong, M. Bloomston et al., "Surgery versus intra-arterial therapy for neuroendocrine liver metastasis: A multicenter international analysis," *Annals of Surgical Oncology*, vol. 18, no. 13, pp. 3657–3665, 2011.

[22] A. Zerbi, V. Capitanio, L. Boninsegna et al., "Treatment of malignant pancreatic neuroendocrine neoplasms: Middle-term (2-year) outcomes of a prospective observational multicentre study," *HPB*, vol. 15, no. 12, pp. 935–943, 2013.

[23] D. J. Birnbaum, O. Turrini, L. Vigano et al., "Surgical management of advanced pancreatic neuroendocrine tumors: short-term and long-term results from an international multiinstitutional study," *Annals of Surgical Oncology*, vol. 22, no. 3, pp. 1000–1007, 2015.

[24] S. Partelli, M. Inama, A. Rinke et al., "Long-term outcomes of surgical management of pancreatic neuroendocrine tumors with synchronous liver metastases," *Neuroendocrinology*, vol. 102, pp. 68–76, 2015.

[25] X. Xu, X. Han, L. Liu, Y. Ji, J. Li, and W. Lou, "Clinical analysis and comprehensive treatment of nonfunctional pancreatic neuroendocrine tumor with liver metastases: A retrospective single-center study," *Pancreas*, vol. 44, no. 6, pp. 995-996, 2015.

[26] K. A. Yao, M. S. Talamonti, A. Nemcek et al., "Indications and results of liver resection and hepatic chemoembolization for metastatic gastrointestinal neuroendocrine tumors," *Surgery*, vol. 130, no. 4, pp. 677–685, 2001.

[27] D. Elias, P. Lasser, M. Ducreux et al., "Liver resection (and associated extrahepatic resections) for metastatic well-differentiated

endocrine tumors: A 15-year single center prospective study," *Surgery*, vol. 133, no. 4, pp. 375–382, 2003.

[28] D. Elias, D. Goéré, G. Leroux et al., "Combined liver surgery and RFA for patients with gastroenteropancreatic endocrine tumors presenting with more than 15 metastases to the liver," *European Journal of Surgical Oncology*, vol. 35, no. 10, pp. 1092–1097, 2009.

[29] M. C. De Jong, M. B. Farnell, G. Sclabas et al., "Liver-directed therapy for hepatic metastases in patients undergoing pancreaticoduodenectomy: A dual-center analysis," *Annals of Surgery*, vol. 252, no. 1, pp. 142–148, 2010.

[30] S. C. Mayo, M. C. De Jong, C. Pulitano et al., "Surgical management of hepatic neuroendocrine tumor metastasis: Results from an international multi-institutional analysis," *Annals of Surgical Oncology*, vol. 17, no. 12, pp. 3129–3136, 2010.

[31] G. A. Poultsides, L. C. Huang, Y. Chen et al., "Pancreatic neuroendocrine tumors: Radiographic calcifications correlate with grade and metastasis," *Annals of Surgical Oncology*, vol. 19, no. 7, pp. 2295–2303, 2012.

[32] M. Krausch, A. Raffel, M. Anlauf et al., ""cherry picking", a multiple non-anatomic liver resection technique, as a promising option for diffuse liver metastases in patients with neuroendocrine tumours," *World Journal of Surgery*, vol. 38, no. 2, pp. 392–401, 2014.

[33] S. Du, J. Ni, L. Weng et al., "Aggressive Locoregional Treatment Improves the Outcome of Liver Metastases from Grade 3 Gastroenteropancreatic Neuroendocrine Tumors," *Medicine (United States)*, vol. 94, no. 34, p. e1429, 2015.

[34] E. Bertani, M. Falconi, C. Grana et al., "Small intestinal neuroendocrine tumors with liver metastases and resection of the primary: Prognostic factors for decision making," *International Journal of Surgery*, vol. 20, pp. 58–64, 2015.

[35] J. E. Maxwell, S. K. Sherman, T. M. O'Dorisio, A. M. Bellizzi, and J. R. Howe, "Liver-directed surgery of neuroendocrine metastases: What is the optimal strategy?" *Surgery*, vol. 159, no. 1, pp. 320–333, 2016.

[36] U. Plockinger and B. Wiedenmann, "Endocrine tumours of the gastrointestinal tract. Management of metastatic endocrine tumours," in *Best Practice & Research: Clinical Gastroenterology*, vol. 19, pp. 553–576, 2005.

[37] J. C. Yao, M. H. Shah, and T. Ito, "Everolimus for advanced pancreatic neuroendocrine tumors," *The New England Journal of Medicine*, vol. 364, no. 6, pp. 514–523, 2011.

[38] S. Scigliano, R. Lebtahi, and F. Maire, "Clinical and imaging follow-up after exhaustive liver resection of endocrine metastases: a 15-year monocentric experience," *Endocrine-Related Cancer*, vol. 16, pp. 977–990, 2009.

[39] J. Strosberg, A. Nasir, D. Coppola, M. Wick, and L. Kvols, "Correlation between grade and prognosis in metastatic gastroenteropancreatic neuroendocrine tumors," *Human Pathology*, vol. 40, no. 9, pp. 1262–1268, 2009.

[40] P. G. Schurr, T. Strate, K. Rese et al., "Aggressive surgery improves long-term survival in neuroendocrine pancreatic tumors: An institutional experience," *Annals of Surgery*, vol. 245, no. 2, pp. 273–281, 2007.

[41] S. E. Carty, R. T. Jensen, and J. A. Norton, "Prospective study of aggressive resection of metastatic pancreatic endocrine tumors," *Surgery*, vol. 112, no. 6, pp. 1024–1032, 1992.

[42] J. M. Sarmiento, G. Heywood, J. Rubin, D. M. Ilstrup, D. M. Nagorney, and F. G. Que, "Surgical treatment of neuroendocrine metastases to the liver: a plea for resection to increase survival," *Journal of the American College of Surgeons*, vol. 197, no. 1, pp. 29–37, 2003.

[43] R. E. Morgan, S. J. Pommier, and R. F. Pommier, "Expanded criteria for debulking of liver metastasis also apply to pancreatic neuroendocrine tumors," *Surgery*, vol. 163, no. 1, pp. 218–225, 2018.

[44] J. R. Howe, K. Cardona, D. L. Fraker et al., "The surgical management of small bowel neuroendocrine tumors," *Pancreas*, vol. 46, no. 6, pp. 715–731, 2017.

[45] D. L. Fraker, J. A. Norton, H. R. Alexander, D. J. Venzon, and R. T. Jensen, "Surgery in Zollinger-Ellison syndrome alters the natural history of gastrinoma," *Annals of Surgery*, vol. 220, no. 3, pp. 320–330, 1994.

[46] J. A. Norton, D. L. Fraker, H. R. Alexander et al., "Surgery increases survival in patients with gastrinoma," *Annals of Surgery*, vol. 244, no. 3, pp. 410–419, 2006.

[47] H. Ahlman, B. Wängberg, S. Jansson et al., "Interventional treatment of gastrointestinal neuroendocrine tumours," *Digestion*, vol. 62, no. 1, pp. 59–68, 2000.

[48] C. G. Moertel, M. Lefkopoulo, S. Lipsitz, R. G. Hahn, and D. Klaassen, "Streptozocin-doxorubicin, streptozocin-fluorouracil, or chlorozotocin in the treatment of advanced islet-cell carcinoma," *The New England Journal of Medicine*, vol. 326, no. 8, pp. 519–523, 1992.

[49] A. P. Venook, "Embolization and chemoembolization therapy for neuroendocrine tumors," *Current Opinion in Oncology*, vol. 11, no. 1, pp. 38–41, 1999.

[50] D. O'Toole and P. Ruszniewski, "Chemoembolization and other ablative therapies for liver metastases of gastrointestinal endocrine tumours," *Best Practice & Research Clinical Gastroenterology*, vol. 19, no. 4, pp. 585–594, 2005.

[51] T. Shah and M. Caplin, "Biotherapy for metastatic endocrine tumours," *Best Practice & Research Clinical Gastroenterology*, vol. 19, no. 4, pp. 617–636, 2005.

[52] T. Brabander, J. J. M. Teunissen, C. H. J. Van Eijck et al., "Peptide receptor radionuclide therapy of neuroendocrine tumours," *Best Practice & Research Clinical Endocrinology & Metabolism*, vol. 30, no. 1, pp. 103–114, 2016.

[53] J. C. Yao, M. Pavel, C. Lombard-Bohas et al., "Everolimus for the treatment of advanced pancreatic neuroendocrine tumors: Overall survival and circulating biomarkers from the randomized, Phase III RADIANT-3 study," *Journal of Clinical Oncology*, vol. 34, no. 32, pp. 3906–3913, 2016.

Hindawi
Journal of Oncology
Volume 2018, Article ID 1912438, 7 pages
https://doi.org/10.1155/2018/1912438

Research Article

A Machine Learning Approach for the Association of ki-67 Scoring with Prognostic Factors

E. Dirican [1] **and E. Kiliç** [2]

[1] *Biostatistics, Faculty of Medicine, Mustafa Kemal University, Hatay 31000, Turkey*
[2] *General Surgery, Faculty of Medicine, Mustafa Kemal University, Hatay 31000, Turkey*

Correspondence should be addressed to E. Dirican; emredir44@hotmail.com

Received 1 June 2018; Accepted 23 July 2018; Published 7 August 2018

Academic Editor: Esaki Shankar

ki-67 score is a solid tumor proliferation marker being associated with the prognosis of breast carcinoma and its response to neoadjuvant chemotherapy. In the present study, we aimed to investigate the way of clustering of prognostic factors by ki-67 score using a machine learning approach and multiple correspondence analysis. In this study, 223 patients with breast carcinoma were analyzed using the random forest method for classification of prognostic factors according to ki-67 groups (<14% and >14%). Also the relationship between subgroups of prognostic factors and ki-67 scores was examined by multiple correspondence analysis. There was a clustering of molecular classification LA, 0-3 metastatic lymph node, age <50, absence of LVI, T1 tumor size with ki-67 <14% and grade III, 10 or more metastatic lymph nodes, and presence of LVI and molecular classification LB, age >50, and T3-T4 tumor size categories with ki-67 >14%. The fact that the low scores of ki-67 correlate with early stage diseases and high scores with advanced disease suggests that 14% threshold value is crucial for ki-67 score.

1. Introduction

Machine learning investigates how computers can learn (or improve their performance) based on available data. A main research area for computer programs is to automatically learn to recognize complex patterns and make intelligent decisions based on available data [1]. Random forest (RF) is a supervised machine learning technique and a combination of tree predictors in which each tree depends on the values of a random vector sampled independently and with the same distribution for all the trees in the forest [2].

ki-67 score is the core protein expressed at G1, S, G2, and M phases of tumor cells and a solid tumor proliferation marker being associated with prognosis of breast carcinoma (BC) and its response to neoadjuvant chemotherapy [3]. A threshold value of 14% is determinant for the identification of molecular subtypes BCs (MSBC). Chemotherapy response and progression of MSBCs differ [4, 5].

The molecular subtypes of breast cancer (MSBC) are defined based on the expression of ki-67, estrogen receptor (ER), progesterone receptor (PR), and human epidermal growth factor receptor-2 (HER-2) [6].

In luminal A (LA), ER and/or PR is positive, HER-2 is negative, and the proliferation index is low. In luminal B (LB), tumors are of high grade and may be PR+ or PR- or HER2+ or HER2-. If they are HER2-, they can be distinguished from LA by ki-67 score being >14% [3]. HER-2: HER-2 gene expression is high; however, ER and PR are negative and they are of high grade with ki-67 score of >14% [6]. Typically, triple negative breast carcinoma (TNBC) is the type lacking ER and PR with overexpression of HER2. Compared to other subtypes, TNBC tumors are usually larger [7, 8] and they are associated with 2.5-fold more metastasis within five years after diagnosis [8].

Lymphovascular invasion (LVI) is present in one-third of BCs. As a single indicator of adjuvant chemotherapy [7], LVI is associated with increased lymph node metastasis and the risk of progression to systemic disease [9, 10]. It is a negative effective factor in survival for relapse and survival in node-negative patients [11].

Age is a prognostic factor in BC and varies by geographical region or demographics. In regions with young

populations such as Asia, Africa, and Turkey, BCs are more frequent under the age of 40, and these tumors are found at further stages compared to the Western societies [12]. The presence of axillary lymph node (LN) is one of the most important factors in prognosis estimation for the patients. Metastatic axillary lymph node ratio (mALNR) is known as an important factor in survival for BC [13]. In general, high mALNR indicates poor prognosis [14, 15]. Spread of cancer cells to regional LNs is the most important prognostic factor and, assessing the status of axillary lymph nodes (ALNs) is important for the prediction of long-term survival in BC [16, 17]. In developed countries, histologically node-negative breast carcinoma (HNNBC) accounts for two-thirds of invasive BC [18]. Histologically node-negative BC patients usually have a good prognosis [18, 19].

Histopathological grade is a special prognostic factor. Some recent studies have confirmed the importance of histopathological grading of BC as a predictive and effective factor in survival. Grade 2 and 3 BCs have poorer prognosis [20, 21]. Tumor size (TS) is an independent prognostic factor independent in TNM staging system and it shows a good correlation with nodal metastasis incidence, relapse risk, and survival [22, 23]. In the present study, we aimed to investigate the way of clustering of prognostic factors by ki-67 score using a machine learning approach and multiple correspondence analysis (MCA).

2. Materials and Methods

Patients with BC treated at Mustafa Kemal University, Faculty of Medicine, Research Hospital, General Surgery Clinic, between January 2014 and December 2017, were analyzed. The study was designed retrospectively and conducted at Mustafa Kemal University, Medical School General Surgery Department, following the approval of Mustafa Kemal University Clinical Research Ethics Committee (approval date, March 22,2018; 75).

Data regarding the prognostic factors including patient's age, body mass index (BMI), TS (cm), ki-67 score (%), ER, PR, c-erb-2 receptor status, molecular classification (MC) (LA, LB, Her-2 and TNBC) data, histopathological diagnosis, nuclear grade status (Modified Bloom Richardson), mALNscount (pN1, pN2, pN3), LVI, and the methods of operation were recorded. The way of clustering of ki-67 scores with prognostic variables was examined.

It was included in the range of 18 to 70 years of age in the study, patients with distant metastasis and morbid obesity (BMI ≥ 40) were excluded. Most of patients (86%) had invasive ductal carcinoma. In the case of a sufficient number of patients with a molecular class of TNBC, it was thought that TNBC could cluster with ki-67 classes.

Also, as number of LN, BMI, perivascular invasion (PVI), and histopathological type variables reduced the total inertia (58%) and caused ambiguity for variable clustering, they were excluded from the analysis. Furthermore, as the effect of surgical type variable on ki-67 classification is neglected, it was excluded from the MCA.

Univariate analyses, RF machine learning classification algorithm, and MCA statistical methods were used for data evaluation. For 16 missing values among different prognostic variables in data set, "rfimpute" RF value imputation algorithm was used. RF is a classification method involving a voting method. It is comprised by many decision trees [2]. Decision trees are independent from each other and formed by samples withdrawn from the data set using bootstrap method.

X input vector: (X), $\widehat{C}_{rf}^{B} = majority\ vote\{\widehat{C}(X)\}_1^B$ where $\widehat{C}_b(X)$ is the class prediction of the b_{th}RF tree. During RF classification procedure, relative significance of different variables is also evaluated [24]. This study took the decrease in GINI index into consideration to evaluate the significance of each variable. The GINI index measures the impurity or inequality level of a sample assigned to a node [25].

Supervised machine learning approach was used in analyzing relationship on between as label ki-67 groups and input variables (MC, LVI, age, number of mLN, nuclear grade, TS, number of LNs, BMI, PVI, surgical type, and histopathological type). Thus in this study, classificability of prognostic variables by ki-67 groups (<14% and >14%) was analyzed using RF method. In the train set, 10-fold cross-validation method was applied for the parametric optimization of machine learning algorithm. Test set was used to determine the accuracy of the learned model. For the evaluation of model performance, the Receiver Operating Characteristics (ROC) curve and area under the curve (AUC) were calculated.

In the correspondence analysis, having no distribution assumption except the assumption that the frequencies in the cross table are positive numbers, the correspondence analysis aims to graphically demonstrate the association between the rows and columns in cross tables and develop simple factors by providing this demonstration [26]. In our study, we used MCA to reveal the association of ki-67 with prognostic factors.

3. Results

A total of 223 patients with breast carcinoma were included in this study. A total of 74 cases (32%) had a ki-67 score of <14% with a mean age of 52.5 ± 12.14 years. A total of 149 cases (66.8%) had a ki-67 score of >14% with a mean age of 50.75 ± 11.95 years. As in general terms, our study was built on the association of ki-67 scoring with variables qualified as prognostic factor for BC; the results of RF method were taken into account (Age, Number of mLNs, Histopathological Type and BMI, p = 0.742, p = 0.234, p = 0.403 and p = 0.386, respectively) rather than the nonsignificant p values in Table 1; as significance control for the variables was also performed using the applied RF algorithm. Many cases had the histological type of invasive ductal carcinoma (86%) and the highest grade was Grade II (51.6%). By BMI groups, there were no underweight patients and most of the patients (56.9%) were in the obese group. The distribution of nonmetastatic lymph node count (nmLN) varies by ki-67 groups and classes (p = 0.07).

Using m_{try} = 3 as number of discriminant variables in decision trees and ntree = 100 as number of used trees,

Table 1: Patient characteristics (discrete data are given as numbers, continuous as the mean ± standard deviation) (n = 223).

Variable		Ki-67 ≤ 14%	Ki-67 > 14%	p
Ki-67 Proliferation		74 (33.2)	149 (66.8)	0.001
Molecular Classification				
	LA	37 (50)	1 (0.7)!	0.001
	LB	28 (37.8)	112 (75.2)	
	Her-2	6 (8.2)	27 (18.1)	
	TN	3 (4)	9 (6)	
Lymphovascular Invasion				
	-	36 (48.6)	32 (21.5)	0.001
	+	38 (51.4)	117 (78.5)	
Age				
	Age <50	38 (51.4)	80 (53.7)	0.742
	Age >50	36 (48.6)	69 (46.3)	
Number of Metastatic Lymph Nodes				
	0-3 LNm	27 (36.5)	38 25.5)	0.234
	4-9 LNm	8 (10.8)	18 (12.1)	
	10 LNm	39 (52.7)	93 (62.4)	
Nuclear Grade				
	Grade I	26 (35.1)	16 (10.7)	0.001
	Grade II	33 (44.6)	82 (55)	
	Grade III	15 (20.3)	51 (34.2)	
Tumor Size				
	T1	32 (43.2)	41 (27.5)	0.01
	T2	38 (51.4)	82 (55)	
	T3 and T4∗∗	4 (5.4)	26 (17.4)	
Body Mass Index				
	18.5-24.9	7 (9.5)	18 (12.1)	0,386
	25-29.9	28 (37.8)	43 (28.9)	
	30^{+}	39 (52.7)	88 (59.1)	
Surgical Type				
	Mastectomy	55 (74.3)	77 (51.7)	0,001
	Segmental Mastectomy	19 (25.7)	72 (48.3)	
Histopathological Type				
	IDC	61 (82.4)	131 (87.9)	0,403
	ILC	6 (8.1)	6 (4)	
	Other∗	7 (9.5)	12 (8.1)	
Perivascular Invasion				
	-	52 (70.3)	36 (24.2)	0.01
	+	22 (29.7)	113 (75.8)	
Number of Lymph Nodes				
		2.39 ± 4.62	3.74 ± 6.3	0.07

∗: 6 mucinous carcinomas, 7 DCIS, 6 neuroendocrine carcinomas. **!:** "rfinput" imputation. **Molecular classification:** LA: luminal A, LB: luminal B, and TNBC: triple negative breast carcinoma; **BMI:** underweight <18.50, normal range 18.50-24.99, overweight ≥ 25.00, and obese ≥ 30.00.

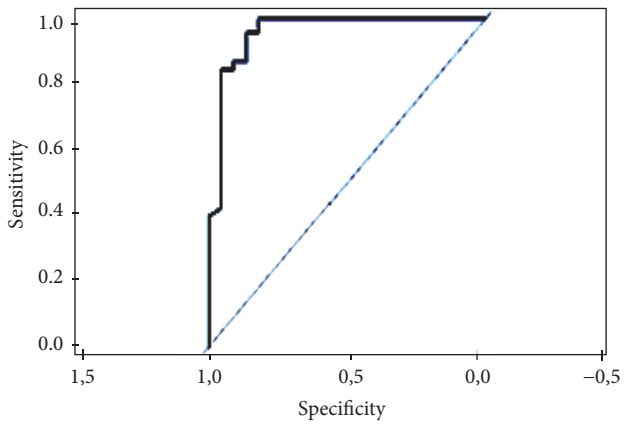

Figure 1: ROC Curve for RF performance.

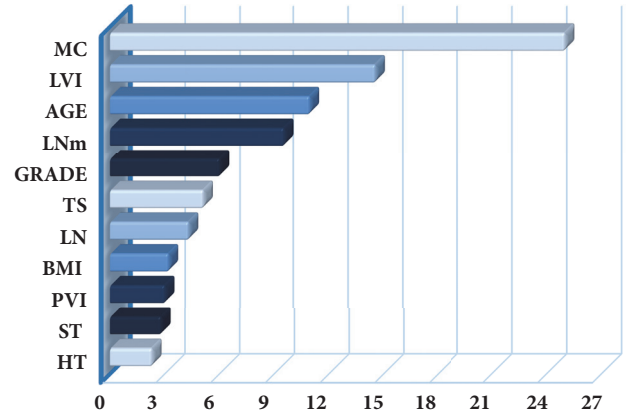

Figure 2: Mean decrease GINI. *MC: molecular classification, LVI: lymphovascular invasion, LNm: number of metastatic lymph nodes, TS: tumor size, LN: number of metastatic/nonmetastatic lymph nodes, BMI: body mass index, PVI: perivascular invasion, ST: surgical type/procedure,* and *HT: hypertension.*

RFClassification Algorithm was applied to the data set involving 223 cases. Using all these arguments, the obtained accuracy was 0.91. For the evaluation of the performance of the obtained model, the ROC curve and AUC were calculated. Using the analysis, AUC was found at 0.95 (Figure 1).

According to the association of ki-67 with the prognostic variables for breast carcinoma, the variables with high and low significance are shown in Figure 2. Figure 2 was designed based on the mean decrease in GINI. According to this figure, the variable with the most contribution to ki-67 classification is MC (25), followed by LVI (14.6), age (11), number of mLN (9.6), nuclear grade (6), TS (5.1), number of LNs (4.3), BMI (3.2), PVI (3), and surgical type (2.8) in descending order with the variable in the GINI index with the least contribution to the classification being histopathological type (2.3).

MCA was performed to determine the association of ki-67 proliferation with other variables. For this analysis, MC, LVI, age, number of mLNs, nuclear grade, and TS variables were taken from Figure 2.

The association of variables in two dimensions in MCA was explained by 76.303% (Dim. 1 + Dim. 2 = 41.093 + 35.209 = 76.303). According to this analysis, in case of ki-67 tumor proliferation over 14%, clustering for grade III, 10 or more mLNs, presence of LVI, LB, age over 50 years, and T3-T4 was observed. In cases of ki-67 tumor proliferation below 14%, clustering for LA, 0-3 mLNs, absence of LVI, age below 50 years, and T1 was observed. However, none of the ki-67 groups showed clustering for Grades I and II, T2, Her 2, and TNBC, 4-9 mLNs (Figure 3).

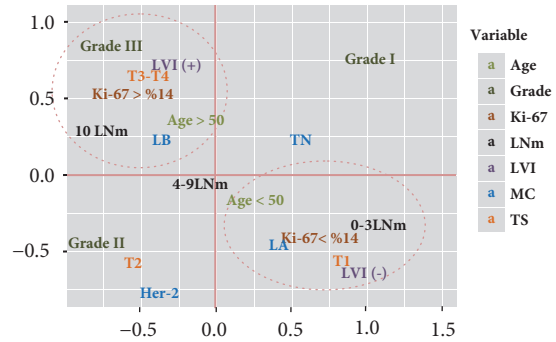

Figure 3: MCA plot of variables association with ki-67. *LNm: number of metastatic lymph nodes, LVI: lymphovascular invasion, MC: molecular classification, TS: tumor size, LA/LB: luminal A/B,* and *Her-2: Her-2 breast carcinoma.*

4. Discussion

4.1. Molecular Subtype Breast Carcinoma and ki-67 Scoring. ki-67 is the core protein expressed at G1, S, G2, and M phases of tumor cells and a solid tumor proliferation marker [3]. In this study, ki-67 groups (<14%/>14%) and MSBC were determined according to St. Gallen consensus [4]. 74 (33.2%) cases had ki-67 score of < 14%, and 149 cases (66.8%) had >14% (p = 0.001).

4.1.1. Luminal A, Luminal B, and Her-2. While normally ki-67 >14% class should not have LA, as imputation was performed for the parameters with missing data using "rfinput" command in the "RandomForest" package in R software, one LA was present in this section. To avoid that these missing data decrease the safety of the analysis, even though they are very few, this random procedure was not interfered. 37.8% of the cases with ki-67 score of <14% and 75.2% of the cases with >14% were LB. In this study, while there were 6 patients (8.2%) with Her-2 molecular type with ki-67 score of <14% and 27 patients (18.1%) with Her-2 molecular type with ki-67 score of >14%. Molecular subtyping was detected to be the most important factor decreasing the mean GINI index and, consistent with the literature, LB showed clustering with ki-67 score of >14% and LA with ki-67 of <14%. Her-2 did not show clustering in neither of the groups.

4.1.2. Triple Negative Breast Cancer. ki-67 score of <14% was detected in 3 (4%) cases and ki-67 of >14% in 9 (6%) cases with TNBC. However, it did not show clustering with ki-67 scores (see Figure 3). The reason that TNBC did not show

clustering with any of the subgroups of prognostic factors in MCA is the insufficient number of TNBC in data set.

4.1.3. Lymphovascular Invasion . In this study, LVI distribution was detected as 38 cases (51.4%) for ki-67 score of <14% and 117 cases (78.5%) for ki-67 of >14%. LVI showed significant clustering with the other prognostic variables and ki-67 groups (ki-67>14%--LVI(+) and ki-67<14%--LV(-)). It is based on 14% of the ki-67 score which is similar to our study [27] reporting that patients with high ki-67 expression had significantly high rates of LVI. Coexistence of LVI and ki-67 score of >14% was considered to indicate poor prognosis and systemic disease [28].

4.1.4. Metastatic/Nonmetastatic Lymph Node Count. Axillary lymph node metastasis is an important biological feature of BC, and it leads to poor prognosis and death [29]. LVI is a powerful predictor of axillary metastasis [30]. mALNs are grouped as 0-3, 4-9, and ≥10; mLNs and nmLNs were detected to be comparable for both groups [31]. ≥10 mALN showed clustering for ki-67 group of >14% and 0-3 mALN for ki-67 of <14%. As aforementioned ki-67 score of >14% showed clustering with LVI (+) and ≥10 mALN [29] (see Figure 3). nmALN was detected to be 2.39 ± 4.62 in ki-67 group of <14% and 3.74 ± 6.3 in ki-67 group of >14% ($p = 0.07$). As the mean GINI index was low, it was excluded from the MCA.

4.1.5. Nuclear Grade. The histopathological grade was determined using the modified Scarff-Bloom-Richardson grading system (Nottingham Combined Histological Grade) [32]. When the groups were assessed for nuclear grade, grade 2 was significantly more in both groups ($p = 0.001$). Clustering was observed for grade III group with ki-67 class of >14%, and no clustering was observed for Grades I and II with any of ki-67 scores (Figure 3). This was considered to develop due to grade and ki-67 scores increased secondarily to nuclear proliferation developed at G1, S, G2, and M phases [3]. Consistent with previous studies, nuclear grade and ki-67 were found to be of positive correlation between scores [33].

4.1.6. Age. In the present study, the number of 50-year-old or younger patients was more in both ki-67 score groups ($p = 0.742$). The association of age groups with ki-67 score classes was evaluated, and clustering was observed for ki-67 of >14% with 50-year-old or older patients and for ki- 67 of <14% with patients younger than 50 years (Figure 3).

The variable of age and ki-67> 14% scores in study showed negative correlation [34] in contrast to our study; the positive correlation was found. This situation is thought to be caused by the difference of the population in which the sample is drawn.

4.1.7. Tumor Size. Although, in many studies, there was no correlation between TS size and ki-67 score [35–37] in the present study, clustering was observed between T3/4 and ki-67 class of >14% and T1 and ki-67 of <14%. However, T2 did not show clustering with any of ki-67 classes (Figure 3). For the tumors at the same T stage, the risk of progression to advanced stage disease increases with the increasing size [31]. TS was considered to increase secondary to progression development with high ki-67 score.

Successful results were obtained in the study using [38] "k-Means clustering" classification method. However, as "k-Means clustering" method lays equal weight to each attribute during the classification, it may cause predicaments for unrelated attributes. Hence, in our study which also examines the association of the data, there are also attributes with no association with ki-67 scoring. Along with the aforementioned parameters, RF method was applied using R 3.3.3 program and the accuracy was found 91%. For validity of the results, the ROC analysis was conducted to evaluate the performance in our study, and AUC was found 0.95.RF method, it was preferred because of its advantages such as possibility of evaluating the relative importance of the variables in classification, the ability to identify variable interactions, and the short operation time.

As a graphical method is used during the analysis of the association between the categories of variables in MCA, it is considered to be more successful than the clustering analysis. In the study examining the prognostic factors correlated with ki-67 [35], the association was examined using univariate analysis such as ANOVA and chi-square test.

In our study of which the majority of data is categorical, a type of multivariate analysis MCA which also takes the visual dimension of the association into account was used. For MCA, the variance for two dimensions was found 76.30%. Among the variables contributing to inertia, the association of grade, mLN, MC, LVI, age, and TS was examined.

5. Conclusion

Luminal B, nuclear grade III, age ≥50 years, LVI (+), number of mLNs ≥10, tumor size T3/4, and ki-67 > 14% clusters were observed in the analysis of the relation between ki-67 threshold value and prognostic factors. Luminal A, age <50 years, LVI (-), number of mLNs 0-3, and tumor T1 were clustered with ki-67 < 14% score. The fact that the low scores of ki-67 correlate with early stage diseases and high scores with advanced disease suggests that 14% threshold value is crucial for ki-67 score.

Data Availability

Access to data is restricted, because the institution from which the data is received does not allow the sharing of data with third parties in terms of patient privacy.

Conflicts of Interest

The authors declare that they have no conflicts of interest.

References

[1] J. Han, M. Kamber, and J. Pei, *Data Mining Concepts and Techniques*, Morgan Kaufmann, 3rd edition, 2012.

[2] L. Breiman, "Random forests," *Machine Learning*, vol. 45, no. 1, pp. 5–32, 2001.

[3] R. L. Jones, J. Salter, R. A'Hern et al., "The prognostic significance of Ki67 before and after neoadjuvant chemotherapy in breast cancer," *Breast Cancer Research and Treatment*, vol. 116, no. 1, pp. 53–68, 2009.

[4] A. Goldhirsch, W. C. Wood, A. S. Coates, R. D. Gelber, B. Thürlimann, and H.-J. Senn, "Strategies for subtypes-dealing with the diversity of breast cancer: highlights of the St Gallen international expert consensus on the primary therapy of early breast cancer 2011," *Annals of Oncology*, vol. 22, no. 8, pp. 1736–1747, 2011.

[5] A. Goldhirsch, E. P. Winer, A. S. Coates, R. D. Gelber, M. Piccart-Gebhart, B. B. Thürlimann et al., "Personalizing the treatment of women with early breast cancer: highlights of the St Gallen International Expert Consensus on the Primary Therapy of Early Breast Cancer 2013," *Annals of Oncology*, vol. 24, no. 9, pp. 2206–2223.

[6] J. Peppercorn, C. M. Perou, and L. A. Carey, "Molecular subtypes in breast cancer evaluation and management: Divide and conquer," *Cancer Investigation*, vol. 26, no. 1, pp. 1–10, 2008.

[7] B. D. Lehmann, J. A. Bauer, X. Chen et al., "Identification of human triple-negative breast cancer subtypes and preclinical models for selection of targeted therapies," *The Journal of Clinical Investigation*, vol. 121, no. 7, pp. 2750–2767, 2011.

[8] R. Dent, M. Trudeau, K. I. Pritchard et al., "Triple-negative breast cancer: clinical features and patterns of recurrence," *Clinical Cancer Research*, vol. 13, no. 15, pp. 4429–4434, 2007.

[9] L. B. Cornwell, K. M. McMasters, and A. B. Chagpar, "The impact of lymphovascular invasion on lymph node status in patients with breast cancer," *The American Surgeon*, vol. 77, no. 7, pp. 874–877, 2011.

[10] J. Wong, A. O'Neill, A. Recht et al., "The relationship between lymphatic vessel invasion, tumor size and pathologic nodal status: Can we predict who can avoid a third field in the absence of axillary dissection," *International Journal of Radiation Oncology • Biology • Physics*, vol. 42, no. 1, p. 251, 1998.

[11] A. H. S. Lee, S. E. Pinder, R. D. Macmillan et al., "Prognostic value of lymphovascular invasion in women with lymph node negative invasive breast carcinoma," *European Journal of Cancer*, vol. 42, no. 3, pp. 357–362, 2006.

[12] G. Agarwal, P. V. Pradeep, V. Aggarwal, C.-H. Yip, and P. S. Y. Cheung, "Spectrum of breast cancer in Asian women," *World Journal of Surgery*, vol. 31, no. 5, pp. 1031–1040, 2007.

[13] W. A. Woodward, V. Vinh-Hung, N. T. Ueno et al., "Prognostic value of nodal ratios in node-positive breast cancer," *Journal of Clinical Oncology*, vol. 24, no. 18, pp. 2910–2916, 2006.

[14] V. Vinh-Hung, H. M. Verkooijen, G. Fioretta et al., "Lymph node ratio as an alternative to pN staging in node-positive breast cancer," *Journal of Clinical Oncology*, vol. 27, no. 7, pp. 1062–1068, 2009.

[15] S. H. Ahn, H. J. Kim, J. W. Lee et al., "Lymph node ratio and pN staging in patients with node-positive breast cancer: A report from the Korean breast cancer society," *Breast Cancer Research and Treatment*, vol. 130, no. 2, pp. 507–515, 2011.

[16] F. J. A. Gujam, J. J. Going, J. Edwards, Z. M. A. Mohammed, and D. C. McMillan, "The role of lymphatic and blood vessel invasion in predicting survival and methods of detection in patients with primary operable breast cancer," *Critical Review in Oncology/Hematology*, vol. 89, no. 2, pp. 231–241, 2014.

[17] A. M. Thompson, "New standards of care in the management of the axilla," *Current Opinion in Oncology*, vol. 24, no. 6, pp. 605–611, 2012.

[18] N. Harbeck and C. Thomssen, "A new look at node-negative breast cancer.," *The Oncologist*, vol. 16, pp. 51–60, 2011.

[19] L. A. Habel, S. Shak, M. K. Jacobs et al., "A population-based study of tumor gene expression and risk of breast cancer death among lymp node-negative patients," *Breast Cancer Research*, vol. 8, no. 3, p. R25, 2006.

[20] M. J. Engstrøm, S. Opdahl, A. I. Hagen et al., "Molecular subtypes, histopathological grade and survival in a historic cohort of breast cancer patients," *Breast Cancer Research and Treatment*, vol. 140, no. 3, pp. 463–473, 2013.

[21] S. Luangdilok, N. Samarnthai, and K. Korphaisarn, "Association between pathological complete response and outcome following neoadjuvant chemotherapy in locally advanced breast cancer patients," *Journal of Breast Cancer*, vol. 17, no. 4, pp. 376–385, 2014.

[22] F. A. Tavasolli and P. Devilee, *World Health Organisation Classification of Tumours. Pathology and Genetics of the Breast and Female Genital Organs*, IARC Press, Lyon, France, 2003.

[23] F. A. Tavasolli, *Pathology of the Breast*, Connecticut: Appelton and Lange, 2nd edition, 1999.

[24] P. O. Gislason, J. A. Benediktsson, and J. R. Sveinsson, "Random forests for land cover classification," *Pattern Recognition Letters*, vol. 27, no. 4, pp. 294–300, 2006.

[25] C. Zhang and Y. Ma, *Ensemble Machine Learning: Methods and Applications*, Springer, New York, NY, USA, 2012.

[26] R. Alpar, *Uygulamali çok değişkenli istatistiksel yöntemler*, Detay Yayıncılık, Ankara, Turkey, 4th edition, 2013.

[27] S. Shen, G. Xiao, R. Du, N. Hu, X. Xia, and H. Zhou, "Predictors of lymphovascular invasion identified from pathological factors in Chinese patients with breast cancer," *Oncotarget* , vol. 9, no. 2, 2018.

[28] E. Ermiah, A. Buhmeida, F. Abdalla et al., "Prognostic value of proliferation markers: Immunohistochemical Ki-67 expression and cytometric S-phase fraction of women with breast cancer in Libya," *Journal of Cancer*, vol. 3, no. 1, pp. 421–431, 2012.

[29] W. L. Donegan, "Tumor-related prognostic factors for breast cancer," *CA: A Cancer Journal for Clinicians*, vol. 47, no. 1, pp. 28–51, 1997.

[30] J. L. B. Bevilacqua, M. W. Kattan, J. V. Fey, H. S. Cody III, P. I. Borgen, and K. J. Van Zee, "Doctor, what are my chances of having a positive sentinel node? A validated nomogram for risk estimation," *Journal of Clinical Oncology*, vol. 25, no. 24, pp. 3670–3679, 2007.

[31] N. G. Coburn, M. A. Chung, J. Fulton, and B. Cady, "Decreased Breast Cancer Tumor Size, Stage, and Mortality in Rhode Island: An Example of a Well-Screened Population," *Cancer Control*, vol. 11, no. 4, pp. 222–230, 2017.

[32] C. W. Elston and I. O. Ellis, "Pathological prognostic factors in breast cancer. I. The value of histological grade in breast cancer: experience from a large study with long-term follow-up. C. W. Elston & I. O. Ellis. *Histopathology* 1991; 19; 403–410," *Histopathology*, vol. 41, no. 3a, pp. 151–153, 2002.

[33] E. C. Inwald, M. Klinkhammer-Schalke, F. Hofstädter et al., "Ki-67 is a prognostic parameter in breast cancer patients: Results of a large population-based cohort of a cancer registry," *Breast Cancer Research and Treatment*, vol. 139, no. 2, pp. 539–552, 2013.

[34] N. Klauber-DeMore, "Tumor biology of breast cancer in young women," *Breast Disease*, vol. 23, pp. 9–15, 2005.

[35] S.-H. Madani, M. Payandeh, M. Sadeghi, H. Motamed, and E. Sadeghi, "The correlation between Ki-67 with other prognostic

factors in breast cancer: A study in Iranian patients," *Indian Journal of Medical and Paediatric Oncology*, vol. 37, no. 2, pp. 95–99, 2016.

[36] A. S. Nahed and M. Y. Shaimaa, "Ki-67 as a prognostic marker according to breast cancer molecular subtype," *Cancer Biology & Medicine*, vol. 13, no. 4, p. 496, 2016.

[37] S. Haroon, A. A. Hashmi, A. Khurshid et al., "Ki67 Index in Breast Cancer: Correlation with Other Prognostic Markers and Potential in Pakistani Patients," *Asian Pacific Journal of Cancer Prevention*, vol. 14, no. 7, pp. 4353–4358, 2013.

[38] X. M. Lopez, O. Debeir, C. Maris et al., "Clustering methods applied in the detection of Ki67 hot-spots in whole tumor slide images: an efficient way to characterize heterogeneous tissue-based biomarkers," *Cytometry Part A*, vol. 81, no. 9, pp. 765–775, 2012.

Hindawi
Journal of Oncology
Volume 2018, Article ID 1828791, 8 pages
https://doi.org/10.1155/2018/1828791

Research Article

S100A4 May Be a Good Prognostic Marker and a Therapeutic Target for Colon Cancer

Sabahattin Destek[1] **and Vahit Onur Gul**[2]

[1]*Bezmialem Vakıf University School of Medicine, Vatan Street, 34093 Fatih, Istanbul, Turkey*
[2]*Department of General Surgery, Gulhane Education and Research Hospital, Ankara, Turkey*

Correspondence should be addressed to Sabahattin Destek; sebahattindestek@yahoo.com

Received 13 April 2018; Accepted 25 June 2018; Published 9 July 2018

Academic Editor: Kalayarasan Srinivasan

Background. Globally, the colorectal cancers rank the third in terms of cancer incidence and rank the fourth in cancer-associated deaths. S100A4, an important member of the S100 protein family, serves to promote tumor progression and metastasis. By conducting this study, we aim to examine the role of S100A4 in the prognosis of colon cancer and to demonstrate its prognostic significance. *Methods*. Tissue samples of colon cancer from 148 patients who underwent colon resection due to colon cancer were analyzed by immunohistochemical staining to determine the protein expression levels of S100A4. The protein expression levels of S100A4 in tumor tissue were matched with the clinicopathologic factors including patient survival. *Results*. Cytoplasmic expression of S100A4 protein was demonstrated in the tumor tissue of 132 patients (89.2%) out of a total of 148 study patients. Statistically, the expression levels of the cytoplasmic S100A4 protein correlated significantly with the TNM stages and patient survival. The distribution of the S100A4 protein staining in the tumor tissue was associated with the age groups, tumor localization, TNM staging, and patient survival with statistical significance. The levels of S100A4 protein expression were found to be an independent prognostic factor for TNM staging and poor survival. *Conclusion*. Expression of the S100A4 protein in colon cancers may be an indicator of tumor progression and lymph node metastasis and may be useful for predicting the overall survival of the patients with colon cancer. In patients with colon cancer, it may be used as an indicator of poor prognosis.

1. İntroduction

It is estimated that, in 2012, 14.1 million new cancer cases have emerged and 8.2 million deaths have occured due to cancer globally [1]. Lung (12.9%), breast (11.9%), and colorectal cancers (CRC) (9.7%) are the most common types of cancer. Among the most common causes of cancer-related deaths, colorectal cancers (8.5%) are in the fourth rank, preceded by lung, liver and stomach cancers [1].

CRC ranks the third in the USA, among all cancer types, with 10.3% incidence and 8.9% mortality rates [2]. On the other hand, it is in the second rank in Europe, among all cancer types, with 13% incidence and 12.2% mortality rates [3]. In our country, colorectal cancers are the third most common types of cancer (9%) according to the 2015 cancer statistics in Turkey [4].

Approximately 90% of cancer-related deaths are due to the metastatic dissemination of the primary tumors [5]. Tumor-node-metastasis (TNM) staging is an important prognostic parameter describing the depth of tumor invasion, lymph node involvement, metastasis status, and the stage of the tumor. Early diagnosis of tumors and metastases is critical to improving the treatment strategies and patient outcomes.

S100 proteins are dimeric, intracellular, and low-molecular-mass proteins binding Ca^{2+} [5]. S100A4 is found in the nucleus, cytoplasm, and the extracellular space, bearing a wide range of biological functions including angiogenesis, cell survival, motility, and regulation of intercellular adhesion [6]. High S100A4 expression levels are associated with aggressive tumor growth, metastases, and poor prognosis in colorectal cancers [5, 6]. In this study, we examined the

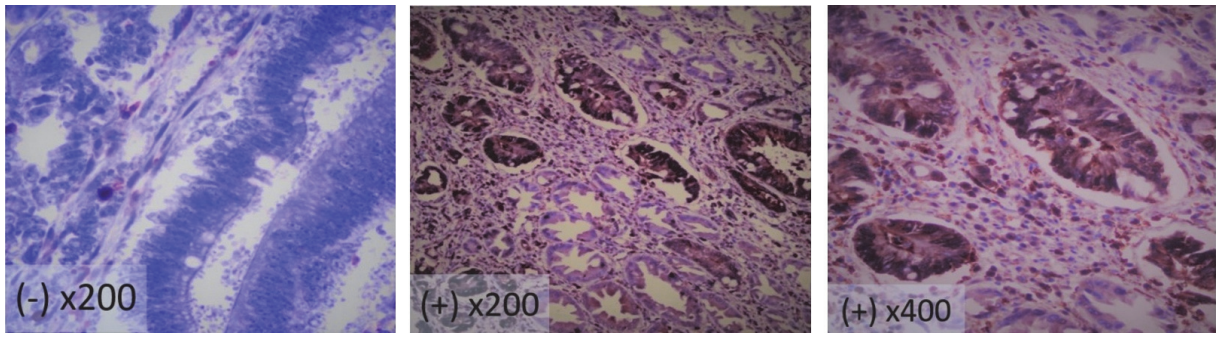

Figure 1: Expression of S100A4 in colonic mucosa (- and + cytoplasmic staining).

association between the levels of S100A4 protein expression in the CRC tissue with the TNM stage.

2. Methods

A total of 148 patients, consisting of 89 males and 59 females, were included in the study. The hospital records were reviewed retrospectively and the following patient data were recorded including age, gender, tumor localization, type of the surgical intervention, tumor size, the grade of the tumor differentiation, and the presence of perivascular or perineural invasion; T, N, and M stages of the tumor; mortality and the duration of survival. S100A4 immunohistochemical staining was applied to the new slides prepared from the paraffin blocks and the levels of S100A4 protein expression were attained.

Patients with rectal cancer and patients having other types of tumors were excluded from the study. The patients with comorbid diseases were excluded from the study if these comorbidities led to the death of the patient during the follow-up period.

2.1. Immunohistochemistry. 4-6 micrometer thick sections from the paraffin blocks of the tissue samples of the 148 patients were mounted onto the slides and were incubated at 37°C for 12 hours. After the sections to be stained with S100A4 were deparaffinized with xylene and high concentrations of alcohol, they were incubated in 3% hydrogen peroxide solution for 10 minutes to eliminate the endogenous peroxidase activity. For the antigen retrieval, they were boiled in a 6.0 pH-citric acid buffer for 10 minutes and then left for cooling at room temperature for 20 minutes. Following this step, 2-3 drops of Ultra V Block solution (LabVision, Fremont, USA) were dropped on the slides and they were left for 3-5 minutes. Then 1/100 diluted rabbit S100A4 antibody (DAKO, Carpinteria, CA, USA) was dropped onto the sections and they were incubated for 60 minutes at room temperature. After adding 2-3 drops of biotinylated rabbit antipolyvalent solution on the sections, they were left for 20 minutes. Between these steps, the sections were left in phosphate buffered saline washing solution for 3-5 minutes. Subsequently 2-3 drops of streptavidin-peroxidase solution were dropped on the sections and they were left for 20 minutes. After the sections were incubated in diaminobenzidine chromogen (Sigma, St Louis, MO, USA) for 5-10 minutes, they were stained with hematoxylin for 20 minutes for balancing. Alcohol was applied to the sections and they were dried in the drying oven.

2.2. Evaluation of the Immunohistochemical Staining. All sections subjected to immunohistochemistry were examined by two independent observers in a double-blinded fashion. Based on the diaminobenzidine chromogen brown, the valuation was performed examining the cytoplasmic staining for S100A4.

A section from a melanoma tissue sample was used as a positive control. Non-specific immune serum was used as the negative control. The tumor cells with brown-stained cytoplasms were classified as positive on the immunohistochemical evaluation of the sections. The S100A4 protein expression of the tumor cells was evaluated according to the ratio of the brown-stained tumor cells (Figure 1). In the presence of the tumor cells staining over 10%, it was accepted that the tumor expressed the S100A4 protein [5].

2.3. Statistical Evaluation. The data obtained in this study were analyzed by the IBM SPSS Statistics Version 20 software. Shapiro Wilks test was used to assess whether the variables were normally distributed. Relations between the groups of nominal variables were examined with the Chi-square analysis. Fisher's Exact Test and Pearson Chi-square analysis were applied when the volume of the expected values was insufficient. The significance level was accepted to be 0.05 while interpreting the results. A p value < 0.05 indicated a significant association between the variables, whereas $p>0.05$ indicated a nonsignificant association.

3. Results

Of 148 study patients, 89 (60%) were males and 59 (40%) were females. The age range of the patients was between 20 and 91 with a mean of 61.7 years. Of the study patients, 57% were 60 years old or older and 43% were younger than 60 years old. The majority of the patients were diagnosed with stage II colon cancers; more commonly having moderately differentiated adenocancers with diameters below 5 cm located in the right colon 89.19% of the patients had S100A4 expression in

Table 1: The Association between the S100A4 expression status, the staining status of the tumor tissue, and clinicopathologic variables.

(a) S100A4 expression.

Clinicopathologic features	Variables	Absent		Present		Total		Chi-square Test
		n	%	n	%	n	%	p
TNM Stage	I	5	31.3	6	4.6	11	7.4	0.001
	II	9	56.3	55	41.7	64	43.2	
	III	0	0	38	28.8	38	25.7	
	IV	2	12.5	33	25	35	23.7	
Duration of Survival	< 2 years	5	31.3	95	72	100	67.6	0.003
	2-5 years	3	18.3	17	12.9	20	13.5	
	5-10 years	8	50	20	15.2	28	18.9	

(b) Distribution of tumor tissue staining.

Clinicopathologic features	Variables	Absent		Superficial		Deep		Complete		Total		Chi-square Test
		n	%	n	%	n	%	n	%	n	%	p
Age Groups	< 60 years	4	25	22	55	10	66.7	28	36.4	64	43.2	0.026
	> 60 years	12	75	18	45	5	33.3	49	63.6	84	56.8	
Colon-Tumor Localization	Right	9	56.3	23	57.5	5	33.3	37	48.1	74	50	0.003
	Transverse	0	0	5	12.5	3	20	18	23.4	26	17.6	
	Left	4	25	7	17.5	1	6.7	10	13	22	14.9	
	Sigmoid	0	0	3	7.5	0	0	9	11.7	12	8.11	
	Multicentric	3	18.6	2	5	6	40	3	3.9	14	9.46	
TNM Stage	I	5	31.3	4	10	0	0	2	2.6	11	7.43	0.001
	II	9	56.3	25	62.5	8	53.3	22	28.6	64	43.2	
	III	0	0	4	10	3	20	31	40.3	38	25.7	
	IV	2	12.5	7	17.5	4	26.7	22	28.6	35	23.65	
Duration of Survival	< 2 years	5	31.3	28	70	8	53.3	59	76.6	100	67.6	0.002
	2-5 years	3	18.8	2	5	4	26.7	11	14.3	20	13.5	
	5-10 years	8	50	10	25	3	20	7	9.09	28	18.9	

the tumor tissues revealed by immunohistochemical staining with a complete staining distribution of 52.03%. The tumor diameters ranged between 15 and 116 mm with a mean of 51.4 mm. Metastatic lymph nodes were identified in 72 (49%) patients. The number of the lymph nodes per patient ranged from 1 to 25 (mean 5). Distant organ metastases were present in 35 (24%) patients. The duration of survival ranged from 1 to 113 (mean 37.3) months.

As regards the association between the status of S100A4 expression and the clinicopathologic variables, no statistically significant associations were observed with the gender, age groups, tumor location, tumor size, tumor grade, the presence of vascular or neural invasions, mortality, or recurrence ($p > 0.05$). On the other hand, there was a statistically significant relationship between the S100A4 expression status and TNM stages ($p < 0.05$). The primary stage was II in 56.25% of the patients without S100A4 expression and in 41.67% of the patients with S100A4 expression, whereas the primary stage was I in 31.25% of the patients without S100A4 protein expression and in 4.55% of the patients with S100A4 expression. There was a statistically significant association between the S100A4 expression status and duration of survival ($p < 0.05$). The duration of survival was shorter than 2 years in 31.25% of the patients without S100A4 expression and in 71.97% of the patients with S100A4 expression. On the other hand, the duration of survival was in a range of 2-5 years in 18.75% of the patients without S100A4 protein expression and in 12.88% of the patients with S100A4 expression (Table 1).

A statistically significant association between the status of S100A4 staining in the tumor tissue and the age groups was observed ($p < 0.05$). 45% of the patients with superficial staining, 33.3% of the patients with deeper staining, and 63.6% of the patients with complete staining were older than 60 years.

There was a statistically significant association between tumor tissue staining and the tumor localization ($p < 0.05$). 57.5% of the patients with superficial staining, 33.3% of those with deeper staining, and 48.6% of those with complete staining had tumor localization in the right colon.

A statistically significant association between the status of staining in the tumor tissue and the TNM stages was present ($p < 0.05$). 62.5% of the patients with superficial staining of the tumor tissues, 53.3% of the patients with deeper staining, and 28.6% of the patients with complete staining were diagnosed with TNM stage II tumors; however, 10% of the patients with superficial staining of the tumor tissues and 2.6% of the patients with complete staining were diagnosed with a primary stage of TNM I.

Table 2: The association of the variables with the tumor stages and nodal stages.

(a) Tumor stage

Pathologic features	Variables	T1		T2		T3		T4		Total		Chi-square Test
		Number	%	Number	%	Number	%	Number	%	Number	%	p
S100A4 expression	Absent	1	100	4	36.4	3	18.6	8	6.7	16	10.8	0.001
	Present	0	0	7	63.6	13	81.3	112	93.3	132	89.2	
	Total	1	100	11	10	16	100	120	100	148	100	
Distribution Of Tumor Tissue Staining	Absent	1	100	4	36.4	3	18.8	8	6.7	16	10.8	0.007
	Superficial	0	0	4	36.4	4	25	32	26.7	40	27	
	Deep	0	0	0	0	3	18.8	12	10	15	10.1	
	Complete	0	0	3	27.3	6	37.5	68	56.7	77	52	
	Total	1	100	11	100	16	100	120	100	148	100	

(b) Nodal stage

Pathologic features	Variables	N0		N1		N2		Total		Chi-square Test
		Number	%	Number	%	Number	%	Number	%	p
S100A4 expression	Absent	15	19.7	0	0	1	2.6	16	10.8	0.001
	Present	61	80.3	34	100	37	97.4	132	89.2	
	Total	76	100	34	100	38	100	148	100	
Distribution Of Tumor Tissue Staining	Absent	15	19.7	0	0	1	2.6	16	10.8	0.001
	Superficial	29	38.2	8	23.5	3	7.9	40	27.0	
	Deep	8	10.5	2	5.9	5	13.2	15	10.1	
	General	24	31.6	24	70.6	29	76.3	77	52.0	
	Total	76	100	34	100	38	100	148	100	

There was a statistically significant association between the status of tumor tissue staining and survival duration ($p < 0.05$). 70% of the patients with superficial staining, 53.3% of the patients with deep staining, and 76.6% of the patients with complete staining had survival durations less than 2 years (Table 1).

No statistically significant associations of the tumor tissue staining status to gender, tumor grade, the presence of vascular or neural invasions, the diameter of the tumor, mortality, or recurrences were identified.

A statistically significant association between the tumor stages and S100A4 staging was present ($p < 0.05$). S100A4 expression was identified in 63.6% of the patients at the T2 stage, in 81.3% of the patients at the T3 stage, and in 93.3% of the patients at the T4 stage.

A statistically significant association between the tumor stages and the status of staining in the tumor tissue was present ($p < 0.05$). Of the patients with T2 tumors, 36.7% had superficial staining and 27.3% had complete staining of their tumor tissues. Of the patients with T3 tumors, 25% displayed superficial staining, 18.8% displayed deeper staining, and 37.5% displayed complete staining. Of the patients with T4 tumors, the staining was superficial in 26.8%, deeper in 10%, and complete in 56.7% (Table 2). There were no significant associations between the distribution of tumor staining and other clinicopathologic variables.

A statistically significant association between the nodal stages and S100A4 expression was present ($p < 0.05$). S100A4 expression was identified in 80.26% of the patients with N0 disease, in 100% of the patients with N1 disease, and in 97.4% of the patients with N2 disease.

A statistically significant association between the nodal stages and the distribution of staining in the tumor tissue was present ($p < 0.05$). Of the patients with N0 disease, 38.2% had superficial staining, 10.5% had deeper staining, and 31.6% had complete staining of their tumor tissues. Of the patients with N1 disease, 23.5% displayed superficial staining, 5.9% displayed deeper staining, and 70.6% displayed complete staining. Of the patients with N2 disease, the staining was superficial in 7.9%, deeper in 13.2%, and complete in 76.3% (Table 2).

There were no statistically significant associations of the metastasis stage to S100A4 expression or staining distribution in the tumor tissues.

4. Discussion

Colorectal cancer is one of the most common types of cancer especially in the developed countries and its incidence is on the rise. Approximately 1.4 million new colorectal cancer cases and 693,900 deaths due to CRC occurred in 2012. Increasing by 60% till 2030, these figures are predicted to reach 2.2 million new cases and 1.1 million deaths [7]. It is estimated that CRC will occur approximately in 5% of the global Western population [8]. The male/female ratio is 1.3 in colon cancer [1]. In our series, the male to female

ratio was found to be 1.5. Colon cancers are more common between 60 and 75 years of age [2]. In our series, 57% of the patients were older than 60 years old. Colon cancer is most frequently found in the right colon with a rate of 25-30% [8]. In our series, half of the patients had right colon tumors.

The well-recognized prognostic factors for survival are the grade of the tumor, its depth of invasion, the presence of regional lymph node involvement, and distant metastases in CRC [9, 10]. Therefore, there is a need to develop reliable biomarkers and simple tests, which will be routinely applied for the early diagnosis of CRC, detection of its progression, determination of the prognosis, and the surveillance of the CRC patients [5, 10, 11].

S100 proteins were introduced for the first time in 1965 by Moore [12]. Found only in vertebrates, the S100 protein family consists of Ca^{2+} binding proteins at varying structures and sizes ranging from 9 to 13 kD. The number of the members of the S100 protein family has reached 25 currently [11, 13]. Their names originate from their solubility in 100% ammonium sulfate at the neutral pH [13]. S100 proteins are typically symmetrical dimers with each S100 subunit containing four α-helical segments. A major portion of these proteins contains a common calcium-binding motif called EF-hand [14, 15].

The S100 proteins do not display enzymatic activities. With the increased serum calcium levels, Ca^{2+} bound S100 proteins show their autocrine, paracrine, and systemic effects [13, 15]. S100 proteins interact with several target proteins intracellularly, including the enzymes, cytoskeletal structures like actin and myosin, several receptors, transcription factors, and nucleic acids, playing roles in homeostasis, energy metabolism, inflammation, migration, invasion, proliferation, differentiation, apoptosis, and intracellular Ca^{2+} regulation [13, 15].

Most of the members of the S100 family may take part in or initiate several biological functions contributing to malignancies, including proliferation, metastasis, angiogenesis, and protection from the immune response [12, 15]. S100 proteins may have specific activities on some target proteins such as NF-κB, p53, and β-catenin [14, 15]. S100 proteins are expressed variably in various malignancies. Although their expressions decrease in some malignancies, they are usually increased [15]. The same S100 protein may be suppressive in a specific cancer type but may activate tumor generation in another type of cancer [15]. S100A4, which is a multifunctional Ca^{2+} signaling protein found in the cytoplasm and extracellular space, is also called metastasin (Mts1), pEL-98, 18A2, 42A, p9Ka, CAPL, calvasculin, and fibroblast-specific protein (FSP1) [11, 12, 16]. S100A4 was first described in 1984 and its expression was demonstrated first in 1989 [11, 17]. The human S100A4 gene is located on the chromosome 1q21 [15, 16]. The S100A4 expression has been reported in several cell types including fibroblasts, monocytes, macrophages, T-lymphocytes, neutrophilic granulocytes, and endothelial cells [6, 11].

The effect of S100A4 protein has been identified in several malignant, benign, or inflammatory diseases [12, 15]. The expression levels of S100A4 increase in rheumatoid arthritis, osteoarthritis, psoriasis, idiopathic inflammatory myopathies, inflammatory bowel diseases like Crohn's disease, cardiac hypertrophy, hepatic hemangiomas, and autoimmune diseases [6, 12, 18, 19]. S100A4 protein expression activates the proinflammatory processes mediated by tumor necrosis factor (TNF)-α, IL-1p and IL-6, and toll-like receptor (TLR)-4, augmenting the inflammation [12, 18, 19].

Several studies are available in the literature on the effects of S100A4 on tumor growth and metastases [12, 15]. Not only does S100A4 protein contribute to the expression levels during the course of aggressive disease processes but it also contributes directly to the progression of the disease as well [16]. S100A4 expression has been demonstrated in several malignancies such as malignancies of the pancreas, stomach, breasts, ovaries, kidneys, lungs, liver, prostate, and bones, in tumors of the urinary bladder, and in melanomas [6, 12, 15].

WNT-β-catenin signaling is one of the most important signaling pathways in the S100A4 protein associated colon carcinogenesis. Wnt proteins bind to the Frizzled receptors and coreceptors via the low-density lipoprotein receptor-related proteins (LRP) 5/6 and activate the receptor-specific signal flow, increasing the β-catenin in the cytoplasm. The increased β-catenin moves to the nucleus and forms a complex with the transcription factor 4 (TCF-4), initiating the S100A4 protein expression by transcription from the S100A4 target gene. The S100A4 protein expressed intracellularly moves to the extracellular space leading to the migration, invasion, and metastasis of the tumor cells [12–14, 20]. The adenomatous polyposis coli (APC) or mutations of the Smad4 gene found almost in 90% of the colorectal cases cause increased β-catenin levels in the cytoplasm. The accumulation of β-catenin in the nucleus causes tumor growth and leads to the expression of the genes taking part in tumor invasion [12, 16, 21].

The capacity for migration is a precondition for the cancer cell to enter the circulation. Matrix metalloproteinases (MMP) play important roles in this process. It is suggested that MMP is stimulated transcriptionally by the S100A4 protein, contributing to the angiogenesis and invasion of the tumor cells [6, 11, 16].

In the cell, the S100A4 protein interacts with the cytoskeletal proteins like nonmuscle myosin heavy chain (NMMHC) IIA, tropomyosin, actin, and filaments. S100A4 protein inhibits the activities of tropomyosin and NMMHC IIA in a Ca^{2+} dependent way binding calcium. Eventually, this increases the cellular mobility and migration [12, 14, 15]. The S100A4 protein interacts with liprin beta 1 and induces the invasiveness of the primary tumors [14]. S100A4 binds to the C-terminal of the p53 protein inhibiting the tumor suppressive effect of p53. This leads the tumor cell to act more aggressively [6, 12, 13].

The receptor for advanced glycation end products (RAGE) and annexin II mediates some of the extracellular functions of the S100A4 protein [6]. After being activated by the extracellular S100A4 protein binding, RAGE activates the mitogen-activated protein kinase (MAPK)/extracellular

signal-regulated kinase (ERK) and NF-κB signaling pathways, augmenting the potency for tumor growth, cell migration, and invasion in colon cancer [12, 15, 16].

The transformation process of the epithelial cells to the mesenchymal cell derivatives is called epithelial-mesenchymal transition (EMT). Induction of EMT leads to rapid tumor growth, invasion, and metastasis [12, 16, 22]. The target signaling protein for Wnt, the S100A4 gene expression, induces the EMT process, facilitating the progression of CRC and its potential for metastasis [14, 16, 22]. The protein expression of the gene encoding the LIM and SH3 domain protein (LASP1) enhances the S100A4 protein expression and leads to the activation of transforming growth factor β (TGF-β) through the activation of the Smad pathway. On the other hand, TGF-β facilitates the EMT induction and increases the levels of mitogenic growth factors leading to immunosuppressor and pro-angiogenic effects to occur [15, 16, 23].

The activation of the phosphatidylinositol 3-kinase (PI3K)/Akt/mTOR/p70S6K signaling pathway by the S100A4 protein causes migration, the expression of vascular endothelial growth factor, and E-cadherin downregulation [14, 16, 24]. When the E-cadherin expression is missing in the nucleus, the accumulated β-catenin in the cytoplasm increases the expression of S100A4, leading to the malignant EMT process and metastatic progression [6, 12, 16, 22].

Several studies demonstrated that various medications interacted with the S100A4 protein. Medications like cromolyn, amlexanox, phenothiazine, statins, propofol, arecoline, niclosamide, paquinimod, and sulindac decrease the activity of S100A4 protein [15, 16]. The antihelmintic medication niclosamide displays its anticancer effects by inhibiting the S100A4 promoter activity and by inhibiting the Wnt/β-catenin signaling pathway, which is a major regulatory pathway for the initiation of cancer, tumor growth, cell differentiation, and metastasis [15, 16]. The anti-inflammatory medication sulindac decreases the S100A4 activation and expression mediated by β-catenin, displaying antitumoral and anti-metastatic effects [6, 12, 15, 16].

Some chemotherapeutic medications may also be the treatment of choice as they have an impact on the S100A4 protein. It has been reported that paclitaxel can inhibit the S100A4 expression in the nucleus. Sorafenib can decrease the expressions of S100A4 mRNA and S100A4 protein. Calcimycin is a structural inhibitor of the active Wnt/β-catenin pathway signals and of the S100A4-promoter activity. By decreasing the expression of S100A4, it decreases the cellular motility and metastasis induced by S100A4 [12, 14–16].

The studies in the literature noted significant associations of the higher levels of S100A4 expression with the tumor localization, lymph node metastasis, TNM stages, and the depth of tumor invasion in patients with CRC [6, 11, 13]. On the other hand, it was reported that no significant associations of the higher levels of S100A4 expression existed with the age, gender, tumoral differentiation, the size of the tumor, the presence of vascular invasion, distant metastases, and presence of recurrences in CRC [11]. Unlike these findings, some studies observed increased rates of metastases during the surveillance of the patients with S100A4 expression [6, 15]. Higher S100A4 expression levels are associated with poor prognosis and lower rates of survival [11, 12, 20, 25].

In our study, too, an exaggerated S100A4 protein expression was demonstrated in 89% of all CRC patients. A statistically significant relationship was found between the S100A4 expression status and TNM stages. S100A4 protein expression is found in 54.5% of the TNM stage I patients: in 85.9% of the stage II patients, in 100% of the stage III patients, and in 94.2% of the stage IV patients. As the TNM stages advanced, the rate of the S100A4 protein expression increased. Parallel to the previous studies, our study did not demonstrate a significant association of the S100A4 expression with the age, gender, tumoral differentiation, the size of the tumor, the presence of vascular invasion, distant metastases, and presence of recurrences in CRC.

In our study, a statistically significant relationship was found between the S100A4 expression status and TNM stages in CRC. Similarly, a statistically significant relationship was found between the S100A4 expression status and the duration of survival. While the patients with S100A4 expression had a 34.5-month mean duration of survival, the mean duration of survival was 60 months in patients without S100A4 expression. S100A4 expression was demonstrated in 93% of the patients with a 5-year survival and in the 95% of the patients with a survival duration of 2 years or less. The survival parameters decreased along with the increased S100A4 expression.

The distribution of the S100A4 staining in the tumor tissue was assessed in order to understand the patterns of the superficial, deep, and complete staining. It was found that the S100A4 staining distribution was statistically associated with the age, localization of the tumor, TNM stages, and survival. In patients younger than 60 years old, a deeper staining pattern was observed. However, in patients older than 60 years old, a complete staining was displayed. In the right colon tumors, in TNM stage II patients, and in patients with a 2-year survival, the staining was complete.

As regards the statistically significant associations between the TNM stages and the levels of S100A4 protein expression, S100A4 expression was identified in 63.6% of the T2 stage patients, in 81.3% of the T3 patients, and in 93.3% of the T4 patients. As the stage of the tumor advanced, the rate of the S100A4 protein expression increased.

There was a statistically significant association between the TNM stages and staining distribution in the tumor tissues. 27.3% of the T2 patients, 37.5% of the T3 patients, and 56.7% of the T4 patients demonstrated complete staining. As the stage of the tumor advanced, the distribution of complete staining for S100A4 protein increased.

A statistically significant association between the TNM nodal stages and S100A4 expression was present. S100A4 expression was identified in 80.26% of the patients with N0 disease, in 100% of the patients with N1 disease, and in 97.4% of the patients with N2 disease. As the nodal stage of the tumor advanced, the rate of the S100A4 protein expression increased.

There was a statistically significant association between the TNM nodal stages and staining distribution in the tumor

tissues. 31.6% of the N0 patients, 70.6% of the N1 patients, and 76.3% of the N2 patients had complete staining of their tumor tissues. As the nodal stage advanced, the distribution of complete staining for S100A4 protein increased. There were no statistically significant associations of the metastasis stage to S100A4 expression or staining distribution in the tumor tissues.

5. Conclusion

As our study has demonstrated, too, the exaggerated expression of the S100A4 protein indicates the capacity of the tumor for invasion and metastasis rather than the capacity for initiating a tumor formation. Our study has noted that as the T and N stages advanced, the exaggerated expression of S100A4 increased as well. The close association of the stage defining parameters with the S100A4 is significant in terms of prognosis. In this study of ours, it was noted that the S100A4 protein was a factor increasing the aggressiveness of the tumor and the occurrence of lymph node metastases. On the other hand, the facilitation of the S100A4 expression along with the advanced stages of the tumor is the most significant finding as the tumor staging is the most important factor in terms of the prognostic value. The S100A4 protein may be a beneficial marker to predict the carcinogenesis, tumor progression, and prognosis in colorectal cancers. We are of the opinion that this may affect the selection of the treatment regimens.

Data Availability

The [Statistical Study and Full Text Article] data used to support the findings of this study have been deposited in the [Harvard Dataverse] repository [https://doi.org/10.7910/DVN/EMCRNZ] (https://www.re3data.org/repository/r3d100010051). The [DATA TYPE] data used to support the findings of this study have been deposited in the [NAME] repository ([DOI or OTHER PERSISTENT IDENTIFIER]) (https://fairsharing.org/biodbcore-001080). The [DATA TYPE] data used to support the findings of this study are included within the supplementary information file(s).

Ethical Approval

Authors declared that the research was conducted according to the principles of the World Medical Association Declaration of Helsinki "Ethical Principles for Medical Research Involving Human Subjects" (amended in October 2013).

Conflicts of Interest

No conflicts of interest were declared by the authors.

Authors' Contributions

All authors read and approved the final version of the manuscript.

References

[1] J. Ferlay, I. Soerjomataram, R. Dikshit et al., "Cancer incidence and mortality worldwide: sources, methods and major patterns in GLOBOCAN 2012," *International Journal of Cancer*, 2014.

[2] A. Jemal, R. Siegel, E. Ward, Y. Hao, J. Xu, and M. J. Thun, "Cancer statistics, 2009," *CA: A Cancer Journal for Clinicians*, vol. 59, no. 4, pp. 225–249, 2009.

[3] J. Ferlay, E. Steliarova-Foucher, J. Lortet-Tieulent et al., "Cancer incidence and mortality patterns in Europe: estimates for 40 countries in 2012," *European Journal of Cancer*, vol. 49, no. 6, pp. 1374–1403, 2013.

[4] V. Ercolak, "Kolorektal Kanserlerde Epidemiyoloji ve Risk Faktörler," *Klinik Tip Aile Hekimliği*, vol. 8, pp. 11–15, 2016, http://dergipark.gov.tr/ktah/issue/30812/333316.11-15.

[5] U. Stein, S. Burock, P. Herrmann et al., "Diagnostic and prognostic value of metastasis inducer S100A4 transcripts in plasma of colon, rectal, and gastric cancer patients," *Journal of Molecular Diagnostics*, vol. 13, no. 2, pp. 189–198, 2011.

[6] K. Boye and G. M. Mælandsmo, "S100A4 and Metastasis," *The American Journal of Pathology*, vol. 176, no. 2, pp. 528–535, 2010.

[7] M. Arnold, M. S. Sierra, M. Laversanne, I. Soerjomataram, A. Jemal, and F. Bray, "Global patterns and trends in colorectal cancer incidence and mortality," *Gut*, vol. 66, no. 4, pp. 683–691, 2017.

[8] J. B. O'Connell, M. A. Maggard, and C. Y. Ko, "Colon cancer survival rates with the new American Joint Committee on Cancer sixth edition staging," *Journal of the National Cancer Institute*, vol. 96, no. 19, pp. 1420–1425, 2004.

[9] K. Naxerova, J. G. Reiter, E. Brachtel et al., "Origins of lymphatic and distant metastases in human colorectal cancer," *Science*, vol. 357, no. 6346, pp. 55–60, 2017.

[10] A. K. Ghazali, K. I. Musa, N. N. Naing, and Z. Mahmood, "Prognostic factors in patients with colorectal cancer at hospital universiti sains Malaysia," *Asian Journal of Surgery*, vol. 33, no. 3, pp. 127–133, 2010.

[11] Y. Liu, W. Tang, J. Wang et al., "Clinicopathological and prognostic significance of S100A4 overexpression in colorectal cancer: a meta-analysis," *Diagnostic Pathology*, vol. 8, article 181, 2013.

[12] M. Dahlmann, D. Kobelt, W. Walther, G. Mudduluru, and U. Stein, "S100A4 in Cancer Metastasis: Wnt Signaling-Driven Interventions for Metastasis Restriction," *Cancers*, vol. 8, no. 6, p. 59, 2016.

[13] P. Moravkova, D. Kohoutova, S. Rejchrt, J. Cyrany, and J. Bures, "Role of S100 Proteins in Colorectal Carcinogenesis," *Gastroenterology Research and Practice*, vol. 2016, Article ID 2632703, 7 pages, 2016.

[14] R. Donato, B. R. Cannon, and G. Sorci, "Functions of S100 proteins," *Current Molecular Medicine*, vol. 13, no. 1, pp. 24–57, 2013.

[15] A. R. Bresnick, D. J. Weber, and D. B. Zimmer, "S100 proteins in cancer," *Nature Reviews Cancer*, vol. 15, no. 2, pp. 96–109, 2015.

[16] F. Fei, J. Qu, M. Zhang, Y. Li, and S. Zhang, "S100A4 in cancer progression and metastasis: A systematic review," *Oncotarget*, vol. 8, no. 42, pp. 73219–73239, 2017.

[17] A. Ebralidze, E. Tulchinsky, M. Grigorian et al., "Isolation and characterization of a gene specifically expressed in different metastatic cells and whose deduced gene product has a high degree of homology to a Ca2+-binding protein family," *Genes & development*, vol. 3, no. 7, pp. 1086–1093, 1989.

[18] M. Grigorian, N. Ambartsumian, and E. Lukanidin, "Metastasis-inducing S100A4 protein: Implication in non-malignant human pathologies," *Current Molecular Medicine*, vol. 8, no. 6, pp. 492–496, 2008.

[19] F. Fei, J. Qu, C. Li, X. Wang, Y. Li, and S. Zhang, "Role of metastasis-induced protein S100A4 in human non-tumor pathophysiologies," *Cell & Bioscience*, vol. 7, no. 1, 2017.

[20] U. Sack and U. Stein, "Wnt up your mind - intervention strategies for S100A4-induced metastasis in colon cancer," *General Physiology and Biophysics*, vol. 28, no. Focus Issue, 2009.

[21] Y. Atlasi, R. Noori, I. Marolin et al., "The role of S100a4 (Mts1) in Apc- and Smad4-driven tumour onset and progression," *European Journal of Cancer*, vol. 68, pp. 114–124, 2016.

[22] U. Stein, F. Arlt, W. Walther et al., "The Metastasis-Associated Gene S100A4 Is a Novel Target of β-catenin/T-cell Factor Signaling in Colon Cancer," *Gastroenterology*, vol. 131, no. 5, pp. 1486–1500, 2006.

[23] H. Wang, J. Shi, Y. Luo et al., "LIM and SH3 protein 1 induces TGFβ-mediated epithelial-mesenchymal transition in human colorectal cancer by regulating S100A4 expression," *Clinical Cancer Research*, vol. 20, no. 22, pp. 5835–5847, 2014.

[24] H. Wang, L. Duan, Z. Zou et al., "Activation of the PI3K/Akt/mTOR/p70S6K pathway is involved in S100A4-induced viability and migration in colorectal cancer cells," *International Journal of Medical Sciences*, vol. 11, no. 8, pp. 841–849, 2014.

[25] K. Flatmark, K. B. Pedersen, J. M. Nesland et al., "Nuclear localization of the metastasis-related protein S100A4 correlates with tumour stage in colorectal cancer," *The Journal of Pathology*, vol. 200, no. 5, pp. 589–595, 2003.